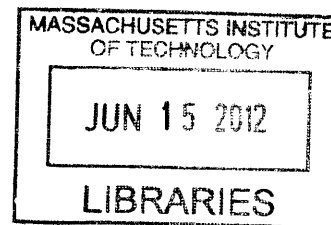


Design and Synthesis of Cyclometalated Transition Metal Complexes as Functional Phosphorescent Materials

by
Shuang Liu

B.S. (With Honors) Chemistry
Fudan University, 2004
M.S. (With Honors) Chemistry
Fudan University, 2007



ARCHIVES

SUBMITTED TO THE DEPARTMENT OF CHEMISTRY
IN PARTIAL FULFILLMENT OF THE REQUIREMENTS FOR THE DEGREE OF

DOCTOR OF PHILOSOPHY IN CHEMISTRY
AT THE
MASSACHUSETTS INSTITUTE OF TECHNOLOGY

JUNE 2012

© 2012 Massachusetts Institute of Technology. All rights reserved.

Signature of Author: _____
Department of Chemistry
June 1, 2012

Certified by: _____
John D. MacArthur Professor of Chemistry
Thesis Supervisor
Timothy M. Swager

Accepted by: _____
Robert W. Field
Haslam and Dewey Professor of Chemistry
Chairman, Departmental Committee on Graduate Students

This doctoral thesis has been examined by a Committee of the Department of Chemistry as follows:

Professor Richard R. Schrock: _____ Thesis Committee Chair

Professor Timothy M. Swager: _____ Thesis Supervisor

Professor Stephen L. Buchwald: _____ Department of Chemistry

Dedicated to My Family
献给我的家人

Design and Synthesis of Cyclometalated Transition Metal Complexes as Functional Phosphorescent Materials

by
Shuang Liu

Submitted to the Department of Chemistry on June 1st of 2012
in Partial Fulfillment of the requirements
for the Degree of Doctor of Philosophy in Chemistry

Abstract

Cyclometalated Ir(III) and Pt(II) compounds are among the most promising phosphorescent emitters for various applications, such as organic light emitting diodes (OLEDs), chemical sensors and bioimaging labels. This family of complexes exhibits high thermal and photo-stability, excellent quantum efficiency, and relatively short lifetime. More importantly, their luminescent properties can be fully tunable by modifying the coordinating ligands.

In this thesis, a series of 2-(1,2,3-triazol-4-yl)-pyridine derivatives, referred to as the “click” ligands, are used to build phosphorescent Ir(III) and Pt(II) compounds. The robust and tolerant nature of the copper mediated 1,3-dipolar cycloaddition reactions offers great flexibility in the molecular design.

Chapter 1 and Chapter 2 focus on the synthesis of heteroleptic cyclometalated Ir(III) and Pt(II) complexes by utilizing the Cu(I) triazolide intermediates generated in “click” reactions as transmetalating reagents. Ligand synthesis and metalation can be achieved in one pot under mild reaction conditions. For the Ir(III) system, the “click” ligands show switchable coordination modes, between the C, N- and N, N-chelation. These ligands act as C, N, N-bridging units to form unique zwitterionic dinuclear complexes with two cyclometalated Pt(II) units.

In Chapter 3, cyclometalated Pt(II) complexes with N, N-chelating “click” ligands are synthesized. Their aggregation-induced solid-state emission is highly responsive to environmental stimuli, such as solvents, heat and mechanical force. This family of compounds represents the first thermotropic Col(h) liquid crystals with only one side-chain. Furthermore, the combined liquid crystalline and mechanochromic properties make them attractive functional materials.

Thesis advisor: Timothy M. Swager
Title: John D. MacArthur Professor of Chemistry

Table of Contents

Title page	1
Signature page	3
Dedication	4
Abstract	5
Table of Contents	6
List of Figures	8
List of Tables	10
List of Schemes	11
Chapter 1. "Click" Synthesis of Heteroleptic Tris-cyclometalated Iridium(III) Complexes	12
1.1 Introduction	13
1.2 Results and Discussion	16
1.2.1 Synthesis and structural characterization	16
1.2.2 Isomerization	22
1.2.3 Electronic Spectroscopy	26
1.3 Conclusion	32
1.4 Experimental Section	32
1.4 References	43
1.5 Appendix: photo isomerization of <i>mer</i> -Ir(ppy) ₂ (trpy), packing diagrams of compounds 6b and 7b, NMR spectra of all the compounds.	47
Chapter 2. Zwitterionic dinuclear cyclometalated Pt(II) complexes based on "click" ligands	67
2.1 Introduction	68
2.2 Results and Discussion	70
2.2.1 Synthesis	70
2.2.3 Structural characterization	73
2.2.4 DFT Calculations	79
2.2.5 Photophysical properties	84
2.2.6 Aggregation-induced luminescence	84
2.3 Experimental Section	88
2.4 References	99
2.5 Appendix: photophysical properties and NMR spectra	103

Chapter 3. Platinum(II) complexes with responsive phosphorescence to environmental stimuli	119
3.1 Introduction	120
3.2 Results and Discussion	121
3.2.1 Synthesis and structural characterizations	121
3.2.2 Polymorphs	126
3.2.3 Photophysical properties	127
3.2.4 Aggregation-induced luminescence	130
3.2.5 Mechanochromism	132
3.2.6 Counterion effect	136
3.2.7 Side-chain effect	138
3.2.8 Liquid crystalline properties	139
3.3 Experimental Section	145
3.4 References	155
3.5 Appendix: frontier orbitals, photophysical properties, experimental setup for the mechanochromic effect study, DSC data, and NMR spectra	157
Curriculum Vitae	181
Acknowledgement	184

List of Figures

Figure 1.1. Functionalized 1,2,3-triazoles as chelating ligands	15
Figure 1.2. Ortep diagrams of 2a and 2b	19
Figure 1.3. Ortep diagram of 6b and 7b	22
Figure 1.4. Photoisomerization of 2a in DMSO- <i>d</i> ₆ , monitored by ¹ H NMR.	24
Figure 1.5. UV-vis absorption and emission spectra of all the <i>mer</i> -Ir(C [^] N) ₂ (trpy) compounds	27
Figure 1.6. UV-vis absorption and emission spectra of the [Ir(C [^] N) ₂ (N [^] N_trpy)] ⁺ compounds	29
Figure 1.7. Contour plots of frontier orbitals of <i>mer</i> -Ir(ppy) ₂ (trpy) and [Ir(ppy) ₂ (N [^] N_trpy)] ⁺	30
Figure 2.1. Ortep diagrams of the two molecules in the asymmetric unit of DiPt-1	74
Figure 2.2. Ortep diagrams of the two molecules in the asymmetric unit of DiPt-3b	75
Figure 2.3. ROESY spectrum of DiPt-3a and the assignment of the aromatic protons	78
Figure 2.4. ROESY spectrum of DiPt-3b and the assignment of the aromatic protons	79
Figure 2.5. Contour plots of frontier orbitals of the model compounds of DiPt-1	80
Figure 2.6. Simulated vertical excitations and the experimental UV-vis absorption spectrum (orange) of DiPt-1	81
Figure 2.7. Contour plots of frontier orbitals of the model compounds of DiPt-2 with <i>trans</i> and <i>cis</i> pyridyl coordination	81
Figure 2.8. UV-vis absorption and emission spectra of the dinuclear Pt(II) compounds in THF	83
Figure 2.9. The photoluminescence spectra of DiPt-3a and DiPt-3b in PMMA thin films	85
Figure 2.10. The packing diagram of DiPt-1	86
Figure 2.11. The packing diagram of DiPt-3b	87
Figure 3.1. ROESY spectrum of Pt1_SbF₆ in DMSO- <i>d</i> ₆ and the assignment of the aromatic protons	124

Figure 3.2. ROESY spectrum of Pt1_SbF₆ in CD ₂ Cl ₂ and the assignment of the aromatic protons	125
Figure 3.3. Polymorphs and the switchable luminescence exhibited by [Pt(ppy)(trpy-C ₆ H ₁₃)]SbF ₆ (Pt1_SbF₆)	127
Figure 3.4. UV-vis absorption and emission spectra of Pt1_SbF₆	128
Figure 3.5. Solid-state emission spectra of Pt1_SbF₆ ($\lambda_{\text{ex}} = 400 \text{ nm}$)	129
Figure 3.6. XRD pattern of the polymorphs of Pt1_SbF₆	130
Figure 3.7. Solid-state emission spectra of [Pt(ppy)(trpy-C ₆ H ₁₃)]SbF ₆ (Pt1_SbF₆) when doped into polymer matrixes	131
Figure 3.8. Mechanochromic luminescence exhibited by [Pt(ppy)(trpy-C ₆ H ₁₃)]SbF ₆ (Pt1_SbF₆)	133
Figure 3.9. Schematic illustration of the X-scan measurement	134
Figure 3.10. Significant red-shift of the PL spectra around the pin during the X-scan of Pt1_SbF₆	135
Figure 3.11. Consistent red shift of the PL spectra around the pin during the Z-scan of Pt1_SbF₆	135
Figure 3.12. UV-vis absorption spectra of Pt1_X (X = SbF ₆ ⁻ , PF ₆ ⁻ , BF ₄ ⁻ , OTf ⁻)	136
Figure 3.13. (a) Solid-state emission spectra of Pt1_X (X = SbF ₆ ⁻ , PF ₆ ⁻ , BF ₄ ⁻ , OTf ⁻)	137
Figure 3.14. Photophysical properties of Pt1_SbF₆ , Pt2_SbF₆ and Pt3_OTf	139
Figure 3.15. DSC trace of Pt1_SbF₆	140
Figure 3.16. POM images of the Col _h phase of Pt1_SbF₆	141
Figure 3.17. POM images of the Col _h phase of Pt1_PF₆	142
Figure 3.18. POM images of the Col _h phase of Pt1_PF₆	142
Figure 3.19. POM images of Pt1_BF₄	143
Figure 3.20. POM images of the Col _h phase of Pt1_OTf	144
Figure 3.21. POM images of Pt2_SbF₆	144

List of Tables

Table 1.1. Selected bond lengths (Å) and bond angles (deg) for compounds 2a , 2b , 6b and 7b	18
Table 1.2. Selected photophysical data of complexes 2-7	28
Table 2.1. Selected bond lengths (Å) and bond angles (deg) for compound DiPt-1	74
Table 2.2. Selected bond lengths (Å) and bond angles (deg) for compound DiPt-3b	76
Table 2.3. Selected photophysical data of DiPt-1 , DiPt-2 , DiPt-3a , and DiPt-3b	84

List of Schemes

Scheme 1.1. Synthesis of tris-cyclometalated iridium(III) complexes	16
Scheme 1.2. Thermal and photochemical isomerization of compounds 2a and 2b	23
Scheme 1.3. Failed attempts to synthesize tris-cyclometalated iridium(III) complexes by literature methods	25
Scheme 2.1. Synthesis of the starting materials Pt-A , Pt-B , Pt-C	70
Scheme 2.2. Synthesis of the dinuclear cyclometalated Pt(II) compounds	71
Scheme 2.3. Stepwise approach as the control reaction	72
Scheme 3.1. Synthesis of Pt1_X (X = SbF ₆ ⁻ , PF ₆ ⁻ , BF ₄ ⁻ , OTf)	122
Scheme 3.2. Synthesis of Pt2_SbF₆ and Pt3_ONTf	123

Chapter 1

“Click” Synthesis of Heteroleptic Tris-cyclometalated Iridium(III) Complexes

Adapted and reprinted in part with permission from:
Shuang Liu, Peter Müller, Michael K. Takase, Timothy M. Swager*. “Click” Synthesis of
Heteroleptic Tris-Cyclometalated Iridium(III) Complexes: Cu(I) Triazolide Intermediates
as Transmetalating Reagents. *Inorganic Chemistry*, 2011, 7598

1.1 Introduction

Phosphorescence-based organic light emitting diodes (OLEDs) have drawn significant attention due to their ability to harvest both singlet and triplet excitons for electroluminescence.¹ Cyclometalated iridium(III) complexes stand out as the most promising high performance emitters due to their strong Ir-C bonds, which ensure good photo and thermal stability and destabilize the thermally accessible, non-emissive metal centered (MC) states.² This family of complexes exhibits favorable photophysical properties, such as high quantum efficiency, short excited state lifetimes, and, most importantly, tunable emission colors. The triplet emission originates from a mixture of metal-to-ligand charge transfer (³MLCT) and ligand centered (³LC) excited states. This strong coupling between the d-orbitals of iridium and the p-orbitals of the ligands allows facile color tuning through the cyclometalating and ancillary ligands.^{3,4} Aside from their appealing applications as OLEDs, cyclometalated compounds can also be used in light-emitting electrochemical cells (LECs),^{5,6} and as chemical sensors⁷⁻¹¹ and bioimaging labels.¹²⁻¹⁶ Therefore, efficient and versatile synthetic methods that allow access to a library of cyclometalated compounds will greatly facilitate the screening process for various applications.

Bis- and tris-cyclometalated Ir(III) complexes are commonly synthesized from chloro-bridged Ir(III) dimers $[\text{Ir}(\text{C}^{\wedge}\text{N})_2\text{Cl}]_2$, which can be readily prepared from $\text{IrCl}_3 \cdot n\text{H}_2\text{O}$ and cyclometalating ligands. Thompson *et al.* reported the first selective synthesis of *mer* and *fac* isomers by controlling the reaction temperatures,¹⁷ which stimulated studies on differentiating the photophysical properties of the two isomers. More recently, μ -hydroxy-bridged Ir(III) dimers and solvated monomeric Ir(III)

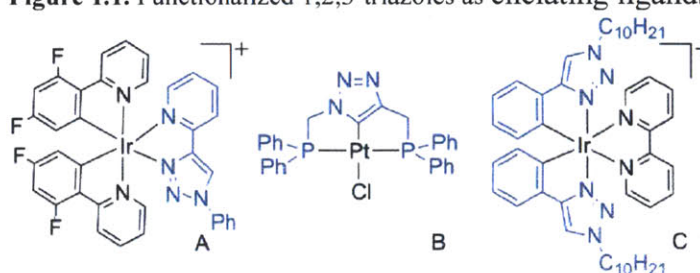
precursors have also been used to achieve *fac/mer* selectivity under mild reaction conditions.¹⁸

Transmetalation of metal-halide bonds with organometallic reagents has also been studied as an alternative approach. For example, Hg(ppy)Cl (ppy = 2-phenylpyridine) has been used to prepare mono-cyclometalated Ir(III) compounds.¹⁹ However, this method has not been extensively applied due to reluctance to work with Hg compounds. Recently, organozinc reagents were used to selectively generate meridional tris-cyclometalated Ir(III) complexes.²⁰ The organozinc reagents were prepared *in-situ* via metal exchange reactions after the ligands were treated with *n*-BuLi. In all instances, the ligands were pre-functionalized to facilitate the lithiation. Unfortunately, the need for highly reactive *n*-BuLi and additional synthetic procedures limited the scope of this method. Organolithiums have proven to be inferior to organozincs due to the low stability,²⁰ despite their applications in the synthesis of bis-cyclometalated Pd(II)/Pt(II) complexes.²¹⁻²³ Therefore, it is highly desirable to explore new organometallic reagents that show high functional group tolerance and ease of preparation.

One of the most popular protocols of copper mediated reactions is the Huisgen 1,3-dipolar cycloaddition reaction of organic azides and alkynes. This well-known “click” reaction provides high yields and regioselectivities under mild reaction conditions, and has found numerous applications in organic synthesis, material science and biological chemistry.²⁴ The catalytic cycle has been widely accepted to proceed via a Cu(I)-acetylide intermediate and a weakly coordinating azide, followed by cyclization and then hydrolysis of the Cu-C bond.²⁴⁻²⁶ Similar mechanistic steps have been convincingly characterized in a series of studies on Au(I) triazolides wherein the stable

Au-C bond allows for the isolation of an intermediate similar to the postulated Cu(I) intermediate in “click” chemistry.^{27,28} Moreover, Wu *et al.* reported that the Cu(I)-triazolide intermediate can be trapped with electrophiles, such as ICl, to give 1,4,5-trisubstituted triazoles.²⁹ These encouraging results indicate that organocopper intermediates can act as potential transmetalating reagents to “click” the *in-situ* generated triazole ligands onto metal centers, which is the critical step in the synthesis of cyclometalated iridium compounds.

Figure 1.1. Functionalized 1,2,3-triazoles as chelating ligands



1,4-disubstituted 1,2,3-triazole derivatives prepared by “click” chemistry have been recently investigated as ligands for a variety of transition metals. This family of so called “click ligands” shows versatile coordination modes when combined with other functional groups. For example, they can act as N[^]N and N[^]N[^]N multi-dentate donors for Ru(III),³⁰⁻³² Pt(II),^{33,34} Ir(III) (Figure 1.1A)^{30,35,36} and other transition metals³⁷ as bipyridine and terpyridine equivalents. The resulting coordination complexes have potential applications as light-emitting materials³⁵ and in LECs.³⁸ Gandelman *et al.* developed a family of 1,2,3-triazole-based pincer ligands that react with Na₂PdCl₄ or (COD)PtCl₂ (COD = cyclooctadiene) to give cyclometalated Pd(II) and Pt(II) complexes, compound B in Figure 1.1.³⁹⁻⁴¹ Schubert *et al.* reported a series of bis-cyclometalated Ir(III) complexes using 4-phenyl-1*H*-[1,2,3]triazoles as cyclometalating ligands (Figure

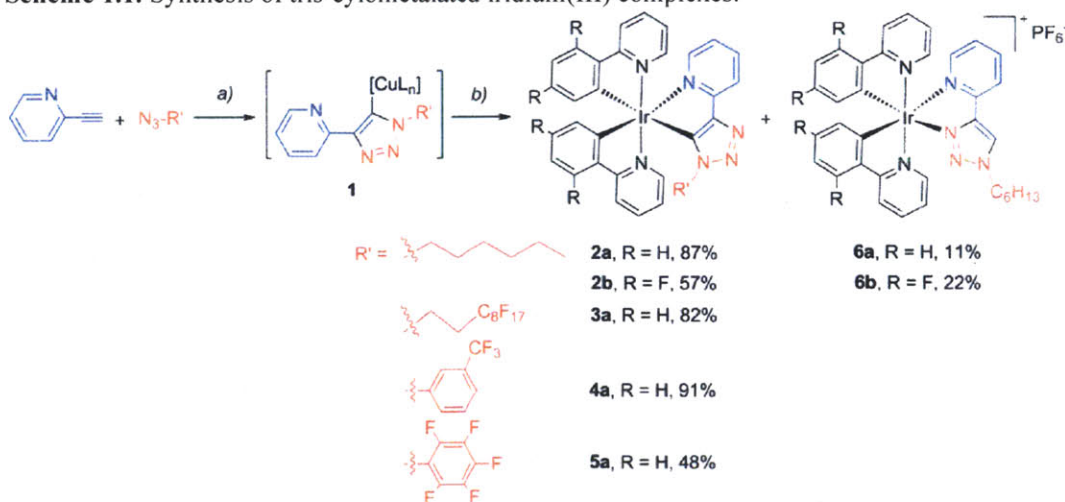
1.1C).³⁶ It is important to note that all these 1,2,3-triazole type ligands were synthesized, isolated and purified separately before the cyclometalation was performed.

Herein, we present a highly efficient one-pot procedure to synthesize heteroleptic tris-cyclometalated Ir(III) complexes, ligated by derivatives of 2-phenylpyridine (ppy) and 2-(1*H*-[1,2,3]triazol-4-yl)pyridine (trpy) ligands. The Cu(I)-triazolide intermediates formed in the reaction of organoazides and commercially available 2-ethynylpyridine was used to transmetalate trpy as the third cyclometalating ligand on to the Ir(III) center.

1.2 Results and Discussion

1.2.1 Synthesis and structural characterization

Scheme 1.1. Synthesis of tris-cyclometalated iridium(III) complexes.



a) $\text{Cu}(\text{MeCN})_4\text{PF}_6$, NaH, $\text{Et}_3\text{N}/\text{THF}$, RT, 2 hours; b) $[\text{Ir}(\text{ppy})_2\text{Cl}]_2$ or $[\text{Ir}(\text{Fppy})_2\text{Cl}]_2$, 65 °C, 2-4 hours.

Scheme 1.1 represents the general route to prepare tris-cyclometalated Ir(III) complexes using the *in-situ* generated Cu(I)-triazolides (**1**) as transmetalating reagents. 2-Ethynylpyridine was treated with stoichiometric $\text{Cu}(\text{MeCN})_4\text{PF}_6$ in THF in the presence of NaH and Et_3N , before the addition of 1-azidohexane. Proton NMR spectra of the

reaction mixture showed that the cyclization was very efficient and usually proceeded to completion within one hour at room temperature. To the organocopper compound containing mixture was added $[\text{Ir}(\text{ppy})_2\text{Cl}]_2$ or $[\text{Ir}(\text{FFppy})_2\text{Cl}]_2$ (FFppy = 2-(2,4-difluorophenyl)pyridine) at room temperature and the reaction was heated to 65 °C for 4 hours. Crystalline $\text{Ir}(\text{ppy})_2(\text{trpy})$ (**2a**) and $\text{Ir}(\text{FFppy})_2(\text{trpy})$ (**2b**) were isolated in moderate to high yields, after purification by column chromatography. In order to maximize the yield of either **2a** or **2b**, it was essential to prevent intermediate **1** from being quenched by other electrophiles before the transmetalation reaction could occur. Therefore, a strong base, such as sodium hydride, was used as an efficient proton scavenger.

The tolerant and robust nature of the click reaction provides an ideal route to introduce different functional groups to the cyclometalated system. Alkyl, perfluoroalkyl and aryl azides, readily prepared from the respective halides in one step, were tested in this case. The 1,3-dipolar cycloaddition and subsequent transmetalation proceeded smoothly to give compounds **3a-5a** in high yields (> 80%). We attribute the slightly lower isolated yield of compound **5a** to repeated purification procedures. All the isolated compounds exhibit good solubility in common organic solvents, such as tetrahydrofuran, dichloromethane and toluene.

The tris-cyclometalated compounds obtained by this approach are expected to be meridional isomers. The pyridyl nitrogen atoms adopt a *trans* configuration in the dimeric Ir(III) precursors as confirmed by X-ray crystallography.¹⁸ This coordination geometry has been proven to be stable and able to survive relatively harsh reaction conditions. Therefore, we hypothesized that the tris-cyclometalated Ir(III) complexes obtained would be meridional.²⁰ This hypothesis is supported by comparing the NMR

spectra of **2a** and **2b** to literature compounds containing [Ir(ppy)₂]/[Ir(FFppy)₂] fragments.¹⁷

Table 1.1. Selected bond lengths (Å) and bond angles (deg) for compounds **2a**, **2b**, **6b** and **7b**

	2a	2b^a		6b	7b
Ir(1)-C(11) ^b	2.016(3)	2.003(4)	2.000(3)	2.007(3)	2.008(2)
Ir(1)-C(31) ^c	2.053(4)	2.048(3)	2.054(3)	2.004(3)	2.0044(19)
Ir(1)-C(47) ^d /N(4) ^e	2.088(4)	2.081(3)	2.091(3)	2.118(2)	2.1200(19)
Ir(1)-N(1)	2.046(3)	2.045(3)	2.039(3)	2.048(2)	2.051(2)
Ir(1)-N(2)	2.062(3)	2.059(3)	2.057(3)	2.047(3)	2.039(2)
Ir(1)-N(3)	2.188(3)	2.183(3)	2.184(3)	2.151(2)	2.172(2)
C(11)-Ir(1)-N(1)	79.93(13)	80.80(14)	80.69(14)	80.39(11)	80.62(9)
C(31)-Ir(1)-N(2)	79.73(13)	79.54(13)	79.93(14)	80.52(12)	80.56(10)
N(3)-Ir(1)-C(47) ^d /N(4) ^e	76.58(13)	77.27(13)	77.34(13)	76.18(9)	76.46(9)

^a Data for the Δ (left column) and Λ (right column) isomers in the asymmetric unit cell. ^b *Trans* to Ir-N(trpy). ^c *Trans* to Ir-C(trpy). ^d For compound **2a** and **2b**. ^e For compound **6b** and **7b**.

Two representative compounds, **2a** and **2b**, were characterized by X-ray crystallography, using single crystals obtained from slow evaporation of respective dichloromethane/hexane solutions. Both compounds crystallize in the monoclinic space group $P2_1/c$, as racemates of the D and L enantiomers/helimers. Only the thermal ellipsoid plots of the D isomers are depicted in Figure 1.2 for simplicity. Details of the data quality and a summary of the residual values of the refinements are listed in Table 1.1, and selected bond lengths and angles are listed in Table 1.1. Full tables of bond lengths, bond angles and atomic coordinates are provided in the supporting information.

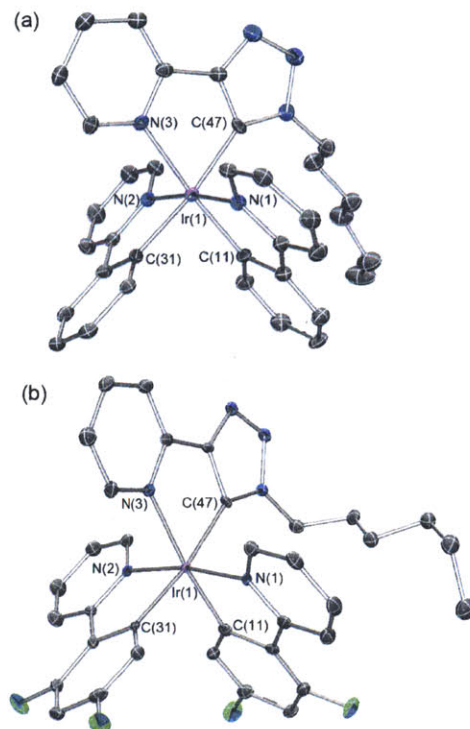


Figure 1.2. Ortep diagrams of **2a** (a) and **2b** (b). Thermal ellipsoids are drawn at the 50% probability level. Hydrogen atoms are omitted for clarity.

Both tris-cyclometalated compounds adopt the meridional configuration, with the phenyl groups of the two ppy ligands mutually *cis* to each other. The *in-situ* generated trpy ligand completes the octahedral coordination sphere through the pyridyl nitrogen and triazolyl carbon at the 5-position. Compounds **2a** and **2b** are rare examples of crystallographically characterized complexes with the trpy ligands acting as C^N chelates, even though other binding modes have been reported before.^{30,38}

The bond lengths and bond angles of **2a** are consistent with values reported for other meridional Ir(III) complexes in the literature. As the X-ray structure of *mer*-Ir(ppy)₃ is not available in the Cambridge Structural Database (CSD), the averaged bond lengths of the Λ and Δ isomers of *mer*-Ir(ppy)₂(tpy) (tpy = 2-(*p*-tolyl)pyridine)⁴² are used as references. The length of the Ir-C(ppy) bond *trans* to Ir-N(trpy) in **2a** is 2.016(3) Å,

which is comparable to its equivalent in *mer*-Ir(ppy)₂(trpy) (2.010 Å). However, the Ir-C(ppy) bond *trans* to Ir-C(trpy) (2.053(4) Å) is shorter than that of the Ir-C(ppy) *trans* to Ir-C(tpy) (2.074 Å). Meanwhile, the Ir-C(trpy) bond (2.088(4) Å) is longer than the Ir-C(tpy) bond (2.074 Å). Such variation in bond lengths suggests that the Ir-C(ppy) and Ir-C(tpy) bonds have a stronger *trans* influence relative to Ir-C(trpy). In other words, trpy appears to be a weaker cyclometalating ligand than the ppy derivatives based on the bond length analysis. This is probably due to the strongly σ electron-withdrawing nature of the triazolyl group.

The structure of **2b** resembles that of **2a**, except that the asymmetric unit of **2b** consists of two crystallographically independent molecules with little variation in individual bond lengths and bond angles (Table 1.2). The average bond lengths of the mutually *trans* Ir-C(FFppy) (2.051 Å) and Ir-C(trpy) (2.086 Å) bonds are the same as those observed in **2a**, indicating little perturbation upon fluorination of the ppy ligand. The two Ir-N(FFppy) bonds *trans* to each other have slightly longer bond lengths than those of *mer*-Ir(FFppy)₃.⁴³ The Ir-N(trpy) bond is elongated by roughly 0.13 Å in comparison with the *trans* Ir-N(FFppy) bonds.

It is worth noting that a minor Ir(III)-containing product **6a** was also isolated from the reaction mixture of **2a**. High resolution mass spectra (HRMS) of the minor product revealed a parent ion of $m/z = 731.2446$ m/e, which is the same as that of **2a** ($m/z = 731.2498$ m/e). The ¹H NMR spectrum of **6a** appeared to be similar to that of **2a**, with one additional peak as a sharp singlet at 8.75 ppm. Careful examination of the gCOSY NMR spectrum revealed that the ppy ligands and the pyridyl group of the trpy were intact and the extra proton giving rise to the new singlet was completely isolated. Addition of

base to a solution of **6a** had no effect on its ^1H NMR spectrum, excluding the possibility of **6a** being a protonated version of **2a**. The ^{19}F NMR spectrum had a doublet signal at -72.99 ppm ($J = 711.0$ Hz), suggesting the presence of fluorophosphate anions (PF_6^-). Based on these characterizations, this minor product was tentatively assigned as a cationic $[\text{Ir}(\text{ppy})_2(\text{N}^{\wedge}\text{N_trpy})]^+$ complex similar to those reported in the literature.^{30,38} The counterion PF_6^- was obtained from the reagent $\text{Cu}(\text{MeCN})_4\text{PF}_6$. The formation of a similar minor product **6b** (22%) was also observed during the synthesis of **2b**. The ^1H NMR spectrum of **6b** also showed a sharp singlet at 8.78 ppm, in addition to the characteristic ^{19}F NMR signal for PF_6^- . Extensive heating or prolonged reaction time were found to increase the yields of **6a** and **6b**. However, no isolable amount of side products was obtained in other cases.

Single crystal structure of **6b** confirmed the formation of positively charged $[\text{Ir}(\text{FFppy})_2(\text{N}^{\wedge}\text{N_trpy})]^+$. As shown in Figure 1.3a, the two Ir-N(FFppy) bonds remain *trans* to each other. The pseudo-octahedral geometry of the $[\text{Ir}(\text{FFppy})_2]$ fragment is completed by the pyridyl group and N at the 3-position of the triazole. The Ir-C(trpy) bond in **2b** is cleaved and the triazolyl group flips to offer a $\text{N}^{\wedge}\text{N}$ binding mode. The hydrogen atom of the newly formed triazolyl C-H bond is located on the residual electron density map and gives rise to the sharp singlet ^1H NMR signal. One hexafluorophosphate anion is also found in the asymmetric unit, in agreement with the ^{19}F NMR spectrum. The two Ir-N(FFppy) bonds *trans* to each other (2.048(2) and 2.047(3) Å) are the same as those previously reported for $[\text{Ir}(\text{FFppy})_2(\text{N}^{\wedge}\text{N_trpy})]\text{BF}_4$ (2.056 and 2.048 Å), where $\text{N}^{\wedge}\text{N_trpy}$ refers to pyridine-N-biphenyl-1,2,3-triazole.³⁸ The two trpy-based Ir-N bonds are elongated due to the strong *trans* influence of the Ir-C(FFppy) bonds. It is interesting

to note that the Ir-N(triazolyl_trpy) bond (2.118(2) Å) is shorter than the N(pyridyl_trpy) bond (2.151(2) Å).

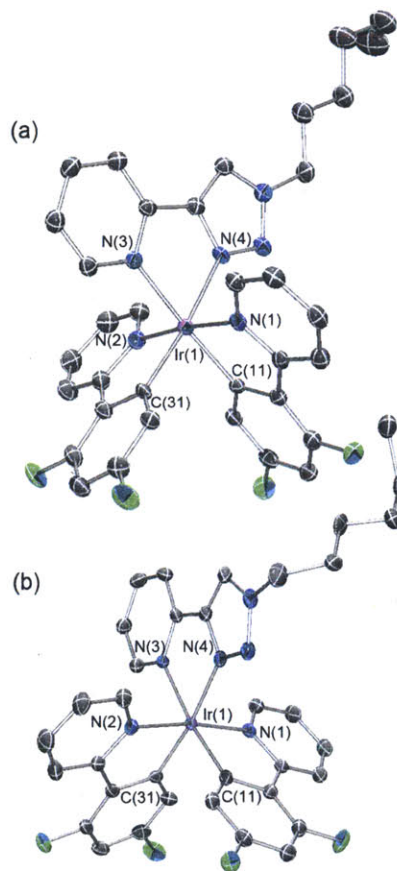


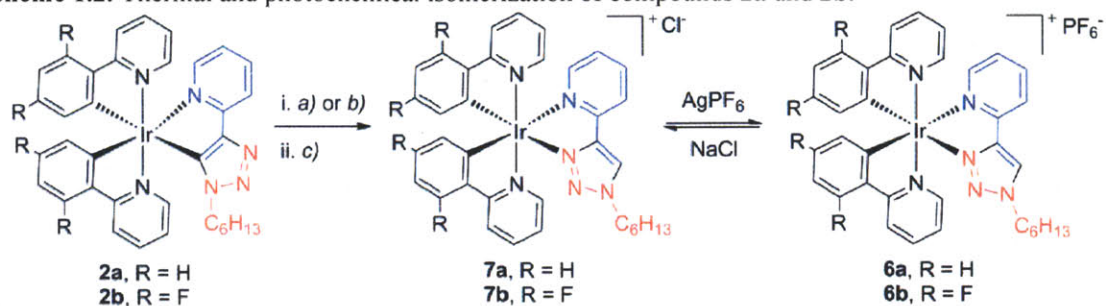
Figure 1.3. Ortep diagram of **6b** (a) and **7b** (b). Thermal ellipsoids are drawn at the 50% probability level. Hydrogen atoms and counter ions are omitted for clarity.

1.2.2 Isomerization

In an attempt to obtain *fac*-Ir(C^N)₂(trpy), **2a** and **2b** were heated in glycerol at 200 °C for twenty hours before treated with saturated NaCl solution (Scheme 1.2). Unlike previous cases reported in the literature, ligand scrambling products were not observed, based on ¹H NMR and HRMS characterization of the crude reaction mixture.

Nevertheless, ^1H NMR spectra indicated that compounds **7a** and **7b** had similar structure to **6a** and **6b**. The characteristic singlet peak from the triazolyl C-H bond was shifted downfield to 9.07 ppm and 10.95 ppm for **7a** and **7b**, respectively. Additionally, a PF_6^- signal was not observed in the ^{19}F NMR spectrum.

Scheme 1.2. Thermal and photochemical isomerization of compounds **2a** and **2b**.



a) glycerol, 200 °C, 20 hours; b) DMSO-*d*₆, UV, 88 hours; c) aqueous NaCl.

Single crystals of compound **7b** were obtained by slow diffusion of hexane into a dichloromethane solution. It is worth noting that **7b** crystallizes in the $P2_1$ space group ($Z = 2$) with only the Δ helimer (Figure 1.3b). Such enrichment of one optical isomer from a racemic mixture is very rare for transition metal complexes with bidentate ligands. Limited literature reports on the separation of Δ and Λ isomers of cyclometalated compounds indicate the need for either rigid chiral ligands⁴⁴ or chiral chromatography techniques⁴⁵. The coordination around the Ir(III) center in **7b** greatly resembles that of **6b**, with the trpy ligand acting as a neutral N^N chelate. However, the counter anion is a chloride ion in this case, which likely arise from the saturated brine solution used during the work-up procedure. Indeed, **6b** and **7b** are interchangeable through simple ion exchange reactions. Treatment with one equivalent of AgPF₆ in dichloromethane, affords **6b** from **7b** quantitatively. Conversely, **6b** can be converted back to **7b** using excess NaCl.

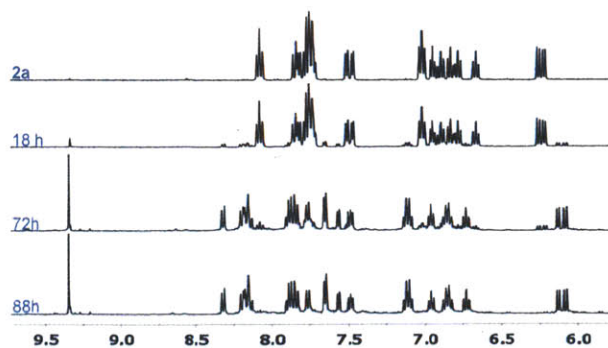


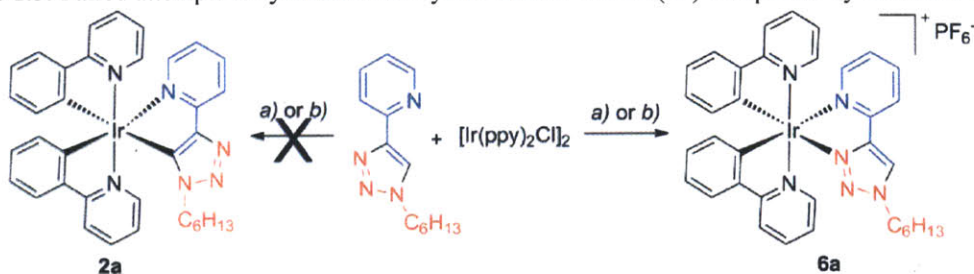
Figure 1.4. Photoisomerization of **2a** in DMSO- d_6 , monitored by ^1H NMR.

Such switching of the binding mode of trpy ligands, from $\text{C}^{\wedge}\text{N}$ to $\text{N}^{\wedge}\text{N}$, could also be achieved photochemically. Broadband UV radiation of DMSO- d_6 solutions of **2a** and **2b** afforded the respective cationic Ir(III) species. The conversion was monitored by ^1H NMR spectroscopy, and only a single product was observed (Figure 1.4). After the isomerization was completed, the reaction mixtures were treated with excess saturated NaCl solution. The isolated products showed identical NMR and HRMS spectra to those of **7a** and **7b**, respectively. Evidence of the formation of *fac*-Ir($\text{C}^{\wedge}\text{N}$) $_2$ (trpy) under either the thermal or the photochemical conditions was not obtained. Moreover, treatment of **2a** with acetic acid and silica gel in dichloromethane also failed to produce the *fac* isomer.⁴⁶

The mechanism of the *mer*-to-*fac* isomerization of tris-cyclometalated Ir(III) compounds is believed to involve the dissociation of one of the mutually transoid nitrogen atoms and protonation of at least one of the Ir-C bonds as indicated by the unavoidable ligand scrambling.^{17,42} The proton source is either the alcoholic solvent or the activated C-H bond of an incoming ligand. The energy needed for the C-H activation is compensated by the rearrangement of the coordination geometry and the chelation effect. However, the trpy ligand used in this study can offer both $\text{C}^{\wedge}\text{N}$ and $\text{N}^{\wedge}\text{N}$

coordination modes, the latter being an analogue of the commonly-used bipyridine ligand. As discussed in the previous section, the Ir-C(trpy) bond is considerably longer than the Ir-C(ppy) bonds in **2a** and **2b**. Therefore, it is most likely to be activated prior to either the Ir-C(ppy) or Ir-C(FFppy) fragments upon heating or UV radiation. Once the triazole C-5 is protonated, the N[^]N chelating mode of the trpy offers a thermodynamically stable product, which prevents isomerization of the ppy ligands. It should be pointed out that the proton source is the glycerol solvent during the thermal isomerization, as previously reported for the *mer*-to-*fac* isomerization.^{17,42} The counterion during the thermal isomerization is likely to be glycerolate ions before the addition of NaCl. In the case of photochemical isomerization, the integration of the singlet corresponding to the triazolyl C-H increased proportionally with other aromatic protons from the ppy and trpy ligands, which precluded the formation of C-D bond (see Appendix). A slight increase of the pH values of the reaction mixture was also observed, in agreement with the formation of hydroxide counterions. Therefore, it is likely that the residual water acted as the proton source instead of DMSO-*d*₆.

Scheme 1.3. Failed attempts to synthesize tris-cyclometalated iridium(III) complexes by literature methods.



a) (1) AgPF₆, MeCN; (2) *o*-dichlorobenzene, 100 °C, 48 hours; b) AgPF₆, 2-ethoxyethanol, 140 °C, 24 hours.

This speculation is further supported by attempts to prepare heteroleptic cyclometalated Ir(III) compounds following the established procedures (Scheme 1.3).^{18,47}

However, only the N^N chelating complexes could be isolated even in refluxing ethoxyethanol. Therefore, the transmetalation approach described in this work is most likely the only way to use the trpy ligand as a C^N chelator.

1.2.3 Electronic Spectroscopy

The absorption spectra of all the meridional tris-cyclometalated Ir(III) complexes are given in Figure 1.5a. Compounds **2a-5a** show intense absorption between 235 and 350 nm, which can be assigned to ligand-centered transitions.³ These spin-allowed π - π^* bands are accompanied by weaker spin-allowed and spin-forbidden charge transfer transitions in the visible region up to 480 nm. The band shapes and extinction coefficients are comparable to other ppy-based cyclometalated complexes, such as *mer*-Ir(ppy)₃.¹⁷

All the ppy-based meridional isomers show green phosphorescence at room temperature. Normalized photoluminescence (PL) spectra recorded in deoxygenated THF solutions and poly(methyl methacrylate) (PMMA) thin films are provided in Figure 1.5. Broad and structureless PL emission bands are observed across the series of *mer*-Ir(ppy)₂(trpy) in solution. In contrast, blue-shifted and relatively structured emission spectra and higher quantum yields are observed in the solid state. These observations suggest that the phosphorescence is based on excited states with strong ³MLCT character. The low quantum efficiency and short triplet state lifetime in solutions likely arise from the distortion or even cleavage of Ir-N and Ir-C bonds upon excitation, which may be responsible for the photoisomerization processes described in the previous section.

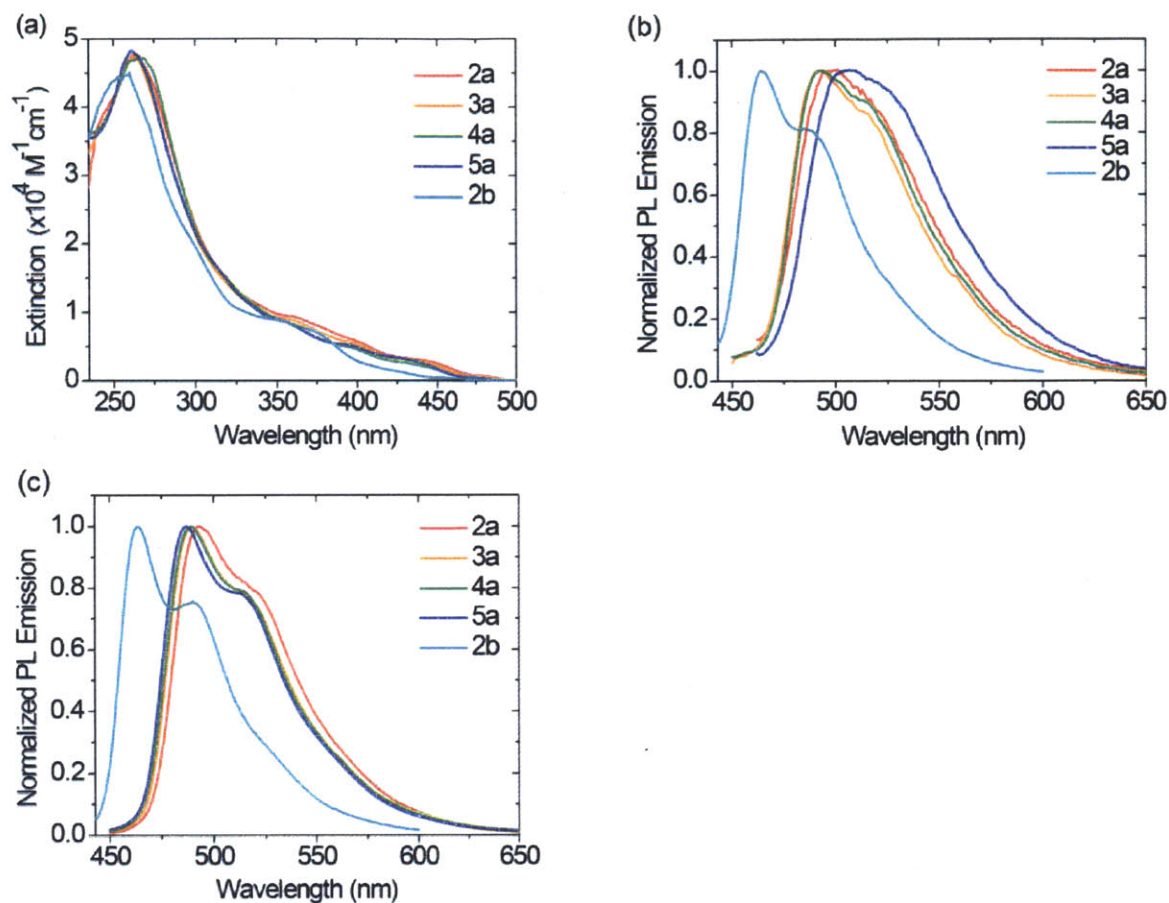


Figure 1.5. UV-vis absorption (a) and emission (b) spectra of all the *mer*-Ir(C^N)₂(trpy) compounds in THF (10⁻⁶ M, under Ar), as well as the photoluminescence spectra in PMMA thin films (c).

The absorption spectrum of FFppy-based **2b** exhibits similar spectral features as found for **2a**, except for a hypsochromic shift, consistent with the absorption spectra of the free ppy and FFppy ligands. Unlike its ppy-based analogues, **2b** exhibits a more structured and narrower PL spectrum in solution, with an emission maximum at 464 nm. Similar trends have also been observed with other Ir and Pt compounds bearing FFppy ligands.^{17,48} It has been recognized that the difluoro substitution stabilizes the HOMO more than the LUMO level, resulting in an increase in the band gap.^{4,49}

Table 1.2. Selected photophysical data of complexes **2-7**

	Solution ^a				Thin film ^c	
	λ_{\max} [nm] ($\epsilon \times 10^{-3} \text{ M}^{-1} \text{ cm}^{-1}$)	λ_{em} [nm]	Φ_{em} ^b	τ [μs]	λ_{em} [nm]	Φ_{em} ^d
2a	263(47.7), 355(9.5), 397(6.0), 440(3.0)	500	0.002	0.90	493	0.10
2b	254(44.1), 346(9.1), 372(7.4), 427(1.3)	464, 485	0.003	0.40	464, 490	0.09
3a	262(47.3), 356(9.0), 396(5.6), 436(2.9)	492	0.007	1.6	490	0.17
4a	266(47.1), 359(8.3), 393(5.1), 432(2.6)	493	0.003	0.23	489	0.09
5a	263(48.0), 355(8.8), 396(5.2), 429(3.2)	505	0.015	1.9	488	0.07
6a	256(37.9), 384(4.8), 411(3.7)	477, 507	0.20	1.7	478, 508	0.35
6b	249(37.5), 362(5.1), 387(3.7)	453, 482	0.24	2.0	454, 483	0.57
7a^c	255(44.0), 386(4.6), 415(3.0)	479, 508	0.35	3.5	479, 508	0.28
7b	248(47.1), 364(4.2), 390(1.7)	454, 483	0.45	3.5	455, 483	0.51

^a Measured in deoxygenated THF solution ($\sim 10^{-5}$ M) at room temperature. ^b Determined by comparison with Coumarin-343 (ethanol, $\Phi = 0.63$).⁵³ ^c Measured in PMMA films doped with 2-5 wt % of the Ir(III) compounds. ^d Determined by comparison with perylene (PMMA film, QY = 0.98)³⁴ and 9,10-diphenylanthracene (PMMA film, QY = 0.83).⁵⁵ ^e Measured in THF with 5% v/v of CH_2Cl_2 due to the low solubility of **7a** in THF.

Although there is little change in terms of the band shape or emission color of compounds with different substituents on the trpy ligands (**2a-5a**), greater differences are observed in the luminescence efficiency (Table 1.2). The perfluorooctyl pedant chain rigidifies the molecule and provides efficient insulation between individual molecules.⁵⁰ As a result, aggregation-induced quenching processes are minimized. Consistent with these arguments, **3a** exhibits the highest quantum yield (17%) in the solid state across the series. On the other hand, the pentafluorophenyl group introduces strong intermolecular interactions. Accordingly, aggregation-induced bathochromic shift in the PL spectrum of **5a** is observed even when the concentration is as low as 4×10^{-6} M. Moreover, crystals of **5a** exhibit yellow phosphorescence under UV radiation instead of the green emission observed for all the other *mer*-Ir(ppy)₂(trpy) complexes. Differences are also evident in terms of lifetimes. Compounds **2a** and **4a** show comparable lifetimes to those of previously reported meridional tris-cyclometalated Ir(III) complexes, such as *mer*-Ir(ppy)₃ (0.15 ms),¹⁷ while highly fluorinated **3a** and **5a** both show longer lifetimes. Hence, it can be established that certain photophysical properties can be tuned by varying

the substituents on the triazole ring. Many potential applications can be envisioned considering the huge library of organo azides established in the literature.

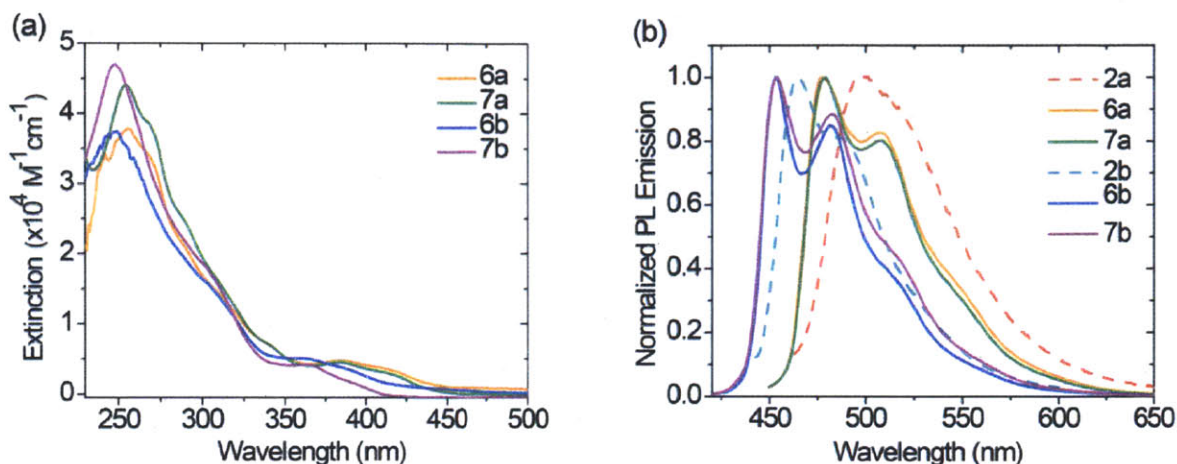


Figure 1.6. UV-vis absorption (a) and emission (b) spectra of the $[\text{Ir}(\text{C}^{\text{N}})_2(\text{N}^{\text{N}}_{\text{trpy}})]^+$ compounds in THF (10^{-6} M, under Ar).

The positively charged $[\text{Ir}(\text{C}^{\text{N}})_2(\text{N}^{\text{N}}_{\text{trpy}})]^+$ complexes exhibit photophysical properties distinct from those of their tris-cyclometalated counterparts (Figure 1.6). The absorption spectra show well defined absorption bands at around 385 nm for **6a/7a** and 363 nm for **6b/7b**. The room temperature solution PL spectra show well-resolved vibronic structures typical of this type of complexes.^{30,38} These highly-structured emission spectra indicate that the excited state is primarily ligand based. The emission maximum is also slightly blue shifted relative to the corresponding meridional compounds. For complexes with PF_6^- and Cl^- anions, the excited state lifetimes and PL quantum efficiencies show counter ions dependency, despite their nearly identical absorption and PL spectra. The excited states of the chlorides **7a** and **7b** display longer lifetimes and higher quantum yields than **6a** and **6b**, respectively. This difference has been observed previously between $[\text{Ir}(\text{FFppy})_2(\text{N}^{\text{N}}_{\text{trpy}})]\text{PF}_6$ and $[\text{Ir}(\text{FFppy})_2(\text{N}^{\text{N}}_{\text{trpy}})]\text{BF}_4$, and it is attributed to different packing interactions when the

cations are not fully solvated.³⁸ Indeed, an examination of the packing diagrams of **6b** and **7b** reveals that PF_6^- and Cl^- ions show different H-bonding interactions with the FFppy and trpy ligands in the solid state (see the Appendix).

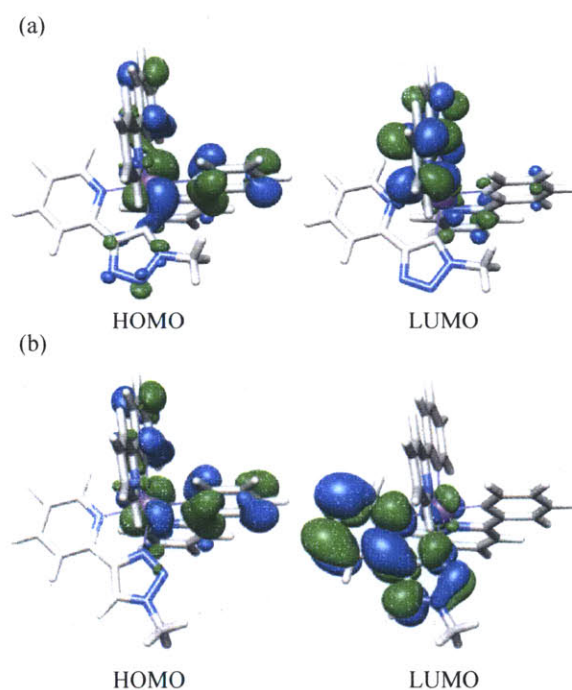


Figure 1.7. Contour plots of frontier orbitals of *mer*-Ir(ppy)₂(trpy) (a) and [Ir(ppy)₂(N[^]N_trpy)]⁺ (b).

In order to gain insights into the different electronic structures and photophysical properties of the neutral and cationic Ir(III) complexes, density functional theory (DFT) calculations were performed on two simplified structures *mer*-Ir(ppy)₂(trpy) and [Ir(ppy)₂(N[^]N_trpy)]⁺. The optimized ground-state geometries closely resemble the solid state structures determined by X-ray diffraction. The most important frontier orbitals of the two model compounds are shown in Figure 1.7. The highest occupied molecular orbitals (HOMOs) of the two model compounds are both composed of a mixture of the d-

orbitals of iridium and the p-orbitals of the two ppy-based phenyl groups, typical for bis- or tris-cyclometalated Ir(III).^{3,4} However, the lowest unoccupied molecular orbitals (LUMOs) appear to be remarkably different. As for *mer*-Ir(ppy)₂(trpy), the LUMO is localized primarily on the ppy ligand that has transoid Ir-C bond with the trpy. Such atomic orbital composition of the frontier molecular orbitals is very typical for meridional bis-cyclometalated Ir(III) complexes.¹⁷ The absence of a significant contribution from the substituted triazolyl group to the frontier orbitals explains the almost identical absorption and emission spectra observed for **2a-5a**. The LUMO for [Ir(ppy)₂(N[^]N₋trpy)]⁺, on the other hand, is dominated by the p*-orbital of the N[^]N₋trpy ligand with little overlap with the HOMO. The orbital diagram of the Ir(III) cation greatly resembles that of bis-cyclometalated complexes with neutral diimine ligands, such as 2,2'-bipyridine (bpy) and 1,10-phenanthroline. The HOMO of [Ir(ppy)₂(bpy)]⁺ is also a mixture of iridium d and phenyl p-orbitals, while the LUMO is primarily on the bpy ligand.^{51,52} Studies on the excited states have confirmed the mixed ³MLCT and ligand-to-ligand charge transfer (³LLCT) character of the low-lying triplet states. Therefore, the low energy absorption of *mer*-Ir(ppy)₂(trpy) can be attributed to excitation to mixed ³MLCT and ³LC excited states of ppy, while the low-lying excited states of [Ir(ppy)₂(N[^]N₋trpy)]⁺ have an important ³LLCT character between the ppy and trpy ligands. This is in good agreement with the highly structured emission spectra and longer phosphorescence lifetimes observed for **6-7** relative to their C[^]N₋trpy counterparts. Since the neutral N[^]N₋trpy ligands are better p acceptors than the anionic C[^]N₋trpy, stronger back bonding from the metal center to N[^]N₋trpy would further stabilize the Ir d-orbitals while destabilized the ligand p*-

orbitals. This stabilization of the HOMO and destabilization LUMO led to the hypsochromic shift observed upon switching from the C[^]N chelating mode to N[^]N.

1.3 Conclusion

In summary, we demonstrated that Cu(I)-triazolides generated by click chemistry can be used to facilitate the synthesis of tris-cyclometalated Ir(III) complexes. This route represents an efficient one-pot procedure for both ligand preparation and cyclometalation. *mer*-Ir(C[^]N)₂(trpy) with various substituents of the triazole groups are isolated in moderate to high yields and fully characterized. These meridional Ir(III) compounds show short-lived phosphorescence at room temperature, and their quantum efficiencies can be perturbed by varying the cyclometalating ligands. The robust nature of the click chemistry affords the possibility of introducing different lateral functional groups to the ligand that can act as sensing receptors or anchor groups. Many potential applications can be envisioned considering the diversity of organo azides established in the literature. The isomerization of neutral *mer*-Ir(C[^]N)₂(trpy) to positively charged [Ir(C[^]N)₂(N[^]N_trpy)]⁺ is also discussed in detail. The neutral N[^]N chelating mode is thermodynamically favored comparing to the anionic C[^]N mode. Therefore, the transmetalation approach described in this work is required to utilize trpy as a cyclometalating ligand.

1.4 Experimental Section

General Methods and Instrumentation. All reactions were performed under an argon atmosphere, using oven-dried glassware and standard Schlenk techniques. ¹H and ¹³C{¹H}NMR spectra were recorded on either a Bruker 400 MHz or Varian 500 MHz

spectrometer and referenced to the residual proton or carbon resonance of the deuterated solvent. ^{19}F NMR spectra were recorded on a Varian 300 MHz spectrometer and referenced to an external standard CFCl_3 (0 ppm). Electrospray ionization (ESI) high resolution mass spectrometry (HRMS) was measured on a Bruker Daltonics APEXIV 4.7 Tesla Fourier Transform Ion Cyclotron Resonance Mass Spectrometer and the most abundant masses are reported.

UV/Vis spectra were recorded on an Agilent 8453 diode-array spectrophotometer. Emission spectra were acquired on a SPEX Fluorolog fluorometer (model FL-321, 450 W xenon lamp) using either right-angle detection (solution measurements) or front-face detection (thin film measurements). All room temperature solution samples for emission spectra were degassed by at least three freeze-pump-thaw cycles in an anaerobic cuvette. Solution photoluminescence quantum yields were determined against Coumarin-343 (ethanol, $\text{QY} = 0.63$)⁵³ and corrected for solvent refractive index and absorption differences at the excitation wavelength. Thin films were prepared by spin-coating a chloroform solution of poly(methyl methacrylate) (PMMA) and the target compound (5-10 % w/w relative to PMMA). Perylene (PMMA film, $\text{QY} = 0.98$)⁵⁴ or 9,10-diphenylanthracene (PMMA film, $\text{QY} = 0.83$)⁵⁵ were used as the reference materials. Phosphorescence lifetimes were determined by time-resolved phosphorescence spectroscopy. The radiation source was an Oriel nitrogen laser (Model 79111) with a 5 ns pulse width operating at approximately 25 Hz. The emitted light was dispersed in an Oriel MS-260i spectrograph with a 600 lines/mm grating. The detector was an Andor Technologies Intensified CCD camera (1024 x 128 pixels) with an onboard delay generator and a minimum gate width of 5 ns operating in full vertical binning mode and

triggered by a TTL prepulse from the nitrogen laser. The detector was calibrated with a Hg(Ar) pencil-style calibration lamp. Solution data was acquired with a horizontal binning of 2 or 3. 15 spectra at different delay times after the laser pulse were taken per lifetime measurement, the integrated intensities of which were fit to a single-exponential function.

Materials and Synthesis. Iridium(III) chloride hydrate ($\text{IrCl}_3 \cdot n\text{H}_2\text{O}$) and *tetrakis*(acetonitrile)copper(I) hexafluorophosphate ($\text{Cu}(\text{MeCN})_4\text{PF}_6$) were purchased from Strem Chemicals. 2-Ethynylpyridine, 2-(2,4-difluorophenyl)pyridine, NaH (60 % dispersion in mineral oil), and all other reagents were obtained from Aldrich Chemicals and used as received. Anhydrous tetrahydrofuran was obtained from a solvent purification system (Innovative Technologies). Triethylamine (Et_3N) was distilled over sodium hydroxide pellets and stored under argon. *m*-chloro-bridged Ir(III) dimers¹⁷, 1-azidohexane,⁵⁶ 1-azido-2-(perfluorooctyl)ethane,⁵⁷ 1-azido-3-(trifluoromethyl)benzene⁵⁸ and 1-azidopentafluorobenzene⁵⁸ were prepared according to the literature methods.

CAUTION: There have been safety concerns about handling organoazides, especially the ones with short alkyl groups. Therefore, all the organoazides used in this report were synthesized on small scales and handled with great care.

Preparation of *mer*-Ir(ppy)₂(trpy-C₆H₁₃) (2a). 2-Ethynylpyridine (41 mg, 0.4 mmol) in THF (8 ml)/ Et_3N (0.1 ml) was added to a mixture of $\text{Cu}(\text{MeCN})_4\text{PF}_6$ (149 mg, 0.4 mmol) and NaH (19 mg, 0.8 mmol), and the resulting suspension was stirred for 0.5 h at room temperature before 1-azidohexane (51 mg, 0.4 mmol) in THF (2 ml) was added.

After stirring at room temperature for another 1-1.5 h, $[\text{Ir}(\text{ppy})_2\text{Cl}]_2$ (107 mg, 0.1 mmol) was added to the mixture as a solid and heated to 65 °C for 4 h. After cooling, the solvent was removed under reduced pressure and the residue was purified by chromatography on silica gel, using CH_2Cl_2 /ethyl acetate (15:1) as the eluent to remove small amount of side product **6a**, then CH_2Cl_2 /ethyl acetate (6:1) to collect the desired product **2a**. After recrystallization from CH_2Cl_2 /hexane, **2a** was isolated as bright yellow crystals (127 mg, 87%). HRMS (ESI): 731.2498 [calcd for $(\text{M}+\text{H})^+$: 731.2415]. ^1H NMR (400 MHz, $\text{DMSO}-d_6$, ppm): 0.76 (t, $J=7.2$ Hz, 3 H), 0.87-1.00 (m, 4 H), 1.06 (m, 2 H), 1.21 (m, 2 H), 3.4 (m, 2H), 6.27 (d, $J=7.2$ Hz, 1 H), 6.31 (d, $J=7.6$ Hz, 1 H), 6.72 (t, $J=7.4$ Hz, 1 H), 6.83 (t, $J=7.4$ Hz, 1 H), 6.88 (t, $J=7.4$ Hz, 1 H), 6.95 (t, $J=7.6$ Hz, 1 H), 6.99 (t, $J=6.3$ Hz, 1 H), 7.07 (m, 2 H), 7.52 (d, $J=5.4$ Hz, 1 H), 7.56 (d, $J=5.7$ Hz, 1 H), 7.75-7.84 (m, 5 H), 7.87 (d, $J=5.7$ Hz, 1 H), 7.91 (d, $J=7.9$ Hz, 1 H), 8.12 (d, $J=7.9$ Hz, 1 H), 8.13 (d, $J=7.9$ Hz, 1 H). ^{13}C NMR (126 MHz, CD_2Cl_2 , ppm): 14.4, 23.1, 26.7, 32.7, 51.1, 118.1, 119.0, 119.5, 120.4, 121.5, 122.1, 122.5, 123.2, 124.6, 124.9, 130.0, 130.6, 131.6, 132.3, 136.0, 137.0, 138.2, 143.5, 145.5, 149.4, 151.1, 152.5, 154.1, 158.8, 162.8, 168.1, 169.4, 170.1.

Compound **6a** was isolated as a bright yellow solid (20 mg, 11%).

HRMS (ESI): 731.2446 [calcd for $(\text{M}-\text{PF}_6)^+$: 731.2415]. ^1H NMR (400 MHz, $\text{DMSO}-d_6$, ppm): 0.84 (t, $J=6.82$ Hz, 3 H), 1.12-1.38 (m, 6 H), 1.83-1.98 (m, 2 H), 4.45 (t, $J=7.4$ Hz, 2 H), 6.30 (d, $J=5.3$ Hz, 1 H), 6.32 (d, $J=5.3$ Hz, 1 H), 6.87 (t, $J=7.5$ Hz, 1 H), 6.93 (t, $J=7.5$ Hz, 1 H), 6.97-7.11 (m, 4 H), 7.30 (t, $J=6.3$ Hz, 1 H), 7.51 (d, $J=5.8$ Hz, 1 H), 7.66-7.71 (m, 2 H), 7.73 (d, $J=7.3$ Hz, 1 H), 7.75-7.82 (m, 2 H), 7.84 (d, $J=5.3$ Hz, 1 H), 7.95 (d, 2 H), 8.02 (t, $J=7.6$ Hz, 1 H), 8.22 (d, $J=7.8$ Hz, 1 H), 8.75 (s, 1 H). ^{13}C NMR (126 MHz, CD_2Cl_2 , ppm): 14.2, 22.9, 26.3, 30.2, 31.4, 53.1, 120.1, 120.2, 122.7, 123.3, 123.5,

123.6, 123.9, 124.9, 125.3, 126.2, 127.0, 130.4, 131.1, 132.1, 132.4, 138.6, 138.7, 140.2, 144.5, 146.8, 149.0, 149.8, 149.9, 150.0, 150.8, 167.9, 168.5. ^{19}F NMR (282 MHz, CD_2Cl_2 , d ppm): -72.99 (d, J = 711.0 Hz).

Preparation of *mer*-Ir(FFppy) $_2$ (trpy-C $_6$ H $_{13}$) (2b). 2-Ethynylpyridine (21 mg, 0.2 mmol), $\text{Cu}(\text{MeCN})_4\text{PF}_6$ (75 mg, 0.2 mmol), NaH (10 mg, 0.4 mmol), and 1-azidohexane (25 mg, 0.2 mmol) were reacted with $[\text{Ir}(\text{FFppy})_2\text{Cl}]_2$ (61 mg, 0.05 mmol) following the procedure detailed for the synthesis of **2a**. The reaction mixture was purified by chromatography on silica gel, using CH_2Cl_2 /ethyl acetate (10:1 to 8:1) as the eluent to remove small amount of side product **6b**, then CH_2Cl_2 /ethyl acetate (4:1) to collect the desired product **2b**. Compound **2b** was isolated as light yellow crystals (91 mg, 57%). HRMS (ESI): 803.2108 [calcd for $(\text{M}+\text{H})^+$: 803.2101]. ^1H NMR (400 MHz, CD_2Cl_2 , d ppm): 0.82 (t, J = 7.3 Hz, 3 H), 1.04 (quin, J = 7.4 Hz, 2 H), 1.09-1.22 (m, 4 H), 1.33-1.45 (m, 2 H), 3.57-3.74 (m, 2 H), 5.87 (m, 2 H), 6.48 (m, 2 H), 6.83-6.93 (m, 3 H), 7.59-7.65 (m, 2 H), 7.66-7.75 (m, 3 H), 7.97 (d, J = 5.3 Hz, 1 H), 8.02 (br. d, J = 5.3 Hz, 1 H), 8.25 (d, J = 8.3 Hz, 2 H). ^{13}C NMR (126 MHz, CD_2Cl_2 , d ppm): 14.3, 23.1, 26.9, 32.0, 32.8, 51.2, 96.7 (t, J = 27.6 Hz), 98.5 (t, J = 27.6 Hz), 113.4 (dd, J = 16.7, 2.9 Hz), 113.8 (dd, J = 15.3, 2.6 Hz), 118.5, 121.9, 122.9, 123.1 (d, J = 19.6 Hz), 123.5, 123.7 (d, J = 19.0 Hz), 127.8, 128.8, 137.1, 138.1, 138.9, 149.5, 150.9, 154.0, 156.7 (d, J = 6.9 Hz), 158.4, 160.91 (d, J = 13.2 Hz), 161.5 (d, J = 11.5 Hz), 162.8 (d, J = 12.1 Hz), 163.0 (d, J = 13.2 Hz), 163.6 (d, J = 11.5 Hz), 163.8 (d, J = 10.9 Hz), 164.7, 164.8, 165.9 (d, J = 10.9 Hz), 166.5 (d, J = 8.1 Hz), 174.3. ^{19}F NMR (282 MHz, CD_2Cl_2 , d ppm): -111.24 (t, J = 9.2 Hz), -110.16 (t, J = 12.2 Hz), -109.46 (d, J = 9.2 Hz), -108.83 (d, J = 9.2 Hz).

Compound **6b** was isolated as light yellow solids (43 mg, 22%).

HRMS (ESI): 803.2056 [calcd for (M-PF₆)⁺: 803.2101]. ¹H NMR (400 MHz, CD₂Cl₂, d ppm): 0.84 (t, *J*=6.8, 3 H), 1.15-1.30 (m, 6 H), 1.86-1.97 (m, 2 H), 4.46 (t, *J*=7.3 Hz, 2 H), 5.73 (dd, *J*=8.6, 2.1 Hz, 1 H), 5.79 (dd, *J*=8.4, 2.1 Hz, 1 H), 6.55 (ddd, *J*=12.2, 9.5, 2.1 Hz, 1 H), 6.61 (ddd, *J*=12.1, 9.5, 2.2 Hz, 1 H), 7.04 (t, *J*=6.4 Hz, 1 H), 7.10 (t, *J*=6.3 Hz, 1 H), 7.37 (t, *J*=6.4 Hz, 1 H), 7.50 (d, *J*=5.7 Hz, 1 H), 7.64 (d, *J*=5.7 Hz, 1 H), 7.80-7.89 (m, 3 H), 8.08 (td, *J*=7.8, 1.0 Hz, 13 H), 8.26 (d, *J*=8.1 Hz, 1 H), 8.31 (d, 2 H), 8.78 (s, 1 H). ¹³C NMR (126 MHz, CD₂Cl₂, d ppm): 14.2, 22.9, 29.3, 30.1, 31.3, 53.3, 99.2 (t, *J*=27.1 Hz), 99.7 (t, *J*=27.1 Hz), 114.5, 114.6 (d, *J*=12.1 Hz), 114.7 (d, *J*=12.1 Hz), 114.8, 123.9, 124.0, 124.2-124.3 (m), 126.7, 127.3, 128.5, 139.6, 139.7, 140.9, 148.8, 149.1, 149.9, 150.0, 150.4 (d, *J*=6.9 Hz), 150.7, 153.8 (d, *J*=6.3 Hz), 160.5 (d, *J*=12.7 Hz), 160.9 (d, *J*=12.7 Hz), 162.5 (d, *J*=8.6 Hz), 162.6 (d, *J*=9.2 Hz), 163.0 (d, *J*=12.7 Hz), 163.1 (d, *J*=12.7 Hz), 164.5-164.6 (m), 165.1-165.2 (m). ¹⁹F NMR (282 MHz, CD₂Cl₂, d ppm): -111.09 (1 F), -109.23 (1 F), -107.75 (1 F), -106.85 (1 F), -72.86 (d, *J*=717.2 Hz, 6 F).

Preparation of *mer*-Ir(ppy)₂(trpy-C₂H₄C₈F₁₇) (3a). 2-Ethynylpyridine (41 mg, 0.4 mmol), Cu(MeCN)₄PF₆ (149 mg, 0.4 mmol), NaH (19 mg, 0.8 mmol), and 1-azido-2-(perfluorooctyl)ethane (196 mg, 0.4 mmol) were reacted with [Ir(ppy)₂Cl]₂ (107 mg, 0.1 mmol) following the procedure detailed for the synthesis of **2a**. The reaction mixture was purified by chromatography on silica gel, using CH₂Cl₂/ethyl acetate (8:1) as the eluent. Compound **3a** was isolated as bright yellow crystals (133 mg, 61%).

HRMS (ESI): 1093.1473 [calcd for (M+H)⁺: 1091.1503]. ¹H NMR (500 MHz, CD₂Cl₂, ppm): 1.85-2.05 (m, 1 H), 2.10-2.27 (m, 1 H), 3.99-4.12 (m, 2 H), 6.44 (d, *J*=7.2 Hz, 1

H), 6.46 (d, $J=7.7$ Hz, 1 H), 6.78-6.89 (m, 4 H), 6.92 (t, $J=7.6$ Hz, 1 H), 6.96 (t, $J=7.4$ Hz, 1 H), 7.03 (t, $J=7.2$ Hz, 1 H), 7.59-7.76 (m, 7 H), 7.87 (d, 2 H), 7.98 (d, $J=5.4$ Hz, 1 H), 8.06 (d, $J=7.7$ Hz, 1 H). ^{13}C NMR (126 MHz, CD_2Cl_2 , ppm): 32.9 (t, $J=21.3$ Hz), 42.8 (t, $J=4.0$ Hz), 108.9-120.12 (m, CF_2 and CF_3), 118.4, 119.1, 119.7, 120.9, 121.9, 122.4, 122.7, 123.3, 124.9, 125.0, 130.3, 130.8, 131.4, 132.2, 136.2, 137.2, 138.4, 143.3, 145.4, 149.6, 151.2, 151.6, 153.9, 158.5, 163.6, 168.0, 168.7, 170.1. ^{19}F NMR (282 MHz, CD_2Cl_2 , ppm): -126.63, -124.31, -123.21, -122.41, -122.23, -115.20, -81.40.

Preparation of *mer*-Ir(ppy) $_2$ (trpy-C $_6$ H $_4$ CF $_3$) (4a). 2-Ethynylpyridine (21 mg, 0.2 mmol), $\text{Cu}(\text{MeCN})_4\text{PF}_6$ (75 mg, 0.2 mmol), NaH (10 mg, 0.4 mmol), and 1-azido-3-(trifluoromethyl)benzene (37 mg, 0.2 mmol) were reacted with $[\text{Ir}(\text{ppy})_2\text{Cl}]_2$ (54 mg, 0.05 mmol) following the procedure detailed for the synthesis of **2a**. The reaction mixture was purified by chromatography on silica gel, using CH_2Cl_2 /ethyl acetate (15:1) as the eluent. Compound **4a** was isolated as bright yellow crystals (72 mg, 91%).

HRMS (ESI): 791.1709 [calcd for $(\text{M}+\text{H})^+$: 791.1726]. ^1H NMR (400 MHz, CD_2Cl_2 , ppm): 6.08 (d, $J=7.6$ Hz, 1 H), 6.33 (d, $J=7.3$ Hz, 1 H), 6.53 (t, $J=8.1$ Hz, 1 H), 6.75 (t, $J=7.3$ Hz, 1 H), 6.81-6.89 (m, 4 H), 6.92 (t, $J=7.3$ Hz, 1 H), 7.00 (t, $J=7.6$ Hz, 1 H), 7.04 (d, $J=8.1$ Hz, 1 H), 7.28 (d, $J=7.8$ Hz, 1 H), 7.48 (d, $J=7.6$ Hz, 1 H), 7.59-7.69 (m, 6 H), 7.72 (t, $J=7.8$ Hz, 1 H), 7.81 (d, $J=8.1$ Hz, 1 H), 7.84 (d, $J=8.1$ Hz, 1 H), 8.06 (d, $J=5.6$ Hz, 1 H), 8.13 (d, $J=7.8$ Hz, 1 H). ^{13}C NMR (126 MHz, CD_2Cl_2 , ppm): 118.7, 119.1, 119.7, 120.5, 120.9, 122.1, 122.4, 122.5, 123.5, 123.8, 124.6, 124.9, 125.9, 127.6, 129.1, 129.8, 130.8, 131.6, 132.0, 136.2, 137.2, 138.4, 141.1, 143.2, 145.3, 149.5, 150.9, 153.0, 154.1, 158.3, 159.1, 163.8, 167.1, 168.0, 169.8. ^{19}F NMR (282 MHz, CD_2Cl_2 , ppm): -62.82.

Preparation of mer-Ir(ppy)₂(trpy-C₆F₅) (5a). 2-Ethynylpyridine (41 mg, 0.4 mmol), Cu(MeCN)₄PF₆ (149 mg, 0.4 mmol), NaH (19 mg, 0.8 mmol), and 1-azidopentafluorobenzene (84 mg, 0.4 mmol) were reacted with [[Ir(ppy)₂Cl]₂] (107 mg, 0.1 mmol) following the procedure detailed for the synthesis of **2a**. The reaction mixture was purified by chromatography on silica gel, using CH₂Cl₂/ethyl acetate (15:1) as the eluent. Compound **5a** was isolated as bright yellow crystals (77 mg, 48%). Samples for photophysical study were purified by preparative thin layer chromatography (PTLC) to remove trace amount contaminants using CH₂Cl₂/ethyl acetate (30:1) as the eluent.

HRMS (ESI): 813.1367 [calcd for (M+H)⁺: 813.1381]. ¹H NMR (400 MHz, CD₂Cl₂, ppm): 6.15 (d, *J*=7.6 Hz, 1 H), 6.40 (d, *J*=7.1 Hz, 1 H), 6.54 (t, *J*=7.4 Hz, 1 H), 6.72 (t, *J*=7.4 Hz, 1 H), 6.85-6.95 (m, 4 H), 7.00 (t, *J*=7.6 Hz, 1 H), 7.45 (d, *J*=7.6 Hz, 1 H), 7.62-7.78 (m, 6 H), 7.81 (d, *J*=8.3 Hz, 1 H), 7.85 (d, *J*=8.1 Hz, 1 H), 8.10 (d, 2 H). ¹³C NMR (126 MHz, CD₂Cl₂, ppm): 118.8, 118.9, 119.6, 120.2, 122.4, 122.7, 123.4, 123.9, 124.9, 129.3, 130.7, 131.3, 132.3, 136.5, 137.3, 138.6, 143.4, 145.4, 149.5, 151.1, 151.3, 154.1, 157.8, 158.0, 168.0, 168.2, 168.4, 169.8. ¹⁹F NMR (282 MHz, CD₂Cl₂, ppm): -163.24 (d, *J*=24.4 Hz), -163.27 (d, *J*=24.4 Hz), -154.92 (t, *J*=21.4 Hz), -146.87 ~ -146.80 (m).

Thermal Isomerization from 2a to 7a. 20 mg of **2a** was suspended in 5 ml glycerol under Ar. The mixture was heated to 200 °C for 20 h. After cooling to room temperature, the slurry was added with saturated NaCl aqueous solution and extracted with CH₂Cl₂. The crude mixture was subjected to HRMS (ESI), which showed that there is only trace amount of Ir(ppy)(tzpy)₂ (<1%). Compound **7a** was purified by flash chromatography on partially deactivated neutral aluminum oxide (5% H₂O), using CH₂Cl₂/CH₃OH (97:3) as

eluent. After recrystallization from CH₂Cl₂/hexane, **7a** was isolated as light yellow crystals (14mg, 63%).

HRMS (ESI): 731.25 [calcd for (M-Cl)⁺: 731.25]. ¹H NMR (400 MHz, MeOH-*d*₄, d ppm): 0.85 (t, *J*=6.8 Hz, 3 H), 1.10-1.30 (m, 6 H), 1.81-1.95 (m, 2 H), 4.47 (t, *J*=7.1 Hz, 2 H), 6.24 (d, *J*=7.3 Hz, 1 H), 6.31 (d, *J*=7.3 Hz, 1 H), 6.78 (t, *J*=7.0 Hz, 1 H), 6.88 (t, *J*=7.0 Hz, 1 H), 6.93 (t, *J*=7.2 Hz, 1 H), 7.02 (d, *J*=7.1 Hz, 1 H), 7.04 (d, *J*=7.8 Hz, 1 H), 7.09 (t, *J*=6.7 Hz, 1 H), 7.40 (t, *J*=6.2 Hz, 1 H), 7.63 (d, *J*=5.8 Hz, 1 H), 7.73 (d, *J*=7.8 Hz, 1 H), 7.76 (d, *J*=5.6 Hz, 1 H), 7.81 (d, *J*=7.8 Hz, 1 H), 7.84-7.91 (m, 3 H), 8.04-8.14 (m, 3 H), 8.26 (d, *J*=7.8 Hz, 1 H), 9.07 (s, 1 H). ¹³C NMR (126 MHz, CD₂Cl₂, d ppm): 14.2, 22.9, 26.4, 30.4, 31.4, 52.8, 120.0, 120.1, 122.6, 123.1, 123.5, 123.8, 124.8, 125.0, 125.2, 126.5, 129.4, 129.5, 130.3, 131.0, 132.1, 132.4, 138.4, 138.5, 140.2, 144.5, 147.3, 149.1, 149.3, 149.9, 150.2, 150.4, 150.8, 168.0, 168.5.

Thermal Isomerization from 2b to 7b. **7b** was prepared following the procedure outlined for **7a**, and purified by flash column chromatography on partially deactivated neutral aluminium oxide (5% H₂O), using CH₂Cl₂/CH₃OH (97:3) as the eluent. After recrystallization from CH₂Cl₂/hexane, **7b** was isolated as light yellow crystals (12 mg, 58%).

HRMS (ESI): 803.2095 [calcd for (M-Cl)⁺: 803.2101]. ¹H NMR (400 MHz, CD₂Cl₂, ppm): 0.83 (t, *J*=6.6 Hz, 3 H), 1.24 (m, 6 H), 1.83-2.03 (m, 2 H), 4.51 (t, *J*=7.3 Hz, 2 H), 5.73 (dd, *J*=8.6, 2.3 Hz, 1 H), 5.80 (dd, *J*=8.6 Hz, 2.3 Hz, 1 H), 6.54 (ddd, *J*=13.1, 9.4, 2.3 Hz, 1 H), 6.60 (ddd, *J*=12.9, 9.3, 2.3 Hz, 1 H), 7.01 (t, *J*=6.7 Hz, 1 H), 7.06 (t, *J*=6.8 Hz, 1 H), 7.31 (t, *J*=6.6 Hz, 1 H), 7.49 (d, *J*=5.8 Hz, 1 H), 7.65 (d, *J*=5.6 Hz, 1 H), 7.74-

7.90 (m, 3 H), 8.10 (t, $J=7.8$ Hz, 1 H), 8.30 (d, 2 H), 9.26 (d, $J=7.8$ Hz, 1 H), 10.95 (s, 1 H). ^{13}C NMR (126 MHz, CD_2Cl_2 , ppm): 14.2, 23.0, 26.4, 30.2, 31.4, 53.0, 99.0 (t, $J=26.5$ Hz), 99.5 (t, $J=27.1$ Hz), 114.6 (dd, $J=6.9, 2.9$ Hz), 114.7 (dd, $J=6.9, 2.9$ Hz), 123.8, 124.0, 124.1, 124.3, 125.7, 126.8, 128.5, 130.1 (d, $J=23.6$ Hz), 139.5, 139.6, 140.9, 149.2, 150.0, 150.1, 150.6, 150.9 (d, $J=6.9$ Hz), 154.4 (d, $J=6.3$ Hz), 160.5 (d, $J=12.7$ Hz), 160.9 (d, $J=12.7$ Hz), 162.5 (d, $J=11.5$ Hz), 162.6 (d, $J=11.5$ Hz), 163.0 (d, $J=12.7$ Hz), 163.1 (d, $J=12.7$ Hz), 164.5-164.6 (m), 165.1-165.2 (m).

^{19}F NMR (282 MHz, CD_2Cl_2 , ppm): -111.16, -109.37, -107.92, -106.01.

Photochemical Isomerization. 15 mg of **2a** or **2b** was dissolved in $\text{DMSO-}d_6$ in a NMR tube capped with a rubber septum, and purged with Ar for 15 min. The sealed tube was irradiated with a portable pen light with broadband UV radiation, and the reaction completed after 3 days based on ^1H NMR. Saturated NaCl aqueous solution was added and the mixture was extracted with CH_2Cl_2 . **7a** (12 mg, 58%) and **7b** were isolated as light yellow crystals.

Crystal Structure Determinations. Low-temperature diffraction data (φ - and ω -scans) were collected on a Bruker D8 three-circle diffractometer coupled to a Bruker-AXS Smart Apex CCD detector with graphite-monochromated Cu $K\alpha$ radiation ($\lambda = 1.54178$ Å) for the structures of compounds **2a**, **2b** and **6b**, and on a Bruker-AXS X8 Kappa Duo diffractometer coupled to a Smart Apex2 CCD detector with Mo $K\alpha$ radiation ($\lambda = 0.71073$ Å) from an I μ S micro-source for the structure of compound **7b**. The structures were solved by direct methods using SHELXS⁵⁹ and refined against F^2 on all data by

full-matrix least squares with SHELXL-97⁶⁰ following established refinement strategies.⁶¹ All non-hydrogen atoms were refined anisotropically. Except for the two hydrogen atoms on the water molecule in the structure of **7b**, all hydrogen atoms were included into the model at geometrically calculated positions and refined using a riding model. Coordinates for the two water-hydrogen atoms were taken from the difference Fourier analysis and the hydrogens were subsequently refined semi-freely with the help of distance restraints. The isotropic displacement parameters of all hydrogen atoms were fixed to 1.2 times the U value of the atoms they are linked to (1.5 times for methyl groups).

Compounds **2a**, **2b**, and **6b** crystallizes in the monoclinic space group $P2_1/c$, **2a** and **6b** contain one molecule and **2b** contains two molecules in the asymmetric unit. Compound **2a** contains half a molecule of hexane which is located near a crystallographic inversion center and disordered accordingly. Compound **2b** contains two molecules of CH_2Cl_2 , one of which is disordered over three positions. Compound **7b** crystallizes in the monoclinic space group $P2_1$ with one molecule of **7b**, its chloride counter ion, one water molecule and one disordered molecule of dichloromethane. The N-bound *n*-hexyl group is heavily disordered and was modeled to be distributed over three independent, mutually exclusive positions. All disorders in all structures were refined with the help of similarity restraints on 1,2- and 1,3-distances and displacement parameters as well as rigid bond restraints for anisotropic displacement parameters.

CCDC 817543 - 817546 contain the supplementary crystallographic data for this paper. These data can be obtained free of charge from The Cambridge Crystallographic Data Centre via www.ccdc.cam.ac.uk/data_request/cif.

Computational Details. Ground-state geometries of [Ir(ppy)₂(CN-tzpy)] and [Ir(ppy)₂(N[^]N_tzpy)]⁺ were optimized by DFT calculations, which were performed using the Gaussian03 software (Gaussian Inc.)⁶⁰ with a B3LYP exchange-correlation functional and the LANL2DZ basis set under an effective core potential. The initial geometries were based on simplified X-ray structures of **2a** and **6b** respectively, with the hexyl groups replaced with methyl groups and F atoms with H atoms, and optimized without any constraints.

1.5 References

- (1) Yersin, H. *Highly Efficient OLEDs with Phosphorescent Materials*; Wiley-VCH Verlag GmbH & Co. KGaA: Weinheim, Germany, 2008.
- (2) Ulbricht, C.; Beyer, B.; Friebe, C.; Winter, A.; Schubert, U. S. *Adv. Mater.* **2009**, *21*, 4418-4441.
- (3) You, Y.; Park, S. Y. *Dalton Trans.* **2009**, 1267-1282.
- (4) Lowry, M. S.; Bernhard, S. *Chem. Eur. J.* **2006**, *12*, 7970-7977.
- (5) Slinker, J.; Bernards, D.; Houston, P. L.; Abruna, H. D.; Bernhard, S.; Malliaras, G. G. *Chem. Commun.* **2003**, 2392-2399.
- (6) Su, H.-C.; Chen, H.-F.; Fang, F.-C.; Liu, C.-C.; Wu, C.-C.; Wong, K.-T.; Liu, Y.-H.; Peng, S.-M. *J. Am. Chem. Soc.* **2008**, *130*, 3413-3419.
- (7) Zhao, Q.; Li, F.; Huang, C. *Chem. Soc. Rev.* **2010**, *39*, 3007-3030.
- (8) DeRosa, M. C.; Mosher, P. J.; Yap, G. P. A.; Focsaneanu, K.-S.; Crutchley, R. J.; Evans, C. E. B. *Inorg. Chem.* **2003**, *42*, 4864-4872.
- (9) Köse, M. E.; Crutchley, R. J.; DeRosa, M. C.; Ananthakrishnan, N.; Reynolds, J. R.; Schanze, K. S. *Langmuir* **2005**, *21*, 8255-8262.

- (10) Zhao, Q.; Cao, T.; Li, F.; Li, X.; Jing, H.; Yi, T.; Huang, C. *Organometallics* **2007**, *26*, 2077-2081.
- (11) Zhao, Q.; Li, F.; Liu, S.; Yu, M.; Liu, Z.; Yi, T.; Huang, C. *Inorg. Chem.* **2008**, *47*, 9256-9264.
- (12) Zhao, Q.; Huang, C.; Li, F. *Chem. Soc. Rev.* **2011**, *40*, 2508-2524.
- (13) Lo, K. K.-W.; Hui, W.-K.; Chung, C.-K.; Tsang, K. H.-K.; Ng, D. C.-M.; Zhu, N.; Cheung, K.-K. *Coord. Chem. Rev.* **2005**, *249*, 1434-1450.
- (14) Lo, K. K.-W.; Hui, W.-K.; Chung, C.-K.; Tsang, K. H.-K.; Lee, T. K.-M.; Li, C.-K.; Lau, J. S.-Y.; Ng, D. C.-M. *Coord. Chem. Rev.* **2006**, *250*, 1724-1736.
- (15) Lo, K. K.-W.; Tsang, K. H.-K.; Sze, K.-S.; Chung, C.-K.; Lee, T. K.-M.; Zhang, K. Y.; Hui, W.-K.; Li, C.-K.; Lau, J. S.-Y.; Ng, D. C.-M.; Zhu, N. *Coord. Chem. Rev.* **2007**, *251*, 2292-2310.
- (16) Yu, M.; Zhao, Q.; Shi, L.; Li, F.; Zhou, Z.; Yang, H.; Yi, T.; Huang, C. *Chem. Commun.* **2008**, 2115-2117.
- (17) Tamayo, A. B.; Alleyne, B. D.; Djurovich, P. I.; Lamansky, S.; Tsyba, I.; Ho, N. N.; Bau, R.; Thompson, M. E. *J. Am. Chem. Soc.* **2003**, *125*, 7377-7387.
- (18) McGee, K. A.; Mann, K. R. *Inorg. Chem.* **2007**, *46*, 7800-7809.
- (19) Constable, E. C.; Leese, T. A. *J. Organomet. Chem.* **1987**, *335*, 293-299.
- (20) Huo, S.; Deaton, J. C.; Rajeswaran, M.; Lenhart, W. C. *Inorg. Chem.* **2006**, *45*, 3155-3157.
- (21) Chassot, L.; Mueller, E.; von Zelewsky, A. *Inorg. Chem.* **1984**, *23*, 4249-4253.
- (22) Jolliet, P.; Gianini, M.; von Zelewsky, A.; Bernardinelli, G.; Stoeckli-Evans, H. *Inorg. Chem.* **1996**, *35*, 4883-4888.
- (23) Thomas, S. W.; Venkatesan, K.; Müller, P.; Swager, T. M. *J. Am. Chem. Soc.* **2006**, *128*, 16641-16648.
- (24) Meldal, M.; Tornøe, C. W. *Chem. Rev.* **2008**, *108*, 2952-3015.
- (25) Spiteri, C.; Moses, J. E. *Angew. Chem. Int. Ed.* **2010**, *49*, 31-33.
- (26) Nolte, C.; Mayer, P.; Straub, B. F. *Angew. Chem. Int. Ed.* **2007**, *46*, 2101-2103.
- (27) Partyka, D. V.; Updegraff, J. B.; Zeller, M.; Hunter, A. D.; Gray, T. G. *Organometallics* **2007**, *26*, 183-186.
- (28) Partyka, D. V.; Gao, L.; Teets, T. S.; Updegraff, J. B.; Deligonul, N.; Gray, T. G. *Organometallics* **2009**, *28*, 6171-6182.
- (29) Wu, Y.-M.; Deng, J.; Li, Y.; Chen, Q.-Y. *Synthesis* **2005**, 1314-1318.
- (30) Felici, M.; Contreras-Carballada, P.; Vida, Y.; Smits, J. M. M.; Nolte, R. J. M.; De Cola, L.; Williams, R. M.; Feiters, M. C. *Chem. Eur. J.* **2009**, *15*, 13124-13134.
- (31) Richardson, C.; Fitchett, C. M.; Keene, F. R.; Steel, P. J. *Dalton Trans.* **2008**, 2534-2537.
- (32) Fletcher, J. T.; Bumgarner, B. J.; Engels, N. D.; Skoglund, D. A. *Organometallics* **2008**, *27*, 5430-5433.

- (33) Schweinfurth, D.; Pattacini, R.; Strobel, S.; Sarkar, B. *Dalton Trans.* **2009**, 9291-9297.
- (34) Urankar, D.; Pinter, B.; Pevec, A.; De Proft, F.; Turel, I.; Košmrlj, J. *Inorg. Chem.* **2010**, *49*, 4820-4829.
- (35) Juriček, M.; Felici, M.; Contreras-Carballada, P.; Lauko, J.; Bou, S. R.; Kouwer, P. H. J.; Brouwer, A. M.; Rowan, A. E. *J. Mater. Chem.* **2011**, *21*, 2104-2111.
- (36) Beyer, B.; Ulbricht, C.; Escudero, D.; Friebe, C.; Winter, A.; González, L.; Schubert, U. S. *Organometallics* **2009**, *28*, 5478-5488.
- (37) Struthers, H.; Mindt, T. L.; Schibli, R. *Dalton Trans.* **2010**, *39*, 675-696.
- (38) Mydlak, M.; Bizzarri, C.; Hartmann, D.; Sarfert, W.; Schmid, G.; De Cola, L. *Adv. Funct. Mater.* **2010**, *20*, 1812-1820.
- (39) Schuster, E. M.; Botoshansky, M.; Gandelman, M. *Angew. Chem. Int. Ed.* **2008**, *47*, 4555-4558.
- (40) Schuster, E. M.; Botoshansky, M.; Gandelman, M. *Organometallics* **2009**, *28*, 7001-7005.
- (41) Schuster, E. M.; Nisnevich, G.; Botoshansky, M.; Gandelman, M. *Organometallics* **2009**, *28*, 5025-5031.
- (42) McDonald, A. R.; Lutz, M.; von Chrzanowski, L. S.; van Klink, G. P. M.; Spek, A. L.; van Koten, G. *Inorg. Chem.* **2008**, *47*, 6681-6691.
- (43) Karatsu, T.; Nakamura, T.; Yagai, S.; Kitamura, A.; Yamaguchi, K.; Matsushima, Y.; Iwata, T.; Hori, Y.; Hagiwara, T. *Chem. Lett.* **2003**, *32*, 886-887.
- (44) Schaffner-Hamann, C.; von Zelewsky, A.; Barbieri, A.; Barigelletti, F.; Muller, G.; Riehl, J. P.; Neels, A. *J. Am. Chem. Soc.* **2004**, *126*, 9339-9348.
- (45) Coughlin, F. J.; Westrol, M. S.; Oyler, K. D.; Byrne, N.; Kraml, C.; Zysman-Colman, E.; Lowry, M. S.; Bernhard, S. *Inorg. Chem.* **2008**, *47*, 2039-2048.
- (46) Deaton, J. C.; Young, R. H.; Lenhard, J. R.; Rajeswaran, M.; Huo, S. *Inorg. Chem.* **2010**, *49*, 9151-9161.
- (47) Dedeian, K.; Shi, J.; Shepherd, N.; Forsythe, E.; Morton, D. C. *Inorg. Chem.* **2005**, *44*, 4445-4447.
- (48) Brooks, J.; Babayan, Y.; Lamansky, S.; Djurovich, P. I.; Tsyba, I.; Bau, R.; Thompson, M. E. *Inorg. Chem.* **2002**, *41*, 3055-3066.
- (49) Coppo, P.; Plummer, E. A.; De Cola, L. *Chem. Commun.* **2004**, 1774-1775.
- (50) Lim, J.; Swager, T. M. *Angew. Chem. Int. Ed.* **2010**, *49*, 7486-7488.
- (51) Lowry, M. S.; Hudson, W. R.; Pascal, R. A.; Bernhard, S. *J. Am. Chem. Soc.* **2004**, *126*, 14129-14135.
- (52) Costa, R. D.; Ortí, E.; Bolink, H. J.; Graber, S.; Schaffner, S.; Neuburger, M.; Housecroft, C. E.; Constable, E. C. *Adv. Funct. Mater.* **2009**, *19*, 3456-3463.
- (53) Reynolds, G. A.; Drexhage, K. H. *Opt. Commun.* **1975**, *13*, 222-225.
- (54) Melhuish, W. H. *J. Phys. Chem.* **1961**, *65*, 229-235.
- (55) Osaheni, J. A.; Jenekhe, S. A. *J. Am. Chem. Soc.* **1995**, *117*, 7389-7398.

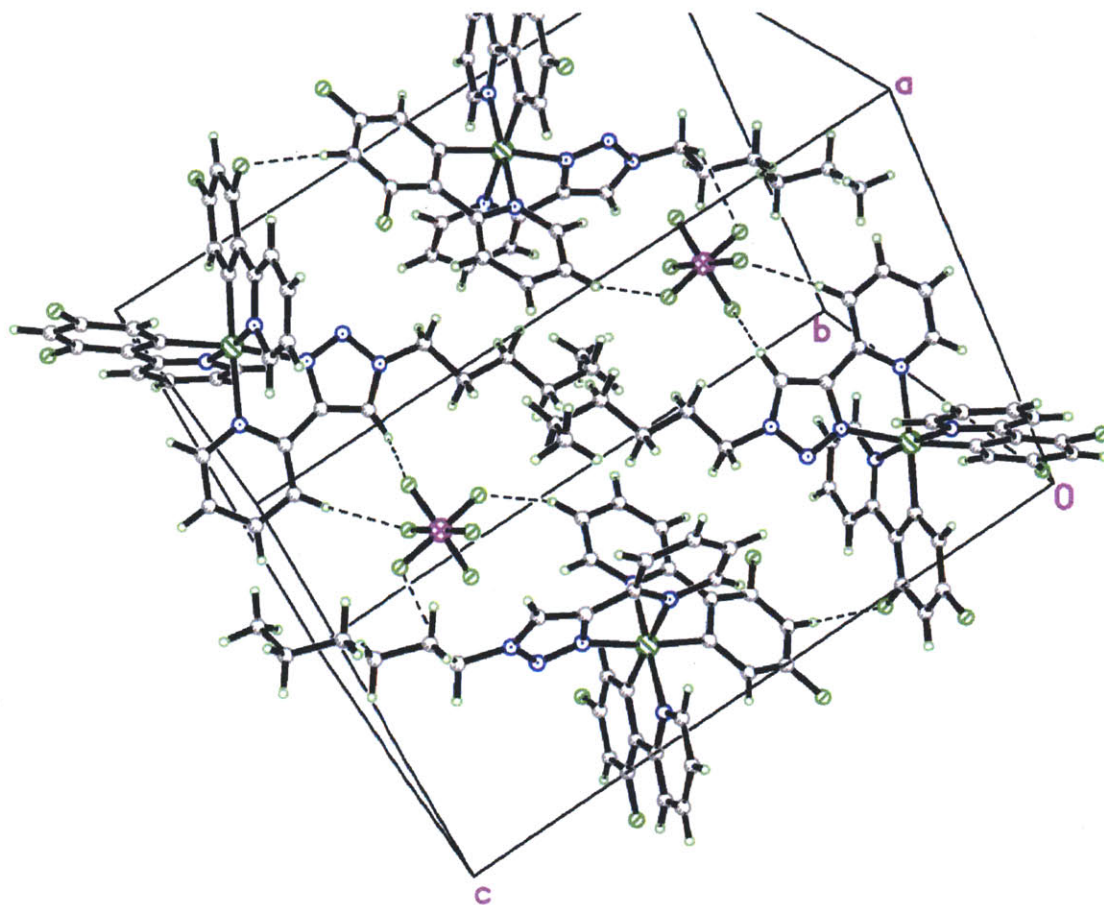
- (56) Lieber, E.; Chao, T. S.; Rao, C. N. R. *J. Org. Chem.* **1957**, *22*, 238-240.
- (57) Gheorghe, A.; Cuevas-Yañez, E.; Horn, J.; Bannwarth, W.; Narsaiah, B.; Reiser, O. *Synlett* **2006**, *2006*, 2767-2770.
- (58) Barral, K.; Moorhouse, A. D.; Moses, J. E. *Org. Lett.* **2007**, *9*, 1809-1811.
- (59) Sheldrick, G. M. *Crystallogr., Sect. A: Found. Crystallogr.* **1990**, *46*, 467-473.
- (60) Sheldrick, G. M. *Crystallogr., Sect. A: Found. Crystallogr.* **2007**, *64*, 112-122.
- (61) Müller, P. *Crystallogr. Rev.* **2009**, *15*, 57-83.
- (62) Frisch, M. J.; Trucks, G. W.; Schlegel, H. B.; Scuseria, G. E.; Robb, M. A.; Cheeseman, J. R.; Montgomery, Jr., J. A.; Vreven, T.; Kudin, K. N.; Burant, J. C.; Millam, J. M.; Iyengar, S. S.; Tomasi, J.; Barone, V.; Mennucci, B.; Cossi, M.; Scalmani, G.; Rega, N.; Petersson, G. A.; Nakatsuji, H.; Hada, M.; Ehara, M.; Toyota, K.; Fukuda, R.; Hasegawa, J.; Ishida, M.; Nakajima, T.; Honda, Y.; Kitao, O.; Nakai, H.; Klene, M.; Li, X.; Knox, J. E.; Hratchian, H. P.; Cross, J. B.; Bakken, V.; Adamo, C.; Jaramillo, J.; Gomperts, R.; Stratmann, R. E.; Yazyev, O.; Austin, A. J.; Cammi, R.; Pomelli, C.; Ochterski, J. W.; Ayala, P. Y.; Morokuma, K.; Voth, G. A.; Salvador, P.; Dannenberg, J. J.; Zakrzewski, V. G.; Dapprich, S.; Daniels, A. D.; Strain, M. C.; Farkas, O.; Malick, D. K.; Rabuck, A. D.; Raghavachari, K.; Foresman, J. B.; Ortiz, J. V.; Cui, Q.; Baboul, A. G.; Clifford, S.; Cioslowski, J.; Stefanov, B. B.; Liu, G.; Liashenko, A.; Piskorz, P.; Komaromi, I.; Martin, R. L.; Fox, D. J.; Keith, T.; Al-Laham, M. A.; Peng, C. Y.; Nanayakkara, A.; Challacombe, M.; Gill, P. M. W.; Johnson, B.; Chen, W.; Wong, M. W.; Gonzalez, C.; and Pople, J. A. *Gaussian 03, Revision C.02*; Gaussian, Inc., Wallingford CT, USA, 2004.

Appendix for Chapter 1

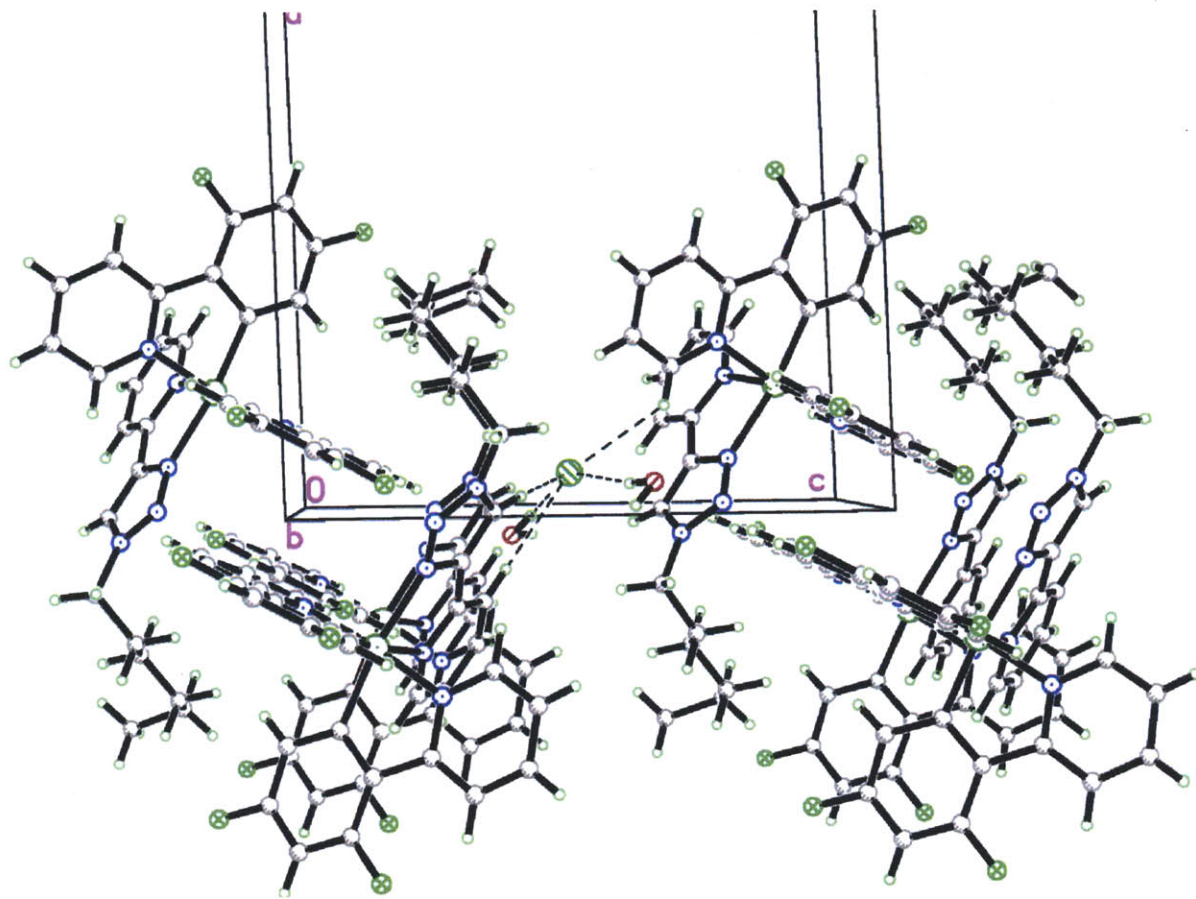
**Photo-isomerization of *mer*-Ir(ppy)₂(trpy)
Packing diagrams of 6b and 7b
NMR spectra**

Crystallographic data for compounds **2a**, **2b**, **6b** and **7b**

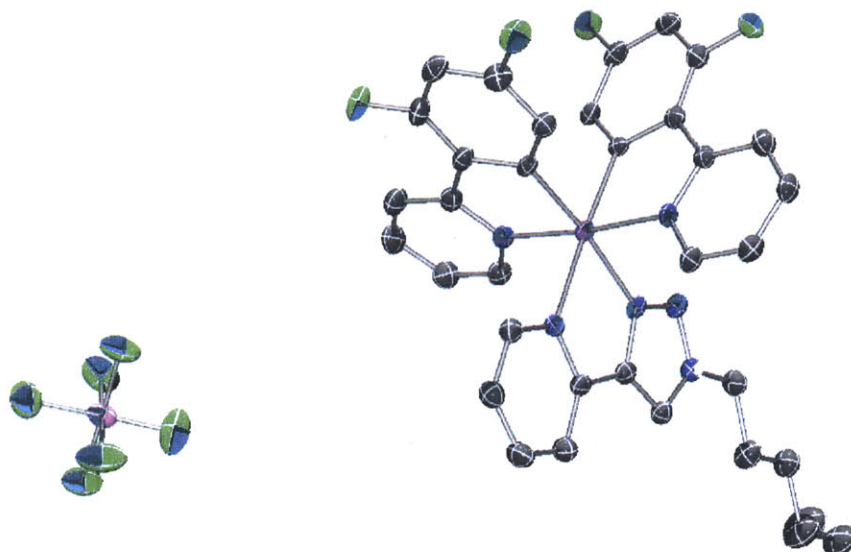
	2a	2b	6b	7b
Empirical formula	C ₃₅ H ₃₃ IrN ₆ · 0.5 C ₆ H ₁₄	C ₃₅ H ₂₉ F ₄ IrN ₆ · CH ₂ Cl ₂	C ₃₅ H ₃₀ F ₁₀ IrN ₆	C ₃₅ H ₃₀ ClF ₄ IrN ₆ · CH ₂ Cl ₂ · H ₂ O
Formula weight	772.96	886.77	947.82	941.24
Crystal system	Monoclinic	Monoclinic	Monoclinic	Monoclinic
Space group	<i>P</i> 2 ₁ / <i>c</i>	<i>P</i> 2 ₁ / <i>c</i>	<i>P</i> 2 ₁ / <i>c</i>	<i>P</i> 2 ₁
<i>a</i> (Å)	20.3916(4)	22.2313(8)	12.9605(2)	12.9937(7)
<i>b</i> (Å)	15.2013(4)	16.1839(6)	14.0627()	10.5037(6)
<i>c</i> (Å)	10.4538(2)	20.5272(8)	18.7948(3)	13.4237(7)
α	90°	90°	90°	90°
β	97.9110(10)°	116.927(2)°	92.2270(10)°	91.4950(10)°
γ	90°	90°	90°	90°
Volume (Å ³)	3209.62(12)	6584.4(4)	3422.95(9)	1831.47(17)
<i>Z</i>	4	8	4	2
Density (calcd) (g/cm ³)	1.600	1.789	1.83	1.707
Absorption coefficient (mm ⁻¹)	8.335	9.861	8.819	3.923
<i>F</i> (000)	1548	3488	1856	928
Θ range for data collection	2.19 to 66.21°	2.23 to 70.07°	3.41 to 67.73°	1.52 to 30.03°
Reflections collected	61406	133671	6186	41064
Independent reflections	5535 [<i>R</i> _{int} = 0.0869]	12423 [<i>R</i> _{int} = 0.0347]	6186 [<i>R</i> _{int} = 0.0486]	10300 [<i>R</i> _{int} = 0.0224]
Data / restraints / parameters	5535 / 57 / 434	12423 / 131 / 942	6186 / 149 / 479	10300 / 388 / 587
Goodness-of-fit on <i>F</i> ²	1.023	1.264	1.068	1.045
Final <i>R</i> indices [<i>I</i> > 2 σ (<i>I</i>)]	<i>R</i> 1 = 0.0264 <i>wR</i> 2 = 0.0626	<i>R</i> 1 = 0.0291 <i>wR</i> 2 = 0.0705	<i>R</i> 1 = 0.0251 <i>wR</i> 2 = 0.0599	<i>R</i> 1 = 0.0178 <i>wR</i> 2 = 0.0441
<i>R</i> indices (all data)	<i>R</i> 1 = 0.0330 <i>wR</i> 2 = 0.0660	<i>R</i> 1 = 0.0294 <i>wR</i> 2 = 0.0706	<i>R</i> 1 = 0.0268 <i>wR</i> 2 = 0.0609	<i>R</i> 1 = 0.0186 <i>wR</i> 2 = 0.0445



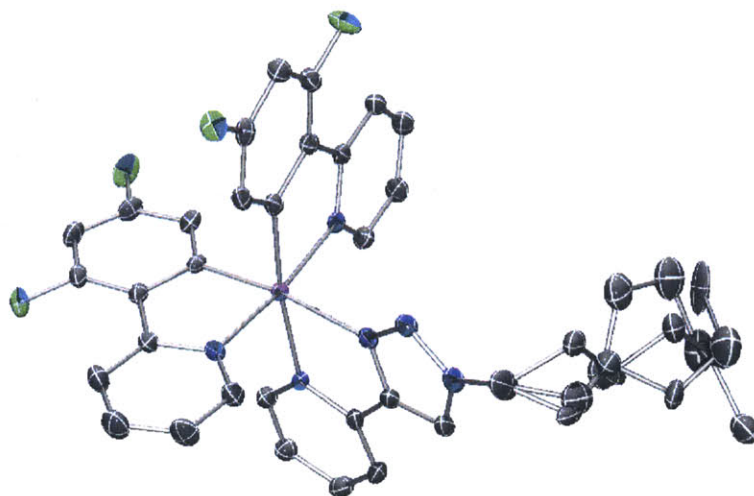
Packing diagram of **6b**.



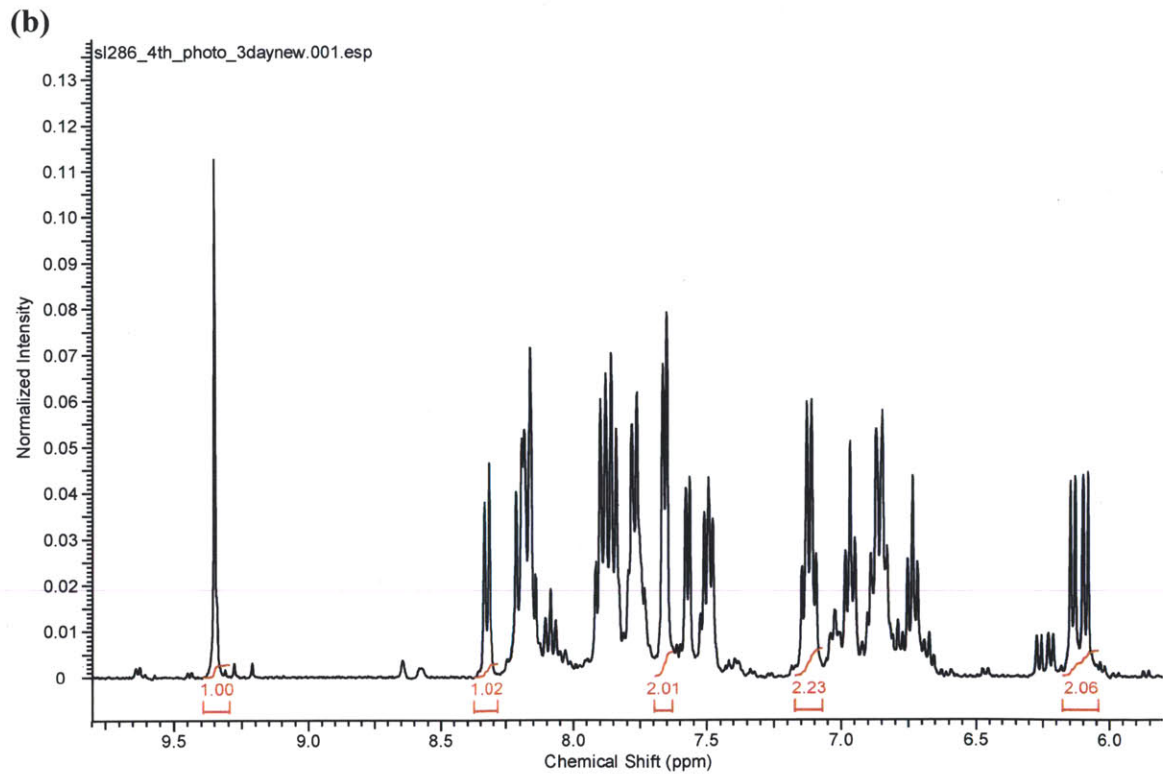
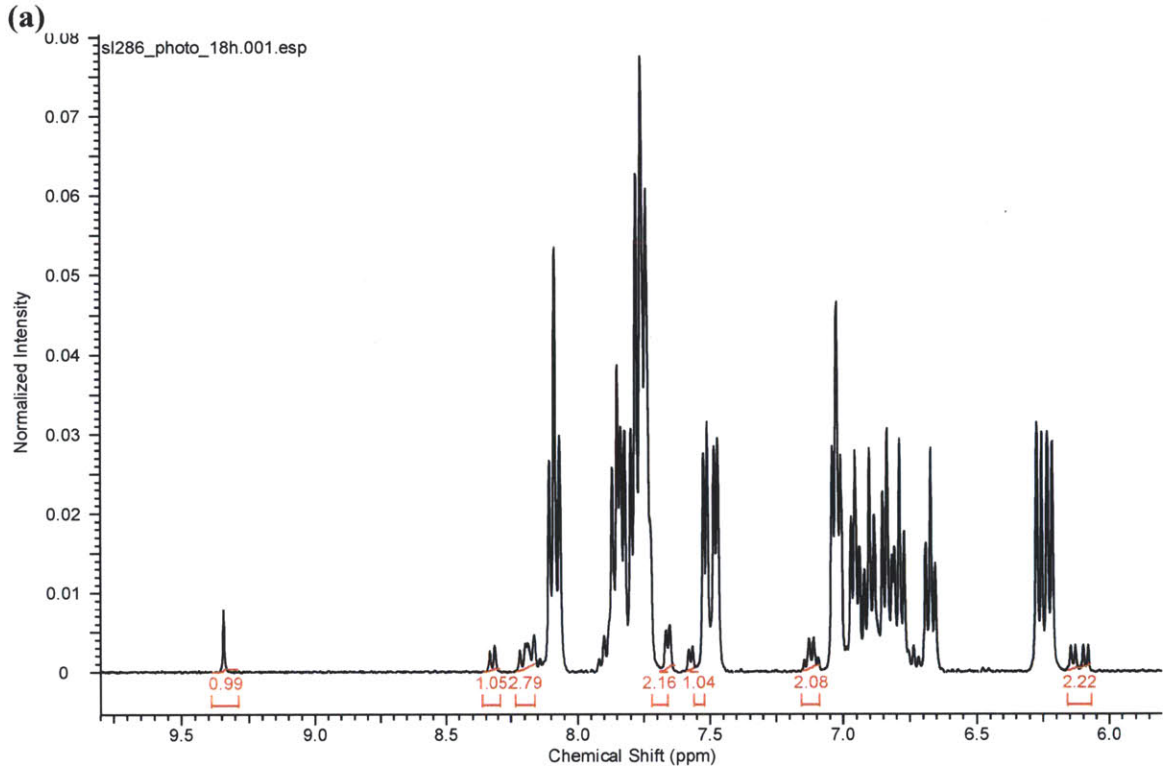
Packing diagram of 7b.

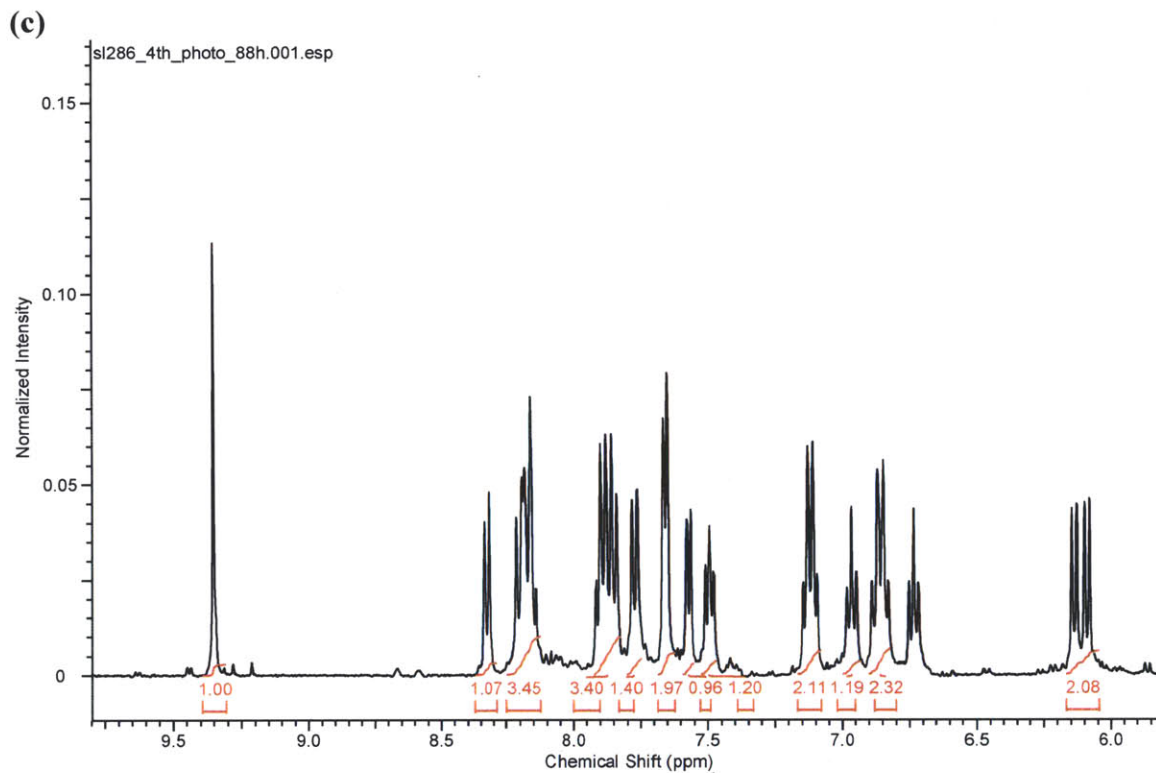


Ortep diagram of **6b**. Thermal ellipsoids are drawn at the 50% probability level.

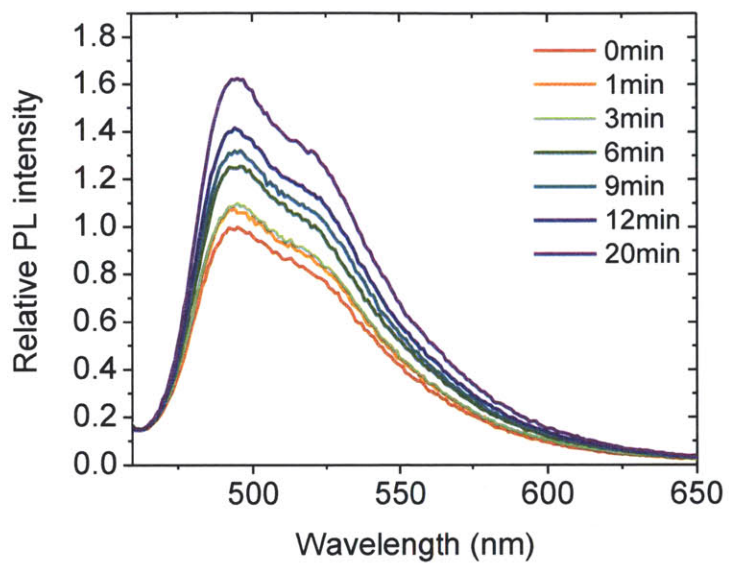


Ortep diagram of **7b**. Thermal ellipsoids are drawn at the 50% probability level.

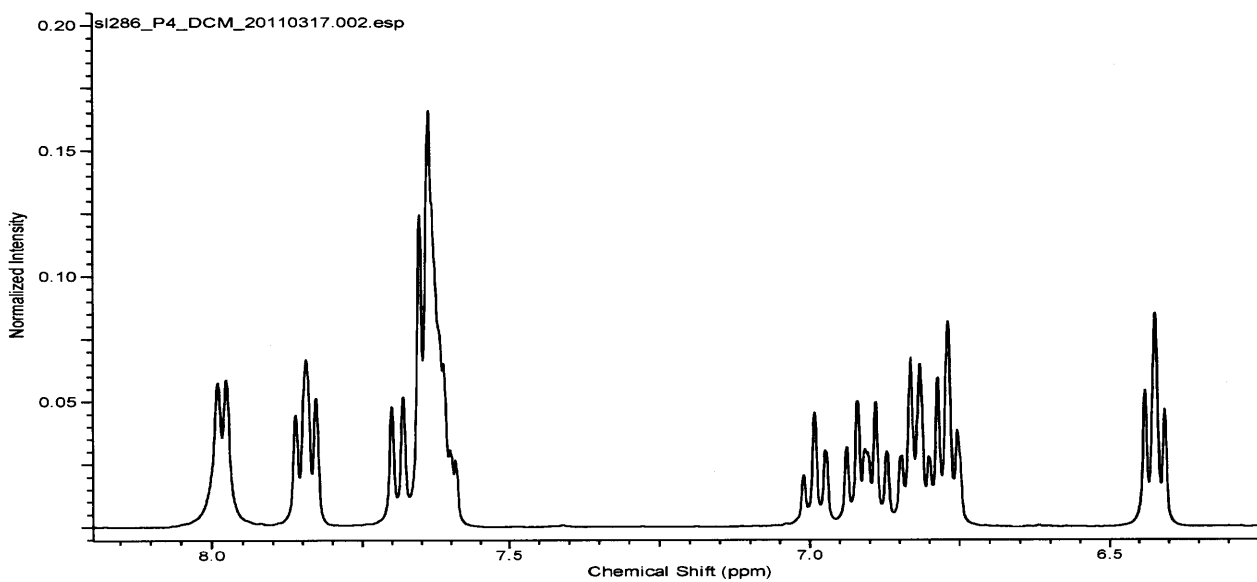




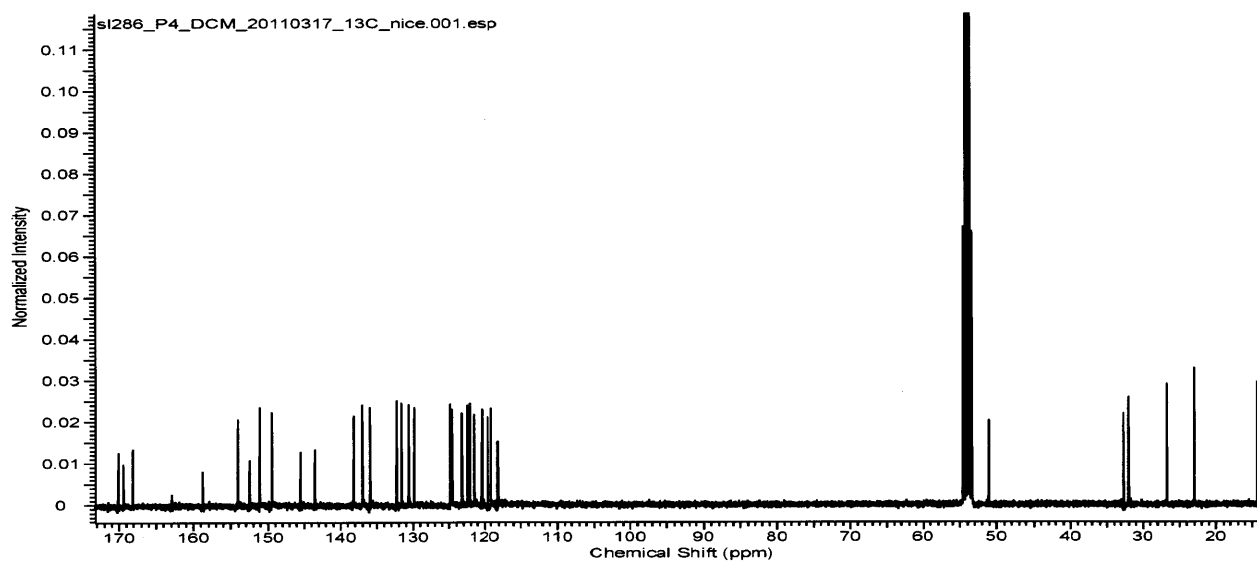
Photoisomerization of **2a** in DMSO- d_6 , monitored by ^1H NMR after exposed to UV radiation for 18 h, 72 h and 88 h. The non-overlapping peaks corresponding to the newly formed $[\text{Ir}(\text{C}^{\wedge}\text{N})_2(\text{N}^{\wedge}\text{N}_{\text{trpy}})]^+$ cation are integrated.



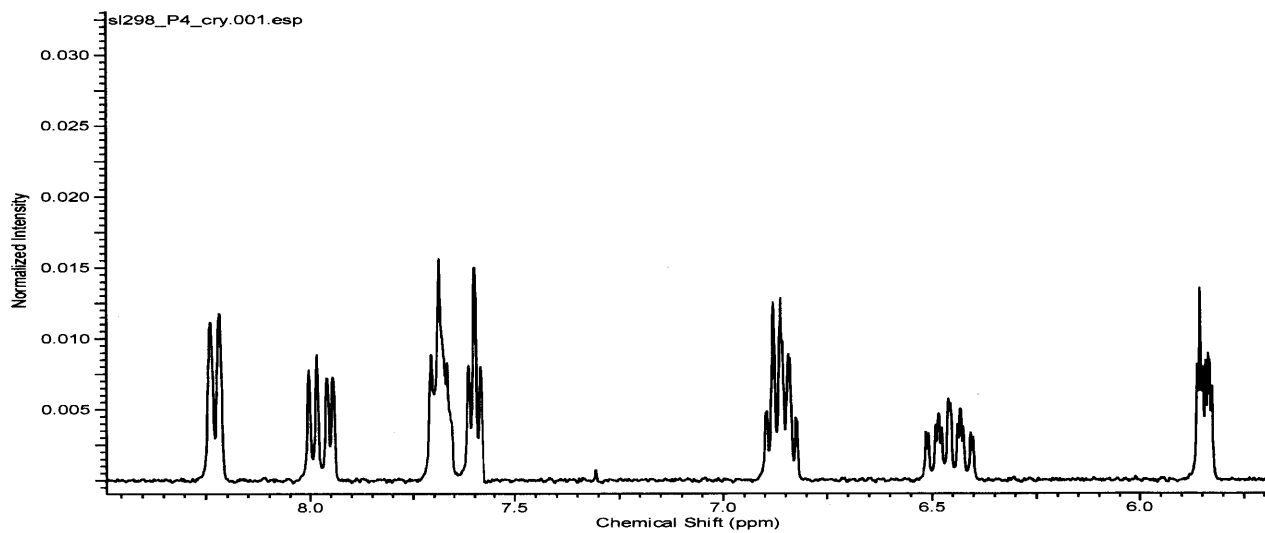
Enhanced photoluminescence of **2a** in deoxygenated THF solution upon broadband UV radiation.



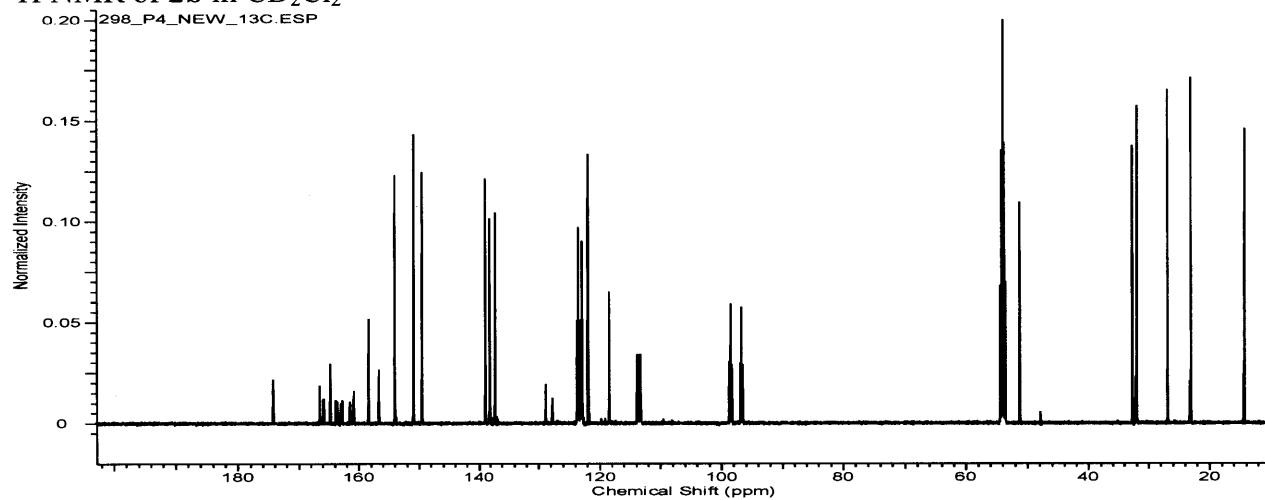
^1H NMR of **2a** in $\text{DMOS-}d_6$



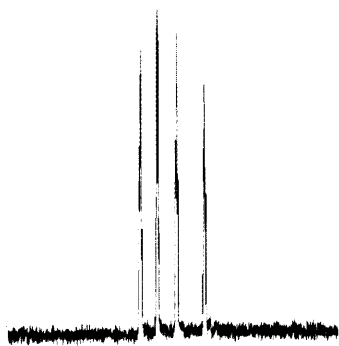
^{13}C NMR of **2a** in CD_2Cl_2



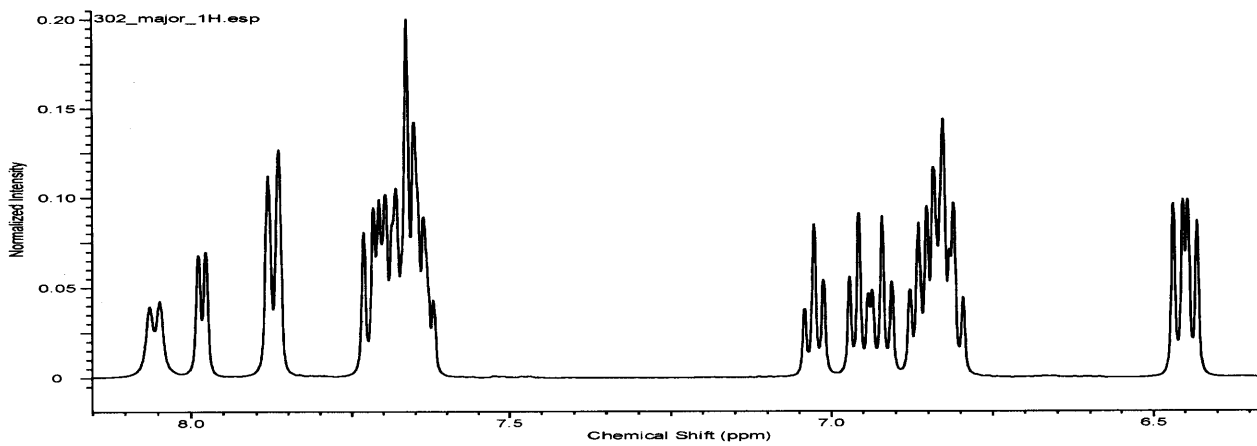
^1H NMR of **2b** in CD_2Cl_2



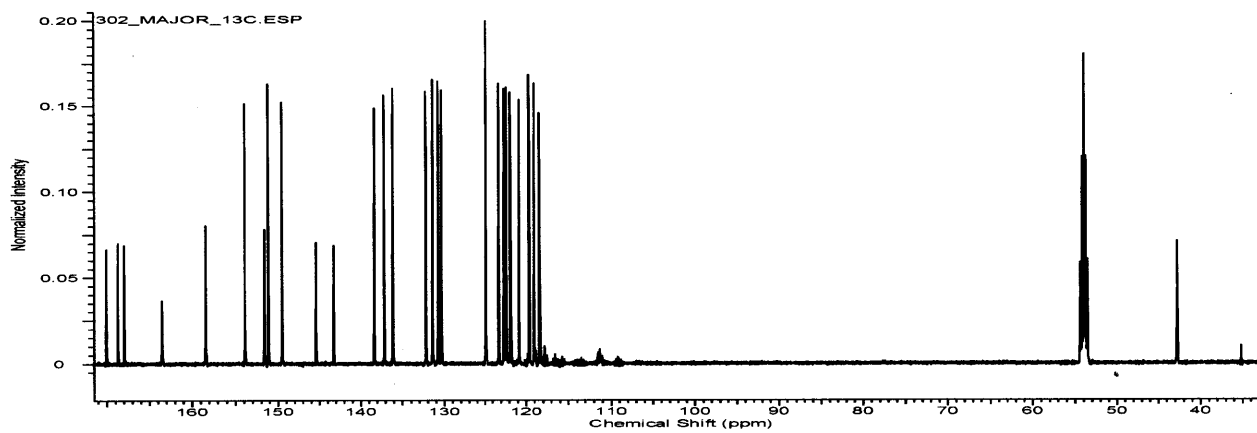
^{13}C NMR of **2b** in CD_2Cl_2



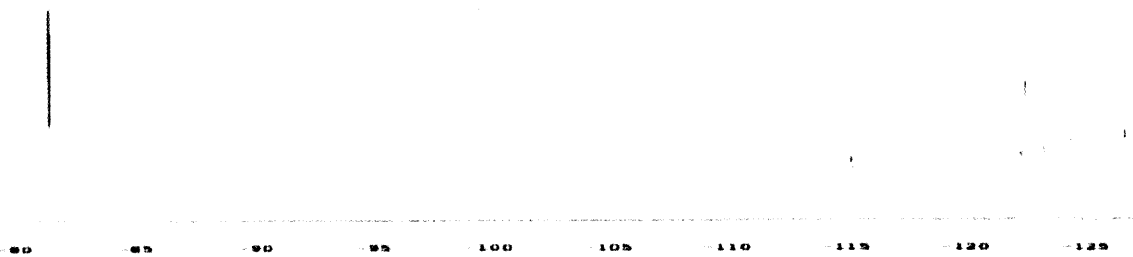
^{19}F NMR of **2b** in CD_2Cl_2



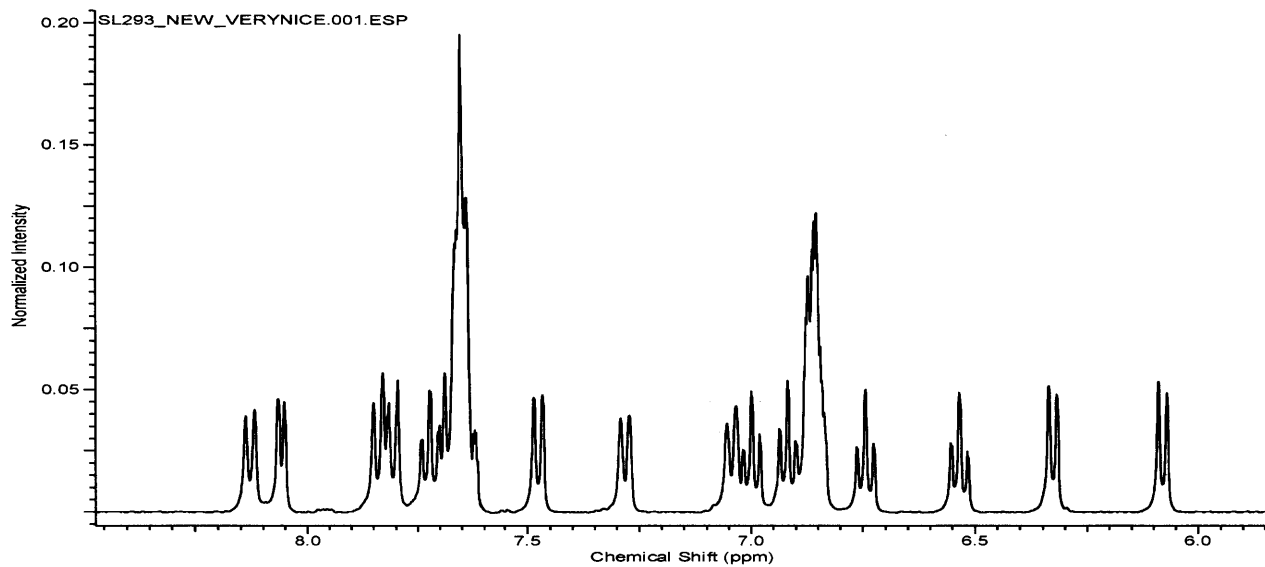
^1H NMR of **3a** in CD_2Cl_2



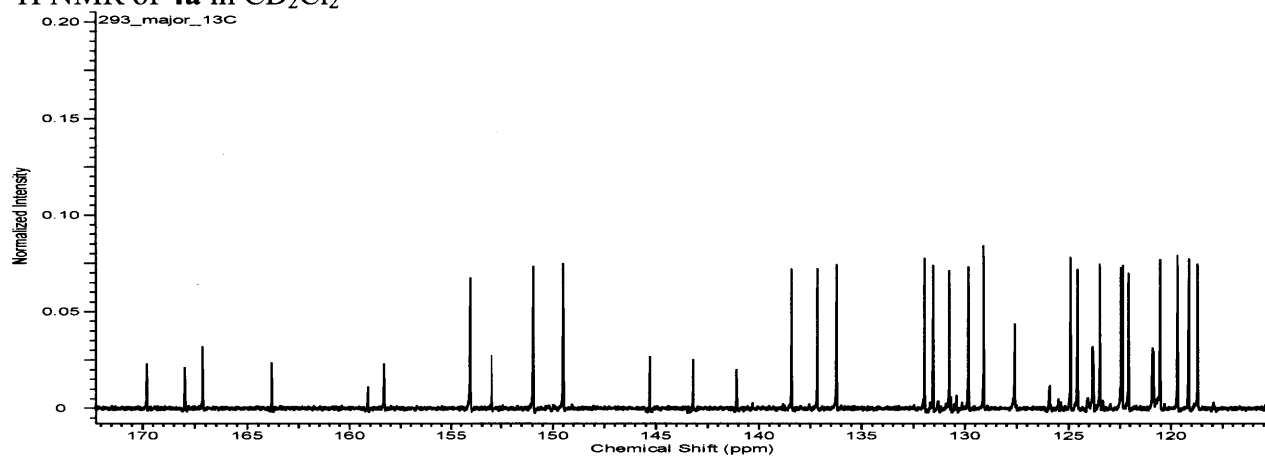
^{13}C NMR of **3a** in CD_2Cl_2



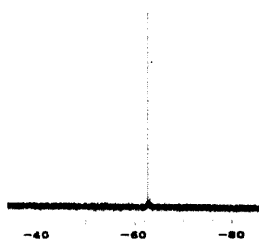
^{19}F NMR of **3a** in CD_2Cl_2



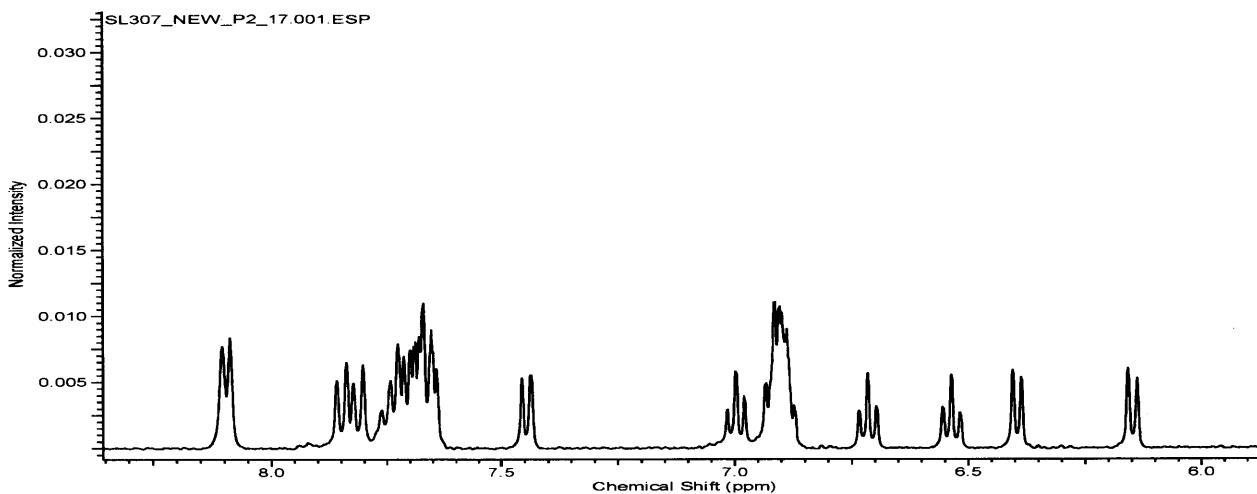
^1H NMR of **4a** in CD_2Cl_2



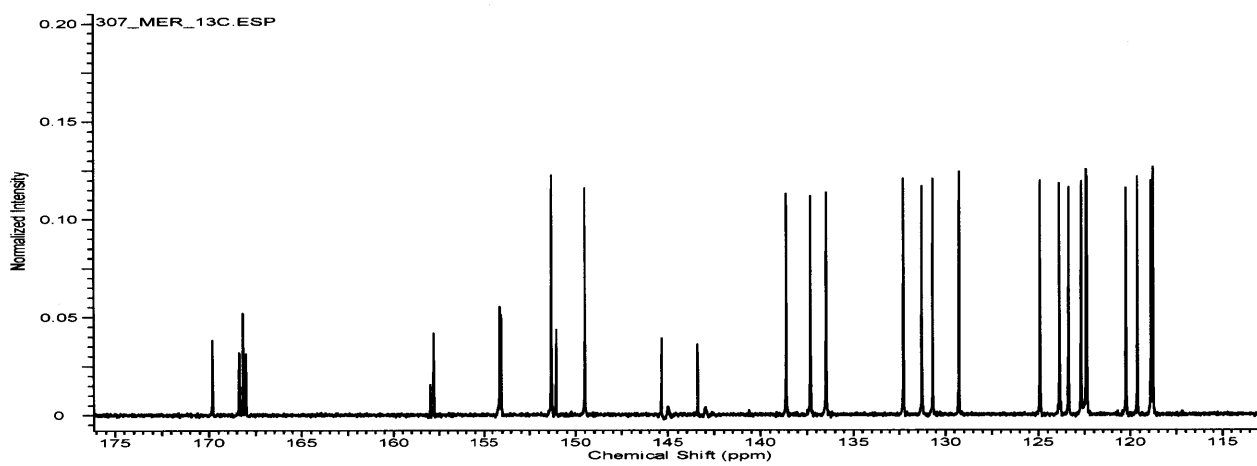
^{13}C NMR of **4a** in CD_2Cl_2



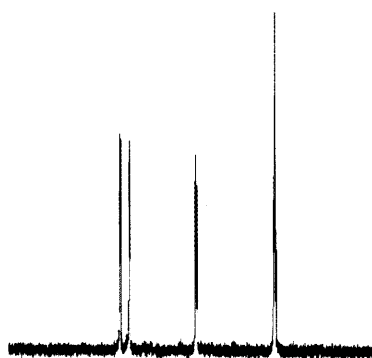
^{19}F NMR of **4a** in CD_2Cl_2



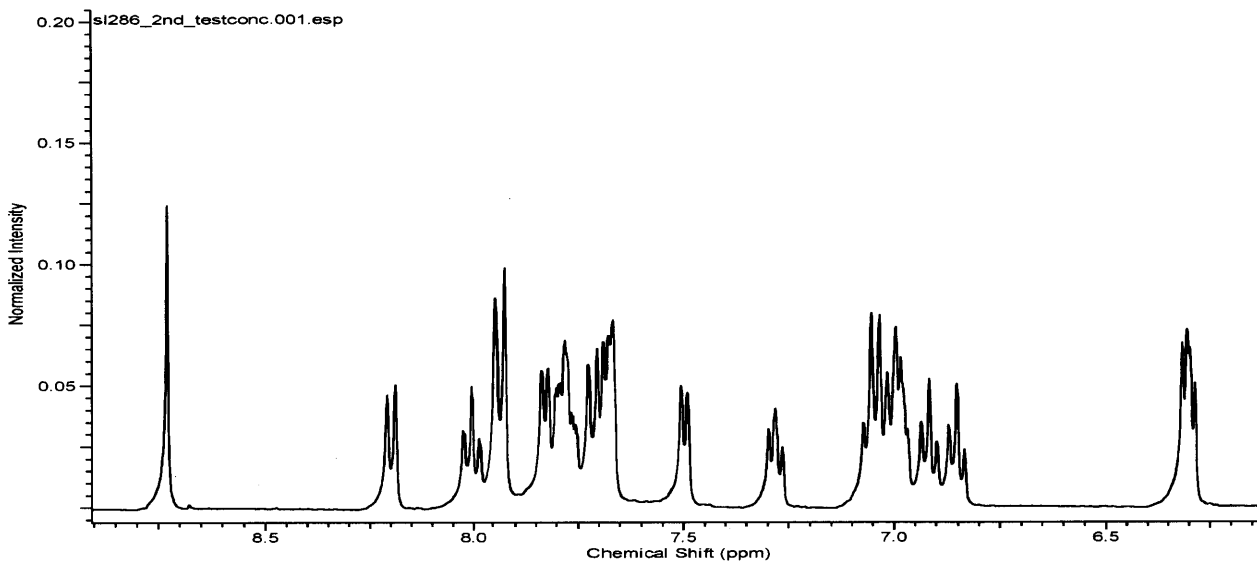
^1H NMR of **5a** in CD_2Cl_2



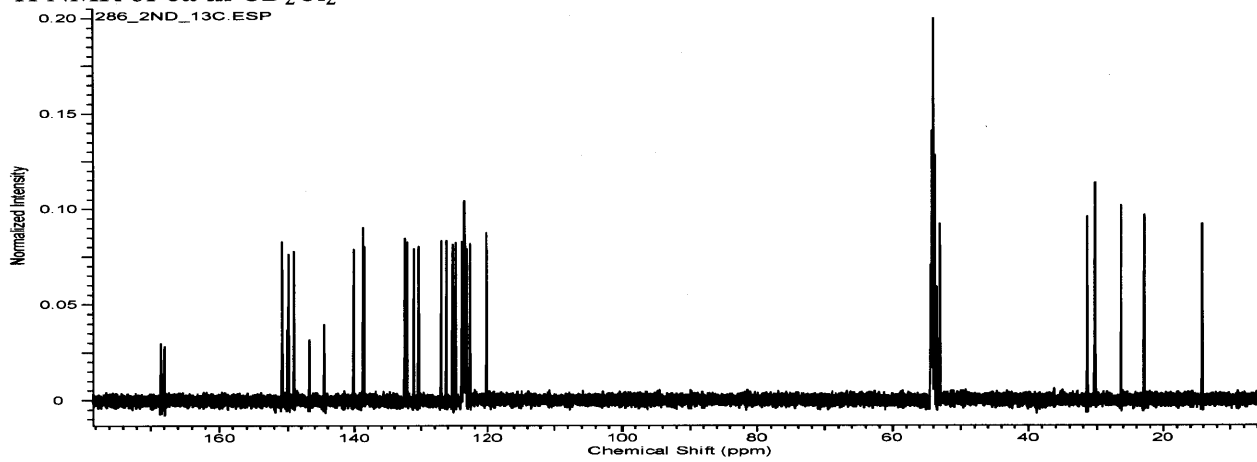
^{13}C NMR of **5a** in CD_2Cl_2



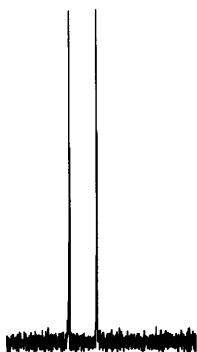
^{19}F NMR of **5a** in CD_2Cl_2



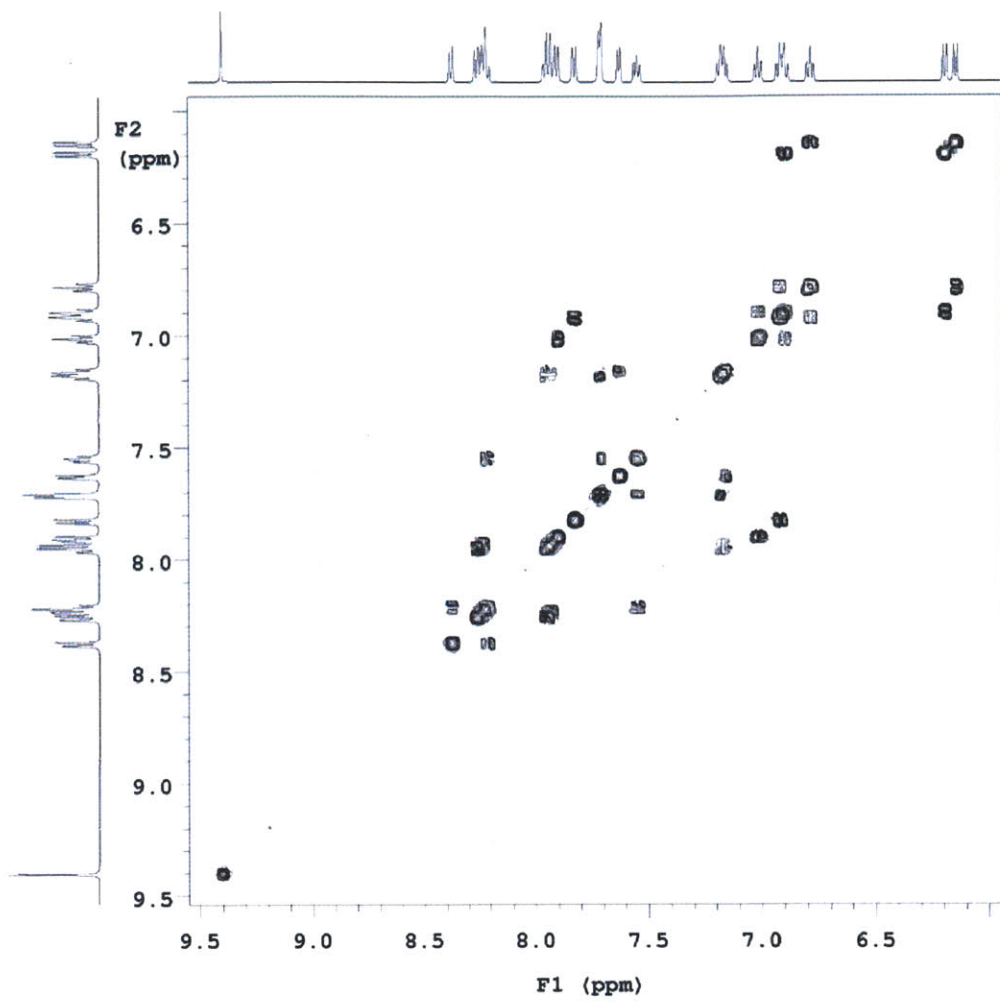
^1H NMR of **6a** in CD_2Cl_2



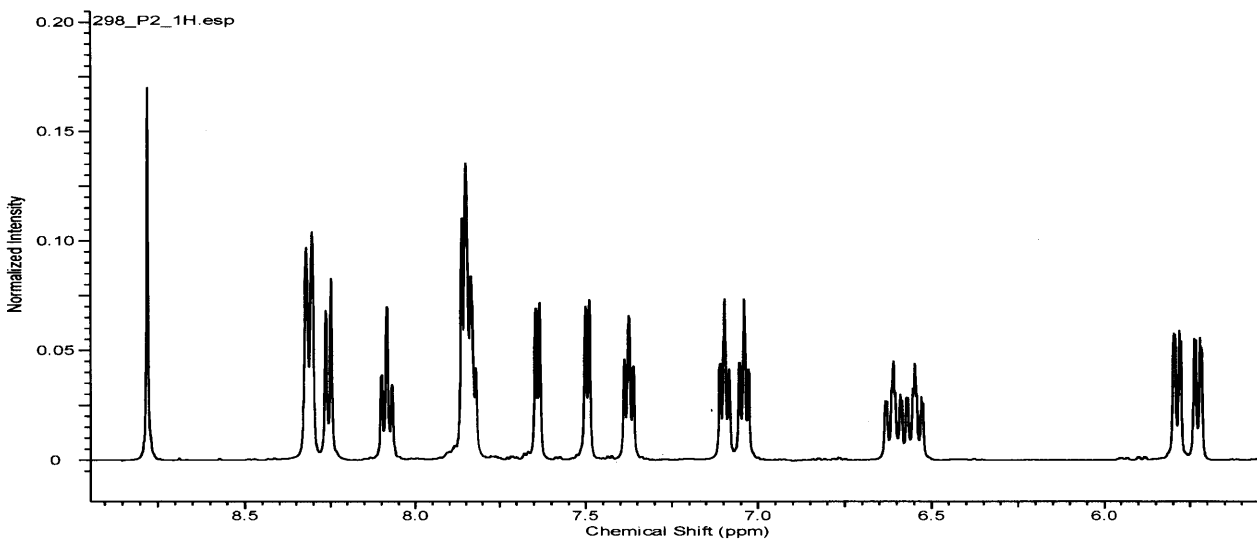
^{13}C NMR of **6a** in CD_2Cl_2



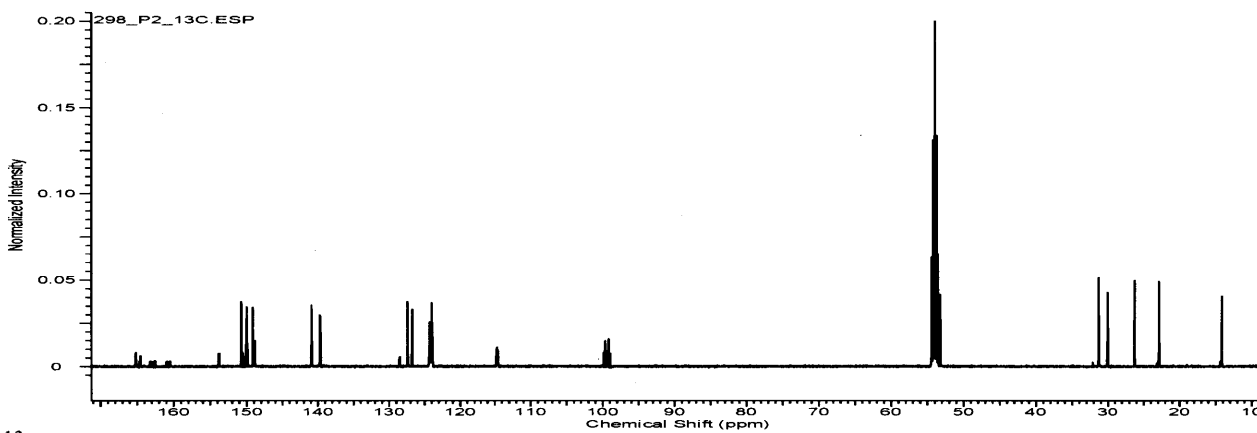
^{19}F NMR of **6a** in CD_2Cl_2



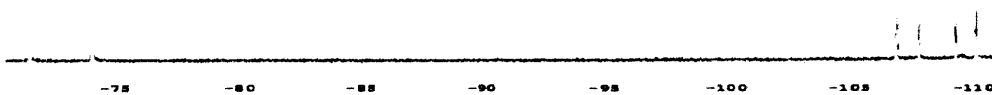
gCOSY of **6a** in $\text{DMOS-}d_6$



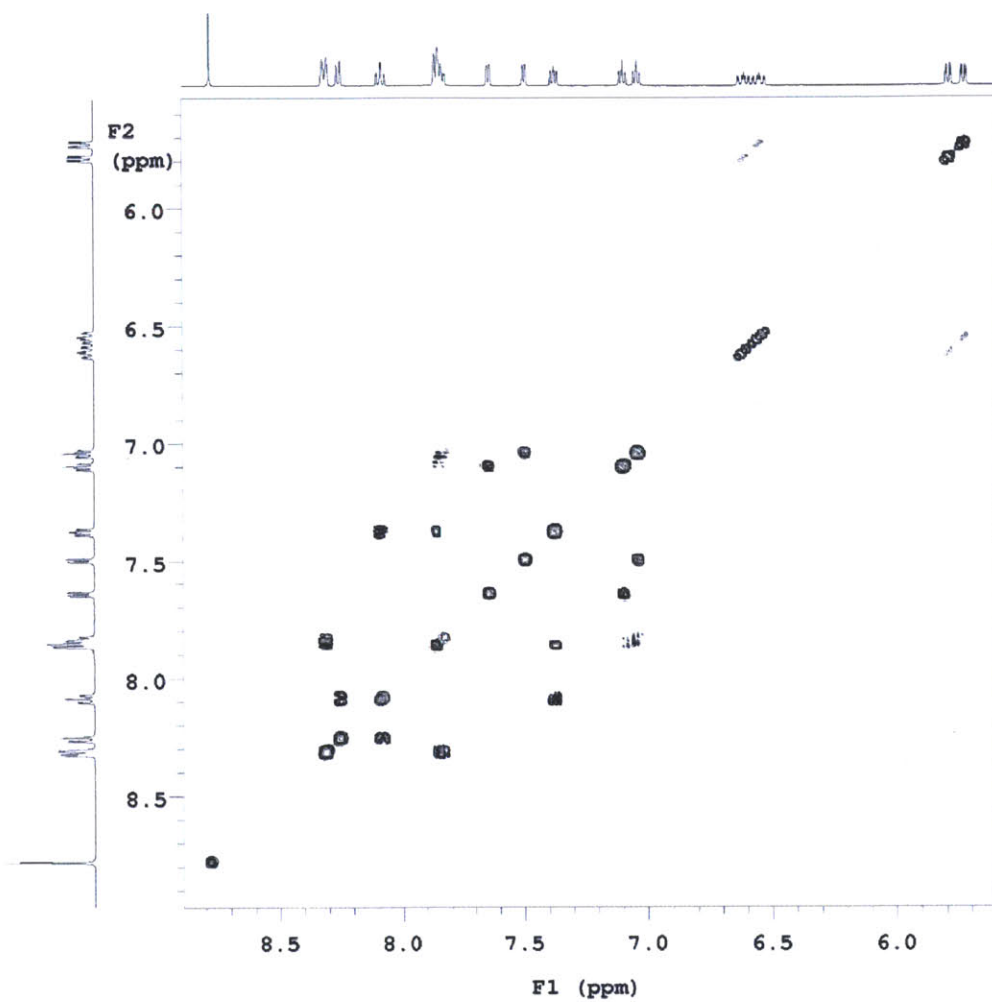
^1H NMR of **6b** in CD_2Cl_2



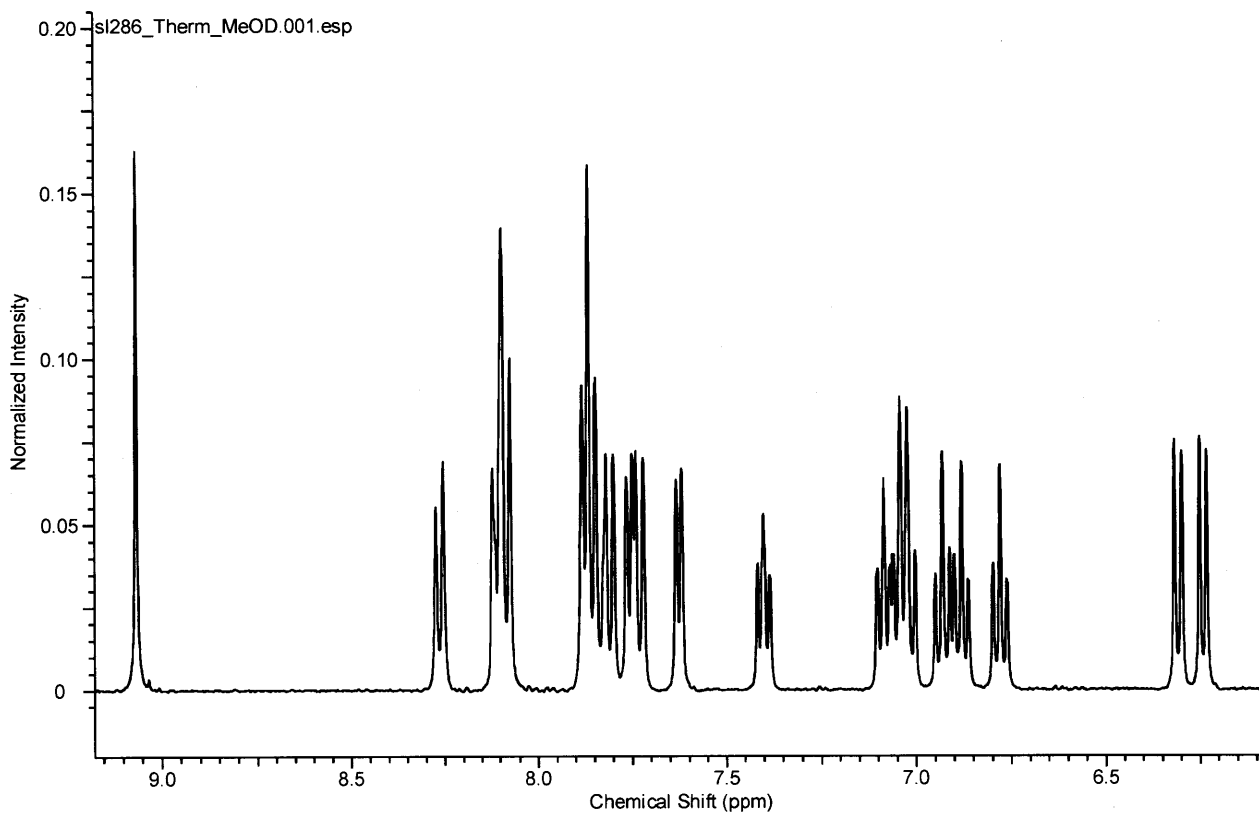
^{13}C NMR of **6b** in CD_2Cl_2



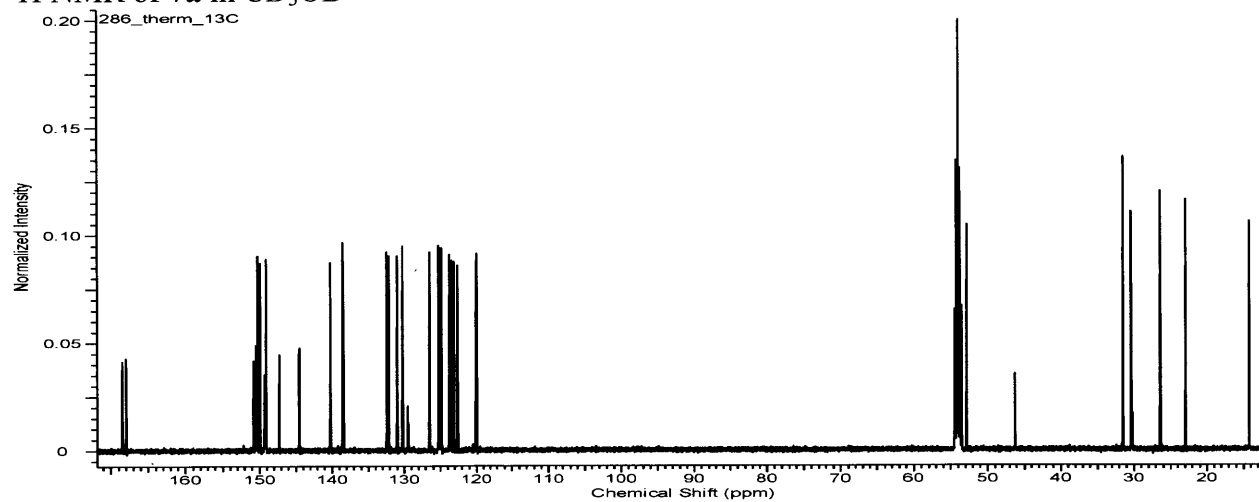
^{19}F NMR of **6b** in CD_2Cl_2



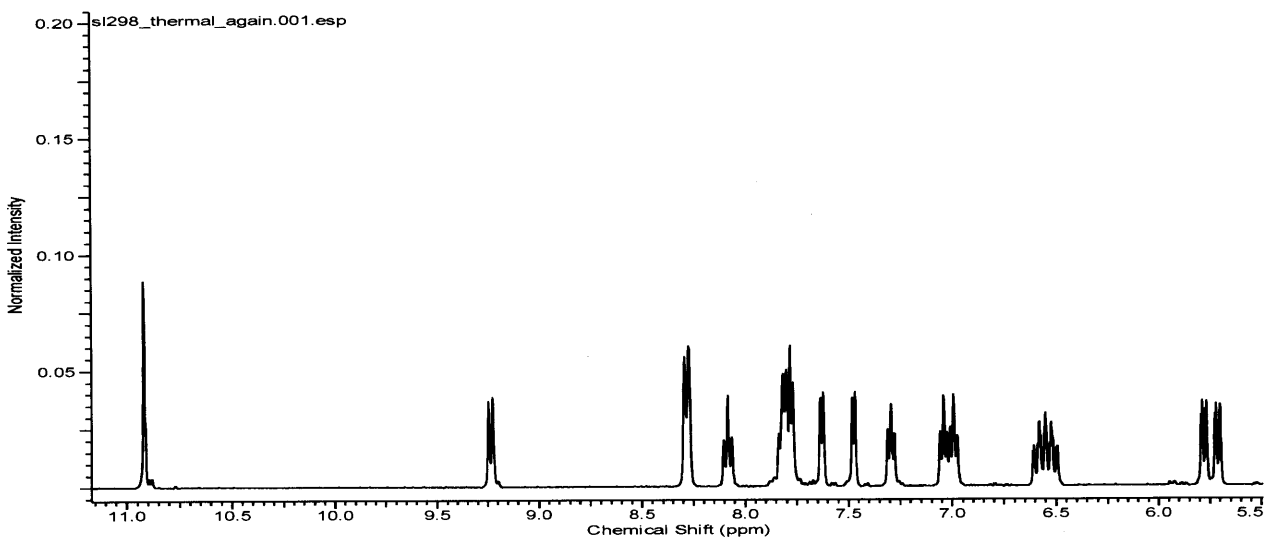
gCOSY of **6b** in CD_2Cl_2



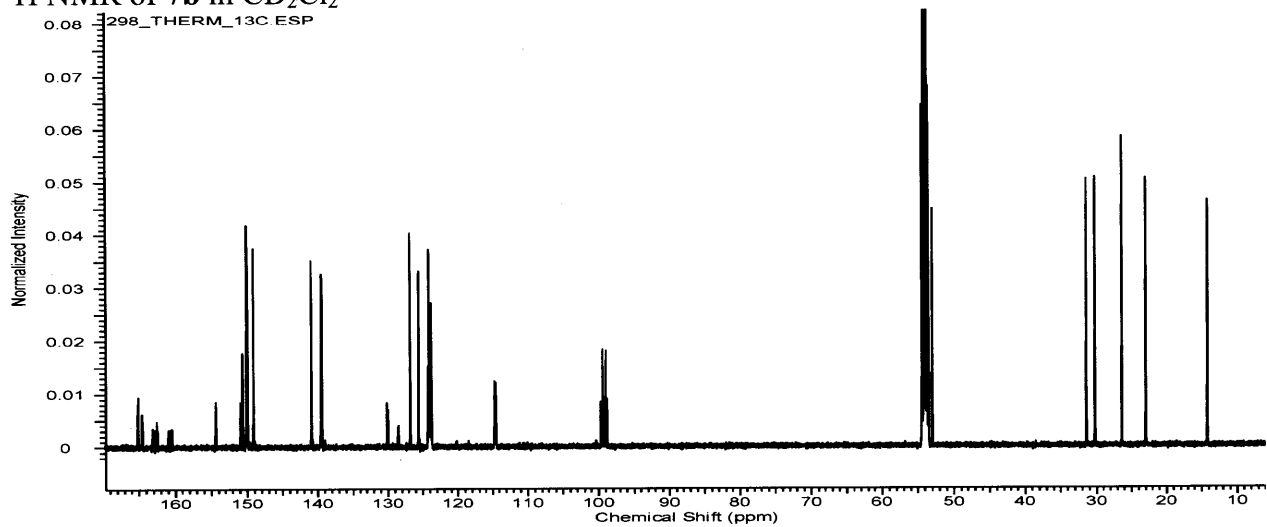
^1H NMR of **7a** in CD_3OD



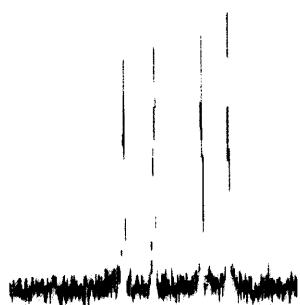
^{13}C NMR of **7a** in CD_2Cl_2



^1H NMR of **7b** in CD_2Cl_2



^{13}C NMR of **7b** in CD_2Cl_2



^{19}F NMR of **7b** in CD_2Cl_2

Chapter 2

Zwitterionic dinuclear cyclometalated Pt(II) complexes based on "click" ligands

2.1 Introduction

Cyclometalated Ir(III) and Pt(II) compounds are among the most promising phosphorescent emitters for various applications. Therefore, this family of complexes has found wide application in the fabrication of phosphorescence-based organic light emitting diodes (OLEDs),¹ chemosensors^{2,3} and bio-imaging.⁴⁻⁷ The structures of cyclometalated Ir(III) and Pt(II) complexes generally consist of at least one five- or six-membered metallacycle.⁸ Ir(III) and Pt(II) centers greatly enhance the rate of intersystem crossing, and offer high quantum efficiency and short excited state lifetime. Furthermore, the strong M-C bond ensures high thermal- and photo-stability. More importantly, the emission color can be tuned by varying the chelating ligands and their functional groups.^{9,10} Triplet emission is key to their photoemission properties and is believed to originate from a mixture of metal-to-ligand charge transfer (³MLCT) and ligand centered (³LC) excited states.^{9,10}

Unlike Ir(III) that usually adopts an octahedral coordination, the d⁸ platinum prefers a square planar configuration. This geometry has two open axial positions that favor non-covalent metal-metal interactions via the exposed metal dz^2 orbitals and π - π stacking between the ligands. The resulting intermolecular interactions leads to the formation of dimers or oligomers, triggering the excimer emission via the metal-metal-to-ligand charge transfer (MMLCT). The aggregation-induced phosphorescence has led to various applications. For instance, the monomer and excimer phosphorescence has been combined to fabricate white light OLEDs based on a single emissive dopant, which greatly simplifies the fabrication process.^{11,12}

In the process of optimizing the ligation environment in search for efficient emitters, the recent developments in organic chemistry have been adopted to facilitate the design of ligands. One good example is the copper catalyzed Huisgen 1,3-dipolar cycloaddition of organic azides and alkynes, also known as the “click” reaction.¹³ When combined with functional groups, such as pyridyl or phenyl, the “click” products based on 1,2,3-triazoles prove to be versatile ligands.¹⁴ This “click-to-chelate” strategy has also been applied to the cyclometalated Pt(II)¹⁵⁻¹⁷ and Ir(III)¹⁸⁻²⁰ compounds with interesting photophysical and catalytic properties. However, the ligands need to be isolated and purified prior to use in all cases.

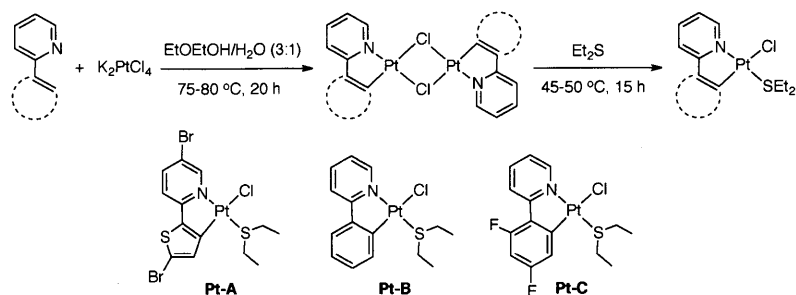
Recently, we have reported a “click” method to synthesize heteroleptic tris-cyclometalated Ir (III) complexes by taking advantage of the Cu(I) triazolide intermediates as transmetalating reagents.²¹ In this approach, the ligand synthesis and metalation can be achieved in one pot under mild reaction conditions. Meridional tris-cyclometalated Ir(III) compounds were isolated readily in high yields, with the in-situ generated 2-(1,2,3-triazol-4-yl)-pyridine (trpy) acting as C[^]N- chelating ligand. The robustness of the “click reaction” provides a general strategy for synthesizing a wide variety of target ligands. Moreover, the “click” ligands can switch from C[^]N- to N[^]N- coordination modes upon thermal and photo-isomerization. As part of our continuing effort to implement the transmetalation strategy, we have examined this approach in preparing heteroleptic cyclometalated Pt(II) compounds.

2.2 Results and Discussion

2.2.1 Synthesis

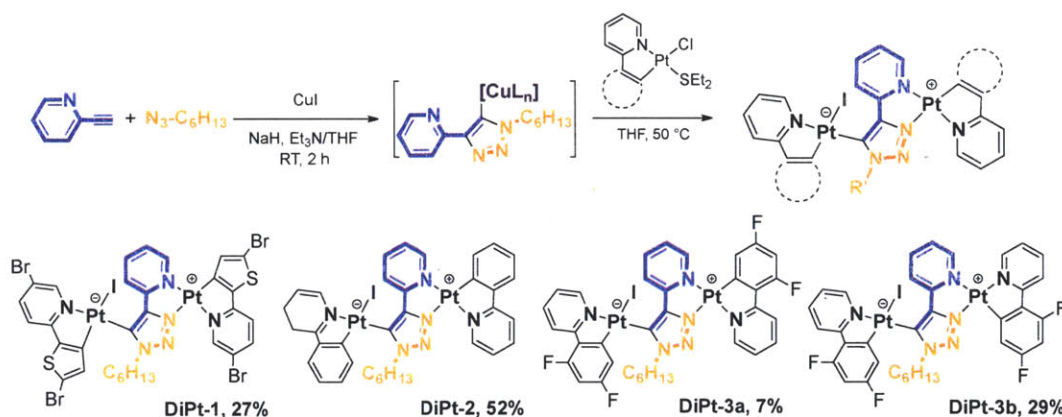
A synthetic route similar to that used in the tris-cyclometalated iridium(III) complexes is adopted, as shown in Scheme 1.²¹ 2-Ethynylpyridine was treated with stoichiometric amount of CuI in THF in the presence of NaH and Et₃N, followed by the addition of 1-azidohexane. The Cu(I)-triazole intermediate was generated within 1 h at room temperature. CuI initially exists in stable clusters and requires a certain concentration of acetylide anion before the reactive complex can be formed. Therefore, NaH is necessary to accelerate the reaction and prevent back-transfer of protons to the copper intermediate. Decomposition of the Pt(II) species to metallic platinum was observed with a large excess of NaH, as confirmed by the isolation of free cyclometalating ligands. This phenomenon has also been reported for other low-valent organometallic compounds, such as gold(I) acetylides.²² Mono-cyclometalated platinum(II) precursor Pt(C[^]N)Cl(Et₂S) (**Pt-A**, **B** or **C**), prepared according to Scheme 2.1, was added to the Cu(I)-triazolide containing mixture at room temperature. The reaction was allowed to proceed for 10 hours at 65 °C. Crystalline solid products were readily purified via column chromatography.

Scheme 2.1. Synthesis of the starting materials **Pt-A**, **Pt-B**, **Pt-C**.



All products exhibit good solubility in common organic solvents, such as tetrahydrofuran, dichloromethane and ethyl acetate. It should be noted that the orange-red **DiPt-1** turned into an insoluble brown residue over time in dichloromethane, but no similar decomposition was observed for the other products. Although the click reaction allows different functional groups to be introduced easily, alkyl groups in the azide were necessary to maintain good solubility of the products. For instance, the product obtained with phenyl or benzyl azides exhibited very low solubility, which hindered further purification and characterization.

Scheme 2.2. Synthesis of the dinuclear cyclometalated Pt(II) compounds.

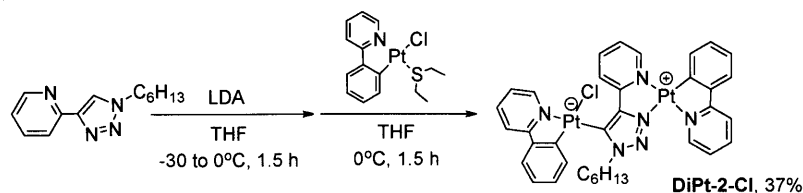


The 1H NMR spectra and HRMS indicate that the structures of the products are more complicated than mononuclear Pt(II) complexes (Scheme 2.2). Take **DiPt-1** as an example, there are two sets of NMR signals originated from the brominated 2-thienylpyridine with different chemical environments but only one set for the newly generated “click” ligand. Therefore, the products are tentatively assigned as dinuclear Pt(II) complexes with a trpy bridging two $[Pt(C^N)]$ units. This result is a natural

extension of the switchable C[^]N- and N[^]N- coordination modes found in cyclometalated Ir(III) compounds.²¹

Attempts to synthesize mononuclear Pt(II) compounds, with either C[^]N- or N[^]N- trpy coordination, did not produce the expected products. Reactions using Cu(I) catalysts with non-coordinating anions, such as Cu(CH₃CN)₄PF₆, did not yield any isolable cyclometalated complexes. Instead, free trpy ligand and a small amount of dimerized bistriazole product were obtained. Formation of the triazole dimers has been attributed to the basic conditions used in this synthesis.²³ Control reactions using stepwise synthetic methods have also been performed, following the method used to prepare bis-cyclometalated Pt(II) complexes.²⁴⁻²⁶ The “click” ligand was prepared and treated with LDA to generate a lithium triazolide,²⁷ a more reactive transmetalating reagent compared to the Cu(I) intermediate (Scheme 2.3). Upon reaction with **Pt-B**, only the dinuclear product **DiPt-2-Cl** was isolated even when excess Pt(II) precursor was used. Its structure is almost identical to that of **DiPt-2**, except for replacing a Pt-Cl bond with a Pt-I bond. Therefore, the trpy ligand prefers to utilize all three coordination sites when associated with Pt(II).

Scheme 2.3. Stepwise approach as the control reaction.



It is worth noting that two products (**DiPt-3a** and **DiPt-3b**) were isolated from the reaction mixture when 2-(2,4-difluorophenyl)pyridine (FFppy) was used as the primary cyclometalating ligand. The two products exhibited very similar properties, both

exhibiting bright orange emission in the solid state at room temperature. Pure samples of **DiPt-3a** and **DiPt-3b** could be obtained by preparative thin layer chromatography (PTLC). High-resolution mass spectra (HRMS) revealed that the parent ions of the two products have similar mass to charge ratios ($m/z = 731.2446$ m/e for **DiPt-3a** and $m/z = 731.2498$ m/e for **DiPt-3b**). The ^1H NMR spectrum of **DiPt-3a** is similar to those of **DiPt-2** and **DiPt-2-Cl**, meanwhile, it is remarkably different from that of **DiPt-3b** in the aromatic region. Therefore, **DiPt-3a** is likely to have similar structure to **DiPt-1** and **DiPt-2**, whereas **DiPt-3b** is expected to be a coordination isomer of **DiPt-3a**.

2.2.3 Structural characterization

The formation of dinuclear Pt(II) complexes has been confirmed by X-ray crystallographic study. Two representative compounds (**DiPt-1** and **DiPt-3b**) were characterized using single crystals obtained from concentrated THF/hexane and dichloromethane/hexane solutions, respectively. **DiPt-1** crystallized in the monoclinic space group $P2_1/n$, while **DiPt-3b** in the triclinic space group $P-1$. Ligands and solvents are severely disordered in both cases. Details of the refinement are provided in the experimental section. Selected interatomic distances and angles are presented in Table 2.1 and Table 2.2, respectively. Full tables of bond lengths, bond angles and atomic coordinates are provided in the appendix of this chapter.

There are two crystallographically independent molecules in the asymmetric unit of **DiPt-1**. Two mono-cyclometalated Pt(II) units are connected by the trpy ligand, through the N[^]N chelation and the Pt-C bond (Figure 2.1). The metal center Pt(1) (or Pt(3)) is located in a distorted square planar environment, with 5-bromo-2-(5-

bromothiophen-2-yl)pyridine (thpy) and the newly-generated click ligand acting as C[^]N and N[^]N chelators, respectively. The two pyridyl groups in thpy and trpy are *trans* to one another. On the other side of the molecule, Pt(2) (or Pt(4)) is coordinated by the triazolyl carbon at the 5-position together with the cyclometalating thpy. The two Pt-C bonds are *cis* to each other as expected. The coordination is further completed by one iodine atom inherited from CuI. The two Pt(II) coordination planes are almost perpendicular to each other. The two molecules in the asymmetric unit are indeed conformational isomers, with the [(C[^]N)PtI] unit rotated by 180° along the Pt-C(trpy) bond.

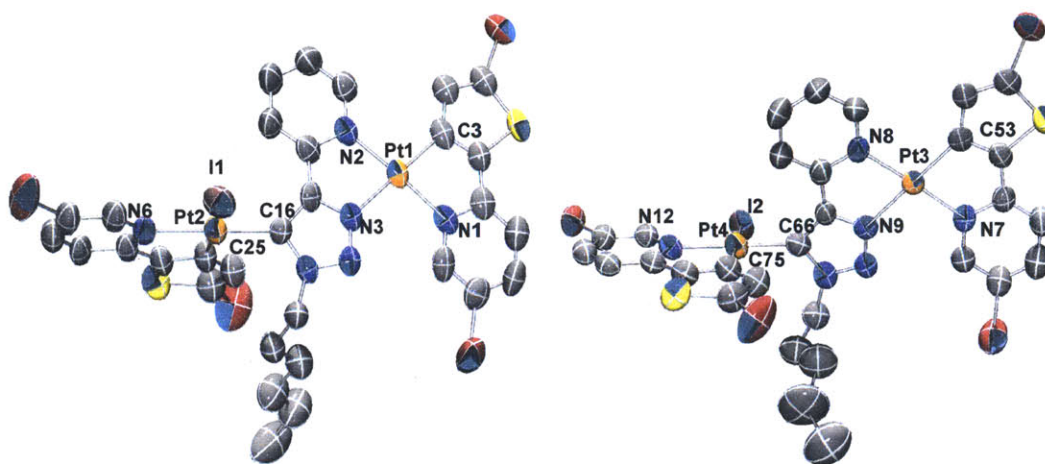


Figure 2.1. Ortep diagrams of the two molecules in the asymmetric unit of **DiPt-1**. Thermal ellipsoids are drawn at the 50% probability level. Hydrogen atoms are omitted for clarity, and only one of the disordered positions was shown.

Table 2.1. Selected bond lengths (Å) and bond angles (deg) for compound **DiPt-1**

Bond lengths (Å)				Bond angles (°)	
Pt(1)-N(1)	2.008(9)	Pt(3)-N(7)	2.017(8)	N(1)-Pt(1)-C(3)	80.8(4)
Pt(1)-C(3)	2.017(10)	Pt(3)-C(53)	2.028(10)	N(2)-Pt(1)-N(3)	78.2(4)
Pt(1)-N(2)	2.045(10)	Pt(3)-N(8)	2.050(9)	C(25)-Pt(2)-N(6)	80.4(6)
Pt(1)-N(3)	2.073(9)	Pt(3)-N(9)	2.084(9)	C(25A)-Pt(2)-N(6A)	79.2(8)
Pt(2)-C(16)	1.975(10)	Pt(4)-C(66)	1.973(11)		
Pt(2)-C(25)	1.963(14)	Pt(4)-C(75A)	1.97(2)	N(7)-Pt(3)-C(53)	80.5(4)
Pt(2)-C(25A)	2.011(19)	Pt(4)-C(75)	1.985(13)	N(8)-Pt(3)-N(9)	78.6(4)
Pt(2)-N(6)	2.107(14)	Pt(4)-N(12)	2.098(14)	C(75)-Pt(4)-N(12)	80.9(6)
Pt(2)-N(6A)	2.11(2)	Pt(4)-N(12A)	2.12(3)	C(75A)-Pt(4)-N(12A)	80.3(10)
Pt(2)-I(1)	2.6298(12)	Pt(4)-I(2)	2.6467(11)		

More importantly, this dinuclear structure can be considered as an intramolecular ion pair, or a zwitterion. The $[(C^{\wedge}N)Pt(N^{\wedge}N)]$ unit carries a formal positive charge, in contrast to the negative charge of $[(C^{\wedge}N)PtI]$. It should be noted that metal containing zwitterionic compounds have been well characterized and applied to catalysis.²⁸ In most of the reported compounds, the negative charge usually rests on the organic ligand. It is less common to find the two metal centers carrying the opposite formal charges.²⁹

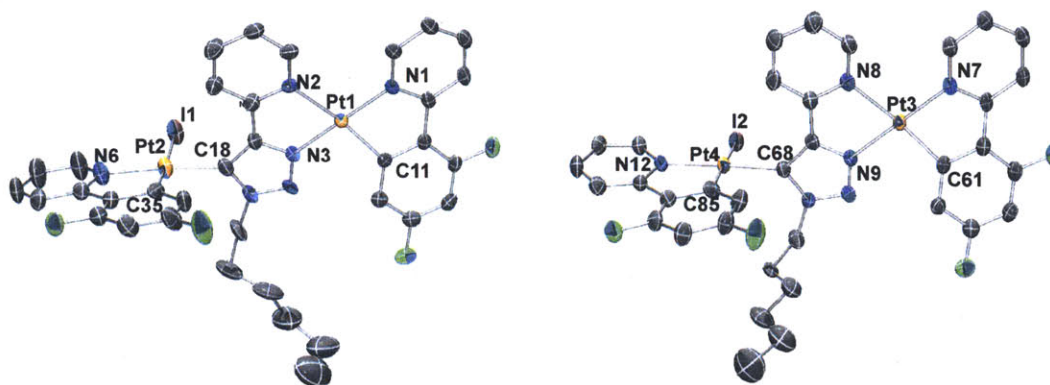


Figure 2.2. Ortep diagrams of the two molecules in the asymmetric unit of **DiPt-3b**. Thermal ellipsoids are drawn at the 50% probability level. Hydrogen atoms are omitted for clarity, and only one of the disordered positions is shown.

The structure of **DiPt-3b** resembles that of **DiPt-1** in terms of the trpy-bridged dinuclear framework (Figure 2.2). However, the $[(C^{\wedge}N)PtI]$ units in the two molecules in the asymmetric unit of **DiPt-3b** are pointing to the same direction. There are only minor variations in the individual bond lengths and angles, as listed in Table 2.2. Moreover, the two pyridyl groups of the $[(C^{\wedge}N)Pt(N^{\wedge}N)]$ moiety adopted a *cis* configuration, instead of the *trans* coordination observed in **DiPt-1**.

The Pt-C and Pt-N bond lengths and the chelating angles in both compounds are all within the expected range of similar cyclometalated platinum compounds. For

instance, the average length of Pt-C(FFppy) bonds in the [(C[^]N)Pt(N[^]N)] and [(C[^]N)PtI] units are 1.9908 Å and 1.9340 Å, respectively. They are consistent with those observed in [(FFppy)Pt(3,5-di-tert-butylcatechol)] (1.976(10) Å)³⁰, but are slightly longer than those in [(FFppy)Pt(CN)₂]⁺ (2.032(3) Å).³¹ However, a close examination of the bond lengths of the two compounds indicates that the Pt-C(FFppy) bonds, in general, are shorter than those in Pt-C(thpy) by 0.03-0.05 Å. Furthermore, the Pt-I bond (avg. 2.6797 Å) in **DiPt-3b** is longer than the one in **DiPt-1** (avg. 2.6383 Å), indicating a stronger *trans* influence executed by the Pt-C(FFppy) compared to Pt-C(thpy). This effect is also observed when comparing the average Pt-N(C[^]N) bond length in **DiPt-3b** (avg. 2.037 Å) to **DiPt-1** (avg. 2.013 Å), with the disordered positions in both molecules in the unit cell accounted for. The Pt-C(trpy) bond lengths are almost identical in both compounds, with 1.974 Å for **DiPt-1** and 1.975 Å for **DiPt-3b**, due to the similar coordination environment.

Table 2.2. Selected bond lengths (Å) and bond angles (deg) for compound **DiPt-3b**

Bond lengths (Å)				Bond angles (°)	
Pt(1)-N(1)	2.042(10)	Pt(3)-N(7)	2.036(9)	C(11)-Pt(1)-N(1)	79.7(6)
Pt(1)-N(1A)	2.030(10)	Pt(3)-N(7A)	2.038(10)	C(11A)-Pt(1)-N(1A)	80.7(6)
Pt(1)-C(11)	1.997(10)	Pt(3)-C(61)	1.973(10)	N(3)-Pt(1)-N(2)	76.6(5)
Pt(1)-C(11A)	1.989(10)	Pt(3)-C(61A)	2.004(10)	N(3A)-Pt(1)-N(2A)	77.7(6)
Pt(1)-N(2)	2.188(9)	Pt(3)-N(8)	2.176(8)	C(35)-Pt(2)-N(6)	81.7(3)
Pt(1)-N(2A)	2.179(10)	Pt(3)-N(8A)	2.196(11)	C(18)-Pt(2)-I(1)	86.6(13)
Pt(1)-N(3)	2.010(9)	Pt(3)-N(9)	2.018(8)	C(18A)-Pt(2)-I(1)	89.7(16)
Pt(1)-N(3A)	2.005(10)	Pt(3)-N(9A)	2.019(11)	C(61)-Pt(3)-N(7)	81.3(5)
Pt(2)-C(18)	1.971(10)	Pt(4)-C(68)	1.981(9)	C(61A)-Pt(3)-N(7A)	79.5(5)
Pt(2)-C(18A)	1.978(11)	Pt(4)-C(68A)	1.970(11)	N(9)-Pt(3)-N(8)	77.2(4)
Pt(2)-C(35)	1.911(7)	Pt(4)-C(85)	1.957(6)	N(9A)-Pt(3)-N(8)	76.2(6)
Pt(2)-N(6)	2.083(6)	Pt(4)-N(12)	2.075(5)	C(85)-Pt(4)-N(12)	81.3(2)
Pt(2)-I(1)	2.6797(7)	Pt(4)-I(2)	2.6822(6)	C(68)-Pt(4)-I(2)	87.7(13)
				C(68A)-Pt(4)-I(2)	89.4(19)

The dinuclear structures were also supported by a series of 2D ^1H NMR studies, such as gCOSY, TOCSY and ROESY NMR. The protons at the *ortho* position of the Pt-C/Pt-N bonds are highly sensitive toward the changes in the coordination modes. The protons ortho- to the Pt-N(thpy) (H^{A} and H^{a}) and those on the thienyl ring (H^{H} and H^{h}) of **DiPt-1** display very different chemical shifts, but the other two protons on the pyridyl groups overlap with their counterparts. The signal for H^{A} is downshifted by 0.3 ppm comparing to H^{a} . This shift is consistent with the fact that the Pt-N(thpy) separation (2.109 Å) of the $[(\text{C}^{\wedge}\text{N})\text{PtI}]$ unit is longer than the one of $[(\text{C}^{\wedge}\text{N})\text{Pt}(\text{N}^{\wedge}\text{N})]$ (2.012 Å), attributed to the stronger *trans* influence of the Pt-C(thpy) comparing to Pt-N(trpy). A more dramatic downfield shift is observed for H^{H} , which is the sharp singlet peak representing the thienyl proton. H^{H} is shifted to the lower field by 0.96 ppm from H^{h} , and this shift has been attributed to the intramolecular steric interactions between H^{H} and H^{l} .³² This argument is further supported by the through-space coupling peak between H^{H} and H^{l} observed on the ROESY spectrum. Similar NMR studies were also performed for **DiPt-2**. In addition to the cross peak between H^{H} and H^{l} , the intra-ligand interactions between H^{D} and H^{E} (H^{d} and H^{e}) can also be located.

2D ^1H NMR techniques have also proven to be helpful for studying the difference between **DiPt-3a** and **DiPt-3b**. The NMR spectra of **DiPt-3a** exhibit a pattern very similar to that of **DiPt-2** (Figure 2.3). Careful examination of the assignment of the peaks suggests that the two pyridyl nitrogen atoms, N(trpy) and N(FFppy) are also *trans* to each other in **DiPt-3a**. However, H^{A} in **Pt-3b** shifted upfield by 1.4 ppm and H^{H} downfield by 1.2 ppm compared to **DiPt-3a** (Figure 2.4). Other proton signals, especially the ones

associated with the FFppy ligand in the $[(C^{\wedge}N)PtI]$ unit, remained mostly unaffected. Moreover, there is strong through space coupling interaction between H^I and H^A in **DiPt-3b**, which is absent in **DiPt-3a**. Therefore, it is clear that the pyridyl groups from the trpy and FFppy ligands are *cis* to each other in **DiPt-3b**, and *trans* to each other in the other dinuclear complexes. As for **DiPt-3a**, H^I and H^H are close to one another and the shielding effect leads to the upfield shift of H^H .³² Similarly, the switch in coordination geometry in **DiPt-3b** leads to the shielding of H^A and deshielding of H^H .

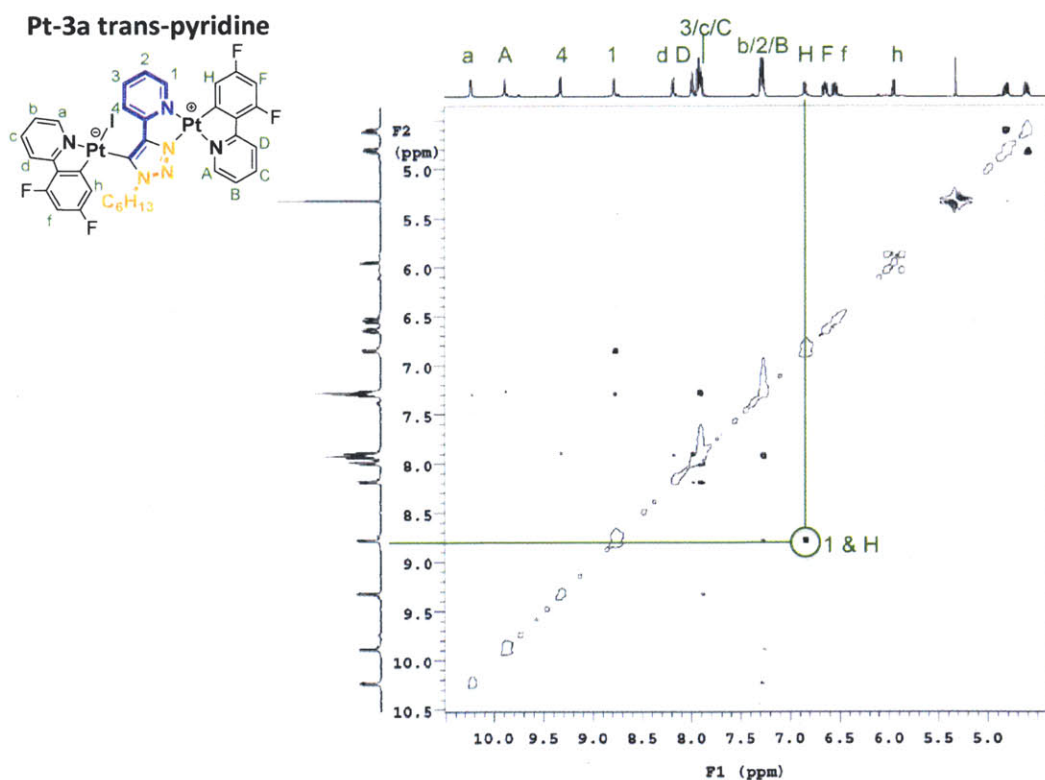


Figure 2.3. ROESY spectrum of **DiPt-3a** and the assignment of the aromatic protons.

Pt-3b cis-pyridine

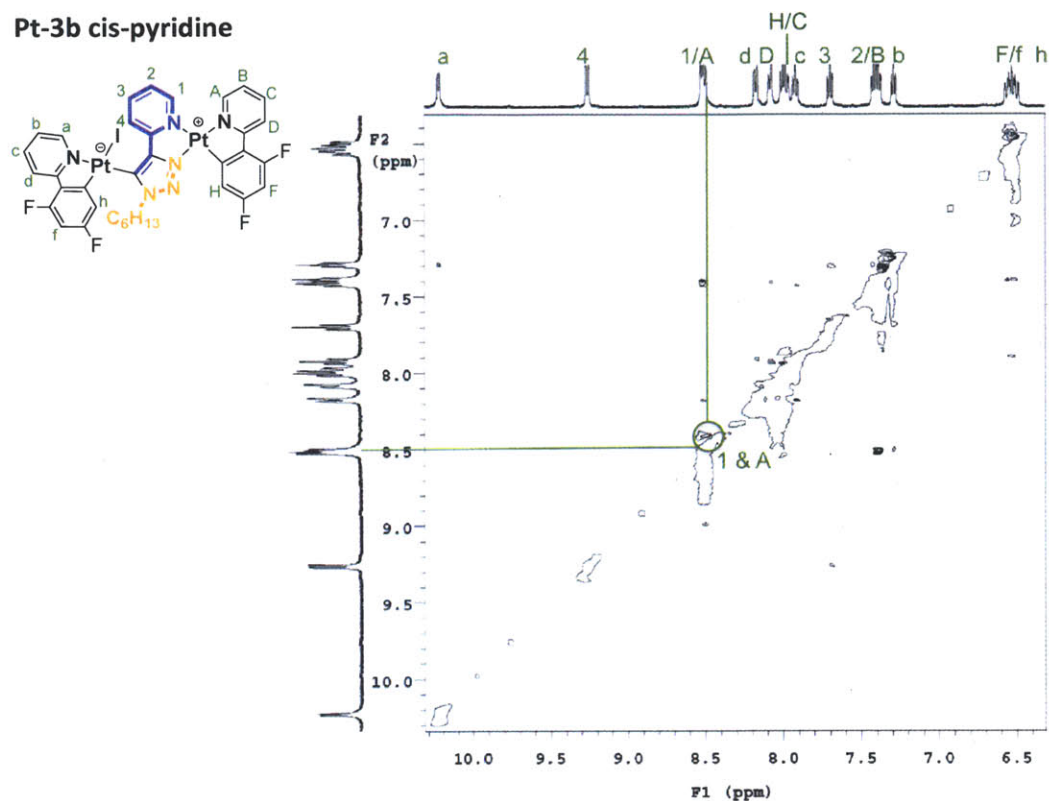


Figure 2.4. ROESY spectrum of DiPt-3b and the assignment of the aromatic protons.

2.2.4 DFT Calculations

Density functional theory (DFT) calculations have been carried out to further understand the electronic properties of these bimetallic compounds. The ground state geometries of two representative structures are optimized based on simplified thpy, 2-phenyl-pyridine (ppy) and trpy ligands. Details of the computational study are provided in the Experimental section. The frontier molecular orbitals of DiPt-1 are plotted in Figure 2.5. The highest occupied molecular orbital (HOMO) is localized within the [(C[^]N)PtI] fragment, with contributions from the platinum center, the thpy ligand and the iodine atom. The lowest unoccupied molecular orbital (LUMO) primarily consists of the π^* orbitals of the thpy and trpy ligands. It is delocalized across the entire [(C[^]N)Pt(N[^]N)]

unit, with almost no contribution from d orbitals of the metal center. This charge separation is in good agreement with the assignment of the zwitterionic structure. The formal positive charge is evenly distributed through the trpy and thpy ligands.

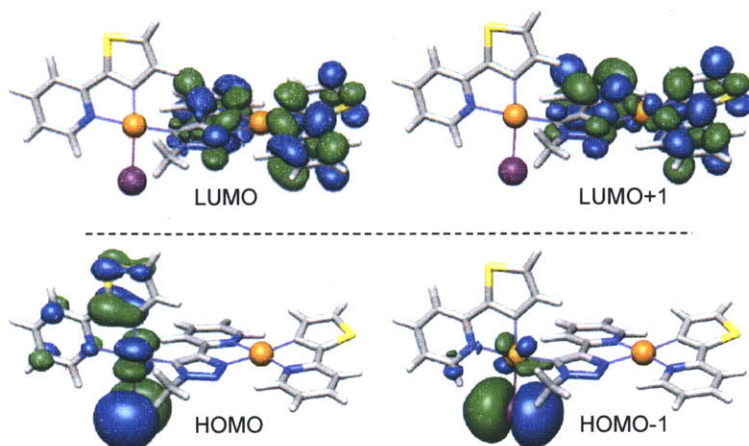


Figure 2.5. Contour plots of frontier orbitals of the model compounds of **DiPt-1**.

Time dependent (TD-DFT) calculations have also been performed on the optimized singlet ground state geometry of the **DiPt-1** analogue. The direct excitation energies of the first 25 singlet states, together with the first 5 triplet transitions, are calculated. In Figure 2.6, the oscillator strengths are plotted against the excitation wavelength, which match well with the peak in the absorption spectrum. The S_0 - S_1 transition is dominated by the HOMO-LUMO transition, indicating an MLCT character. However, the oscillator strength of this excitation is close to zero, likely caused by the minimum overlap between the HOMO and LUMO orbitals. A lower oscillator strength is consistent with the crystal structure, in which the $[(C^N)PtI]$ and $[(C^N)Pt(N^N)]$ units are almost orthogonal to each other. The absorption maximum in the low energy region can be attributed to a transition corresponding to the MLCT/LC excitation within the $[(C^N)PtI]$ fragment.

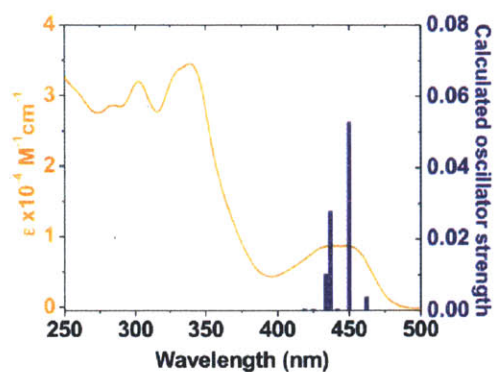


Figure 2.6. Simulated vertical excitations (blue) and the experimental UV-vis absorption spectrum (orange) of **DiPt-1**.

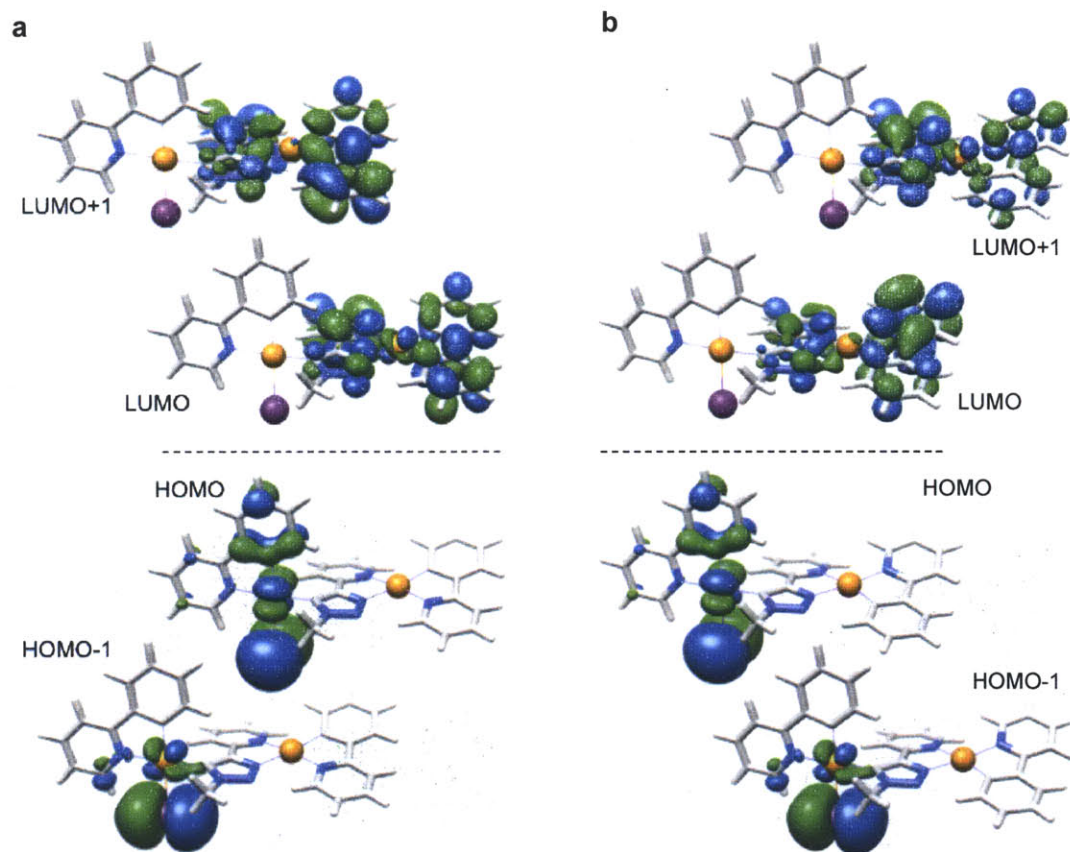


Figure 2.7. Contour plots of frontier orbitals of the model compounds of **DiPt-2** with *trans* (a) and *cis* pyridyl (b) coordination.

The *cis* and *trans* coordination of the pyridyl groups has very little effect on the frontier orbitals of the simplified **DiPt-2** as shown in Figure 2.7. The composition and energies of the orbitals is almost identical for these two configurations, suggesting that the triazolyl and pyridyl groups exhibit similar coordination strengths, which is likely due to the full conjugation across the trpy ligands.

2.2.5 Photophysical properties

UV-vis absorption spectra of all dinuclear compounds were recorded in dilute THF solutions, as depicted in Figure 2.8. Additional photophysical properties are summarized in Table 2.3. There are two broad absorption peaks for **DiPt-1** in the range of 390-480 nm and 270-390 nm. The low energy absorption peak is red-shifted by about 10 nm when dissolved in cyclohexane, indicating the metal-to-ligand charge transfer (MLCT) nature of this peak. As discussed in the previous section, the HOMO consists of mixed metal and ligand contributions. Hence, the HOMO is destabilized in cyclohexane as compared to THF while the ligand-centered (LC) LUMO remained unaffected, resulting in a bathochromic shift in non-polar solvents. The increase in the extinction coefficient was observed in the high-energy region in various solvents is indicative of LC π - π^* transitions. Moreover, **DiPt-1** shows the most intense MLCT transition among all the dinuclear compounds, because the electron-rich nature of the thpy ligand greatly facilitates the electron donation from the cyclometalated Pt(II) center to the π^* orbitals of the ligands. There is no well-resolved MLCT peak for the ppy/FFppy based complexes. Compound **DiPt-2** exhibits weaker absorption than **DiPt-1**, with the featureless spectrum extending into the visible region (up to 450 nm). The two FFppy-based compounds have

similar absorption spectra, except that **DiPt-3b** has an extra peak at around 382 nm. This is consistent with the DFT calculations, which show that the two isomers have very similar electronic properties.

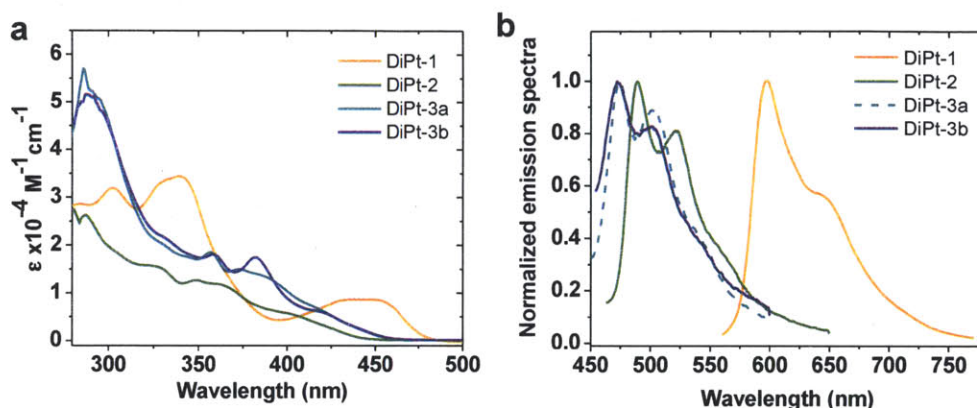


Figure 2.8. UV-vis absorption (left) and emission (right) spectra of the dinuclear Pt(II) compounds in THF ($\sim 10^{-6}$ M, under Ar).

All the compounds are emissive both in the solution and the solid phases at room temperature. Normalized photoluminescence spectra recorded in deoxygenated THF solutions are depicted in Figure 2.8. The emission bands for all compounds are highly structured even at room temperature, with vibronic progressions of $1226\text{-}1256 \text{ cm}^{-1}$. This indicates that the nature of the phosphorescence is mainly due to LC emission. The color of the phosphorescence is controlled by the cyclometalating ligands, varying from orange-red to cyan-blue in the sequence of thpy, ppy and FFppy. The emission of **DiPt-1** shows the lowest transition energy, with the emission maximum at 597 nm, which is attributed to the polarizability of the sulfur atoms and the electron rich nature of thpy ligands.³³ The photoluminescence spectra for **DiPt-3a** and **DiPt-3b** are almost identical, both blue shifted by 15 nm in comparison to that for **DiPt-2**. This hypsochromic shift is caused by fluorination at the 4- and 6-positions of the phenyl groups, as observed with

other Ir and Pt compounds bearing FFppy ligands.³³⁻³⁵ Lifetimes of the triplet excited states of these doubly metalated compounds are on the order of microseconds. The values are comparable to those of mononuclear compounds, such as (ppy)Pt(dmp) (8.9 μ s) and (FFppy)Pt(dmp) (8.1 μ s).³³ The presence of additional heavy atoms, platinum and iodine in particular, has little effect on the lifetimes.

Table 2.3. Selected photophysical data of **DiPt-1**, **DiPt-2**, **DiPt-3a**, and **DiPt-3b**

	Solution			Thin film	
	λ_{\max} [nm] ($\epsilon \times 10^{-3} \text{ M}^{-1} \text{ cm}^{-1}$)	λ_{em} [nm]	τ [ms]	λ_{em} [nm]	
DiPt-1	302(31.9), 339(34.4), 440(8.6)	597, 645	12.0	615	
DiPt-2	287(26.3), 325(15.7), 349(12.7), 400(5.8)	489, 521	8.8	566	
DiPt-3a	289(53.0), 357(18.6), 374(15.0), 415(7.2)	474, 501	8.0	574	
DiPt-3b	288(51.7), 358(18.1), 382(17.5), 420(6.0)	474, 501	8.2	576	

2.2.6 Aggregation-induced luminescence

In addition to the color tuning ability in solution, the luminescence properties in the solid state are also ligand dependent. The solid state photoluminescence spectra were measured with the target phosphors dispersed into the poly(methyl methacrylate) (PMMA) matrix. The emission color of **DiPt-1** remains indistinguishable in both fluid solutions and thin films. In contrast, the photoluminescence of the ppy and FFppy based complexes undergoes dramatic changes in the solid state. The emission color changes gradually from green to yellow with increasing dopant concentration (Figure 2.9). For instance, the emission band of **DiPt-3a** becomes red-shifted and broadened, with a new band growing at around 575 nm, when the concentration is higher than 0.5% by weight relative to PMMA. The ratio of the monomer and the excimer emission changes with the concentration, and the photoluminescence is completely dominated by the featureless

excimer emission with 20% of **DiPt-3a**. **DiPt-3b** has an even greater tendency to aggregate in the solid state, in agreement with the fact that **Pt-3b** showed lower solubility than **DiPt-3a** after crystallization. As seen in Figure 2.9, the aggregation-induced emission band is already present when the concentration of the compound is as low as 0.1%. With only 2% of dopant, **DiPt-3b** can achieve the same degree of aggregation as 20% of **DiPt-3b**. Additionally the monomer emission vanishes completely with 10% of **DiPt-3b**.

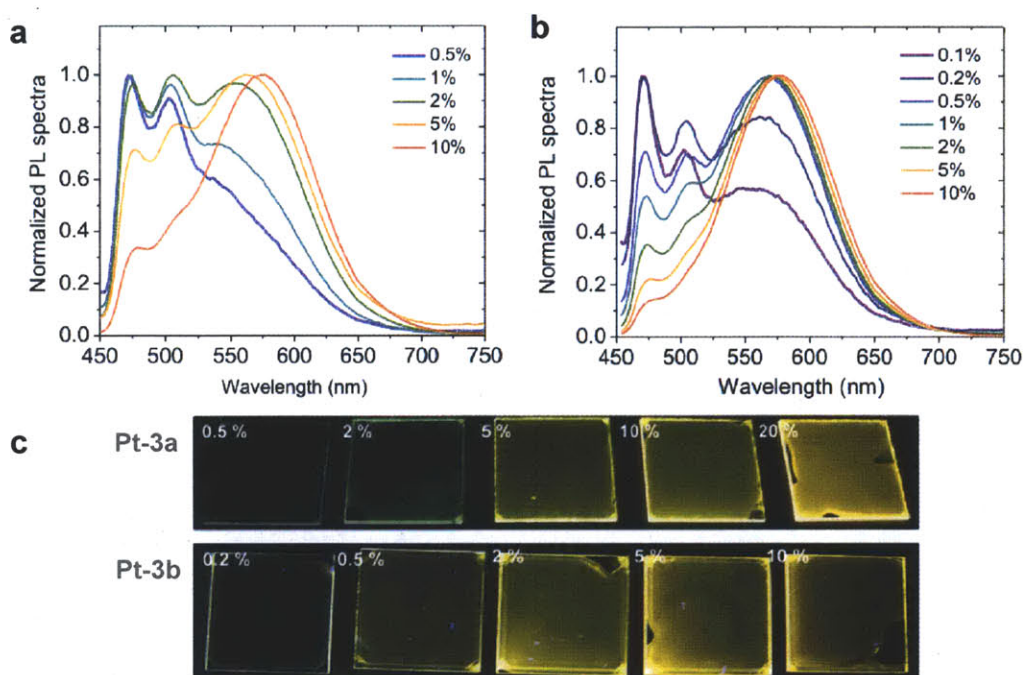


Figure 2.9. The photoluminescence spectra of **DiPt-3a** (a) and **DiPt-3b** (b) in PMMA thin films, and the images of the thin films taken under UV radiation (c).

The difference in the luminescence properties in the solid state can be explained in part by the distinct degree of intermolecular interaction in the solid state. The two molecules in the unit cell of **DiPt-1** form a loose pair without any intermolecular interactions. However, two of these pairs form an interdigitated tetrameric repeating unit,

through the stacking of the $[(C^{\wedge}N)Pt(N^{\wedge}N)]$ units. Figure 2.10 provides a schematic illustration of the overall intermolecular interactions. The blue and orange bars linked together by a grey dotted line represent two molecules from the same asymmetric unit. There are two types of Pt \cdots Pt separations along the one-dimensional array. The Pt \cdots Pt distance observed between molecules labeled by the same color is very short (3.25 Å), indicating strong metallophilic interactions. The Pt \cdots Pt separation is 5.35 Å between different colored molecules. Moreover, the $[(C^{\wedge}N)Pt(N^{\wedge}N)]$ units from different molecular pairs slip away from each other to accommodate weak Pt \cdots S interactions (3.72 Å). This type of Pt-S affinity has been observed in other compounds as well. For instance, neutral $[Pt(8-QNS)_2]$ (8-QNS = 8-quinolinethiolate) and cationic $[Pt(tpy)(Cl)]^+$ are stacked together by alternating Pt \cdots Pt (3.35 Å) and Pt \cdots S (3.85 Å) interaction.³⁶ The mismatch of the coordination disrupts potential Pt \cdots Pt and $\pi\cdots\pi$ interactions, and in turn prevents the formation of long-range conjugation.

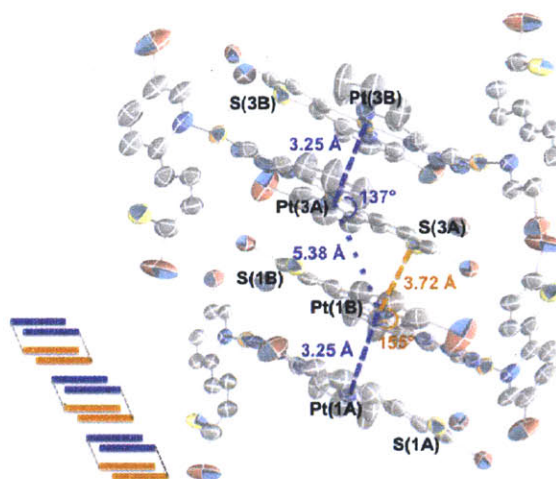


Figure 2.10. The packing diagram of DiPt-1. Thermal ellipsoids are drawn at the 50% probability level. All of the hexyl groups and hydrogen atoms are omitted for clarity, and only one of the disordered positions was shown.

In contrast, the intermolecular interaction for **DiPt-3b** is much stronger. The two molecules in the same unit cell are close to one another. The $[(C^{\wedge}N)Pt(N^{\wedge}N)]$ units sit almost on top of each other, with Pt \cdots Pt distances of 3.36 Å. These dimers stack in a head-to-tail fashion to form infinite chains as indicated in Figure 2.11. Although the Pt \cdots Pt separations (4.54 Å) between these dimeric structures are still larger than the sum of the van der Waals radii of two Pt atoms (3.55 Å), the $\pi\cdots\pi$ stacking interaction is much stronger than that of **DiPt-1**. This dissimilarity can be attributed to the FFppy ligands in **DiPt-3b**. This ligand has been widely used to promote formation of excimers or aggregated structures.^{37–39} Moreover, $[(C^{\wedge}N)Pt]$ units from the adjacent molecules are rotated from each other by roughly 90° to avoid the steric hindrance, wrapping the zig-zag columns formed by the $[(C^{\wedge}N)Pt(N^{\wedge}N)]$ moieties in a pseudo-helical fashion. They act as extended arms to hold the columns together through π - π interactions, with a plane-to-plane spacing of 3.30 Å.

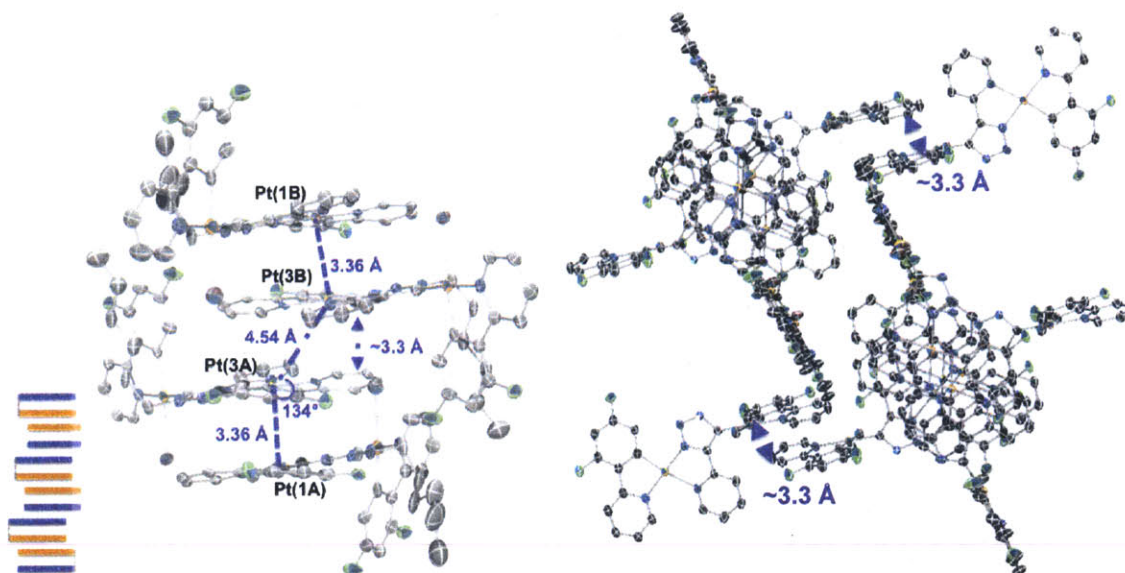


Figure 2.11. The packing diagram of **DiPt-3b**: side-view (left) and top-view (right). All of the hexyl groups and hydrogen atoms are omitted for clarity, and only one of the disordered positions was shown.

2.3 Experimental Section

General Methods and Instrumentation. All reactions were performed under an argon atmosphere, using oven-dried glassware and standard Schlenk techniques. ^1H , gCOSY, TOCSY, ROESY and $^{13}\text{C}\{^1\text{H}\}$ NMR spectra were recorded on either a Bruker 400 MHz or Varian 500 MHz spectrometer and referenced to the residual proton or carbon resonance of the deuterated solvent. ^{19}F NMR spectra were recorded on a Varian 300 MHz spectrometer and referenced to an external standard CFCl_3 (0 ppm). Electrospray ionization (ESI) high-resolution mass spectrometry (HRMS) was measured on a Bruker Daltonics APEXIV 4.7 Tesla Fourier Transform Ion Cyclotron Resonance Mass Spectrometer and the most abundant masses are reported.

UV-vis spectra were recorded on an Agilent 8453 diode-array spectrophotometer. Emission spectra were acquired on a SPEX Fluorolog fluorometer (model FL-321, 450 W xenon lamp) using either right-angle detection (solution measurements) or front-face detection (thin film measurements). All room temperature solution samples for emission spectra were degassed with Ar in an anaerobic cuvette. Solution photoluminescence quantum yields were determined against Coumarin-6 (ethanol, QY = 0.63) and Coumarin-343 (ethanol, QY = 0.63)⁴⁰ and corrected for solvent refractive index and absorption differences at the excitation wavelength. Thin films were prepared by spin-coating a chloroform solution of poly(methyl methacrylate) (PMMA) and the target compound (5-10 % w/w relative to PMMA). Perylene (PMMA film, QY = 0.98)⁴¹ or 9,10-diphenylanthracene (PMMA film, QY = 0.83)⁴² were used as the reference materials. Phosphorescence lifetimes were determined by time-resolved phosphorescence spectroscopy. The radiation source was an Oriel nitrogen laser (Model 79111) with a 5 ns

pulse width operating at approximately 25 Hz. The emitted light was dispersed in an Oriol MS-260i spectrograph with a 600 lines/mm grating. The detector was an Andor Technologies Intensified CCD camera (1024 x 128 pixels) with an onboard delay generator and a minimum gate width of 5 ns operating in full vertical binning mode and triggered by a TTL prepulse from the nitrogen laser. The detector was calibrated with a Hg(Ar) pencil-style calibration lamp. Solution data were acquired with a horizontal binning of 2 or 3. 15 spectra at different delay times after the laser pulse were taken per lifetime measurement, the integrated intensities of which were fitted to a single-exponential function.

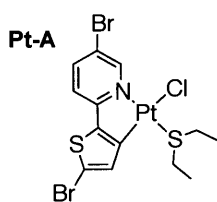
Materials and Synthesis. Potassium tetrachloroplatinate(II) (K_2PtCl_4) and copper(I) iodide (CuI) were purchased from Strem Chemicals. 2-Ethynylpyridine, 2-(2,4-difluorophenyl)pyridine (FFppy), NaH (60 % dispersion in mineral oil), and all other reagents were obtained from Aldrich Chemicals and used as received. Anhydrous tetrahydrofuran was obtained from a solvent purification system (Innovative Technologies). Triethylamine (TEA) and diisopropanolamine (DIPA) were distilled over sodium hydroxide pellets and stored under argon.

The Pt(II) precursor $Pt(ppy)Cl(SEt_2)$ (**Pt-B**) were synthesized from K_2PtCl_4 and corresponding ligands over two steps.²⁴ 5-bromo-2-(5-bromothiophen-2-yl)pyridine (thpy),⁴³ 2-(1-hexyl-1*H*-1,2,3-triazol-4-yl)-pyridine (trpy),⁴⁴ and 1-azidohexane⁴⁵ were prepared according to the literature methods.

CAUTION: There have been safety concerns about handling organoazides, especially the ones with short alkyl groups. All the organoazides used in this report were synthesized on small scales and handled with great care.

Preparation of Pt(thpy)Cl(SEt₂) (Pt-A). K₂PtCl₄ (207 mg, 0.5 mmol) and 5-bromo-2-(5-bromothiophen-2-yl)pyridine (319 mg, 1.0 mmol) in a 3:1 mixture of 2-ethoxyethanol (18 mL) and water (6 mL) was heated under argon for 16 hours at 75 °C. The reaction mixture was cooled down and poured into 150 mL water to yield an orange precipitate. The precipitate was filtered, washed with water, ethanol and diethyl ethyl. The Pt(II) μ -dichloro-bridged dimer was used without characterization due to its low solubility.

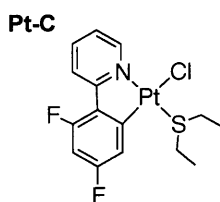
Et₂S (2.0 mL, 18 mmol) was added to the suspension of the Pt(II) μ -dichloro-bridged dimer in dry chloroform, and the mixture was stirred at 50 °C for 12 hours under Ar. The reaction mixture was cooled down and evaporated to yield an oily residue. The orange-red residue was chromatographed on silica gel using CH₂Cl₂/hexane (3:1) as the eluent to yield 115 mg (51% over two steps) of Pt(thpy)Cl(SEt₂) (Pt-A) as an orange powder.



HRMS (ESI): 603.8545 [calculated for (M-Cl)⁺: 603.8552]. ¹H NMR (400 MHz, CD₂Cl₂, ppm): 9.42 (dt, J = 1.8, J_{Pt-H} = 17.7 Hz, 1 H), 7.88 (dd, J = 2.1, 8.5 Hz, 1 H), 7.17 (d, J = 8.5 Hz, 1 H), 7.13 (t, J_{Pt-H} = 10.7 Hz, 4 H), 3.40 - 3.22 (m, 2 H), 3.06 - 2.82 (m, 2 H), 1.39 (t, J = 7.3 Hz, 6 H). ¹³C NMR (126 MHz, CD₂Cl₂, ppm): 13.4, 32.9, 114.6, 116.8, 118.3, 133.7, 140.5, 143.2, 146.0, 150.8, 160.3.

Preparation of Pt(FFppy)Cl(SEt₂) (Pt-C). K₂PtCl₄ (622 mg, 1.5 mmol) and 2-(2,4-difluorophenyl)pyridine (FFppy) (430 mg, 2.3 mmol) in a 3:1 mixture of 2-ethoxyethanol (15 mL) and water (5 mL) was heated under argon for 20 hours at 75 °C. The reaction mixture was cooled down and poured into 150 mL water to yield a light yellow precipitate. The precipitate was filtered, washed with water, ethanol and diethyl ethyl. The Pt(II) μ -dichloro-bridged dimer was used without characterization due to its low solubility.

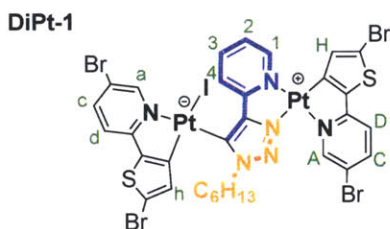
Et₂S (2.0 mL, 18 mmol) was added to the suspension of the Pt(II) μ -dichloro-bridged dimer in dry chloroform, and the mixture was stirred at 45 °C for 17 hours under Ar. The reaction mixture was cooled down and evaporated to yield an oily residue. The yellow red residue was chromatographed on silica gel with using CH₂Cl₂/hexane (2:1) as the eluent to yield 480 mg (67% over two steps) of Pt(FFppy)Cl(SEt₂) (Pt-C) as a light yellow powder.



HRMS (ESI): 475.0618 [calculated for (M-Cl)⁺: 475.0609]. ¹H NMR (400 MHz, CD₂Cl₂, ppm): 9.70 (dt, J = 5.8, J_{Pt-H} = 16.2 Hz, 1 H), 8.08 (d, J = 8.2 Hz, 1 H), 7.96 - 7.86 (m, 1 H), 7.32 (td, J = 9.6, J_{Pt-H} = 26.9 Hz, 1 H), 7.27 (t, J = 6.1 Hz, 1 H), 6.65 (dt, J = 2.4, 8.5 Hz, 1 H), 3.45 - 3.26 (m, 2 H), 3.09 - 2.85 (m, 2 H), 1.40 (t, J = 7.3 Hz, 6 H). ¹³C NMR (126 MHz, CD₂Cl₂, ppm): 13.4, 32.7, 100.2 (t, J_{C-F} = 30.5 Hz), 114.6 (dd, J_{C-F} = 19.6, 2.9 Hz), 122.7 (t, J_{C-F} = 13.8 Hz), 140.6 (d, J_{C-F} = 7.5 Hz), 144.6, 150.5, 159.9 (d, J_{C-F} = 12.7

Hz), 162.0 (d, $J_{C-F} = 12.7$ Hz), 162.7 (d, $J_{C-F} = 12.7$ Hz), 163.6 (d, $J_{C-F} = 6.9$ Hz), 164.7 (d, $J_{C-F} = 12.7$ Hz). ^{19}F NMR (282 MHz, CD_2Cl_2 , ppm): -110.40 (1 F), -107.76 (1 F).

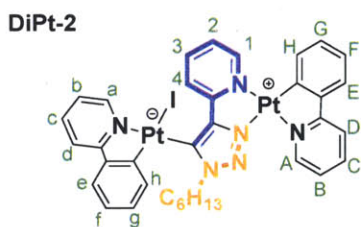
Preparation of DiPt-1. 2-Ethynylpyridine (30.9 mg, 0.3 mmol) in THF (6 mL)/ TEA (0.1 mL) was added to a mixture of CuI (57.1 mg, 0.3 mmol) and NaH (24 mg, 60% in mineral oil, 0.6 mmol), and the resulting suspension was stirred for 0.5 h at room temperature before 1-azidohexane (38.2 mg, 0.3 mmol) in THF (2 mL) was added. After stirring at room temperature for another 1.5 h, Pt(thpy)Cl(SET₂) (**Pt-A**, 153.3 mg, 0.24 mmol) was added to the mixture as a solid and heated to 45 °C for 20 h. After cooling, the solvent was removed under reduced pressure and the residue was purified by chromatography on silica gel, using CH_2Cl_2 /ethyl acetate (15:1) to collect the desired product **DiPt-1**. After recrystallization from THF/hexane, **DiPt-1** was isolated as an orange solid (45 mg, 27%).



HRMS (ESI): 1254.7565 [calculated for $(\text{M-I})^+$: 1254.7564]. ^1H NMR (400 MHz, CD_2Cl_2 , ppm): 10.16 (dd, $J=6.82, 1.00$ Hz, H^a), 9.87 (d, $J=5.30$ Hz, H^A), 9.41 (d, $J=7.33$ Hz, H^4), 8.93 (d, $J=6.06$ Hz, H^1), 7.86 - 7.94 (m, H^C and H^c), 7.82 (m, H^3 and H^D), 7.75 (d, $J=8.08$ Hz, H^d), 7.55 (d, $J=7.07$ Hz, H^e), 7.48 (d, $J=7.80$ Hz, H^E), 7.38 (d, $J=7.83$ Hz, H^H), 7.21 - 7.31 (m, H^b, H^B and H^G), 7.19 (t, $J=6.60$ Hz, H^2), 7.11 (t, $J=7.83$ Hz, H^F), 7.04 (t, $J=7.58$ Hz, H^f), 6.81 (t, $J=7.83$ Hz, H^E), 6.42 (dd, $J=6.80$ Hz, $J_{\text{Pt-H}}=32.80$, H^h), 4.77 - 4.90 (m, 1H- CH_2), 4.58 - 4.69 (m, 1H- CH_2), 1.98 - 2.25 (m, CH_2), 1.19 - 1.45 (m, 3 CH_2),

0.80 (t, $J=7.07$ Hz, CH_3). ^{13}C NMR (126 MHz, CD_2Cl_2 , ppm): 14.5, 23.4, 27.2, 29.7, 32.2, 55.3, 115.1, 116.1, 116.2, 116.6, 118.8, 119.2, 123.0, 124.9, 135.1, 135.3, 139.1, 140.5, 141.8, 142.7, 143.9, 144.1, 145.8, 148.5, 150.4, 152.5, 153.1, 154.6, 155.5, 160.4, 161.6.

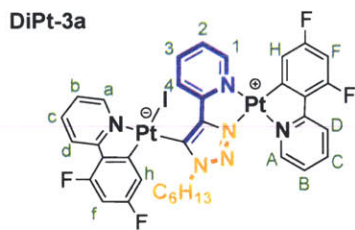
Preparation of DiPt-2. 2-Ethynylpyridine (20.6 mg, 0.2 mmol) in THF (6 mL)/ DIPA (0.1 mL) was added to a mixture of CuI (38.1 mg, 0.2 mmol) and NaH (16 mg, 60% in mineral oil, 0.4 mmol), and the resulting suspension was stirred for 0.5 h at room temperature before 1-azidohexane (30.5 mg, 0.24 mmol) in THF (2 mL) was added. After stirring at room temperature for another 1.5 h, Pt(ppy)Cl(SEt₂) (**Pt-B**, 75.9 mg, 0.16 mmol) was added to the mixture as a solid and heated to 45 °C for 20 h. The reaction was worked up following the procedure detailed for **DiPt-1**. The mixture was purified by column chromatography on silica gel, using CH_2Cl_2 /ethyl acetate (15:1~10:1). After recrystallization from CH_2Cl_2 /hexane, **DiPt-2** was isolated as an orange solid (44 mg, 52%).



HRMS (ESI): 927.2035 [calculated for $(\text{M}-\text{I})^+$: 927.2051]. ^1H NMR (400 MHz, CD_2Cl_2 , ppm): 10.16 (d, $J = 5.6$ Hz, H^a), 9.87 (d, $J = 5.3$ Hz, H^A), 9.41 (d, $J = 7.3$ Hz, H^4), 8.93 (d, $J = 6.1$ Hz, H^1), 7.97 - 7.86 (m, H^c and H^C), 7.86 - 7.78 (m, H^3 and H^d), 7.75 (d, $J = 8.1$ Hz, H^D), 7.55 (d, $J = 7.1$ Hz, H^e), 7.48 (d, $J = 7.3$ Hz, H^E), 7.38 (d, $J = 7.8$ Hz, H^H), 7.30 - 7.21 (m, H^b , H^B and H^G), 7.19 (t, $J = 7.6$ Hz, H^2), 7.11 (t, $J = 8.6$ Hz, H^F), 7.07 - 7.00 (m, $J = 9.3, 9.3$ Hz, H^f), 6.81 (dt, $J = 1.0, 7.5$ Hz, H^g), 6.42 (dd, $J = 6.8, J_{\text{Pt-H}} = 33.6$ Hz, H^h),

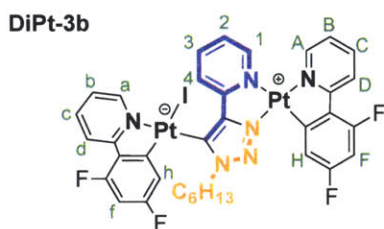
4.88 - 4.76 (m, 1H-CH₂), 4.68 - 4.55 (m, 1H-CH₂), 2.27 - 2.04 (m, CH₂), 1.48 - 1.15 (m, 3CH₂), 0.80 (t, J = 6.8 Hz, CH₃). ¹³C NMR (126 MHz, CD₂Cl₂, ppm): 23.1, 26.9, 29.6, 31.8, 118.9, 119.6, 122.6, 123.0, 123.2, 123.4, 123.6, 124.2, 124.4, 125.2, 130.1, 130.8, 133.7, 133.8, 138.6, 139.2, 140.0, 144.2, 145.5, 145.6, 146.7, 147.4, 150.1, 151.1, 152.6, 154.4, 155.7, 165.9, 167.9.

Preparation of DiPt-3a and DiPt-3b. 2-Ethynylpyridine (30.9 mg, 0.3 mmol) in THF (6 mL)/ TEA (0.1 mL) was added to a mixture of CuI (57.1 mg, 0.3 mmol) and NaH (24 mg, 60% in mineral oil, 0.6 mmol), and the resulting suspension was stirred for 0.5 h at room temperature before 1-azidohexane (38.2 mg, 0.3 mmol) in THF (2 mL) was added. After stirring at room temperature for another 1.5 h, Pt(FFppy)Cl(SEt₂) (**Pt-C**, 122.6 mg, 0.24 mmol) was added to the mixture as a solid and heated to 50 °C for 15 h. The reaction was worked up following the procedure detailed for **DiPt-1**. The mixture was first purified by column chromatography on silica gel, using CH₂Cl₂/hexane (3:1) as the eluent. Extra care should be taken in order to isolate **DiPt-3a** and **DiPt-3b**, respectively. Samples of the two isomers for photophysical studies were purified by preparative thin layer chromatography (PTLC) to remove trace amount contaminants using CH₂Cl₂/hexane (2:1) as the eluent. **DiPt-3a** was isolated as an orange solid (10 mg, 7%), after recrystallization from CH₂Cl₂/hexane.



HRMS (ESI): 999.1652 [calculated for (M-I)⁺: 999.1674]. ¹H NMR (400 MHz, CD₂Cl₂, ppm): 10.23 (d, J = 5.56 Hz, H^a), 9.91 (d, J = 5.81 Hz, H^A), 9.33 (d, J = 7.83 Hz, H⁴), 8.80 (d, J = 5.56 Hz, H¹), 8.18 (d, J = 8.34 Hz, H^d), 8.01 (d, J = 1.00 Hz, H^D), 7.87 - 7.96 (m, H^c, H³ and H^C), 7.24 - 7.37 (m, H^b, H² and H^B), 6.86 (d, J = 9.09 Hz, H^H), 6.65 (td, J = 10.60, 1.00 Hz, H^F), 6.54 (td, J = 10.10, 1.00 Hz, H^f), 5.95 (dd, J = 8.72, J_{Pt-H} = 37.9 Hz, H^h), 4.80 (m, 1H-CH₂), 4.57 - 4.65 (m, 1H-CH₂), 2.06 - 2.24 (m, CH₂), 1.19 - 1.47 (m, 3CH₂), 0.80 (t, J = 6.82 Hz, CH₃). ¹³C NMR (126 MHz, CD₂Cl₂, ppm): 14.3, 23.0, 26.7, 29.6, 31.7, 54.6, 99.4 (t, J = 29.9 Hz), 101.1 (t, J = 27.1 Hz), 115.6 (d, J = 17.9 Hz), 116.6 (d, J = 19.0 Hz), 122.4 - 123.2 (m), 123.5 (t, J = 28.2 Hz), 129.3 - 129.5 (m), 130.5 - 130.8 (m), 139.2, 139.7, 140.5, 144.6, 148.1 (d, J = 6.9 Hz), 150.1, 150.5 (d, J = 22.5 Hz), 150.7, 152.7, 154.8, 155.3, 159.2 - 165.3 (m). ¹⁹F NMR (282 MHz, CD₂Cl₂, d ppm): -110.68 (1 F), -110.30 (1 F), -109.03 (1 F), -106.97 (1 F).

DiPt-3b was isolated as a yellow solid (39 mg, 29%), after recrystallization from CH₂Cl₂/hexane.

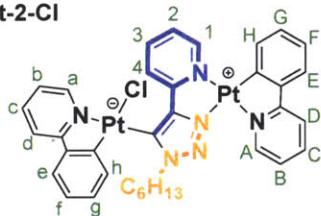


HRMS (ESI): 999.1656 [calculated for (M-I)⁺: 999.1674]. ¹H NMR (400 MHz, CD₂Cl₂, ppm): 10.22 (d, J = 5.56 Hz, H^a), 9.28 (d, J = 7.83 Hz, H⁴), 8.49 - 8.56 (m, H¹ and H^A), 8.18 (d, J = 8.34 Hz, H^d), 8.11 (d, J = 8.34 Hz, H^D), 7.97 - 8.05 (m, H^H and H^C), 7.93 (t, J = 7.96 Hz, H^c), 7.73 (t, J = 7.58 Hz, H³), 7.37 - 7.44 (m, H² and H^B), 7.30 (t, J = 6.57 Hz, H^b), 6.49 - 6.62 (m, H^F and H^f), 5.94 (dd, J = 8.84, J_{Pt-H} = 35.9 Hz, H^h), 4.86 (m, 1H-CH₂),

4.50 - 4.58 (m, 1H-CH₂), 3.66 (m, CH₂), 1.15 - 1.41 (m, 3CH₂), 0.80 (t, J=6.95 Hz, CH₃).
¹³C NMR (126 MHz, CD₂Cl₂, ppm): 14.3, 23.0, 26.8, 29.4, 31.7, 55.0, 99.4 (t, J = 28.2 Hz), 100.9 (t, J = 28.2 Hz), 115.6 (d, J = 19.6 Hz), 117.8 (d, J = 24.2 Hz), 122.7 (t, J = 21.3 Hz), 123.6 (t, J = 20.7 Hz), 124.0, 139.2, 139.4, 140.3, 143.3 - 143.6 (m), 144.3 - 144.6 (m), 148.0, 150.1, 151.0 - 151.4 (m), 153.2 - 153.5 (m), 154.7 - 155.0, 162.8, 165.1. ¹⁹F NMR (282 MHz, CD₂Cl₂, d ppm): -111.54, -110.80, -108.71, -107.49.

Preparation of DiPt-2-Cl. 2-(1-hexyl-1*H*-1,2,3-triazol-4-yl)-pyridine (46.1 mg, 0.2 mmol) was dissolved in THF (5 mL), and was added freshly prepared LDA (0.1 M, 2 mL, 0.2 mmol) at -30 °C. The mixture was slowly warmed up to 0 °C. After stirring at 0 °C for 1 h, Pt(ppy)Cl(SEt₂) (**Pt-B**, 95.0 mg, 0.2 mmol) was added. The reaction was brought to room temperature slowly and stirred for another hour before quenched with NH₄Cl (aq). The solvent was removed under reduced pressure and the residue was extracted with ethyl acetate, and dried with MgSO₄. The oily orange residue from the extract was purified by chromatography on silica gel, using CH₂Cl₂/ethyl acetate (15:1) as the eluent to collect the desired product. After recrystallization from CH₂Cl₂/hexane, **DiPt-2-Cl** was isolated as light yellow crystals (36 mg, 37%).

DiPt-2-Cl



HRMS (ESI): 927.2077 [calculated for (M-Cl)⁺: 927.2051]. ¹H NMR (400 MHz, CD₂Cl₂, ppm): 0.79 (d, J=4.70 Hz, 4 H), 1.18 - 1.32 (m, 7 H), 1.38 (br. s., 3 H), 2.05 - 2.26 (m, 3 H), 4.59 (d, J=6.00 Hz, 1 H), 4.92 (d, J=6.00 Hz, 1 H), 6.44 - 6.67 (m, 1 H), 6.75 (d,

$J=5.02$ Hz, 1 H), 6.92 - 7.05 (m, 2 H), 7.06 - 7.23 (m, 3 H), 7.29 (br. s., 1 H), 7.36 (br. s., 2 H), 7.54 (br. s., 1 H), 7.68 (br. s., 1 H), 7.79 (d, $J=3.24$ Hz, 1 H), 7.83 - 7.95 (m, 2 H), 8.59 - 8.90 (m, 1 H), 8.81 (br. s., 1 H), 9.43 (br. s., 1 H), 9.70 (br. s., 1 H), 9.77 (br. s., 1 H). ^{13}C NMR (126 MHz, CD_2Cl_2 , ppm): 14.4, 23.1, 26.8, 30.2, 31.8, 53.6, 118.6, 119.8, 122.2, 122.7, 122.9, 123.0, 123.1, 124.1, 124.5, 125.0, 130.0, 133.7, 133.1, 135.2, 139.0, 140.0, 143.3, 144.3, 145.4, 146.5, 147.3, 149.0, 150.7, 151.0, 152.1, 155.4, 166.1, 167.5.

Crystal Structure Determination:

Low-temperature diffraction data (ϕ - and ω -scans) were collected on a Bruker-AXS X8 Kappa Duo diffractometer coupled to a Smart Apex2 CCD detector with Mo K_α radiation ($\lambda = 0.71073$ Å) from an $I\mu\text{S}$ micro-source. Structures were solved by direct methods using SHELXS⁴⁶ and refined against F^2 on all data by full-matrix least squares with SHELXL-97,⁴⁷ following established refinement strategies.⁴⁸ All non-hydrogen atoms were refined anisotropically. All hydrogen atoms were included in the model at geometrically calculated positions and refined using a riding model. The isotropic displacement parameters of all hydrogen atoms were fixed to 1.2 times the U value of the atoms they are linked to (1.5 times for methyl groups). All disordered atoms were refined with the help of similarity restraints on 1,2- and 1,3- distances and displacement parameters as well as rigid bond restraints for anisotropic displacement parameters.

Dark red single crystals of **DiPt-1** (X11089) were obtained by slow diffusion of hexane into the saturated THF solution. It crystallizes in the monoclinic space group $P2_1/n$ with two molecules in the asymmetric unit along with 1.54 molecules of THF

which are located at three independent positions. One of the ligands as well as the alkyl chain, on each platinum complex, was modeled as disordered over two positions. All atoms in the disordered aromatic ligand were restrained to be flat within 0.1 \AA^3 . The anisotropic displacement parameters for the eight bromine atoms involved in disorders were constrained to be pairwise equivalent. Two half-occupied THF molecules are located near inversion centers and are disordered accordingly. The third partially occupied THF molecule clashes with the second component of one of the disordered alkyl groups and its occupancy was constrained to be equivalent to the first component of that alkyl group. A direct result of this solvent disorder is the non-integer number of THF molecules per asymmetric unit and the non-integer numbers for the elements C, H, and O in the empirical formula.

Light yellow needle-like single crystals of **DiPt-3b** (X11075) were grown from slow evaporation of the dichloromethane/hexane solution. It crystallizes in the triclinic space group P-1 with two molecules in the asymmetric unit along with two molecules of dichloromethane. One of the two dichloromethane molecules is disordered over two positions. Two of the three ligands on each platinum complex were modeled as two part disorders. In addition to similarity restraints, the anisotropic displacement parameters for nearly overlapping disordered atoms (that is N1/N1A, N9/N9A, N10/N10A, C12/12A, C13/C13A, N7/N7A, N8/N8A, C55/C55A, C5/C5A, C54/C54A, C62/C62A, and F2/F2A) were constrained to be pairwise equivalent. And all aromatic rings were restrained to be flat within 0.1 \AA^3 . The crystal was non-merohedrally twinned. Two independent orientation matrices for the unit cell were determined using the program CELL_NOW,⁴⁹ and data reduction taking into account the twinning was performed with SAINT.⁵⁰ The

program TWINABS⁵¹ was used to perform absorption correction and scaling, and to set up the HKLF5 format file for structure refinement. The twin ratio was refined freely and converged at a value of 0.4648(4).

Computational Details. Ground-state geometries of **DiPt-1** and **DiPt-2** was optimized by DFT calculations, which were performed using the Gaussian03 software (Gaussian Inc.)⁵² with a B3LYP exchange-correlation functional. The LANL2DZ basis set under an effective core potential was used for Pt, S, and I. The initial geometries of the *trans* pyridyl isomers were based on simplified X-ray structures of **DiPt-1**, with the hexyl groups replaced with methyl groups and Br atoms with H atoms, and optimized without any constraints. The initial geometries of the *cis* pyridyl isomers were based on simplified X-ray structures of **DiPt-3b**, with the hexyl groups replaced with methyl groups and F atoms with H atoms, and optimized without any constraints.

2.4 References

- (1) Yersin, H. *Highly efficient OLEDs with phosphorescent materials*; Wiley-VCH, 2007.
- (2) Zhao, Q.; Li, F.; Huang, C. *Chem. Soc. Rev.* **2010**, *39*, 3007–3030.
- (3) Guerchais, V.; Fillaut, J.-L. *Coord. Chem. Rev.* **2011**, *255*, 2448–2457.
- (4) Lo, K. K.-W.; Hui, W.-K.; Chung, C.-K.; Tsang, K. H.-K.; Ng, D. C.-M.; Zhu, N.; Cheung, K.-K. *Coord. Chem. Rev.* **2005**, *249*, 1434–1450.

- (5) Lo, K. K.-W.; Tsang, K. H.-K.; Sze, K.-S.; Chung, C.-K.; Lee, T. K.-M.; Zhang, K. Y.; Hui, W.-K.; Li, C.-K.; Lau, J. S.-Y.; Ng, D. C.-M.; Zhu, N. *Coord. Chem. Rev.* **2007**, *251*, 2292–2310.
- (6) Zhao, Q.; Huang, C.; Li, F. *Chem. Soc. Rev.* **2011**, *40*, 2508–2524.
- (7) Lo, K. K.-W.; Hui, W.-K.; Chung, C.-K.; Tsang, K. H.-K.; Lee, T. K.-M.; Li, C.-K.; Lau, J. S.-Y.; Ng, D. C.-M. *Coord. Chem. Rev.* **2006**, *250*, 1724–1736.
- (8) Albrecht, M. *Chem. Rev.* **2009**, *110*, 576–623.
- (9) You, Y.; Park, S. Y. *Dalton Trans.* **2009**, 1267–1282.
- (10) Lowry, M. S.; Bernhard, S. *Chem. Eur. J* **2006**, *12*, 7970–7977.
- (11) Gather, M. C.; Köhnen, A.; Meerholz, K. *Adv. Mater.* **2010**, *23*, 233–248.
- (12) Wang, Q.; Ma, D. *Chem. Soc. Rev.* **2010**, *39*, 2387–2398.
- (13) Meldal, M.; Tornøe, C. W. *Chem. Rev.* **2008**, *108*, 2952–3015.
- (14) Struthers, H.; Mindt, T. L.; Schibli, R. *Dalton Trans.* **2010**, *39*, 675–696.
- (15) Schuster, E. M.; Botoshansky, M.; Gandelman, M. *Angew. Chem. Int. Ed.* **2008**, *47*, 4555–4558.
- (16) Schuster, E. M.; Nisnevich, G.; Botoshansky, M.; Gandelman, M. *Organometallics* **2009**, *28*, 5025–5031.
- (17) Schuster, E. M.; Botoshansky, M.; Gandelman, M. *Organometallics* **2009**, *28*, 7001–7005.
- (18) Felici, M.; Contreras-Carballada, P.; Vida, Y.; Smits, J. M. M.; Nolte, R. J. M.; De Cola, L.; Williams, R. M.; Feiters, M. C. *Chem. Eur. J.* **2009**, *15*, 13124–13134.
- (19) Juricek, M.; Felici, M.; Contreras-Carballada, P.; Lauko, J.; Bou, S. R.; Kouwer, P. H. J.; Brouwer, A. M.; Rowan, A. E. *J. Mater. Chem.* **2011**, *21*, 2104–2111.
- (20) Beyer, B.; Ulbricht, C.; Escudero, D.; Friebe, C.; Winter, A.; González, L.; Schubert, U. S. *Organometallics* **2009**, *28*, 5478–5488.
- (21) Liu, S.; Müller, P.; Takase, M. K.; Swager, T. M. *Inorg. Chem.* **2011**, *50*, 7598–7609.
- (22) Vicente, J.; Chicote, M.-T.; Abrisqueta, M.-D.; Jones, P. G. *Organometallics* **1997**, *16*, 5628–5636.
- (23) Angell, Y.; Burgess, K. *Angew. Chem., Int. Ed.* **2007**, *46*, 3649–3651.
- (24) Thomas, S. W.; Venkatesan, K.; Müller, P.; Swager, T. M. *J. Am. Chem. Soc.* **2006**, *128*, 16641–16648.
- (25) Chassot, L.; Mueller, E.; Von Zelewsky, A. *Inorg. Chem.* **1984**, *23*, 4249–4253.
- (26) Jolliet, P.; Gianini, M.; von Zelewsky, A.; Bernardinelli, G.; Stoeckli-Evans, H. *Inorg. Chem.* **1996**, *35*, 4883–4888.
- (27) Fukuzawa, S.; Oki, H.; Hosaka, M.; Sugasawa, J.; Kikuchi, S. *Org. Lett.* **2007**, *9*, 5557–5560.
- (28) Stradiotto, M.; Hesp, K. D.; Lundgren, R. J. *Angew. Chem. Int. Ed.* **2010**, *49*, 494–512.
- (29) Sue, T.; Sunada, Y.; Nagashima, H. *Eur. J. Inorg. Chem.* **2007**, *2007*, 2897–2908.

- (30) Hirani, B.; Li, J.; Djurovich, P. I.; Yousufuddin, M.; Oxgaard, J.; Persson, P.; Wilson, S. R.; Bau, R.; Goddard, W. A.; Thompson, M. E. *Inorg. Chem.* **2007**, *46*, 3865–3875.
- (31) Rausch, A. F.; Monkowius, U. V.; Zabel, M.; Yersin, H. *Inorg. Chem.* **2010**, *49*, 7818–7825.
- (32) Cheney, B. V. *J. Am. Chem. Soc.* **1968**, *90*, 5386–5390.
- (33) Brooks, J.; Babayan, Y.; Lamansky, S.; Djurovich, P. I.; Tsyba, I.; Bau, R.; Thompson, M. E. *Inorg. Chem.* **2002**, *41*, 3055–3066.
- (34) Tamayo, A. B.; Alleyne, B. D.; Djurovich, P. I.; Lamansky, S.; Tsyba, I.; Ho, N. N.; Bau, R.; Thompson, M. E. *J. Am. Chem. Soc.* **2003**, *125*, 7377–7387.
- (35) Baranoff, E.; Curchod, B. F. E.; Monti, F.; Steimer, F.; Accorsi, G.; Tavernelli, I.; Rothlisberger, U.; Scopelliti, R.; Grätzel, M.; Nazeeruddin, M. K. *Inorg. Chem.* **2011**, *51*, 799–811.
- (36) Tzeng, B.-C.; Lee, G.-H.; Peng, S.-M. *Inorg. Chem. Commun.* **2003**, *6*, 1341–1343.
- (37) D’Andrade, B. W.; Brooks, J.; Adamovich, V.; Thompson, M. E.; Forrest, S. R. *Adv. Mater.* **2002**, *14*, 1032–1036.
- (38) Adamovich, V.; Brooks, J.; Tamayo, A.; Alexander, A. M.; Djurovich, P. I.; D’Andrade, B. W.; Adachi, C.; Forrest, S. R.; Thompson, M. E. *New J. Chem.* **2002**, *26*, 1171–1178.
- (39) Williams, E. L.; Haavisto, K.; Li, J.; Jabbour, G. E. *Adv. Mater.* **2007**, *19*, 197–202.
- (40) Reynolds, G. A.; Drexhage, K. H. *Opt. Commun.* **1975**, *13*, 222–225.
- (41) Melhuish, W. H. *J. Phys. Chem.* **1961**, *65*, 229–235.
- (42) Osaheni, J. A.; Jenekhe, S. A. *J. Am. Chem. Soc.* **1995**, *117*, 7389–7398.
- (43) Venkatesan, K.; Kouwer, P. H. J.; Yagi, S.; Muller, P.; Swager, T. M. *J. Mater. Chem.* **2008**, *18*, 400–407.
- (44) Fletcher, J. T.; Bumgarner, B. J.; Engels, N. D.; Skoglund, D. A. *Organometallics* **2008**, *27*, 5430–5433.
- (45) Lieber, E.; Chao, T. S.; Rao, C. N. R. *J. Org. Chem.* **1957**, *22*, 238–240.
- (46) Sheldrick, G. M. *Acta Crystallogr., Sect. A* **2007**, *64*, 112–122.
- (47) Sheldrick, G. M. *Acta Crystallogr., Sect. A* **1990**, *46*, 467–473.
- (48) Müller, P. *Crystallogr. Rev.* **2009**, *15*, 57–83.
- (49) Sheldrick, G. M. *CELL_NOW*; University of Göttingen: Germany, 2007.
- (50) Bruker *SAINT*; Bruker-AXS Inc.: Madison, Wisconsin, USA, 2007.
- (51) Sheldrick, G. M. *TWINABS*; University of Göttingen: Germany, 2007.
- (52) Frisch, M. J.; Trucks, G. W.; Schlegel, H. B.; Scuseria, G. E.; Robb, M. A.; Cheeseman, J. R.; Montgomery, Jr., J. A.; Vreven, T.; Kudin, K. N.; Burant, J. C.; Millam, J. M.; Iyengar, S. S.; Tomasi, J.; Barone, V.; Mennucci, B.; Cossi, M.; Scalmani, G.; Rega, N.; Petersson, G. A.; Nakatsuji, H.; Hada, M.; Ehara, M.; Toyota, K.; Fukuda, R.; Hasegawa, J.; Ishida, M.; Nakajima, T.; Honda, Y.; Kitao, O.; Nakai, H.; Klene, M.; Li, X.; Knox, J. E.; Hratchian, H. P.; Cross, J. B.; Bakken,

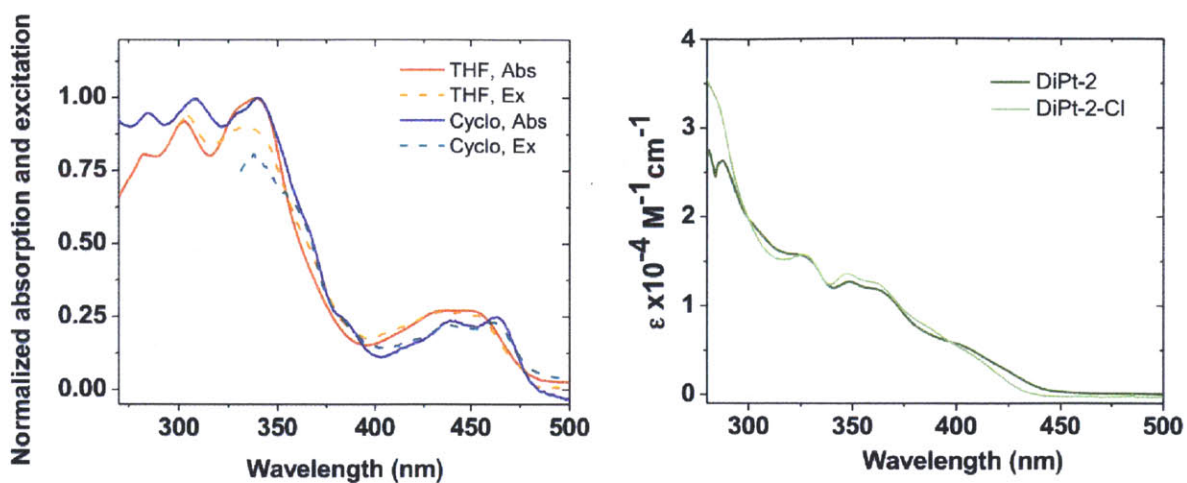
V.; Adamo, C.; Jaramillo, J.; Gomperts, R.; Stratmann, R. E.; Yazyev, O.; Austin, A. J.; Cammi, R.; Pomelli, C.; Ochterski, J. W.; Ayala, P. Y.; Morokuma, K.; Voth, G. A.; Salvador, P.; Dannenberg, J. J.; Zakrzewski, V. G.; Dapprich, S.; Daniels, A. D.; Strain, M. C.; Farkas, O.; Malick, D. K.; Rabuck, A. D.; Raghavachari, K.; Foresman, J. B.; Ortiz, J. V.; Cui, Q.; Baboul, A. G.; Clifford, S.; Cioslowski, J.; Stefanov, B. B.; Liu, G.; Liashenko, A.; Piskorz, P.; Komaromi, I.; Martin, R. L.; Fox, D. J.; Keith, T.; Al-Laham, M. A.; Peng, C. Y.; Nanayakkara, A.; Challacombe, M.; Gill, P. M. W.; Johnson, B.; Chen, W.; Wong, M. W.; Gonzalez, C.; and Pople, J. A. *Gaussian 03, revision C.02*; Gaussian, Inc.: Wallingford, CT, 2004.

Appendix for Chapter 2

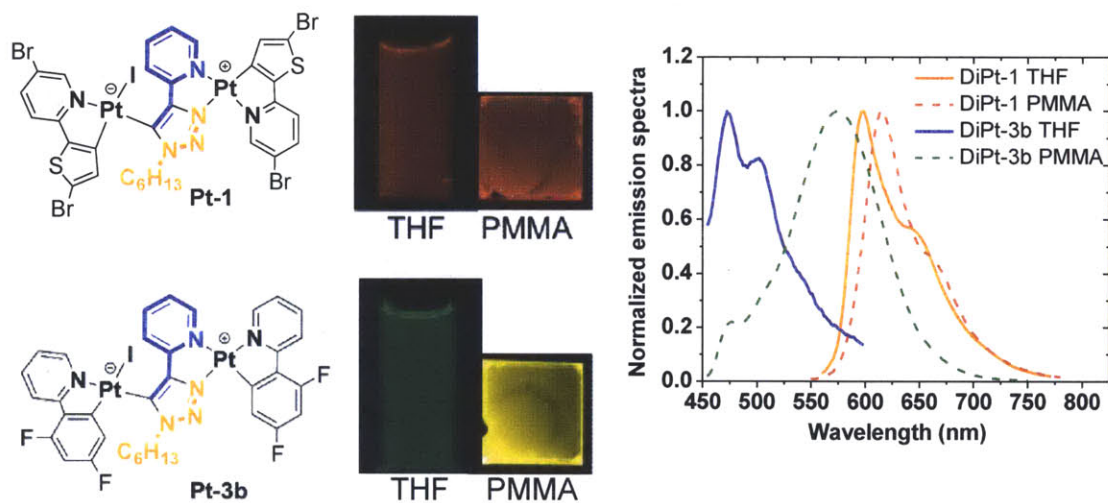
X-ray Crystallography
Photophysical properties
NMR spectra

Crystallographic data for compounds **DiPt-1** and **DiPt-3b**

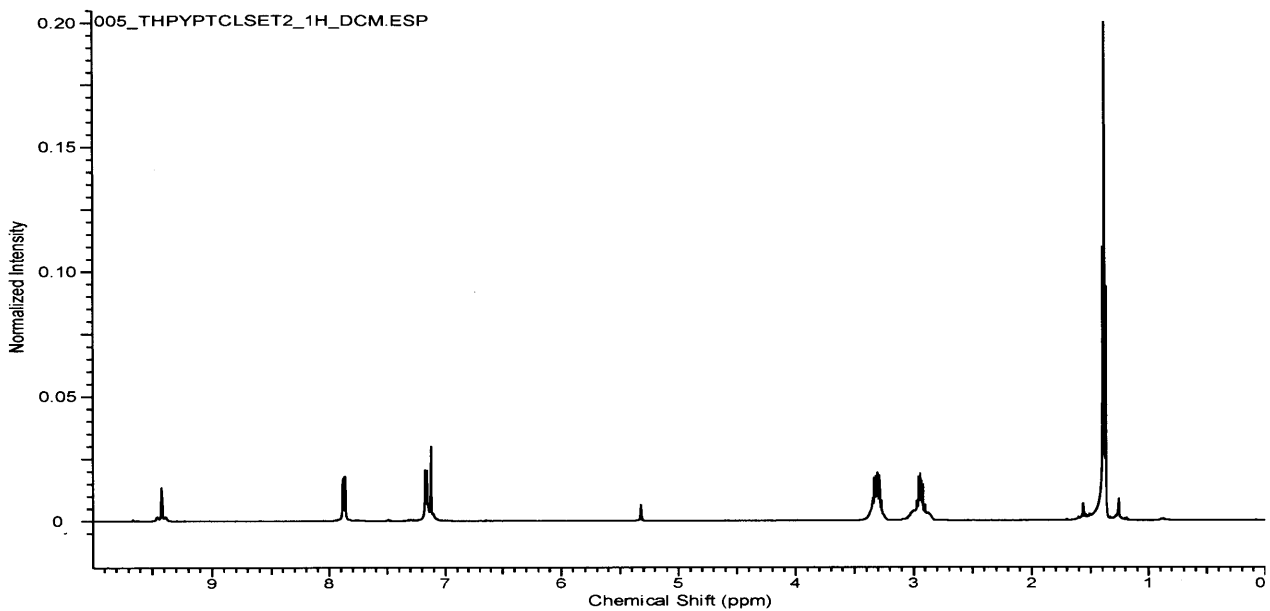
Identification code	DiPt-1	DiPt-3b
Empirical formula	C _{34.09} H _{31.18} Br ₄ I N ₆ O _{0.77} Pt ₂ S ₂	C ₃₆ H ₃₁ Cl ₂ F ₄ I N ₆ Pt ₂
Formula weight	1438.07	1211.65
Temperature	100(2) K	100(2) K
Wavelength	0.71073 Å	0.71073 Å
Crystal system	Monoclinic	Triclinic
Space group	P2(1)/n	P-1
Unit cell dimensions	a = 15.3011(11) Å b = 28.749(2) Å c = 19.7328(14) Å a = 90° b = 103.889(2)° g = 90°	a = 14.2235(15) Å b = 16.6299(18) Å c = 17.8419(19) Å a = 65.616(3)° b = 74.681(3)° g = 78.606(3)°
Volume	8426.4(11) Å ³	3688.4(7) Å ³
Z	8	4
Density (calculated)	2.267 Mg/m ³	2.182 Mg/m ³
Absorption coefficient	11.293 mm ⁻¹	8.616 mm ⁻¹
F(000)	5319	2272
Crystal size	0.30 x 0.08 x 0.08 mm ³	0.35 x 0.05 x 0.05 mm ³
Theta range for data collection	1.52 to 26.37° -19<=h<=19, -35<=k<=35, -24<=l<=24	1.28 to 30.57° -19<=h<=20, -21<=k<=23, 0<=l<=25
Index ranges		
Reflections collected	229127	22545
Independent reflections	17227 [R(int) = 0.0522]	22545 [R(int) = 0.0000]
Completeness to theta = 30.57°	100.00%	99.60%
Absorption correction	Semi-empirical from equivalents	Semi-empirical from equivalents
Max. and min. transmission	0.4653 and 0.1327	0.6726 and 0.1524
Refinement method	Full-matrix least-squares on F ²	Full-matrix least-squares on F ²
Data / restraints / parameters	17227 / 2051 / 1276	22545 / 3768 / 1438
Goodness-of-fit on F ²	1.079	1.08
Final R indices [I>2sigma(I)]	R1 = 0.0577, wR2 = 0.1466	R1 = 0.0369, wR2 = 0.0776
R indices (all data)	R1 = 0.0868, wR2 = 0.1743	R1 = 0.0520, wR2 = 0.0853
Largest diff. peak and hole	4.696 and -2.255 e.Å ⁻³	2.683 and -2.692 e.Å ⁻³



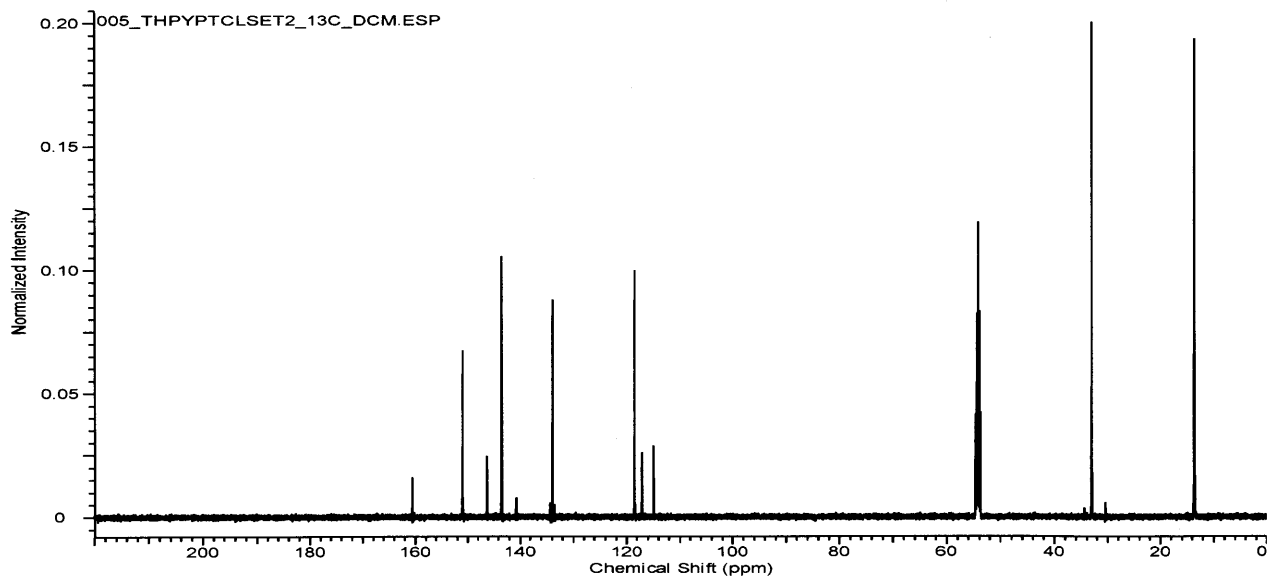
UV-vis and excitation spectra of **DiPt-1** in THF and cyclohexane (left); UV-vis spectra of **DiPt-2** and **DiPt-2-Cl** in THF (right).



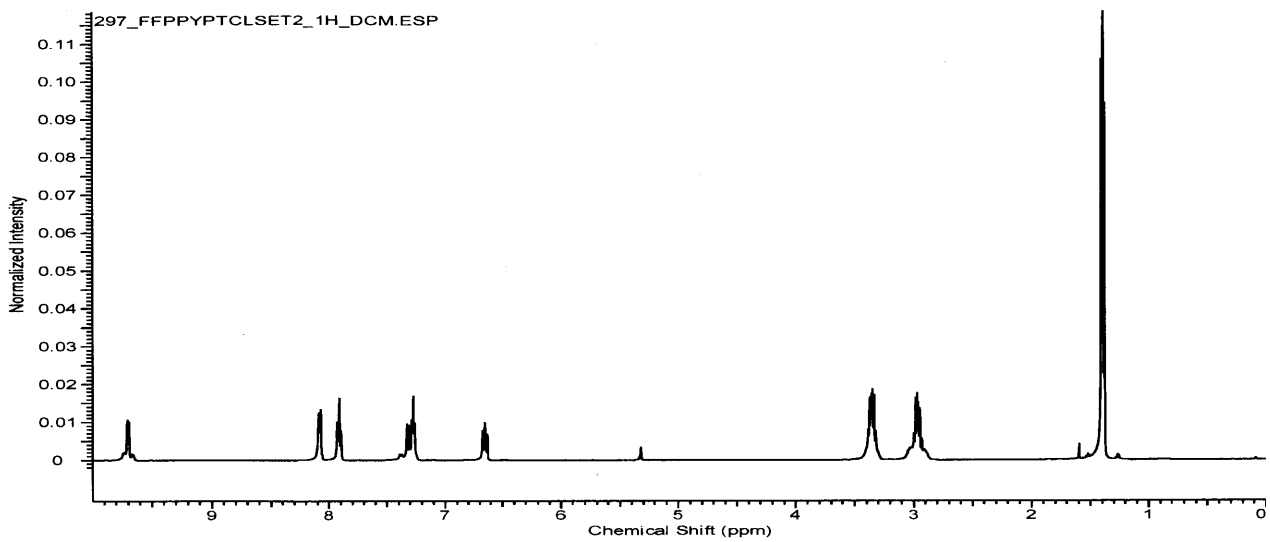
Emission spectra of **DiPt-1** and **DiPt-3b** in THF and the solid state.



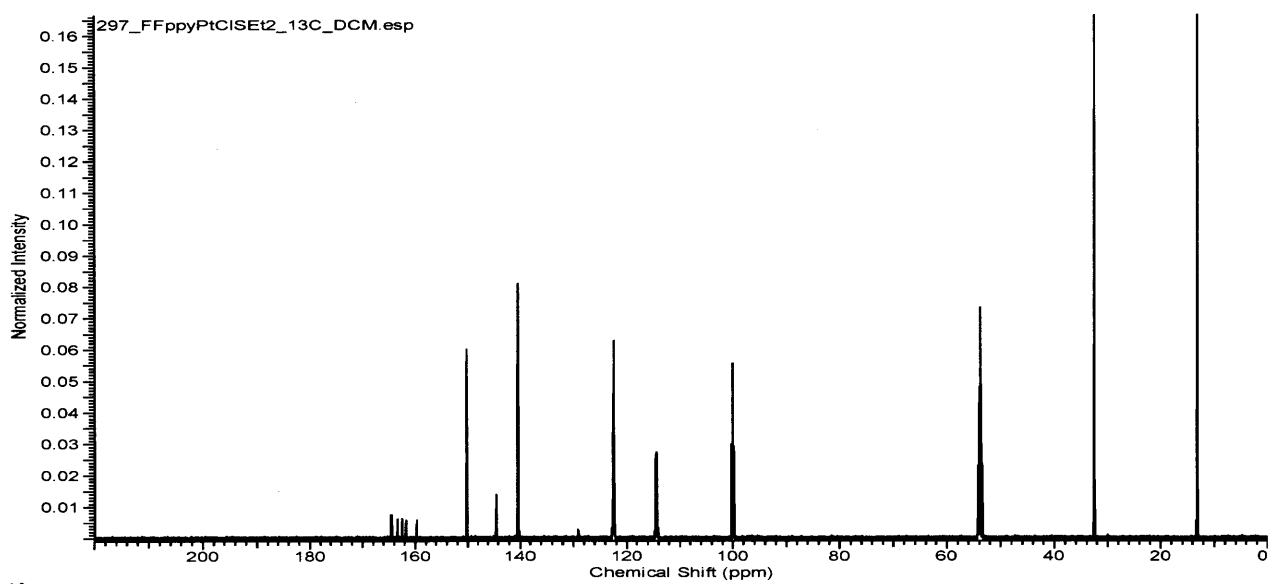
^1H NMR of **Pt-A** in CD_2Cl_2



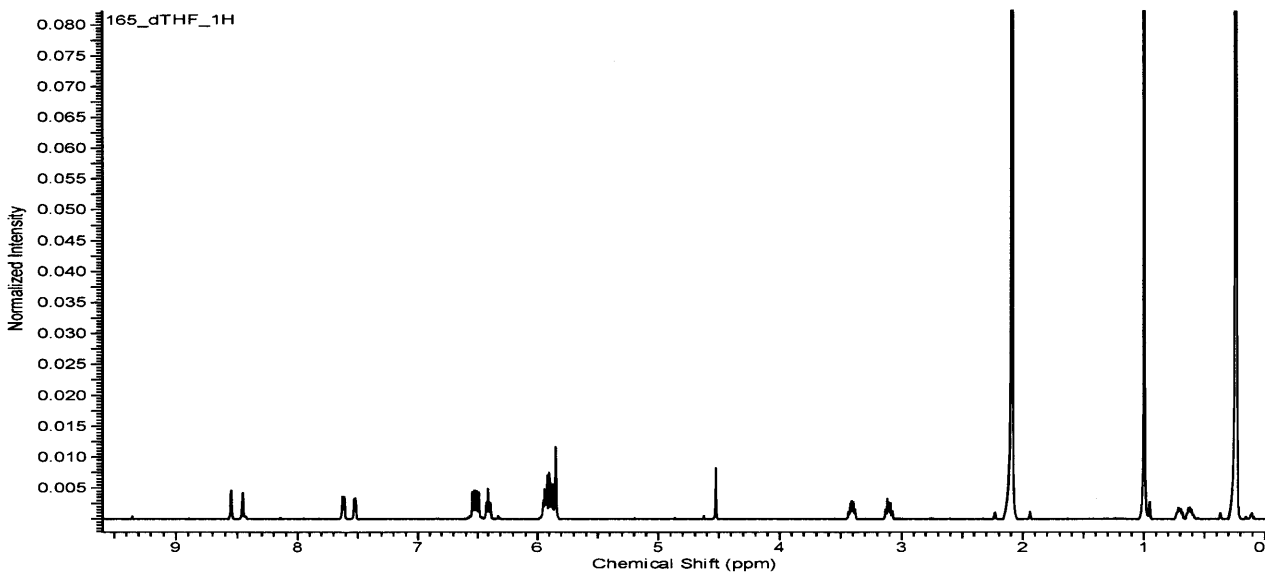
^{13}C NMR of **Pt-A** in CD_2Cl_2



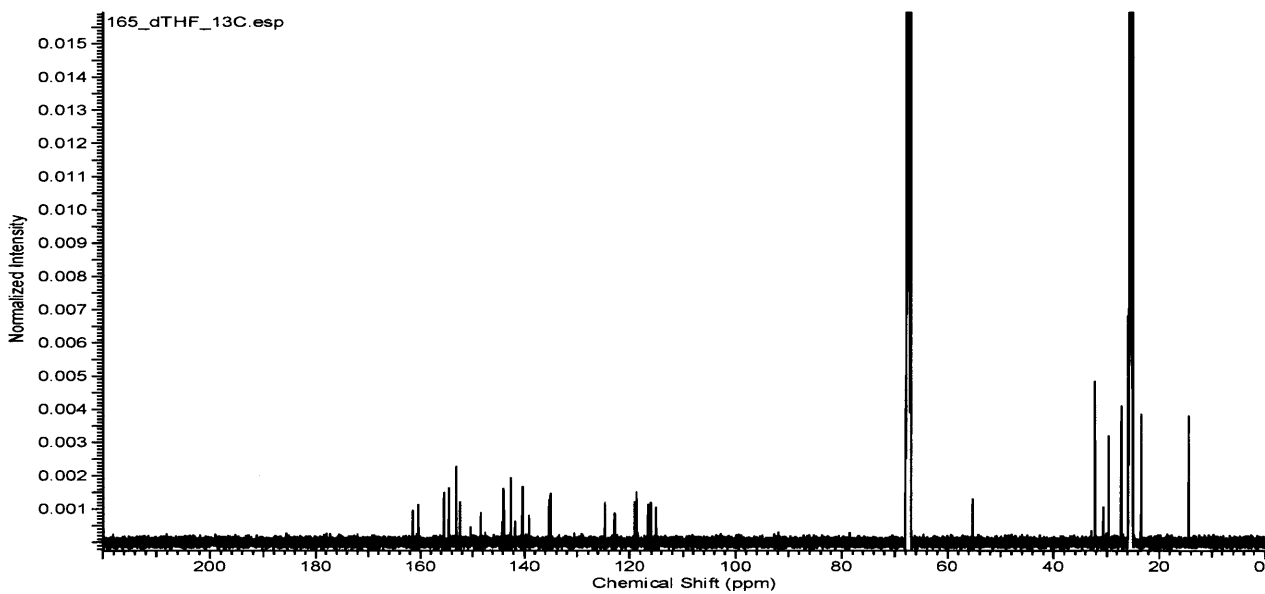
^1H NMR of **Pt-C** in CD_2Cl_2



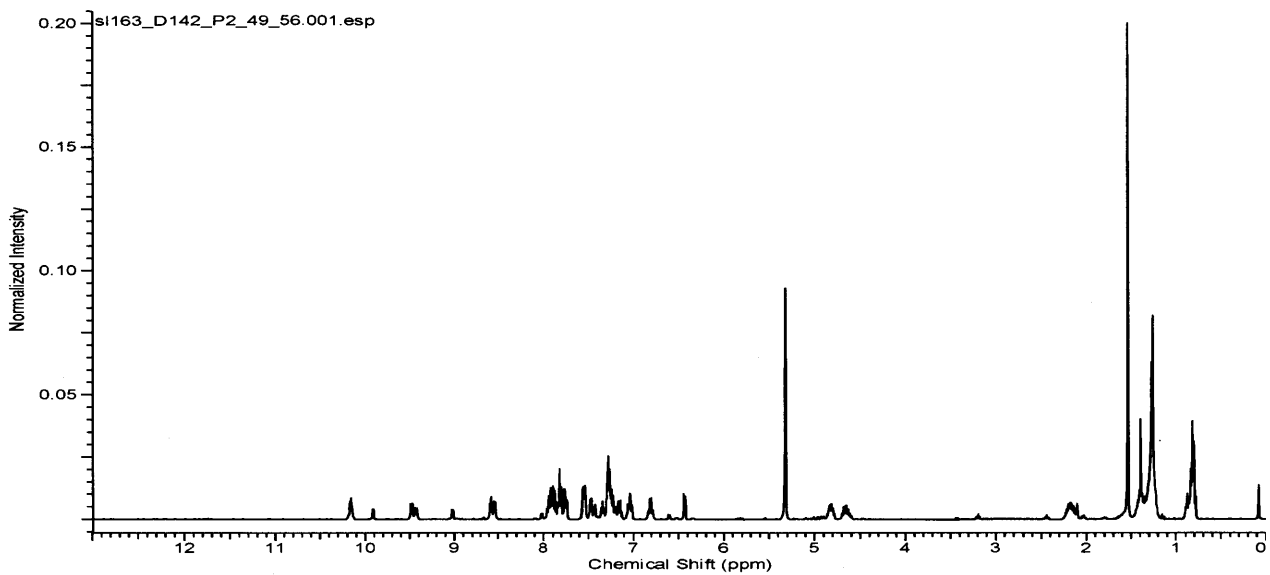
^{13}C NMR of **Pt-C** in CD_2Cl_2



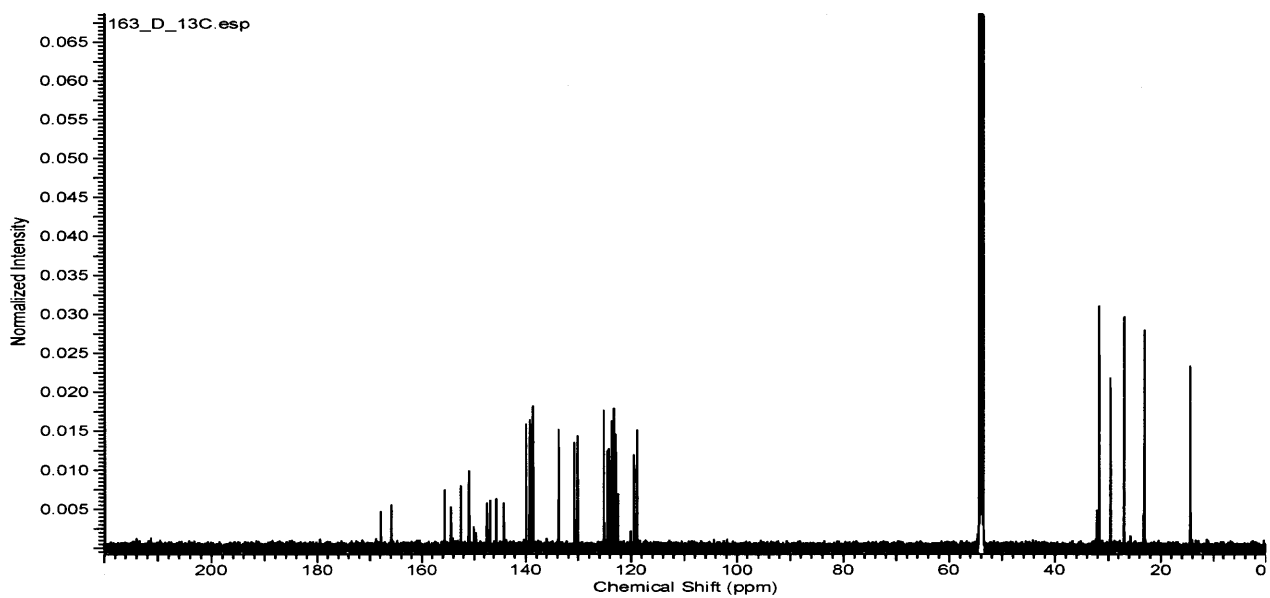
¹H NMR of DiPt-1 in THF-*d*₈



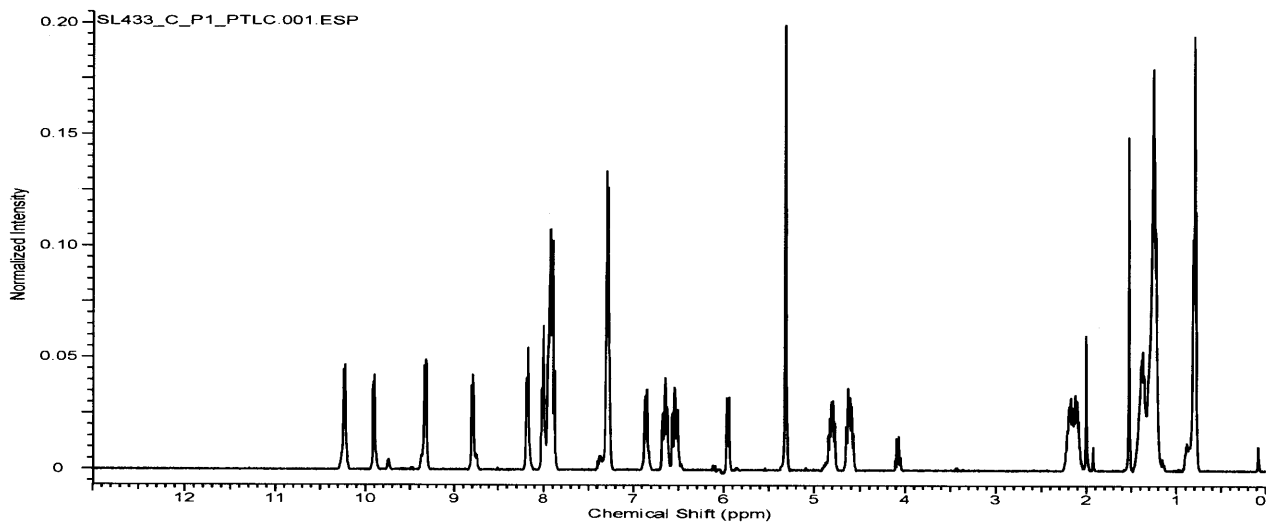
¹³C NMR of DiPt-1 in THF-*d*₈



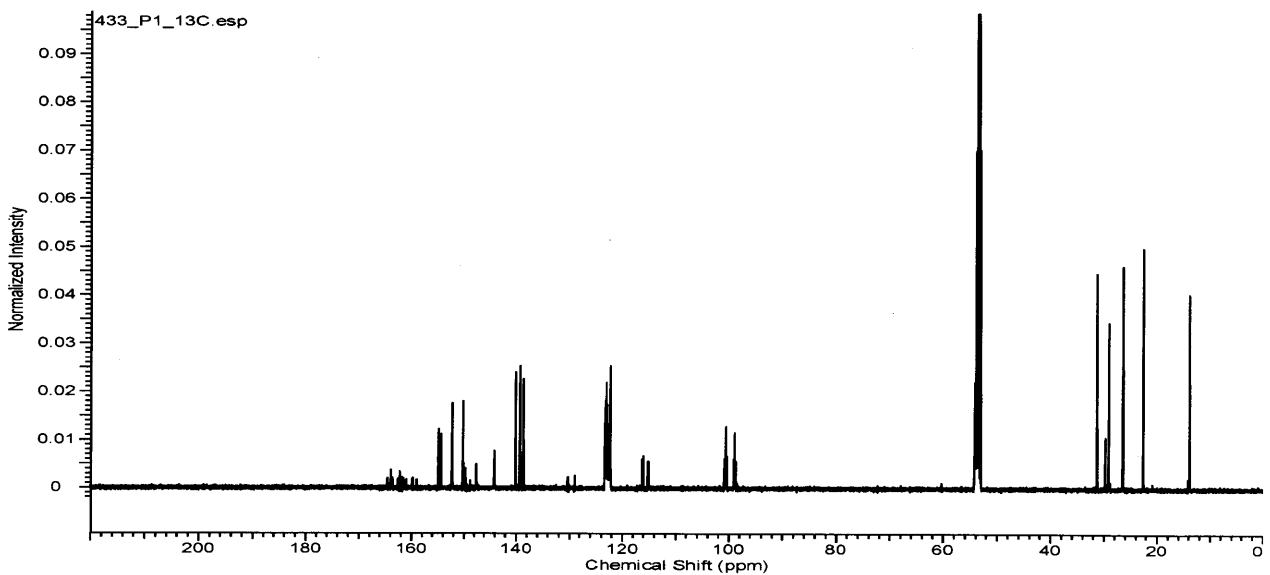
^1H NMR of **DiPt-2** in CD_2Cl_2



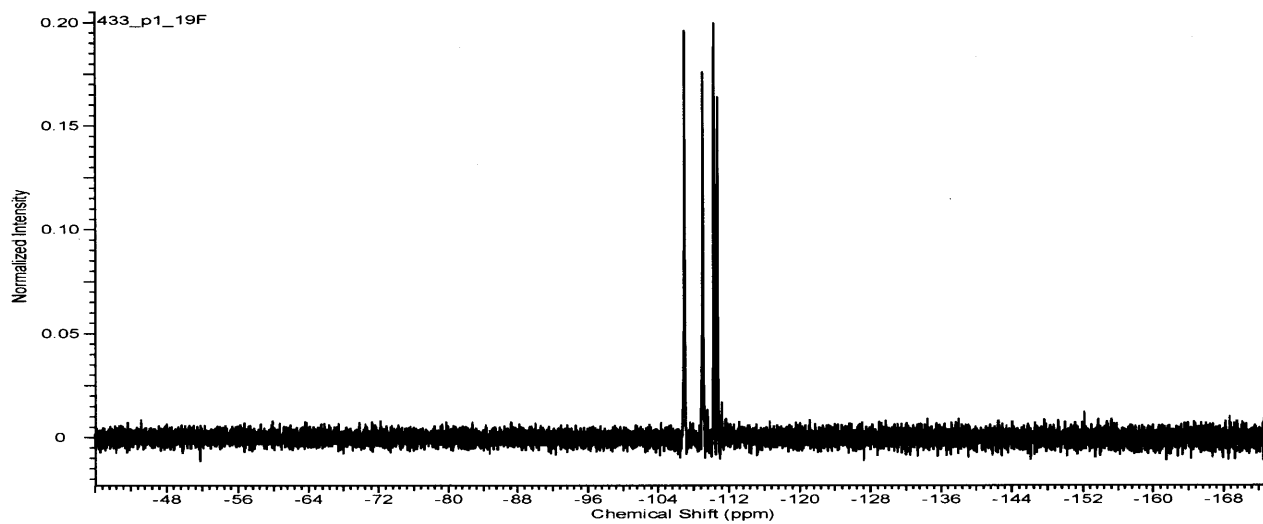
^{13}C NMR of **DiPt-2** in CD_2Cl_2



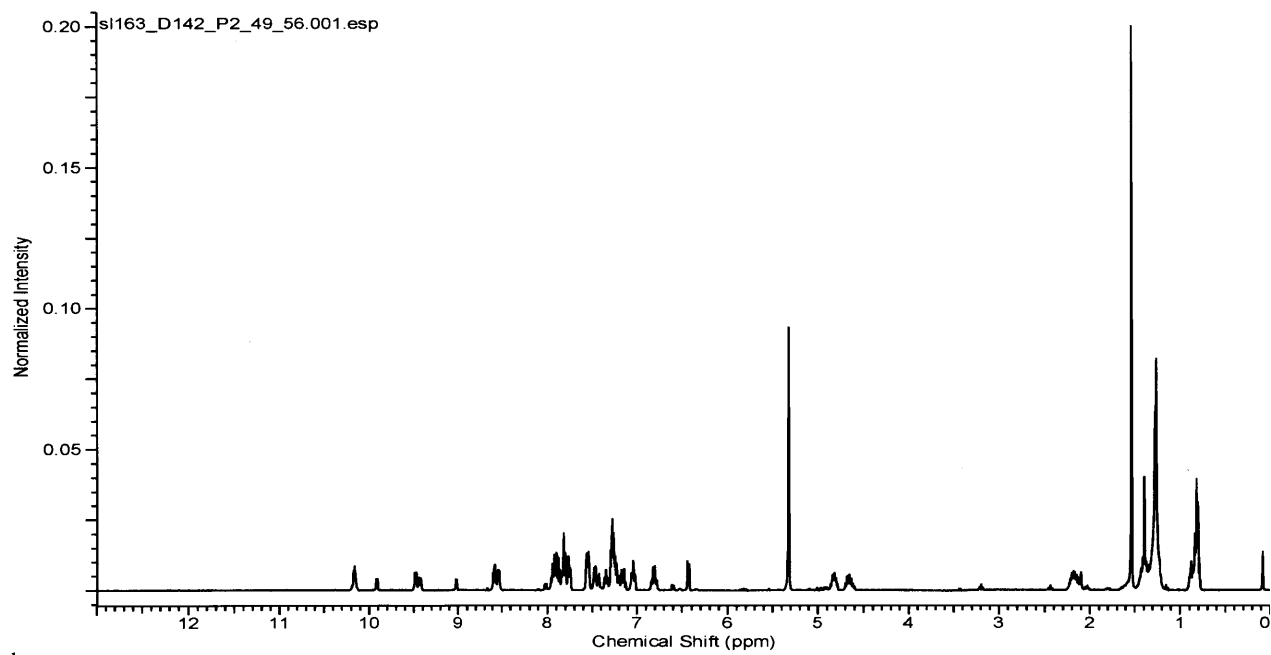
^1H NMR of **DiPt-3a** in CD_2Cl_2



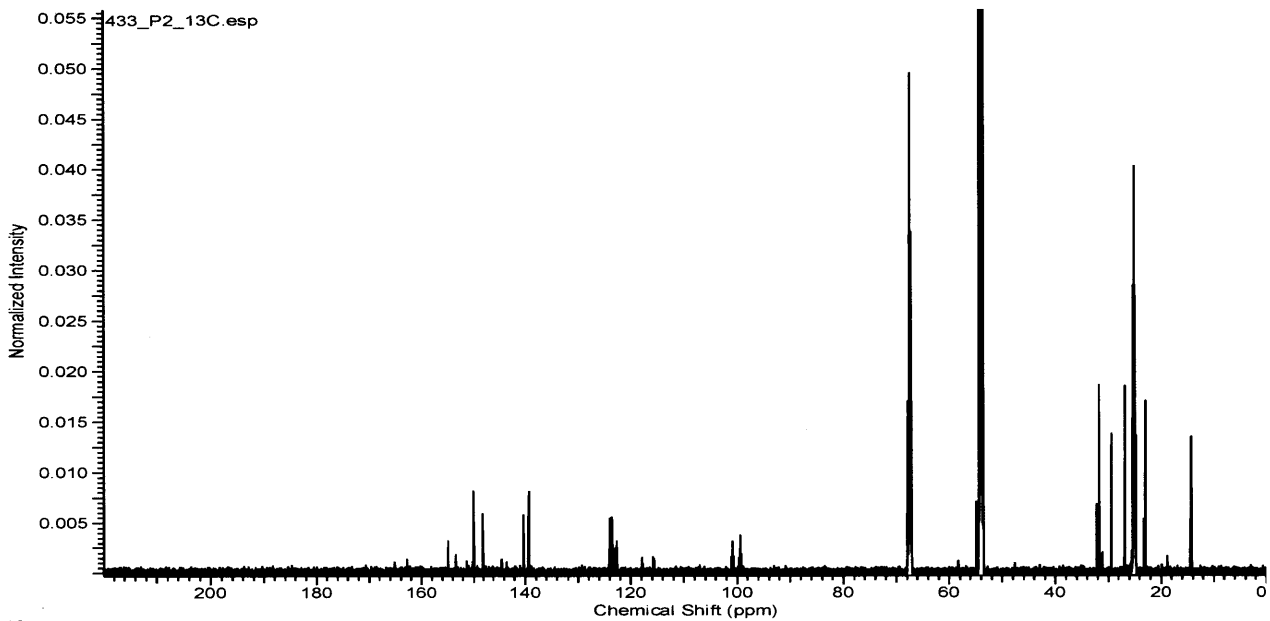
^{13}C NMR of **DiPt-3a** in CD_2Cl_2



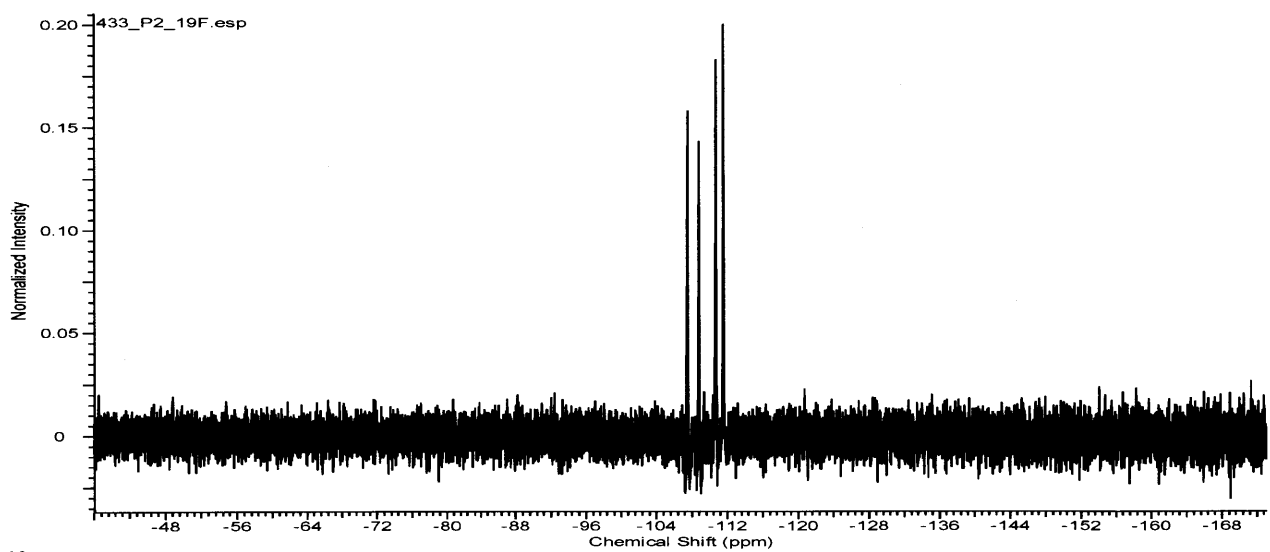
^{19}F NMR of **DiPt-3a** in CD_2Cl_2



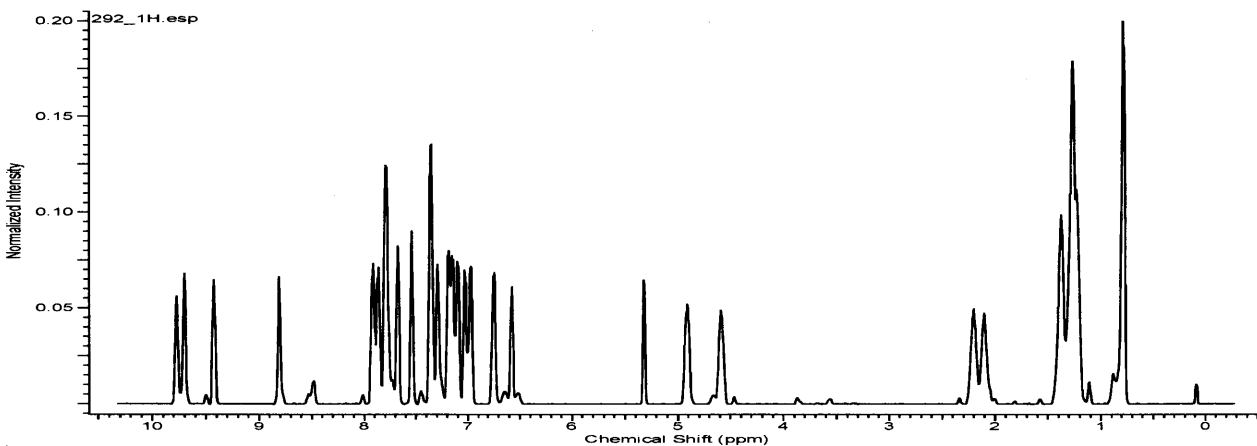
^1H NMR of **DiPt-3b** in CD_2Cl_2



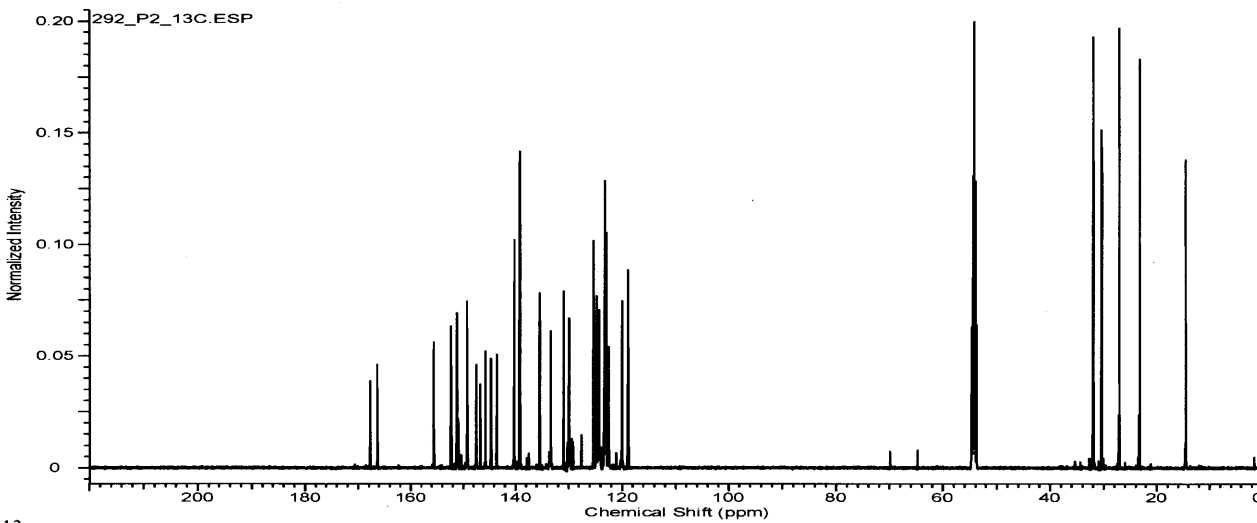
^{13}C NMR of **DiPt-3b** in CD_2Cl_2



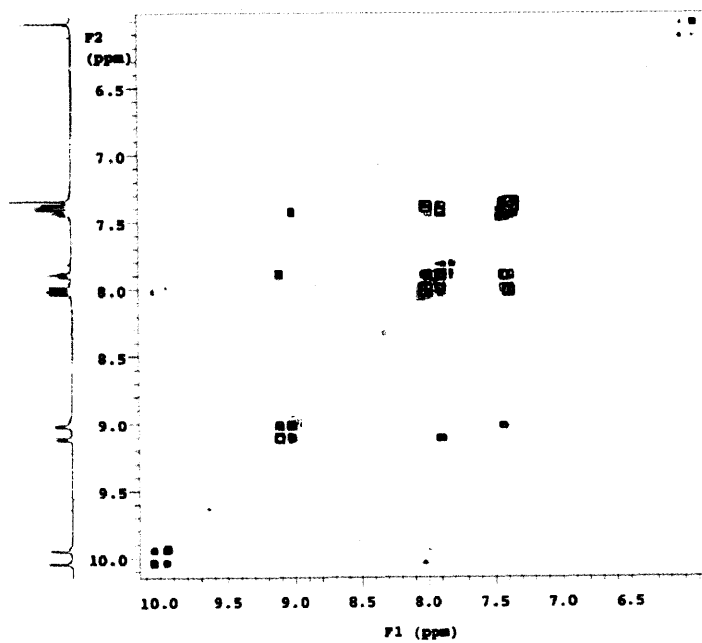
^{19}F NMR of **DiPt-3b** in CD_2Cl_2



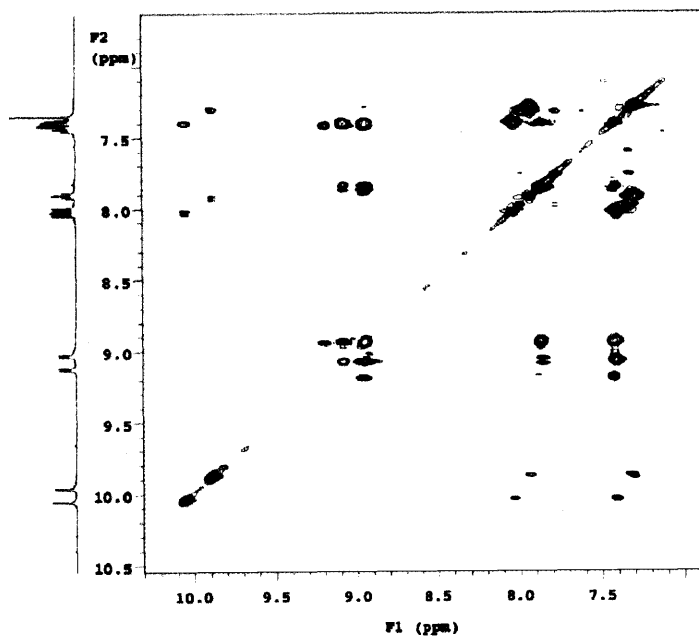
^1H NMR of **DiPt-2-Cl** in CD_2Cl_2



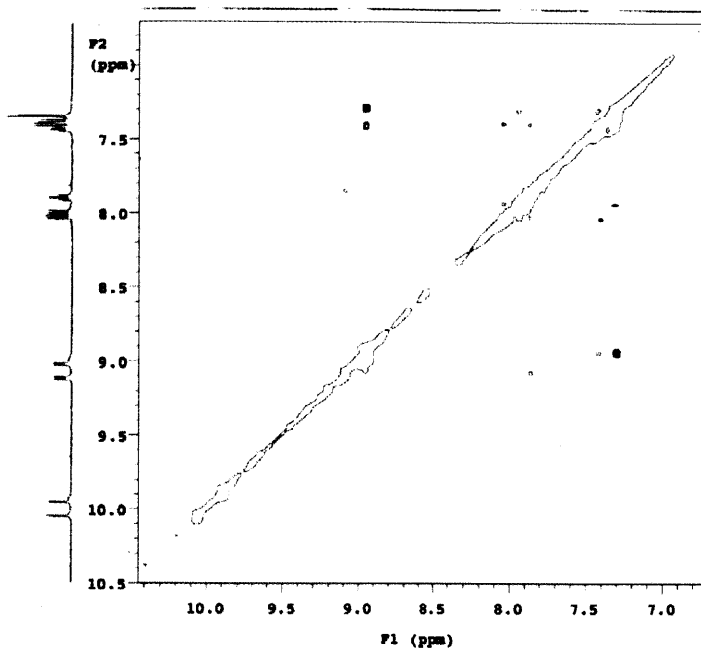
^{13}C NMR of **DiPt-2-Cl** in CD_2Cl_2



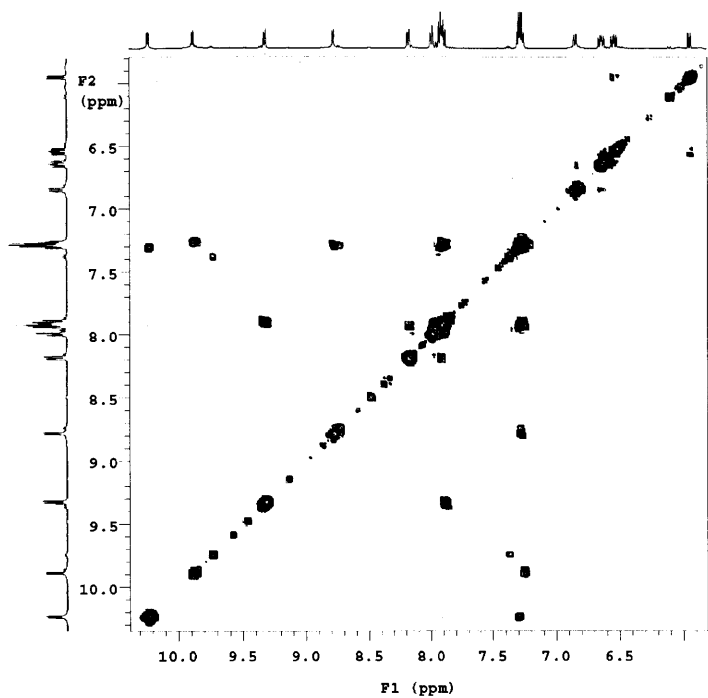
gCOSY of DiPt-3a



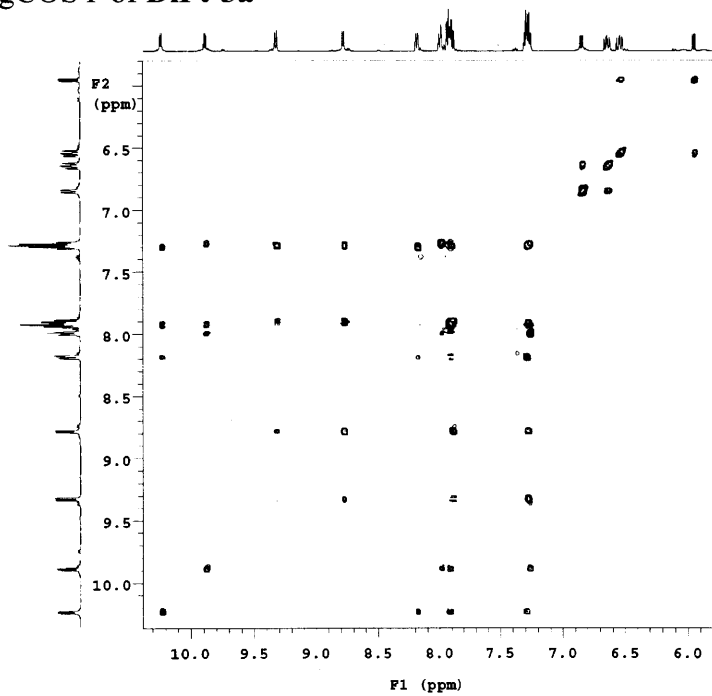
TOCSY of DiPt-3a



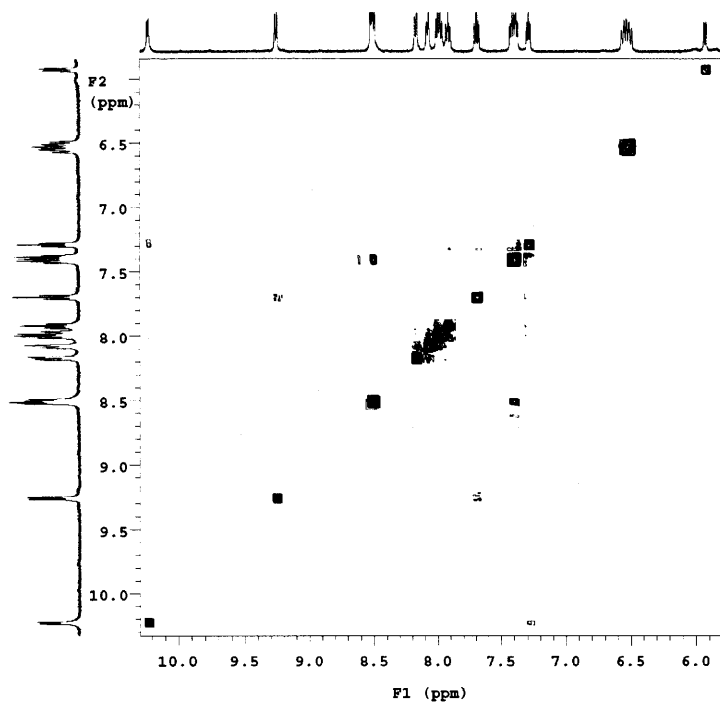
ROESY of DiPt-3a



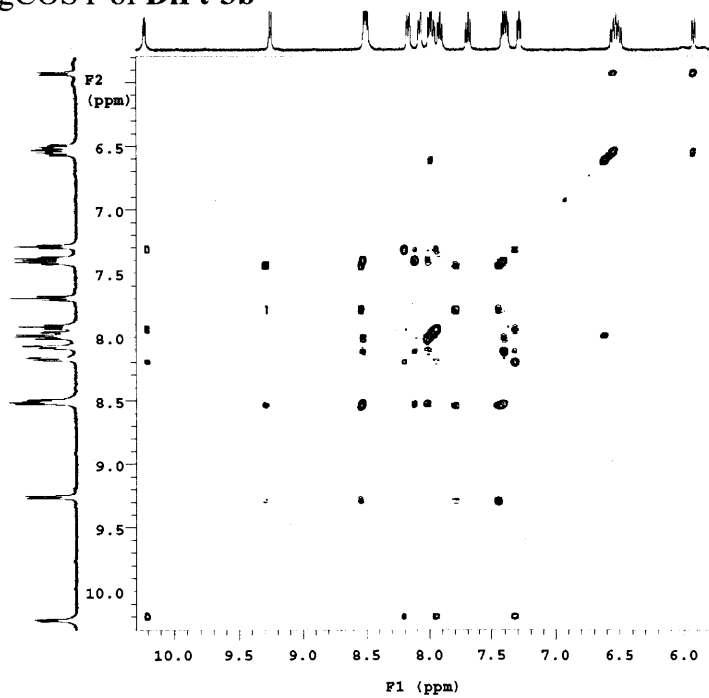
gCOSY of DiPt-3a



TOCSY of DiPt-3a



gCOSY of DiPt-3b



TOCSY of DiPt-3b

Chapter 3

Platinum(II) complexes with responsive phosphorescence to environmental stimuli

3.1 Introduction

The degree of intermolecular interactions of Pt(II) complexes can be effectively controlled by varying the coordinating ligands, functional groups, and counterions. This strategy has been utilized to design functional materials that are responsive toward external stimuli, such as liquid crystals,¹ mechanochromic materials^{2,3} and sensors.⁴

The intermolecular interaction, which controls the photophysical properties of the aggregated compounds, is greatly influenced by the nature of the counterions. Yam *et al.* recently reported that the colors of [Pt(terpy)(CC-R)]X (X = OTf⁻, PF₆⁻, ClO₄⁻, BF₄⁻) in the aggregated states change from yellow to blue, magenta, pink, and orange respectively.⁵ The aggregation is disrupted when bulky ions, such as BPh₄⁻ are used. Similar counterion effect has also been observed with [Pt(terpy)(CC-R)]X (X = Cl⁻, ClO₄⁻, PF₆⁻, BF₄⁻)⁶ and [Pt(terpy)(Cl)]X (X = ClO₄⁻, Cl⁻, PF₆⁻, OTf).⁷ Unfortunately, no simple systematic correlation between the nature of anions and their solid-state colors could be made.

We have utilized a series of 2-(1,2,3-triazol-4-yl)-pyridine (trpy) derivatives prepared by “click” chemistry⁸ to synthesize a variety of Ir(III)⁹ and Pt(II) compounds with interesting photophysical properties. These “click” ligands show versatile coordination modes and can act as C, N- and N, N-chelating ligands as well as C, N, N-bridging units.¹⁰

As discussed in Chapter 2, the trpy-based dinuclear Pt(II) compounds exhibit excimer emission in the solid state or concentrated solutions, depending on the degree of aggregation. The compound bearing 5-bromo-2-(5-bromothiophen-2-yl)pyridine (thpy)

as the cyclometalating ligand (**DiPt-1**) shows slightly red-shifted emission in thin films in comparison to that in solution. However, its 2-(2,4-difluorophenyl)pyridine (FFppy) based counterpart (**DiPt-3b**) exhibits significant photoluminescence changes in the solid state. X-ray crystallography study indicates that **DiPt-3b** forms closely packed infinite zig-zag columns through intermolecular Pt···Pt and $\pi\cdots\pi$ stacking interactions.

In order to take advantage of the photophysical properties of these compounds in their aggregated states, we will focus on the $[(C^{\wedge}N)Pt(N^{\wedge}N)]$ fragment of the dinuclear molecules (**DiPt-1**, **2**, **3**) that is responsible for the strong intermolecular interactions in this chapter. A series of mono-cyclometalated Pt(II) complexes with the general structure of $[(C^{\wedge}N)Pt(N^{\wedge}N)]X$ has been prepared, with the trpy ligands acting as neutral $N^{\wedge}N$ -chelators.

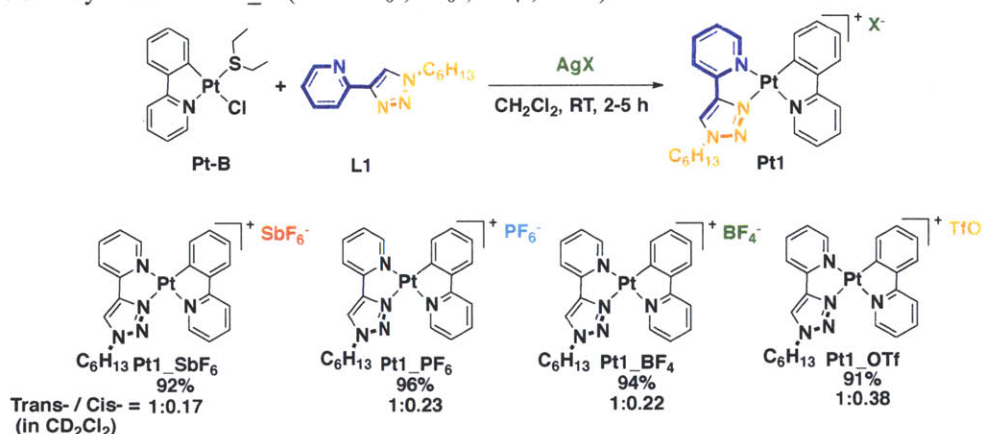
3.2 Results and Discussion

3.2.1 Synthesis and structural characterizations

Instead of the one-pot procedure adopted in the previous two chapters, the synthesis of the cationic $[(C^{\wedge}N)Pt(N^{\wedge}N)]^{+}$ compounds were carried out stepwise (Scheme 3.1). The trpy ligands with different alkyl groups at the 1-position were prepared from 2-ethynylpyridine and the respective alkyl azides in the presence of $CuSO_4$ and sodium ascorbate. The ligands were purified by column chromatography and recrystallization prior to reactions. The Pt(II) compounds were prepared by having the mono-cyclometalated platinum(II) precursor $Pt(ppy)Cl(Et_2S)$ (ppy = 2-phenyl-pyridine, **Pt-B**)

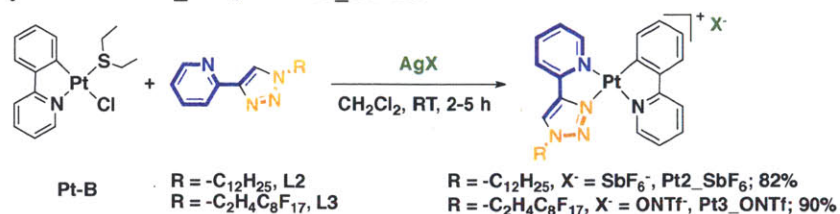
react with 2-(1,2,3-triazol-4-yl)-pyridine (trpy) derivatives in dichloromethane at room temperature for 3 h. One equivalent of silver salts was added to the reaction mixture to facilitate the activation of the Pt-Cl bond. The products precipitated out of the solution immediately after the addition of the silver reagents. The AgCl precipitate was subsequently removed by filtering after the reaction mixture was diluted with dichloromethane. The filtrate was concentrated and added toluene to give pure products in high yields (> 90%).

Scheme 3.1. Synthesis of **Pt1_X** (X = SbF₆⁻, PF₆⁻, BF₄⁻, OTf⁻).



This synthetic approach offers great flexibility in the molecular design and allows quick access to a library of complexes to study the structure-property relationships. The trpy ligands can be modified easily by varying the substituents on 2-ethynylpyridine, as well as the organic azide. The counterions can be controlled simply by choosing the proper silver reagents, or by ion exchange reactions. A series of trpy-C₆H₁₃ (**L1**) based complexes, **Pt1_X** (X = SbF₆⁻, PF₆⁻, BF₄⁻, OTf⁻), were prepared to examine the effect of counterions on the physical properties (Scheme 3.1). Meanwhile, the trpy-C₁₂H₂₅ (**L2**) and trpy-C₂H₄C₈H₁₇ (**L3**) were adopted to yield **Pt2_SbF₆** and **Pt3_ONTf** (ONTf = nonatriflate, C₄H₉SO₃⁻) in order to study the role of the trpy substituents (Scheme 3.2).

Scheme 3.2. Synthesis of Pt2_SbF₆ and Pt3_ONTf.



Regardless of the counterions or substituents, each compound exists as a mixture of two isomers. Take **Pt1_SbF₆** as an example; there are two sets of ¹H NMR signals corresponding to the same number of protons, although the high resolution MS suggests the formation of a single product. The presence of two sharp singlets between 8.5 ppm and 9.9 ppm indicates that the C-H bond at the 5-position of the triazole ring is intact and only the N[^]N-chelation of **L1** is present.⁹ The ratio of the two components changes when the sample is dissolved in different solvents. The ratios of the two isomers in these three solvents are 1:0.17, 1:0.42 and 1:0.91, respectively.

¹H NMR signal corresponding to the proton at the 5-position of the triazole ring shows a significant downfield shift in acetone-*d*₆ and DMSO-*d*₆, as compared to that in CD₂Cl₂. The chemical shift of the triazolyl proton shifts from 8.63 ppm in CD₂Cl₂ to 8.94 ppm in acetone-*d*₆ and 9.28 ppm in DMSO-*d*₆ for the major isomer. Similar downfield shift in polar solvents is also observed for the minor isomer, with the triazolyl singlet at 8.53 ppm in CD₂Cl₂, 8.91 ppm in acetone-*d*₆, and 9.26 ppm in DMSO-*d*₆. This solvent dependence is likely originated from the H-bonding interactions of this acidic C-H bond with acetone and DMSO molecules that can act as H-bond acceptors. This type of interactions has found wide applications in building supramolecular architectures and chemosensors.¹¹

DMSO- d_6 : major : minor = 1:0.91

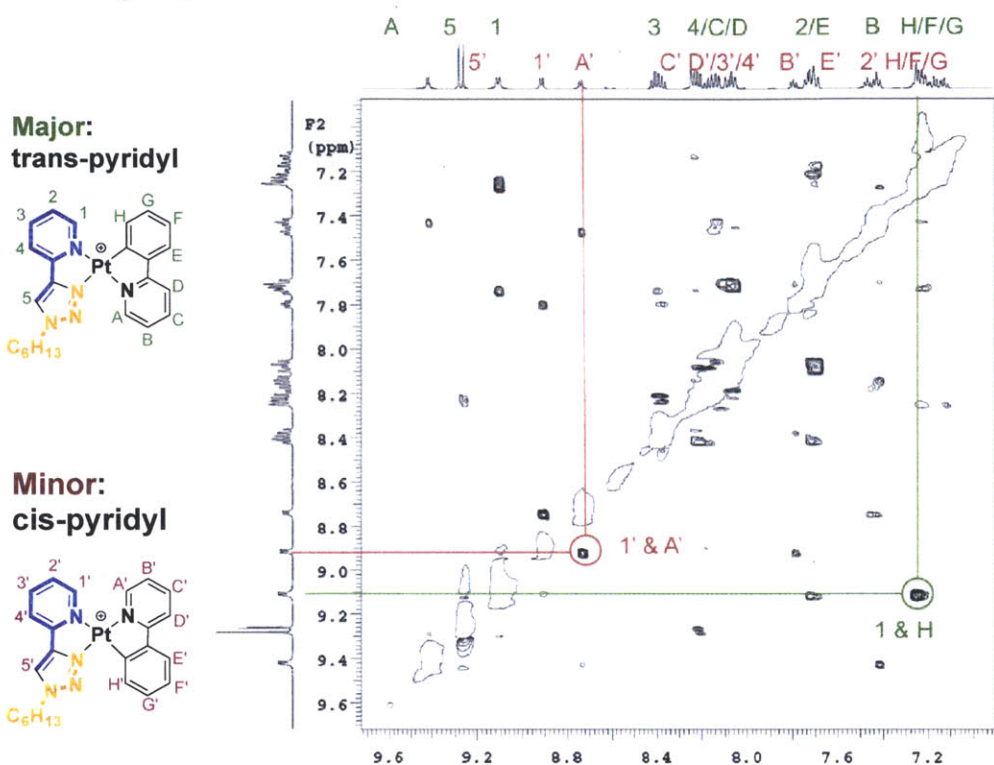


Figure 3.1. ROESY spectrum of **Pt1** SbF_6 in DMSO- d_6 and the assignment of the aromatic protons.

Furthermore, variable-temperature (VT) NMR spectra of **Pt1** SbF_6 were recorded between 22 °C and 100 °C to study the existence of oligomers in the solution.^{12,13} The entire spectrum is shifted downfield with increasing temperature, and the largest shift is observed for the triazolyl proton at the 5-position (H^5 and $\text{H}^{5'}$). Other protons that are close to the platinum center also exhibit large shifts. As the temperature increases, the peaks also become broader and start to merge. No change in the ratio of the two components is observed across the temperature range. The temperature dependent spectral shift is reversible, suggesting dimeric or oligomeric structures are not present in the sample solutions. Moreover, the equilibrium between the *trans* and *cis* isomers is more sensitive to solvent polarity than temperature in this regard.

CD₂Cl₂: major : minor = 1:0.17

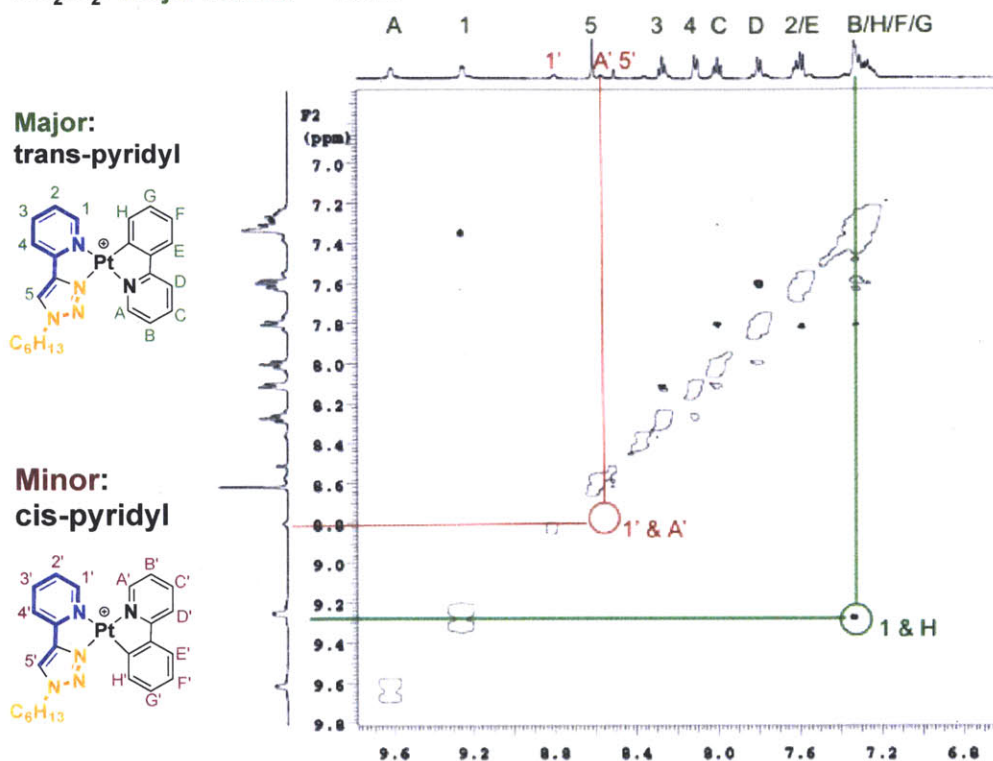


Figure 3.2. ROESY spectrum of Pt1_SbF₆ in CD₂Cl₂ and the assignment of the aromatic protons.

The two coexisting components of Pt1_SbF₆ are assigned as coordination isomers based on a series of 2D ¹H NMR techniques, such as gCOSY, TOCSY and ROESY NMR. As discussed in Chapter 2, the protons at the ortho-positions of the Pt-C/Pt-N bonds are used as probes to study the coordination geometry. As for the major isomer, there is a clear cross peak between the protons at the ortho-position of the Pt-C(ppy) bond (H^H) and the one adjacent to the Pt-N(trpy_Py) bond (H¹) on the ROESY spectrum taken in DMSO-*d*₆ (Figure 3.1). The same through-space coupling between H^H and H¹ is also observed in CD₂Cl₂ (Figure 3.2), indicating that the two pyridyl groups from the ppy and trpy ligands are *trans* to each other (similar to DiPt-1, DiPt-2 and Dipt3a in Chapter 2). On the other hand, the minor component shows coupling interactions between H^{A'} and H^{1'} in DMSO-*d*₆, clearly indicating a *cis* pyridyl configuration. It should be noted that the

$H^A - H^I$ cross peak is weak in Figure 3.2 because of the low solubility of **Pt1_SbF₆** in CD_2Cl_2 . The proton signals of the other **Pt1_X** ($X = PF_6^-$, BF_4^- , OTf^-) complexes can be assigned accordingly, and the ratios of the *trans/cis* isomers in CD_2Cl_2 are listed in Scheme 3.1.

The presence of counterions can be confirmed by ^{19}F NMR spectra for most of the compounds, as evidenced by the characteristic signals for PF_6^- (-72.66 ppm), BF_4^- (-151.30 ppm), and OTf^- (-79.06 ppm). There is only one signal for each compound despite of the coexistence of two isomers in each sample. Poorly resolved ^{19}F NMR resonance is observed for SbF_6^- .

3.2.2 Polymorphs

Interestingly, **Pt1_SbF₆** has two stable polymorphs that are interconvertible at room temperature, as shown in Figure 3.3. **Pt1_SbF₆** is soluble in acetone and dimethyl sulfoxide, and only exhibits limited solubility in CH_2Cl_2 . Unlike other square planar Pt(II) complexes, **Pt1_SbF₆** is not soluble in acetonitrile. Bright yellow crystalline solids (Morph-A) can be isolated from CH_2Cl_2 . This polymorph shows intense yellow emission when exposed to UV radiation. There is also an orange metastable polymorph (Morph-B) formed during rapid precipitation from CH_2Cl_2 , which transforms into the yellow-colored Morph-A in the presence of CH_2Cl_2 . On the contrary, a red solid (Morph-C) with bright red solid-state emission is obtained when the compound is precipitated from its acetone solution. Morph-A and Morph-C are interconvertible by simple solvent annealing.

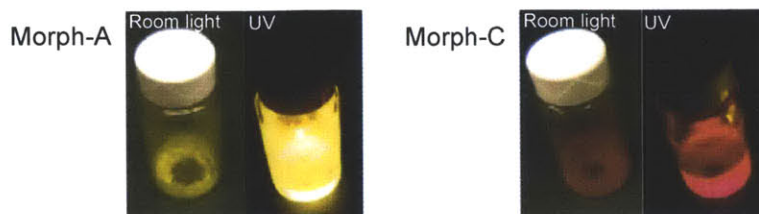


Figure 3.3. Polymorphs of $[\text{Pt}(\text{ppy})(\text{trpy}-\text{C}_6\text{H}_{13})]\text{SbF}_6$ (**Pt1_SbF₆**): yellow crystals recrystallized from $\text{CH}_2\text{Cl}_2/\text{hexane}$ (left) and red solid precipitated rapidly from acetone (right).

Although the two polymorphs of **Pt1_SbF₆** show strong solvatochromic effect, there is no indication of incorporation of neither solvent in the crystal lattice. Thermogravimetric analysis (TGA) shows no weight loss below the decomposition temperature (304°C , $< 5\%$ weight loss). The differential scanning calorimetry (DSC) analysis shows no transition associated with solvent loss, either.

3.2.3 Photophysical properties

The UV-vis absorption and emission spectra of **Pt1_SbF₆** exhibit moderate solvent dependence, as shown in Figure 3.4. Unlike the featureless absorption spectra of **DiPt-3a**, the absorption of **Pt1_SbF₆** shows two well-resolved peaks in the UV region and a broad band in solution. The two intense absorption peaks at 330 nm and 347 nm are assigned to allowed ligand-centered (LC) transitions. The low energy band between 375 nm and 430 nm is mainly due to the metal-to-ligand charge transfer (MLCT), similar to most of the $(\text{C}^{\wedge}\text{N})\text{Pt}(\text{LL})$ complexes.¹⁴ However, the entire spectrum is slightly red shifted in CH_2Cl_2 compared to that in acetone. The low-lying band shows a larger shift (6 nm) than the high-energy peaks (2-3 nm). The spectral shift is likely originated from the hydrogen

bonding interactions between the trpy ligand and the solvent molecules, as evidenced in the ^1H NMR spectra.

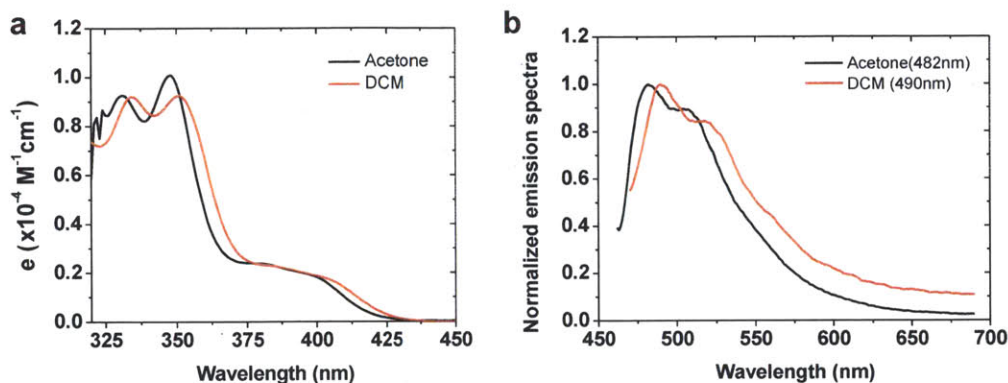


Figure 3.4. UV-vis absorption (a) and emission ($\lambda_{\text{exc}} = 400 \text{ nm}$) (b) spectra of **Pt1_SbF₆** in acetone and dichloromethane ($\sim 10^{-6} \text{ M}$, under Ar).

Compound **Pt1_SbF₆** is only weakly emissive in the solution at room temperature. The low quantum efficiency is commonly observed among heteroleptic platinum complexes, attributable to the presence of a low-lying or thermally accessible $^3\text{d-d}$ excited state.⁴ The photoluminescence obtained in acetone shows fine vibrational slitting patterns. This highly structured emission band suggests that the *trans* and *cis* coordination isomers have very similar photophysical properties, as discussed for **DiPt-3a** and **DiPt-3b** in Chapter 2. The emission band is also red shifted in CH_2Cl_2 by 8 nm, with a growth of emission intensity in the low-energy region. This bathochromic shift is consistent with the formation of close intermolecular interactions in CH_2Cl_2 .

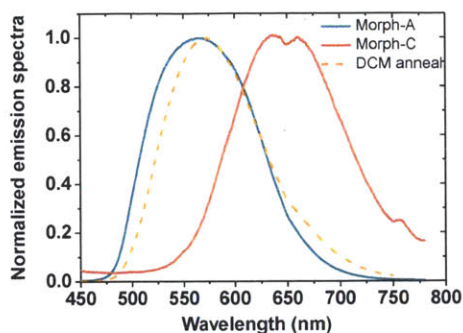


Figure 3.5. Solid-state emission spectra of **Pt1_SbF₆** ($\lambda_{\text{ex}} = 400$ nm).

Pt1_SbF₆ is highly emissive in the solid state, as shown in the luminescence spectra (Figure 3.5). The yellow crystals of Morph-A exhibit broad and featureless emission ($\lambda_{\text{em}} = 565$ nm) in the range of 480-700 nm. This turn-on of luminescence in the solid state is introduced by the self-assembly of **Pt1_SbF₆**. The solid-state emission is attributed to the excited triplet metal-metal-to-ligand charge transfer (³MMLCT) states.^{4,15} The quantum yield reaches 86% in neat films prepared by drop-casting a suspension of **Pt1_SbF₆** in hexane onto glass substrates, which is on par with the best solid-state Pt(II) emitters reported.^{16,17} The red-colored Morph-C shows bright red emission between 550 nm and 800 nm. This band could potentially resolve into two distinct peaks from the *trans* and *cis* isomers, with emission maxima at 635 nm and 660 nm. It is likely that the isomers adopt slightly different emission properties in the aggregated states. In order to demonstrate that the two polymorphs are interconvertible, Morph-C is annealed with CH₂Cl₂ for 10 min, and the emission spectrum is also plotted in Figure 1. The emission band of the annealed sample overlaps with that of Morph-A, and the slightly narrower bandwidth is due to the annealing.

3.2.4 Aggregation-induced luminescence

Preliminary powder X-ray diffraction (XRD) of the polymorphs of **Pt1_SbF₆** shows that they have distinct diffraction patterns. The yellow-colored Morph-A is highly crystalline, as indicated by the sharp diffraction peaks (Figure 3.6). The primary layer spacing is around 6.6 Å. On the contrary, the red-colored Morph-C only has one broad diffraction peak, corresponding to 3.53 Å. The metastable Morph-B (orange-colored) does not have any long-range order. Given that these polymorphs have identical chemical composition and the only structural difference is the intermolecular distance, the difference in the color and luminescence among the polymorphs of **Pt1_SbF₆** is attributed to the extent of intermolecular interactions.

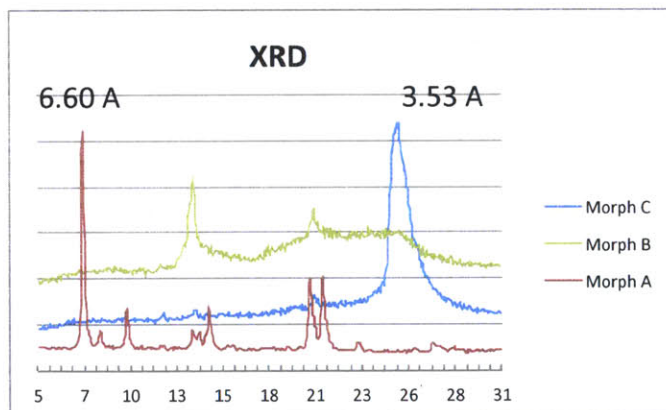


Figure 3.6. XRD patterns of the polymorphs of **Pt1_SbF₆**.

It has been documented that square planar Pt(II) complexes, in particular terpyridine coordinated compounds, show favorable photophysical properties in the aggregated states. Subtle changes in the Pt···Pt distance and $\pi\cdots\pi$, may led to dramatic change in color and emission. For instance, Yam *et al.* has recently reported that [Pt(terpy)(CC-CCH)]OTf crystallizes into two polymorphs with distinct colors.¹⁸ The dark

green crystal form consists of a Pt···Pt separation of 3.388 Å, while the red crystal form contains alternating Pt···Pt distances of 3.394 Å and 3.648 Å.

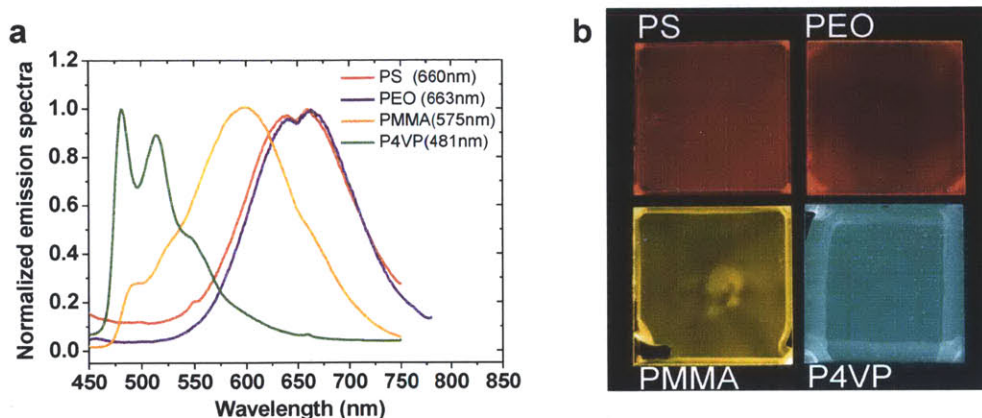


Figure 3.7. (a) Solid-state emission spectra of [Pt(ppy)(trpy-C₆H₁₃)]SbF₆ (**Pt₁_SbF₆**) when doped into polymer matrixes: PS (red), PEO (magenta), PMMA (orange), and P4VP (green); (b) distinctive photoluminescence colors contrast observed under UV radiation (365 nm).

Doping **Pt₁_SbF₆** into different polymer matrixes offers an effective method of controlling the degree of the intermolecular interactions. Four polymers are selected for studying the interactions between **Pt₁_SbF₆** and the host materials, namely polystyrene (PS), polyethylene oxide (PEO), poly(methyl methacrylate) (PMMA) and poly(4-vinylpyridine) (P4VP). Samples for the solid-state emission spectra were prepared by spin-coating a solution of the polymer and **Pt₁_SbF₆** (6-8 % w/w relative to the polymer). The photoluminescence spectra and the images of the films are depicted in Figure 3.7. **Pt₁_SbF₆** exhibits red emission in both PS and PEO, which are acting as inert hosts. The emission in PMMA is concentration-dependent, varying from yellow to orange as the concentration of **Pt₁_SbF₆** increases. The small feature at 490 nm matches the monomer emission of **Pt₁_SbF₆** observed in fluid solutions, suggesting incomplete aggregation. The green emission ($\lambda_{em} = 481$ nm) together with the well-defined

vibrational splitting patterns in P4VP indicates that the emission is based on monomeric **Pt1_SbF₆**. The pyridyl groups in P4VP are ideal to coordinate with the metal center and break up any intermolecular aggregation. In fact, a full-range color tuning based on a single emitter can be envisioned by screening different host materials and dopant concentration.

3.2.5 Mechanochromism

Apart from the organic solvents, **Pt1_SbF₆** also exhibits switchable colors and luminescence in response to mechanical force. The conversion of Morph-A to Morph-C can be achieved by grinding the solid in a mortar (Figure 3.8). Grinding the yellow crystals obtained from CH₂Cl₂ using a pestle causes the color as well as emission to change into orange-red immediately. The fully ground sample exhibits emission similar to that of Morph-C of **Pt1_SbF₆**. The yellow emission can be recovered when it is exposed to CH₂Cl₂, as indicated by the yellow circle in the lower left corner of Figure 3.8.

Despite of the attractive properties of mechanochromic materials, there are only a few examples involving phosphorescent materials. Low coordination Au(I) complexes are one of the most popular candidates, partially due to the strong aurophilic interactions.^{2,3} Only a few Pt(II) compounds have been reported to exhibit luminescence change in response to mechanical force to date.¹⁹⁻²² Recently, cyclometalated Ir(III) compounds have been reported to be piezochromic for the first time.²³ Unfortunately, the mechanism of the mechanochromic transformation is still under debate.

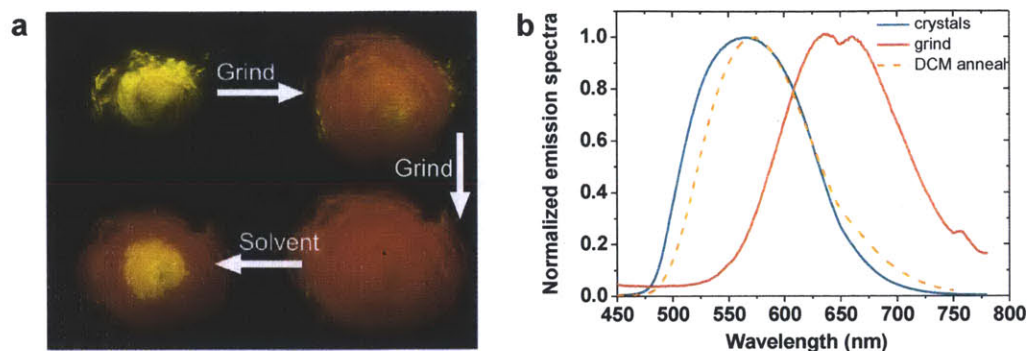


Figure 3.8. Mechanochromic luminescence exhibited by $[\text{Pt}(\text{ppy})(\text{trpy}-\text{C}_6\text{H}_{13})]\text{SbF}_6$ (**Pt1_SbF₆**): (a) crystals recrystallized from $\text{CH}_2\text{Cl}_2/\text{hexane}$ (upper left) were ground with a pestle (upper and lower right); the yellow emission was restored when CH_2Cl_2 was dropped onto the ground sample (lower left). All images were obtained under UV radiation (365 nm); (b) solid-state emission spectra of crystals recrystallized from $\text{CH}_2\text{Cl}_2/\text{hexane}$ (green), the ground solid (red), and the solid annealed with CH_2Cl_2 after grinding (orange) ($\lambda_{\text{ex}} = 400\text{nm}$).

In the pursuit of investigating the nature of this mechanochromic behavior, the photoluminescence (PL) switch is studied in detail in collaboration with Wendi Chang and Gleb Akselrod from Prof. Bulovic's research group at MIT. A motorized metal pin is used to apply controlled mechanical force or pressure onto the neat film of **Pt1_SbF₆** sandwiched between two glass substrates. The displacement of the springs in the setup is proportional to the applied force, and fiber optics is used to collect the PL spectra with a laser excitation. The layout of the experimental setup is provided in the appendix of this chapter. Two types of measurements are performed, namely the X-scan and the Z-Scan.

The PL spectra are recorded within $\pm 500 \mu\text{m}$ of the center of the pin, which is marked as $0 \mu\text{m}$ during the measurement, with a specific force applied to the sample film. Figure 3.9 offers a schematic illustration of the X-scan measurement. The PL spectra are stacked along the X-axis and traces representing the 0.25, median (0.5) and 0.75 of each PL spectrum are plotted against the position relative to the center of the pin. Figure 3.10 summarizes the PL change around the pin, with the displacement of the pin being 4 mm,

5 mm, and 6 mm. In all of the three measurements, the emission spectra are shifted toward longer wavelength. The maximum shift occurs around the center of the pin, where the force is the strongest. According to Figure 1-(d), the degree of red shift increases as the displacement increases. The spectral median shift is as large as 60 nm with a displacement of 6 mm.

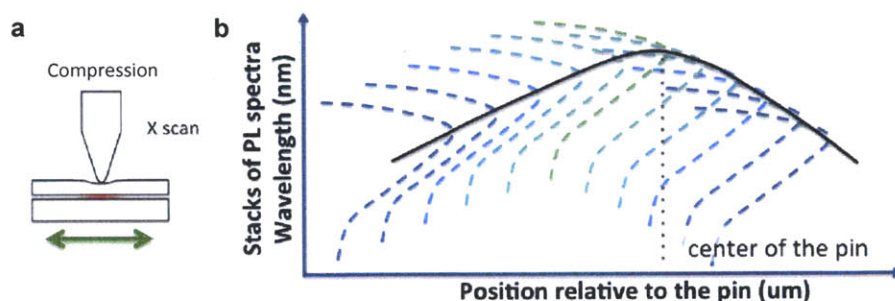


Figure 3.9. Schematic illustration of the X-scan measurement: (a) experimental set up; (b) the PL spectra were recorded within $\pm 500 \mu\text{m}$ of the center of the pin, which is at 0 mm.

Consistent red shift of the PL spectra is observed with increasing pressure during the Z-scan (Figure 3.11). During the Z-scan, the PL spectra are recorded at the center of the pin as a function of the displacement, which directly reflects the force applied to the surface. The turn-on displacement ($\sim 3 \text{ mm}$) is marked by a dotted line. This cut-off force is dependent on the mechanical strength and stiffness of the glass substrates used in the measurement. An overall shift of 80 nm of the emission maximum is observed with a displacement of 10 mm. This is approaching the difference between the emission maxima of Morph-A (565 nm) and Morph-C ($\sim 650 \text{ nm}$) in the solid state. The bathochromic shift of the solid-state emission spectra of **Pt1_SbF₆** during these pressure sensitive measurements clearly indicates that mechanical force provides a driving force for the reorganization of the molecules in the solid state.

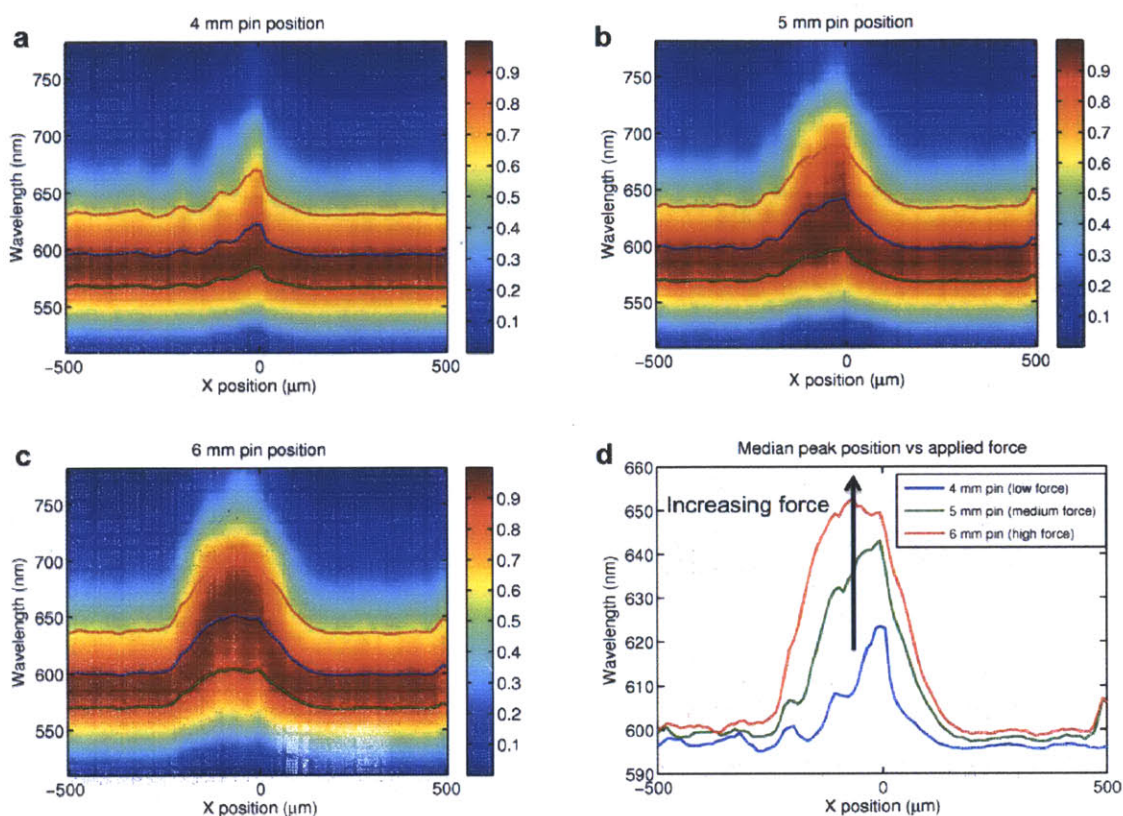


Figure 3.10. Significant red-shift of the PL spectra around the pin during the X-scan of Pt1_SbF_6 , with the displacement of the pin being 4 mm (a), 5 mm (b), and 6 mm (c). The green, blue and red traces represent the 0.25, median (0.5) and 0.75 of each PL spectrum; (d) comparison of the median peak position relative to the applied force.

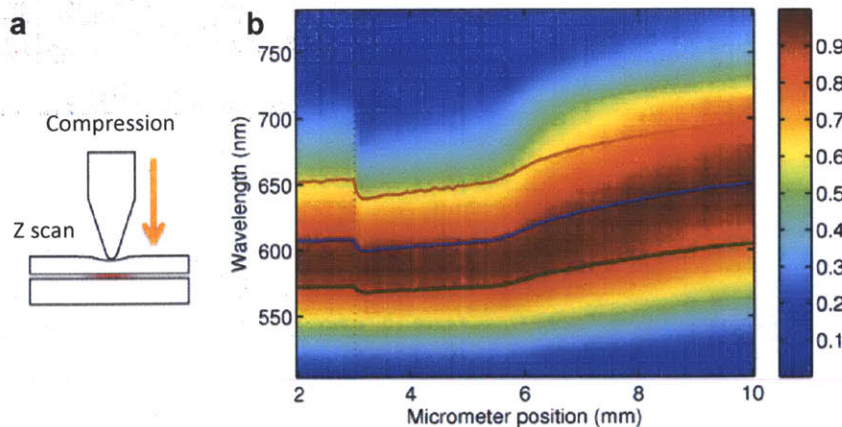


Figure 3.11. Consistent red shift of the PL spectra around the pin during the Z-scan of Pt1_SbF_6 with increasing pin displacement: (a) schematic illustration of the Z-scan measurement; (b) the PL spectra recorded at the center of the pin. The green, blue and red traces represent the 0.25, median (0.5) and 0.75 of the PL spectra.

3.2.6 Counterion effect

In spite of the similarity in the chemical structure, **Pt1_X** exhibit distinct physical properties depending on the anions. **Pt1_SbF₆** only exhibits limited solubility in CH₂Cl₂, but all the other **Pt1_X** complexes are more soluble in this solvent. The solubility increases in the order of **Pt1_SbF₆** < **Pt1_PF₆** < **Pt1_OTf** < **Pt1_BF₄**. All the complexes show very high solubility in acetone and dimethyl sulfoxide.

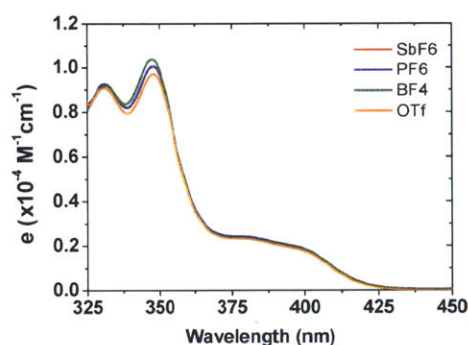


Figure 3.12. UV-vis absorption spectra of **Pt1_X** (X = SbF₆⁻, PF₆⁻, BF₄⁻, OTf⁻) in acetone solution (~10⁻⁶ M).

Compound **Pt1_PF₆** also has the switchable yellow and red polymorphs that are similar to those of **Pt1_SbF₆**. However, **Pt1_BF₄** and **Pt1_OTf** only have a single stable morphology at room temperature. The color of **Pt1_BF₄** solid precipitated from CH₂Cl₂ is orange-yellow, but the color immediately darkens to orange-red when removed from the solution. The orange-yellow color is restored as soon as the sample is exposed to CH₂Cl₂ vapor. On the contrary, no visible color change occurs when **Pt1_BF₄** is annealed in the acetone atmosphere. This fast and selective response to CH₂Cl₂ shows the promise of utilizing **Pt1_BF₄** as colorimetric and luminescent VOC sensors.

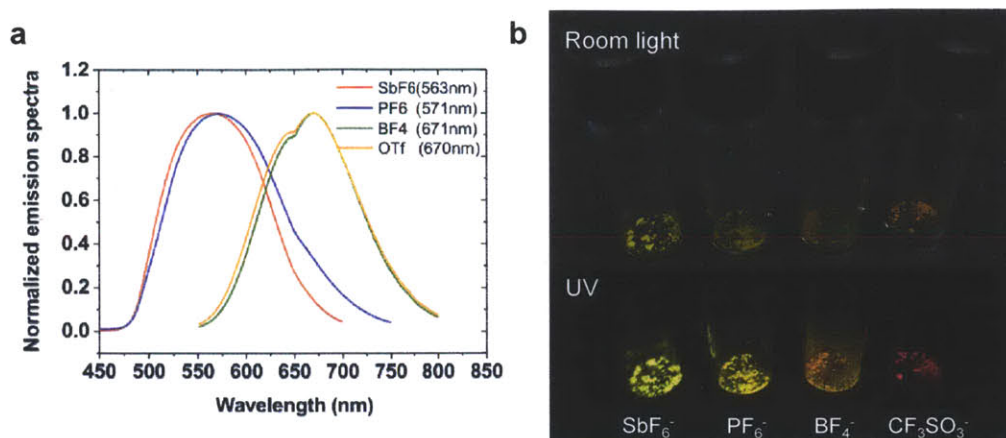


Figure 3.13. (a) Solid-state emission spectra of **Pt1_X** ($X = \text{SbF}_6^-$, PF_6^- , BF_4^- , OTf^-) recrystallized from $\text{CH}_2\text{Cl}_2/\text{hexane}$ ($\lambda_{\text{ex}} = 400 \text{ nm}$ for **Pt1_SbF₆/PF₆**; $\lambda_{\text{ex}} = 430 \text{ nm}$ for **Pt1_BF₄/OTf**); (b) distinctive colors and emission of the four complexes under room light and UV radiation.

In dilute solutions, the counterions exhibit no influence on the photophysical properties of **Pt1_X** ($X = \text{SbF}_6^-$, PF_6^- , BF_4^- , OTf^-). The UV-vis spectra are compared in Figure 3.12. The absorption bands overlap with each other, with a little variation of the extinction coefficient ($\sim 0.7 \times 10^{-3} \text{ M}^{-1} \text{ cm}^{-1}$) at 347 nm. This series of compounds is only weakly emissive in the solution state at room temperature.

The solid-state luminescence of complexes **Pt1_X** shows high counterion dependence. Emission spectra of **Pt1_X** ($X = \text{SbF}_6^-$, PF_6^- , BF_4^- , OTf^-) are recorded using solid samples obtained from CH_2Cl_2 . As shown in Figure 3.13, **Pt1_PF₆** shares similar luminescent profiles with **Pt1_SbF₆**; whereas, the emission maxima of **Pt1_BF₄** and **Pt1_OTf** are red-shifted by 100 nm. The red shift of emission for OTf^- salt comparing to SbF_6^- has also been observed for other Pt(II) complexes, but the origin of the difference remains unclear.¹⁸

3.2.7 Side-chain effect

Compound **Pt2_SbF₆**, which bears a dodecyl group, greatly resembles **Pt1_SbF₆**, since the increase in the length of the alkyl group has little effect on its solubility. The formation of two polymorphs is also observed. However, the stability of Morph-A **Pt2_SbF₆** decreases in comparison to **Pt2_SbF₆**; an orange-colored solid is usually obtained instead of the yellow emitting Morph-A. The solubility of **Pt3_ONTf** in organic solvents is much lower than its non-fluorinated counterparts. It is only slightly soluble in acetone, but more soluble in THF. **Pt3_ONTf** adopts several colors in the solid state, ranging from yellow to red. The most stable polymorph has a unique coral color, and is insensitive to CH₂Cl₂ vapors.

The side chains have little influence on the UV-vis absorption, but greatly affect the solid-state emission properties (Figure 3.14). The absorption spectra for **Pt1_SbF₆** and **Pt2_SbF₆** are identical, yet **Pt3_ONTf** shows slightly higher extinction coefficient. The solid-state emission is measured with samples obtained from CH₂Cl₂ for **Pt1_SbF₆** and **Pt2_SbF₆**, and acetone for **Pt3_ONTf**. The emission of **Pt2_SbF₆** is similar to that of Morph-C of **Pt1_SbF₆**, with a small dip at the emission maximum. The emission color of **Pt3_ONTf** is different from all the cationic Pt(II) complexes studied in this chapter, with the emission maximum at 611 nm. The heavily fluorinated side chain is more rigid comparing with the alkyl groups, and the strong affinity between the fluorous tails, in turn, alter the packing patterns in the solid states.²⁴

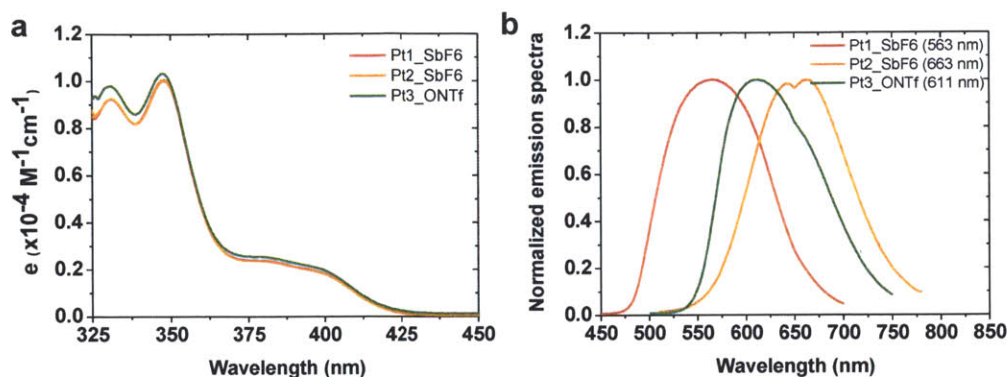


Figure 3.14. Photophysical properties of **Pt1_SbF₆**, **Pt2_SbF₆** and **Pt3_ONTf**: (a) UV-vis absorption spectra in acetone solution ($\sim 10^{-6}$ M); (b) solid-state emission spectra of solid samples ($\lambda_{\text{ex}} = 400$ nm).

3.2.8 Liquid crystalline properties

In fact, the transformation from Morph-A to Morph-C of **Pt1_SbF₆** can also be achieved by heating. The yellow solid of **Pt1_SbF₆** undergoes three heating/cooling cycles from 25 °C to 250 °C with the rate of 10 °C/min, and the DSC trace is plotted in Figure 3.15. The trace for the third cycle is identical to that of the second cycle, indicating good thermal stability of **Pt1_SbF₆**. At the end of the third cycle, the sample is retrieved and subjected to PL study. The emission spectrum of the resulted dark red crystals resembles that of Morph-C and the ground sample. Therefore, heating and mechanical force can both drive the molecular reorganization in the solid states.

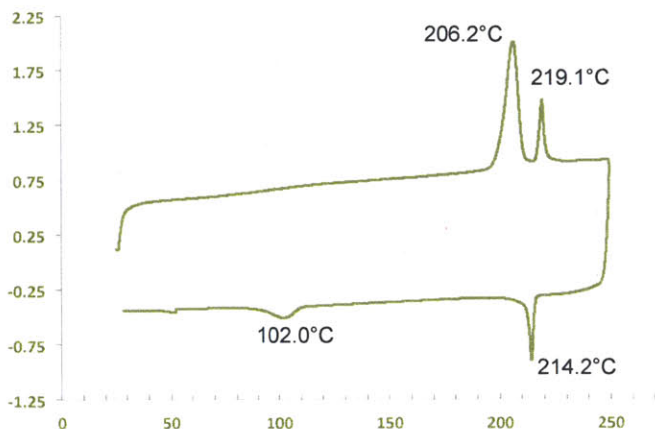


Figure 3.15. DSC trace of **Pt1_SbF₆**.

The absence of the over cooling effect based on the DSC study of **Pt1_SbF₆** led us to study the possible formation of liquid crystal phases. The small temperature difference between the last endothermic transition (219 °C) during the heating cycle and the first exothermic transition (214 °C) during the consecutive cooling cycle indicates that this transition is not the crystallization process. Microcrystals of **Pt1_SbF₆** are heated to the isotropic phase between two glass cover slips, and the cooling process (2 °C/min) is examined by polarized optical microscope (POM). The formation of dendritic optical textures with rectilinear defects (Figure 3.16) confirms that a hexagonal columnar (Col_h) mesophase is formed. The liquid-crystallinity of **Pt1_SbF₆** is surprising since it usually takes six to eight long alkyl groups for the ppy-based Pt(II) compounds to form columnar phases.²⁵⁻²⁷ Moreover, this is the first thermotropic Col_h liquid crystal with only one side chain to the best of our knowledge.

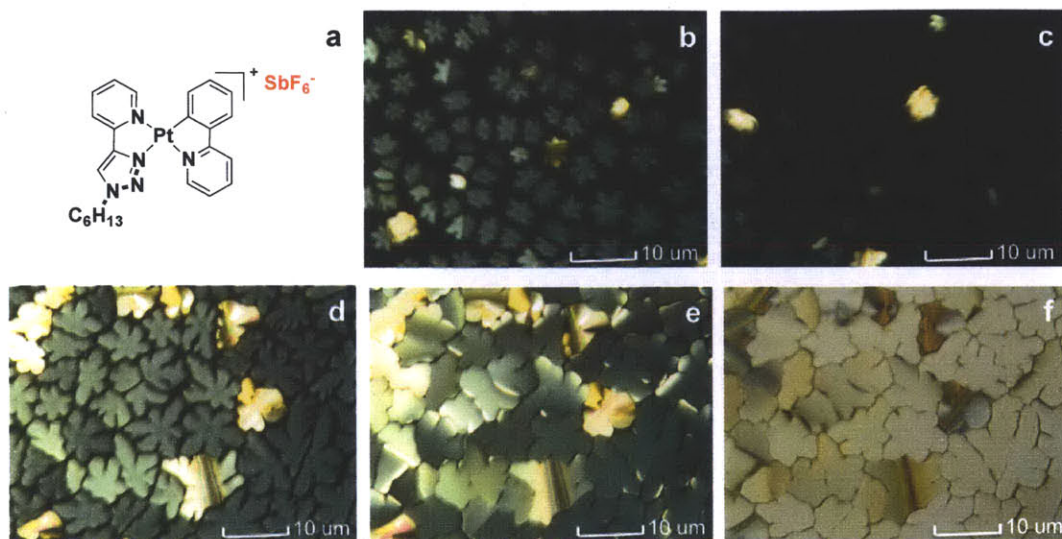


Figure 3.16. POM images of the Col_h phase of $Pt1_SbF_6$: (a) the chemical structure of $Pt1_SbF_6$; (b) 90° polarized at $218^\circ C$; (c) rotated by 45° polarized at $218^\circ C$; (d) 90° polarized at $216^\circ C$; (e) 90° polarized at $203^\circ C$; (f) non-polarized at $203^\circ C$.

Counterions play an important role in determining the liquid crystalline properties. The clearing temperatures decrease in the order of $Pt1_SbF_6$ ($219^\circ C$) > $Pt1_PF_6$ ($203^\circ C$) > $Pt1_BF_4$ ($164^\circ C$) = $Pt1_OTf$ ($164^\circ C$). The trend of clearing temperatures corresponds well with the solubilities of the compounds, both controlled by the strength of the intermolecular interactions.

The mesogen textures observed with $Pt1_PF_6$ are remarkably different from those of $Pt1_SbF_6$. The domain sizes are much smaller (Figure 3.17), and diversified textures are observed in different regions of the sample (Figure 3.18). Moreover, all attempted shearing in the isotropic phase, in the hope of facilitating the alignment, triggers rapid crystallization. Significant overcooling is observed for $Pt1_PF_6$, together with a cold crystallization transition at $115^\circ C$ during the heating cycles of the second and third run. Therefore, any external stimuli would favor crystallization from the overcooled isotropic phase.

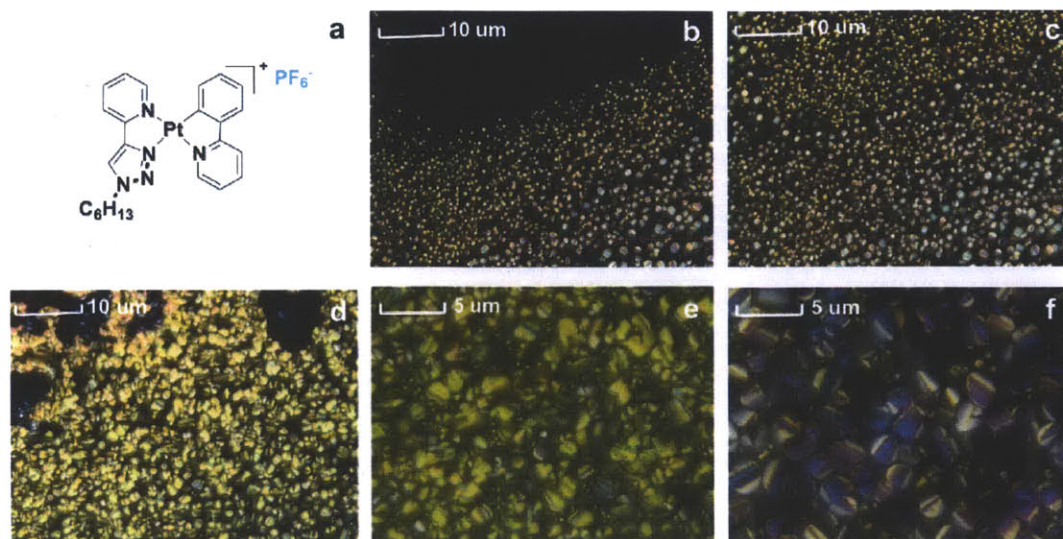


Figure 3.17. POM images of the Col_h phase of $Pt1_PF_6$: (a) the chemical structure of $Pt2_PF_6$; mesogen development (b) at 192 °C; (c) at 191 °C; (d) at 186 °C; (e-f) textures at 180 °C. All the images were captured with 90° polarization.

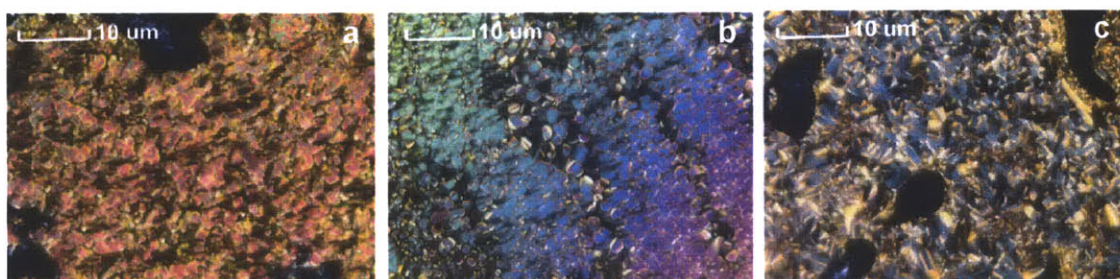


Figure 3.18. POM images of the Col_h phase of $Pt1_PF_6$: (a-b) textures of different regions at 180 °C; (c) textures at room temperature. All the images were captured with 90° polarization.

Only very small mesogenic textures are observed for $Pt1_BF_4$ (Figure 3.19). Meanwhile, the crystallization process is competing with the formation of the liquid crystal phase. Uniform needle-like crystals, instead of the mesogens, would form when the cooling rate is faster than 1 °C/min from the isotropic phase. Once formed, the crystals exhibit remarkably high thermal stability. The sample has to be heated up to 230 °C to melt the crystals completely, which is 52 °C higher than the regular clearing

temperature under the same experimental conditions. The competition between mesogen formation and crystallization can be attributed to the similarity between the transition temperatures for these two processes.

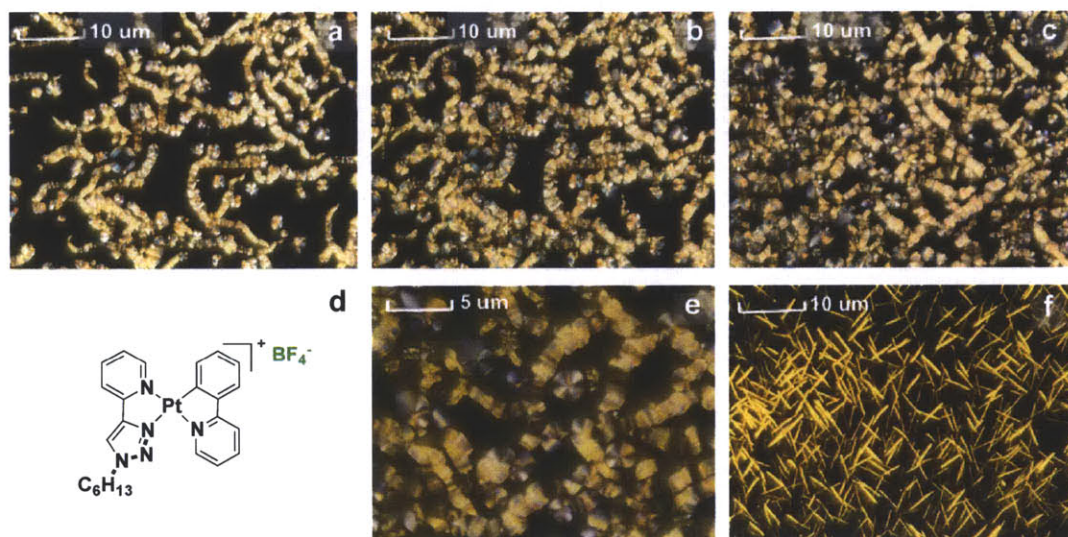


Figure 3.19. POM images of **Pt1_BF₄**: (a-c) mesogen development at 149 °C; (d) the chemical structure of **Pt1_BF₄**; (e) textures at 149 °C; (f) the competing crystallization process. All the images were captured with 90° polarization.

Pt1_OTf exhibits similar liquid crystalline behavior to that of **Pt1_SbF₆**. The characteristic Col_h textures are formed upon cooling (Figure 3.20), and retained even when cooled to room temperature. This is in agreement with the DSC data, which show no transitions for crystallization or cold crystallization. Although **Pt1_OTf** is similar to **Pt1_BF₄** in many aspects, subtle changes in the shapes and electronic properties of the anions have strong influence on the liquid crystal behavior.

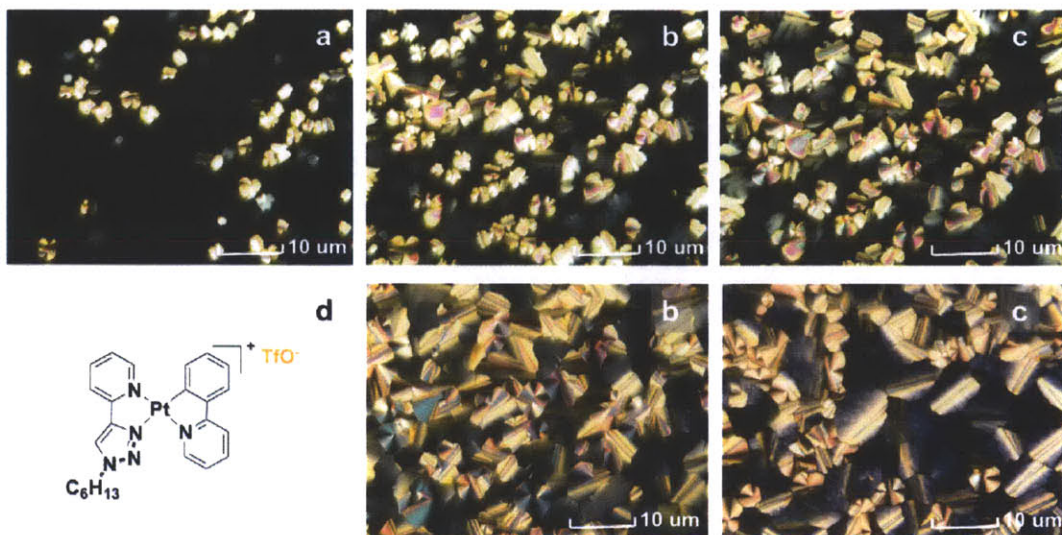


Figure 3.20. POM images of the Col_h phase of **Pt1_OTf**: mesogen development (a) at 164 °C; (b) at 162 °C; (c) at 161 °C; (d) the chemical structure of **Pt1_OTf**; (e) textures at 60 °C; (f) textures at room temperature. All the imaged are captured with 90° polarization.

Although longer alkyl groups usually help to stabilize the mesophases, **Pt2_PF₆** proves to be inferior to **Pt1_SbF₆**. The transitions for mesogen formation and crystallization overlap with each other. Therefore, no mesophase is observed with POM (Figure 3.21). The clearing temperature (219 °C) is identical to that of **Pt1_PF₆**, a compromise between the increase in both molecular weight and entropy by introducing the dodecyl group.

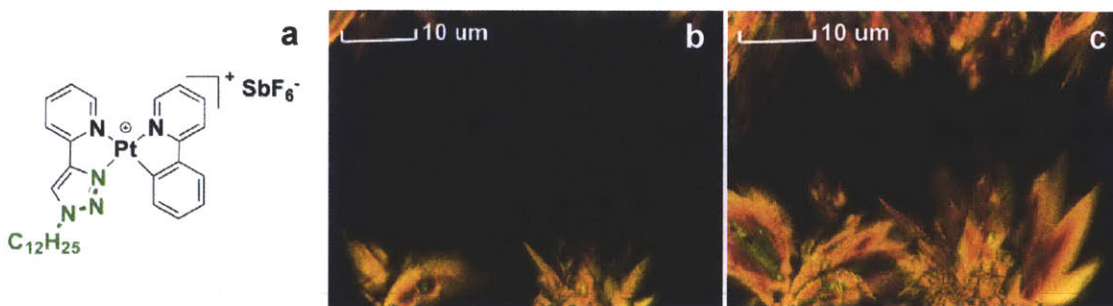


Figure 3.21. POM images of **Pt2_SbF₆**: (a) the chemical structure of **Pt2_SbF₆**; (b-c) the crystallization process at 208 °C. All the imaged were captured with 90° polarization.

In short, **Pt1_X** ($X = \text{SbF}_6^-$, PF_6^- , BF_4^- , OTf^-) represent the first thermotropic Col(h) liquid crystals with only one side chain. Furthermore, the combined liquid crystalline and mechanochromic properties make this family of compounds, especially **Pt1_SbF₆**, very attractive functional materials.²² Detailed XRD study is in progress.

3.3 Experimental Section

General Methods and Instrumentation.

All reactions were performed under an argon atmosphere despite of the stability of the product toward air and moisture, using oven-dried glassware and standard Schlenk techniques. ^1H , gCOSY, TOCSY, ROESY and $^{13}\text{C}\{^1\text{H}\}$ NMR spectra were recorded on either a Bruker 400 MHz or Varian 500 MHz spectrometer and referenced to the residual proton or carbon resonance of the deuterated solvent. ^{19}F NMR spectra were recorded on a Varian 300 MHz spectrometer and referenced to an external standard CFCl_3 (0 ppm). Electrospray ionization (ESI) high-resolution mass spectrometry (HRMS) was measured on a Bruker Daltonics APEXIV 4.7 Tesla Fourier Transform Ion Cyclotron Resonance Mass Spectrometer and the most abundant masses are reported.

UV/Vis spectra were recorded on an Agilent 8453 diode-array spectrophotometer. Emission spectra were acquired on a SPEX Fluorolog fluorometer (model FL-321, 450 W xenon lamp) using either right-angle detection (solution measurements) or front-face detection (thin film measurements). All room temperature solution samples for emission spectra were degassed with Ar in an anaerobic cuvette. Samples for the solid-state emission spectra were prepared by drop-casting a suspension of the target compound in

mixed dichloromethane and hexane onto glass substrates. The solid-state photoluminescence quantum yield (PLQY) was measured with an integrating sphere.

Materials and Synthesis. Potassium tetrachloroplatinate(II) (K_2PtCl_4) and copper(II) sulfate ($CuSO_4$) were purchased from Strem Chemicals. 2-Ethynylpyridine, 2-phenylpyridine, and all other reagents were obtained from Aldrich Chemicals and used as received. Anhydrous CH_2Cl_2 was obtained from a solvent purification system (Innovative Technologies), and stored under argon.

The Pt(II) precursor $Pt(ppy)(SEt_2)Cl$ (**Pt-B**) were synthesized from K_2PtCl_4 and 2-phenylpyridine over two steps.²⁸ 1-azidohexane,²⁹ 1-azido-2-(perfluorooctyl)ethane,³⁰ 2-(1-hexyl-1*H*-1,2,3-triazol-4-yl)-pyridine and 2-(1-dodecyl-1*H*-1,2,3-triazol-4-yl)-pyridine³¹ were prepared according to modified literature methods.

CAUTION: There have been safety concerns about handling organoazides, especially the ones with short alkyl groups. Therefore, all the organoazides used in this report were synthesized on small scales and handled with great care.

Preparation of $[Pt(ppy)(trpy-C_6H_{13})]SbF_6$ (Pt1_SbF6**).** $Pt(ppy)(SEt_2)Cl$ (**Pt-B**, 47.2 mg, 0.1 mmol) and $trpy-C_6H_{13}$ (**L1**, 23.0 mg, 0.1 mmol) were dissolved in dry CH_2Cl_2 (6 ml) under Ar. To the yellow solution, a CH_2Cl_2 solution of $AgSbF_6$ (34.4 mg, 0.1 mmol) was added while protected from light. The mixture was stirred rapidly at room temperature in the dark. After 3 h, the bright yellow suspension was diluted with CH_2Cl_2 , and filtered to remove the $AgCl$ precipitate. The filtrate was concentrated and added toluene, and the resulted bright yellow solid was washed extensively with toluene. After

recrystallization from hot CH₂Cl₂, **Pt1_SbF₆** was isolated as bright yellow crystals (75 mg, 92%). HRMS (ESI): 579.1837 [calcd for (M-SbF₆)⁺: 579.1828].

Major:

¹H NMR (500 MHz, DMSO-*d*₆, ppm): 9.36 (d, J = 5.8 Hz, 1 H), 9.24 (s, 1 H), 9.06 (d, J = 5.8 Hz, 1 H), 8.41 - 8.36 (m, 1 H), 8.19 - 8.15 (m, 1 H), 8.11 (t, J = 7.6 Hz, 1 H), 8.02 (d, J = 8.2 Hz, 1 H), 7.72 - 7.65 (m, 1 H), 7.39 (t, J = 6.6 Hz, 1 H), 7.26 - 7.17 (m, 3 H), 4.61 (t, J = 7.3 Hz, 2 H), 2.03 - 1.94 (m, 2 H), 1.46 - 1.27 (m, 6 H), 0.89 (t, J = 6.9 Hz, 3 H).
¹³C NMR (126 MHz, Acetone-*d*₆, ppm): 14.4, 23.2, 26.8, 30.2, 31.9, 53.6, 120.2, 123.4, 124.1, 125.0, 126.0, 126.3, 127.3, 130.5, 133.3, 141.3, 141.8, 147.0, 148.6, 150.3, 150.5, 151.9, 167.3.

Minor:

¹H NMR (500 MHz, DMSO-*d*₆, ppm): 9.22 (s, 1 H), 8.86 (d, J = 5.5 Hz, 1 H), 8.69 (d, J = 5.8 Hz, 1 H), 8.37 - 8.34 (m, 1 H), 8.22 - 8.19 (m, 1 H), 8.13 (d, J = 4.0 Hz, 1 H), 8.05 (d, J = 8.2 Hz, 1 H), 7.76 (t, J = 6.4 Hz, 1 H), 7.67 - 7.65 (m, 1 H), 7.44 (t, J = 6.6 Hz, 1 H), 7.19 (m, 1 H), 7.16 (t, J = 7.5 Hz, 2 H), 7.10 (t, J = 7.9 Hz, 1 H), 4.61 (t, J = 7.3 Hz, 2 H), 2.03 - 1.94 (m, 2 H), 1.46 - 1.27 (m, 6 H), 0.89 (t, J = 6.9 Hz, 3 H). ¹³C NMR (126 MHz, Acetone-*d*₆, ppm): 14.4, 23.2, 26.8, 30.2, 31.9, 53.8, 120.6, 123.1, 124.2, 124.4, 125.8, 127.2, 130.2, 135.1, 137.9, 140.9, 141.5, 145.4, 148.5, 149.8, 150.7, 152.7, 167.8.

Preparation of [Pt(ppy)(trpy-C₆H₁₃)]PF₆ (Pt1_PF₆). Pt(ppy)(SEt₂)Cl (**Pt-B**, 47.5 mg, 0.1 mmol) and trpy-C₆H₁₃ (**L1**, 23.0 mg, 0.1 mmol) were dissolved in dry CH₂Cl₂ (6 ml). The solution was treated with AgPF₆ (25.3 mg, 0.1 mmol) following the procedure detailed for the synthesis of **Pt1_SbF₆** above. Compound **Pt1_PF₆** was isolated as a yellow orange solid (70 mg, 96%), after recrystallization from CH₂Cl₂/hexane. HRMS

(ESI): 579.1817 [calcd for (M-PF₆)⁺: 579.1828]. ¹⁹F NMR (282 MHz, CD₂Cl₂, ppm): -72.66 (J_{P-F} = 717.2 Hz).

Major:

¹H NMR (500 MHz, CD₂Cl₂, ppm): 9.22 (d, J = 5.5 Hz, 1 H), 8.86 (d, J = 5.5 Hz, 1 H), 8.48 (s, 1 H), 8.06 (t, J = 7.6 Hz, 1 H), 7.87 - 7.82 (m, 1 H), 7.53 (d, J = 7.9 Hz, 1 H), 7.38 (t, J = 6.6 Hz, 1 H), 7.35 - 7.30 (m, 1 H), 7.15 - 7.08 (m, 3 H), 7.02 - 6.99 (m, 1 H), 4.46 (t, J = 7.5 Hz, 2 H), 2.05 - 1.97 (m, 2 H), 1.44 - 1.33 (m, 6 H), 0.91 (t, J = 7.9 Hz, 3 H). ¹³C NMR (126 MHz, Acetone-*d*₆, ppm): 14.4, 23.3, 26.8, 30.1, 31.9, 53.4, 120.1, 123.3, 124.0, 124.9, 125.8, 126.1, 127.1, 130.3, 133.0, 141.1, 141.6, 146.8, 148.3, 150.0, 151.8, 152.4, 167.0.

Minor:

¹H NMR (500 MHz, CD₂Cl₂, ppm): 8.41 (d, J = 5.2 Hz, 1 H), 8.34 (s, 1 H), 8.19 (d, J = 5.5 Hz, 1 H), 7.99 (t, J = 9.2 Hz, 1 H), 7.95 (d, J = 7.6 Hz, 1 H), 7.83 - 7.77 (m, 2 H), 7.51 - 7.48 (m, 2 H), 7.23 (d, J = 7.6 Hz, 1 H), 7.08 - 7.06 (m, 1 H), 7.00 - 6.97 (m, 2 H), 4.46 (t, J = 7.5 Hz, 2 H), 2.05 - 1.97 (m, 2 H), 1.44 - 1.33 (m, 6 H), 0.91 (t, J = 7.9 Hz, 3 H). ¹³C NMR (126 MHz, Acetone-*d*₆, ppm): 14.4, 23.3, 26.8, 30.1, 31.9, 53.4, 120.4, 122.9, 124.2, 125.6, 127.1, 130.1, 137.8, 140.8, 141.3, 145.1, 148.2, 149.5, 149.6, 150.2, 150.5, 167.5.

Preparation of [Pt(ppy)(trpy-C₆H₁₃)]BF₄ (Pt1_BF₄). Pt(ppy)(SEt₂)Cl (Pt-B, 47.5 mg, 0.1 mmol) and trpy-C₆H₁₃ (L1, 23.0 mg, 0.1 mmol) were dissolved in dry CH₂Cl₂ (6 ml). The solution was treated with AgBF₄ (19.5 mg, 0.1 mmol) following the procedure detailed for the synthesis of Pt1_SbF₆ above. Compound Pt1_BF₄ was isolated as an

orange-red solid (63 mg, 94%), after recrystallization from CH₂Cl₂/hexane. HRMS (ESI): 579.1838 [calcd for (M-BF₄)⁺: 579.1828]. ¹⁹F NMR (282 MHz, CD₂Cl₂, ppm): -151.30.

Major:

¹H NMR (500 MHz, CD₂Cl₂, ppm): 10.09 (d, J = 5.5 Hz, 1 H), 9.70 (d, J = 5.8 Hz, 1 H), 9.63 (s, 1 H), 8.97 (t, J = 7.5 Hz, 1 H), 8.88 (d, J = 7.3 Hz, 1 H), 8.78 - 8.73 (m, 1 H), 8.42 (d, J = 7.9 Hz, 1 H), 8.28 (t, J = 6.3 Hz, 1 H), 8.20 - 8.16 (m, 1 H), 8.03 - 7.95 (m, 3 H), 7.93 - 7.88 (m, 1 H), 5.41 (t, J = 7.5 Hz, 2 H), 2.99 - 2.90 (m, 2 H), 2.40 - 2.25 (m, 6 H), 1.86 (t, J = 6.7 Hz, 3 H). ¹³C NMR (126 MHz, CD₂Cl₂, ppm): 14.3, 23.0, 26.6, 30.3, 31.6, 53.5, 119.9, 123.4, 123.6, 124.9, 126.4, 126.6, 130.4, 132.7, 140.8, 141.2, 146.9, 148.1, 150.0, 151.7, 152.0, 166.8.

Minor:

¹H NMR (500 MHz, CD₂Cl₂, ppm): 9.47 (s, 1 H), 9.38 (d, J = 5.5 Hz, 1 H), 9.14 (d, J = 5.5 Hz, 1 H), 8.92 (td, J = 1.0, 7.9 Hz, 1 H), 8.82 (td, J = 1.0, 6.1 Hz, 1 H), 8.73 - 8.69 (m, 1 H), 8.61 - 8.55 (m, 1 H), 8.50 (t, J = 6.3 Hz, 1 H), 8.40 (d, J = 8.2 Hz, 1 H), 8.11 (t, J = 6.3 Hz, 1 H), 8.07 (d, J = 7.0 Hz, 1 H), 7.90 - 7.86 (m, 2 H), 5.29 (t, J = 7.5 Hz, 2 H), 2.92 - 2.85 (m, 2 H), 2.40 - 2.25 (m, 6 H), 1.86 (t, J = 6.7 Hz, 3 H). ¹³C NMR (126 MHz, CD₂Cl₂, ppm): 14.3, 23.1, 26.8, 30.3, 31.7, 53.7, 120.2, 123.0, 124.0, 124.2, 126.1, 127.1, 130.1, 134.7, 138.5, 141.0, 141.0, 147.9, 149.3, 149.8, 150.1, 167.0.

Preparation of [Pt(ppy)(trpy-C₆H₁₃)]OTf (Pt1_OTf). Pt(ppy)(SEt₂)Cl (**Pt-B**, 23.8 mg, 0.05 mmol) and trpy-C₆H₁₃ (**L1**, 11.5 mg, 0.1 mmol) were dissolved in dry CH₂Cl₂ (6 ml). The solution was treated with a THF solution of AgOTf (12.8 mg, 0.05 mmol), following the procedure detailed for the synthesis of **Pt1_SbF₈2%** above. Compound **Pt1_OTf** was isolated as an orange solid (33 mg, 91%), after recrystallization from

CH₂Cl₂/hexane. HRMS (ESI): 579.1834 [calcd for (M-OTf)⁺: 579.1828]. ¹⁹F NMR (282 MHz, CD₂Cl₂, ppm): -79.06.

Major:

¹H NMR (500 MHz, CD₂Cl₂, ppm): 9.26 (d, J = 5.2 Hz, 1 H), 9.00 (d, J = 1.8 Hz, 1 H), 8.89 (d, J = 5.5 Hz, 1 H), 8.14 - 8.04 (m, 1 H), 7.97 (d, J = 5.2 Hz, 1 H), 7.90 - 7.82 (m, 2 H), 7.60 (d, J = 7.9 Hz, 1 H), 7.44 - 7.34 (m, 2 H), 7.20 - 6.97 (m, 3 H), 4.48 (t, J = 7.3 Hz, 2 H), 2.07 - 1.94 (m, 2 H), 1.50 - 1.28 (m, 6 H), 0.91 (t, J = 7.0 Hz, 3 H). ¹³C NMR (126 MHz, CD₂Cl₂, ppm): 14.3, 23.0, 26.5, 30.3, 31.6, 53.4, 119.8, 120.3 (CF₃SO₃⁻), 123.4, 123.6, 124.7, 125.9, 126.4, 126.7, 130.4, 133.0, 140.6, 141.1, 146.6, 148.2, 149.7, 150.2, 151.7, 167.2.

Minor:

¹H NMR (500 MHz, CD₂Cl₂, ppm): 8.80 (s, 1 H), 8.50 (d, J = 4.9 Hz, 1 H), 8.27 (d, J = 5.5 Hz, 1 H), 8.08 - 8.03 (m, 2 H), 7.82 (t, J = 8.5 Hz, 1 H), 7.57 (d, J = 8.2 Hz, 1 H), 7.54 - 7.50 (m, 1 H), 7.27 (d, J = 7.6 Hz, 1 H), 7.17 - 6.98 (m, 4 H), 4.40 (t, J = 7.5 Hz, 2 H), 2.08 - 1.94 (m, 2 H), 1.49 - 1.27 (m, 6 H), 0.93 (t, J = 7.3 Hz, 3 H). ¹³C NMR (126 MHz, CD₂Cl₂, ppm): 14.3, 23.0, 26.5, 30.3, 31.6, 53.4, 120.1, 120.3 (CF₃SO₃⁻), 122.9, 123.1, 124.0, 125.6, 126.8, 130.1, 134.8, 137.4, 140.7, 140.8, 144.8, 148.2, 149.1, 150.2, 152.0, 167.5.

Preparation of trpy-C₁₂H₂₅ (L2). A mixture of 2-ethynylpyridine (309 mg, 3 mmol), 1-azidododecane²⁹ (634 mg, 3 mmol), CuSO₄ (150 mg, 0.6 mmol), and sodium ascorbate (238 mg, 1.2 mmol) in THF (20 ml, with 5% H₂O) was stirred rapidly for 20 h at room temperature. The solvent was evaporated and the brown residue was extracted between CH₂Cl₂ and aqueous NH₄OH. The organic layer was dried over MgSO₄, filtered and

volatiles removed via rotary evaporation to give an off-white solid. The crude product was flash chromatographed on silica gel, using hexane/ethyl acetate (2:1) as the eluent. After recrystallization from CH₂Cl₂/hexane, **L2** was isolated as white crystals (880 mg, 93%). HRMS (ESI): 315.2547 [calcd for (M+H)⁺: 315.2543]. ¹H NMR (400 MHz, CD₂Cl₂, ppm): 9.48 (d, J = 4.6 Hz, 1 H), 9.08 (s, 1 H), 9.06 (d, J = 7.9 Hz, 1 H), 8.70 (dt, J = 1.5, 7.8 Hz, 1 H), 8.14 (dd, J = 5.3, 7.2 Hz, 1 H), 2.86 (t, J = 7.0 Hz, 2 H), 2.31 - 2.24 (m, 2 H), 2.24 - 2.12 (m, 10 H), 1.81 (t, J = 6.9 Hz, 3 H). ¹³C NMR (126 MHz, CD₂Cl₂, ppm): 14.5, 23.3, 27.0, 29.6, 29.9, 30.0, 30.1, 30.2, 30.8, 32.5, 51.0, 120.3, 122.5, 123.2, 137.2, 148.8, 150.0, 151.2.

Preparation of [Pt(ppy)(trpy-C₁₂H₂₅)]SbF₆ (Pt₂_SbF₆). Pt(ppy)(SEt₂)Cl (**Pt-B**, 23.7 mg, 0.05 mmol) and trpy-C₁₂H₂₅ (**L2**, 15.7 mg, 0.05 mmol) were dissolved in dry CH₂Cl₂ (6 ml). The solution was treated with a THF solution of AgSbF₆ (17.2 mg, 0.05 mmol), following the procedure detailed for the synthesis of **Pt1_SbF₆** above. Compound **Pt₂_SbF₆** was isolated as an orange-red solid (37 mg, 82%), after recrystallization from CH₂Cl₂/hexane. HRMS (ESI): 663.2751 [calcd for (M-SbF₆)⁺: 663.2768].

Major:

¹H NMR (400 MHz, CD₂Cl₂ (10% v/v Acetone-*d*₆), ppm): 9.12 (d, J = 5.5 Hz, 1 H), 8.77 (d, J = 5.8 Hz, 1 H), 8.43 (s, 1 H), 8.02 (t, J = 7.3 Hz, 1 H), 7.88 (d, J = 7.6 Hz, 1 H), 7.81 - 7.75 (m, 2 H), 7.46 - 7.42 (m, 1 H), 7.33 (t, J = 6.1 Hz, 1 H), 7.25 - 7.20 (m, 1 H), 7.06 - 6.97 (m, 3 H), 4.44 (t, J = 7.6 Hz, 2 H), 2.01 - 1.91 (quin, J = 7.2 Hz, 2 H), 1.37 (br. s., 4 H), 1.31 - 1.18 (m, 14 H), 0.81 (t, J = 4.6 Hz, 3 H). ¹³C NMR (126 MHz, CD₂Cl₂ (10% v/v Acetone-*d*₆), ppm): 14.3, 23.2, 26.8, 30.0, 32.4, 53.4, 119.7, 122.9, 123.5, 124.6,

125.4, 126.0, 126.7, 130.3, 132.7, 134.7, 140.7, 141.1, 146.6, 148.1, 149.5, 149.8, 151.6, 166.8.

Minor:

^1H NMR (400 MHz, CD_2Cl_2 (10% v/v Acetone- d_6), ppm): 8.36 (d, $J = 5.5$ Hz, 1 H), 8.31 (s, 1 H), 8.16 (d, $J = 5.5$ Hz, 1 H), 7.98 (t, $J = 7.3$ Hz, 1 H), 7.77 - 7.72 (m, 1 H), 7.48 (m, 1 H), 7.25 - 7.21 (m, 1 H), 7.18 (d, $J = 7.3$ Hz, 1 H), 7.09 (t, $J = 6.3$ Hz, 1 H), 7.04 (t, $J = 6.7$ Hz, 2 H), 6.96 - 6.88 (m, 2 H), 4.40 (t, $J = 7.6$ Hz, 2 H), 2.01 - 1.91 (quin, $J = 7.2$ Hz, 2 H), 1.37 (br. s., 4 H), 1.31 - 1.18 (m, 14 H), 0.81 (t, $J = 4.6$ Hz, 3 H). ^{13}C NMR (126 MHz, CD_2Cl_2 (10% v/v Acetone- d_6), ppm): 14.3, 23.2, 26.8, 30.0, 32.4, 53.7, 120.1, 122.7, 123.6, 124.0, 125.3, 125.8, 126.9, 130.1, 136.0, 139.6, 140.9, 141.0, 145.0, 147.9, 149.0, 150.1, 152.2, 167.2.

Preparation of trpy- $\text{C}_2\text{H}_4\text{C}_8\text{H}_{17}$ (L3). A mixture of 2-ethynylpyridine (309 mg, 3 mmol), 1-azido-2-(perfluorooctyl)ethane (1.46 g, 3 mmol), CuSO_4 (150 mg, 0.6 mmol), and sodium ascorbate (238 mg, 1.2 mmol) in THF (20 ml, with 5% H_2O) was stirred rapidly for 20 h at room temperature. The solvent was evaporated and the brown residue was extracted between ethyl acetate and aqueous NH_4OH . The organic layer was dried over MgSO_4 , filtered and volatiles removed via rotary evaporation to give an off-white solid. The crude product was flash chromatographed on silica gel, using CH_2Cl_2 /ethyl acetate (4:1) as the eluent. After recrystallization from CH_2Cl_2 /hexane, **L3** was isolated as white crystals (1.3 g, 73%). HRMS (ESI): 593.0602 [calcd for $(\text{M}+\text{H})^+$: 593.0629]. ^{19}F NMR (282 MHz, CD_2Cl_2 , ppm): -126.60 (CF_2), -123.94 (CF_2), -123.19 (CF_2), -122.36 (CF_2), -122.13 (2CF_2), -114.67 (CF_2), -81.36 (t, $J = 9.2$ Hz, CF_3). ^1H NMR (400 MHz, CD_2Cl_2 , ppm): 8.57 (d, $J = 4.3$ Hz, 1 H), 8.21 (s, 1 H), 8.13 (d, $J = 7.8$ Hz, 1 H), 7.79 (dt,

$J = 1.5, 7.8$ Hz, 1 H), 7.25 (dd, $J = 5.1, 6.8$ Hz, 1 H), 4.76 (t, $J = 7.3$ Hz, 2 H), 2.99 - 2.79 (m, 2 H). ^{13}C NMR (126 MHz, THF- d_4 , ppm): 32.1 (t, $J_{\text{C-F}} = 23.0$ Hz), 42.9, 120.4, 123.4, 123.8, 137.5, 149.5, 150.5, 152.0.

Preparation of [Pt(ppy)(trpy- $\text{C}_2\text{H}_4\text{C}_8\text{H}_{17}$)] $\text{C}_4\text{F}_9\text{SO}_3$ (Pt3_ONTf). Pt(ppy)(SEt₂)Cl (Pt-B, 23.7 mg, 0.05 mmol) and trpy- $\text{C}_2\text{H}_4\text{C}_8\text{H}_{17}$ (L3, 59.0 mg, 0.1 mmol) were dissolved in dry $\text{CH}_2\text{Cl}_2/\text{THF}$ (6 ml/2 ml). The solution was treated with a THF solution of AgSbF_6 (40.7 mg, 0.1 mmol), following the procedure detailed for the synthesis of Pt1_SbF₆ above. Compound Pt3_ONTf was isolated as an orange-red solid (117 mg, 90%), after recrystallization from acetone. HRMS (ESI): 941.0874 [calcd for (M-ONTf)⁺: 941.0860]. ^{19}F NMR (282 MHz, CD_2Cl_2 , ppm): -125.86 (2CF₂), 123.13 (CF₂), -122.50 (CF₂), -121.66 (CF₂), -121.27 (3CF₂), -114.72 (CF₂), -113.41 (CF₂), -81.09 (CF₃), -80.87 (CF₃).

Major:

^1H NMR (500 MHz, Acetone- d_6 , ppm): 9.21 (d, $J = 5.5$ Hz, 1 H), 9.08 (s, 1 H), 8.93 (d, $J = 5.5$ Hz, 1 H), 8.19 (t, $J = 7.6$ Hz, 1 H), 8.01 - 7.96 (m, 2 H), 7.94 - 7.90 (m, 1 H), 7.69 (d, $J = 7.9$ Hz, 1 H), 7.53 (q, $J = 5.9$ Hz, 1 H), 7.40 (dd, $J = 3.2, 6.0$ Hz, 1 H), 7.16 (t, $J = 6.1$ Hz, 1 H), 7.08 - 7.01 (m, 3 H), 5.04 (t, $J = 7.3$ Hz, 2 H), 3.27 - 3.17 (m, 2 H).

Minor:

^1H NMR (500 MHz, Acetone- d_6 , ppm): 9.01 (s, 1 H), 8.62 (d, $J = 5.2$ Hz, 1 H), 8.45 (d, $J = 5.5$ Hz, 1 H), 8.12 (t, $J = 7.6$ Hz, 1 H), 7.97 (s, 1 H), 7.91 - 7.88 (m, 1 H), 7.69 - 7.67 (m, 1 H), 7.51 (br. s., 1 H), 7.34 (d, $J = 7.3$ Hz, 1 H), 7.22 (t, $J = 6.1$ Hz, 1 H), 7.05 - 7.02 (m, 2 H), 6.99 - 6.94 (m, 1 H), 5.04 (t, $J = 7.3$ Hz, 2 H), 3.27 - 3.17 (m, 2 H).

Characterization of liquid crystalline materials.

Optical microscopy was carried out using standard glass microscope slides on a Leica DM RXP Optical Microscope equipped with a Mettler FP82HT hot stage controlled by Linkham TMS 94 Temperature Controller. Differential scanning calorimetry (DSC) experiments were performed on a TA Instruments Q10 DSC. Each sample (3~5 mg), sealed in aluminum pans, was underwent three heating/cooling cycles from 25 °C to 250 °C with the rate of 10 °C/min.

Powder X-ray diffraction (XRD) data were collected using an Inel CPS 120 position sensitive detector using an XRG 3000 generator (Cu K α). Crushed powder samples were loaded onto aluminium sample substrate. XRD data is shown as the intensity as a function of the length of the scattering wave vector q , defined as $q = |q| = 4\pi \sin\theta / n\lambda$, where θ is the scattering angle, n is an integer and λ is the wavelength ($\lambda_{\text{Cu K}\alpha} = 1.54 \text{ \AA}$). The layer spacing at a particular temperature is determined as the maximum of a fit of a Gaussian distribution to the fundamental reflection in inverse space q . Then, the (layer) spacing d was calculated by $d_{001} = 2\pi / q_{FIT}$, where q_{FIT} is the peak position of the fitted curve.

Thin films for luminescence study.

Samples for the solid-state emission spectra were prepared by drop-casting a suspension of the target compound in mixed dichloromethane and hexane onto glass substrates.

Polymer-based thin films were prepared by spin-coating at the rate of 100 rpm, from a solution of the respective polymer and [Pt(ppy)(trpy-C₆H₁₃)]SbF₆ (**Pt1_SbF₆**, 6-8 % w/w relative to the polymer). Different solvents were used to accommodate the solubility of

the polymers. MeOH is used for polyethylene oxide (PEO, $M_w = 20,000$) and poly(4-vinylpyridine) (P4VP, $M_w = 60,000$), while THF(with 5% v/v acetone) for polystyrene (PS, $M_w = 220,000$) and poly(methyl methacrylate) (PMMA, $M_w = 120,000$). All the solutions were filtered through a PTFE syringe filter (0.2 μm) before use.

3.4 References:

- (1) Donnio, B.; Bruce, D. W. In *Palladacycles: Synthesis, Characterization and Applications*; Dupont, J.; Pfeffer, M., Eds.; Wiley-VCH Verlag GmbH & Co. KGaA, 2008; pp. 239–283.
- (2) Balch, A. L. *Angew. Chem. Int. Ed.* **2009**, *48*, 2641–2644.
- (3) Sagara, Y.; Kato, T. *Nat. Chem.* **2009**, *1*, 605–610.
- (4) Wong, K. M.-C.; Yam, V. W.-W. *Acc. Chem. Res.* **2011**, *44*, 424–434.
- (5) Yam, V. W.-W.; Wong, K. M.-C.; Zhu, N. *J. Am. Chem. Soc.* **2002**, *124*, 6506–6507.
- (6) Yam, V. W.-W.; Chan, K. H.-Y.; Wong, K. M.-C.; Zhu, N. *Chem. Eur. J.* **2005**, *11*, 4535–4543.
- (7) Wang, J.; Chen, Y.; Law, Y.-C.; Li, M.; Zhu, M.-X.; Lu, W.; Chui, S. S.-Y.; Zhu, N.; Che, C.-M. *Chem. Asian J.* **2011**, *6*, 3011–3019.
- (8) Meldal, M.; Tornøe, C. W. *Chem. Rev.* **2008**, *108*, 2952–3015.
- (9) Liu, S.; Müller, P.; Takase, M. K.; Swager, T. M. *Inorg. Chem.* **2011**, *50*, 7598–7609.
- (10) Struthers, H.; Mindt, T. L.; Schibli, R. *Dalton Trans.* **2010**, *39*, 675–696.
- (11) Hua, Y.; Flood, A. H. *Chem. Soc. Rev.* **2010**, *39*, 1262–1271.
- (12) Yam, V. W.-W.; Chan, K. H.-Y.; Wong, K. M.-C.; Chu, B. W.-K. *Angew. Chem. Int. Ed.* **2006**, *45*, 6169–6173.
- (13) Kui, S. C. F.; Law, Y.-C.; Tong, G. S. M.; Lu, W.; Yuen, M.-Y.; Che, C.-M. *Chem. Sci.* **2011**, *2*, 221–228.
- (14) Brooks, J.; Babayan, Y.; Lamansky, S.; Djurovich, P. I.; Tsyba, I.; Bau, R.; Thompson, M. E. *Inorg. Chem.* **2002**, *41*, 3055–3066.
- (15) Eryazici, I.; Moorefield, C. N.; Newkome, G. R. *Chem. Rev.* **2008**, *108*, 1834–1895.

- (16) Mydlak, M.; Mauro, M.; Polo, F.; Felicetti, M.; Leonhardt, J.; Diener, G.; De Cola, L.; Strassert, C. A. *Chem. Mater.* **2011**, *23*, 3659–3667.
- (17) Strassert, C. A.; Chien, C.-H.; Galvez Lopez, M. D.; Kourkoulos, D.; Hertel, D.; Meerholz, K.; De Cola, L. *Angew. Chem. Int. Ed.* **2010**, *50*, 946–950.
- (18) McMillin, D. R.; Moore, J. J. *Coord. Chem. Rev.* **2002**, *229*, 113–121.
- (19) Ni, J.; Zhang, X.; Qiu, N.; Wu, Y.-H.; Zhang, L.-Y.; Zhang, J.; Chen, Z.-N. *Inorg. Chem.* **2011**, *50*, 9090–9096.
- (20) Abe, T.; Itakura, T.; Ikeda, N.; Shinozaki, K. *Dalton Trans.* **2009**, 711–715.
- (21) Zhang, X.; Wang, J.-Y.; Ni, J.; Zhang, L.-Y.; Chen, Z.-N. *Inorg. Chem.* **2012**, *51*, 5569–5579.
- (22) Kozhevnikov, V. N.; Donnio, B.; Bruce, D. W. *Angew. Chem. Int. Ed.* **2008**, *47*, 6286–6289.
- (23) Shan, G.-G.; Li, H.-B.; Cao, H.-T.; Zhu, D.-X.; Li, P.; Su, Z.-M.; Liao, Y. *Chem. Commun.* **2012**, *48*, 2000–2002.
- (24) Lim, J.; Swager, T. M. *Angew. Chem. Int. Ed.* **2010**, *49*, 7486–7488.
- (25) Damm, C.; Israel, G.; Hegmann, T.; Tschierske, C. *J. Mater. Chem.* **2006**, *16*, 1808–1816.
- (26) Hegmann, T.; Kain, J.; Diele, S.; Schubert, B.; Bögel, H.; Tschierske, C. *J. Mater. Chem.* **2003**, *13*, 991–1003.
- (27) Serrette, A. G.; Lai, C. K.; Swager, T. M. *Chem. Mater.* **1994**, *6*, 2252–2268.
- (28) Thomas, S. W.; Venkatesan, K.; Müller, P.; Swager, T. M. *J. Am. Chem. Soc.* **2006**, *128*, 16641–16648.
- (29) Lieber, E.; Chao, T. S.; Rao, C. N. R. *J. Org. Chem.* **1957**, *22*, 238–240.
- (30) Gheorghe, A.; Cuevas-Yañez, E.; Horn, J.; Bannwarth, W.; Narsaiah, B.; Reiser, O. *Synlett* **2006**, *2006*, 2767–2770.
- (31) Fletcher, J. T.; Bumgarner, B. J.; Engels, N. D.; Skoglund, D. A. *Organometallics* **2008**, *27*, 5430–5433.

Appendix for Chapter 3

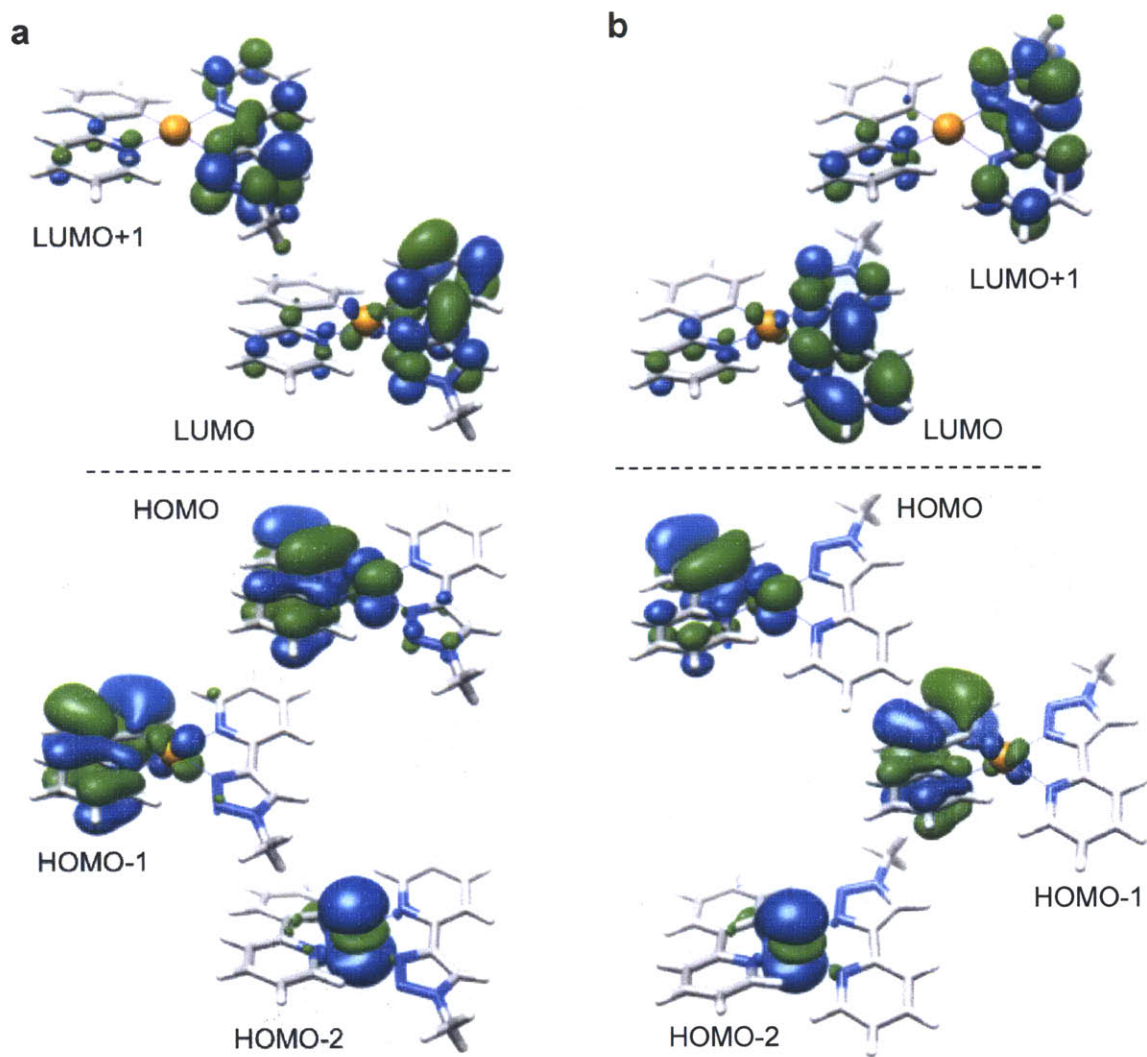
Frontier orbitals

Photophysical properties

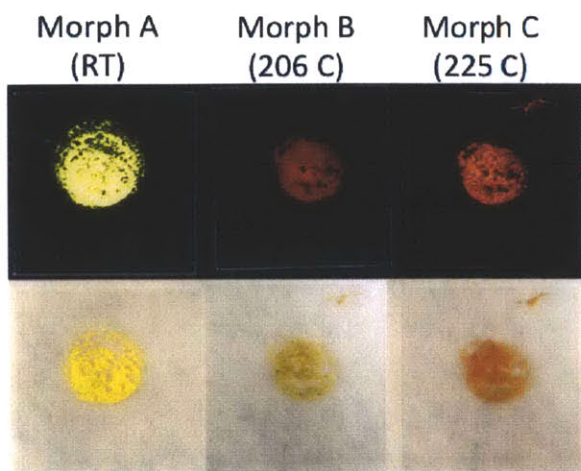
**Experimental setup for the
mechanochromic effect study**

DSC data

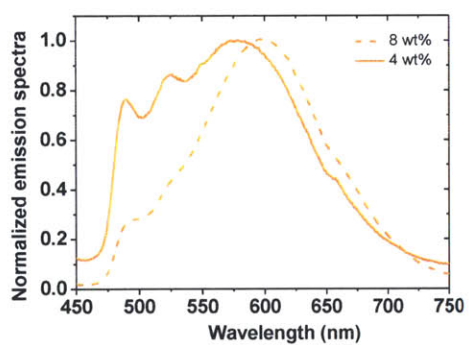
NMR spectra



Frontier orbitals of the *trans* (left) and *cis* isomer (right) of the $[(ppy)Pt(trpy)]^+$

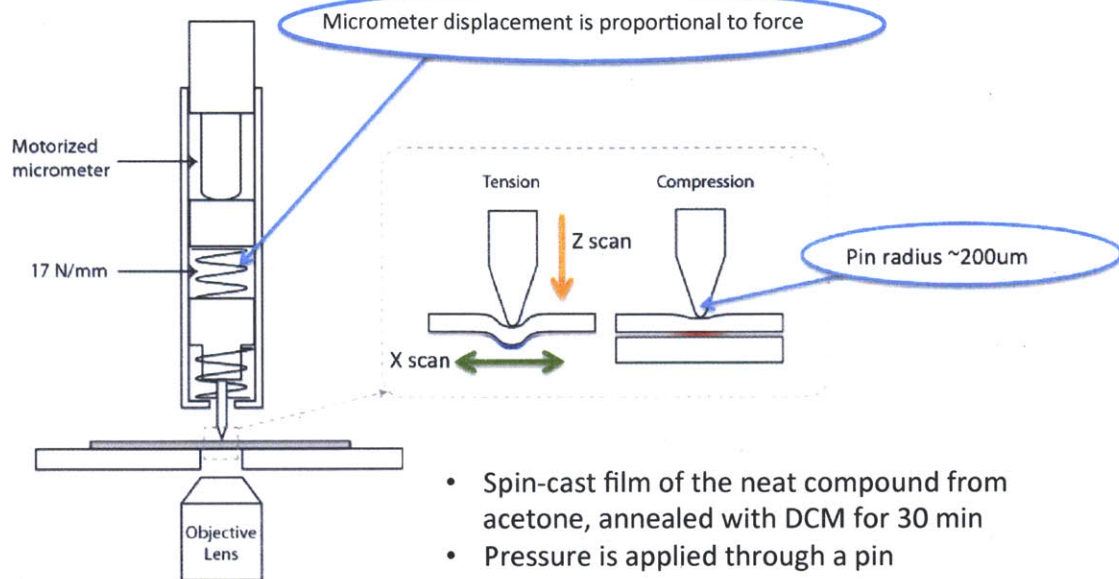


Images of the three polymorphs under UV (upper) and room light (lower)



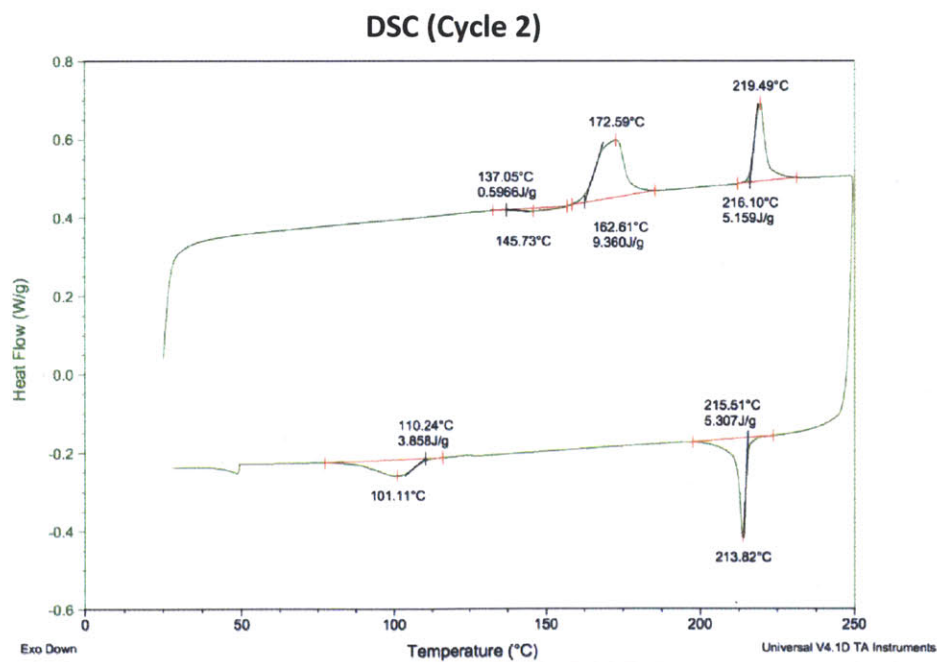
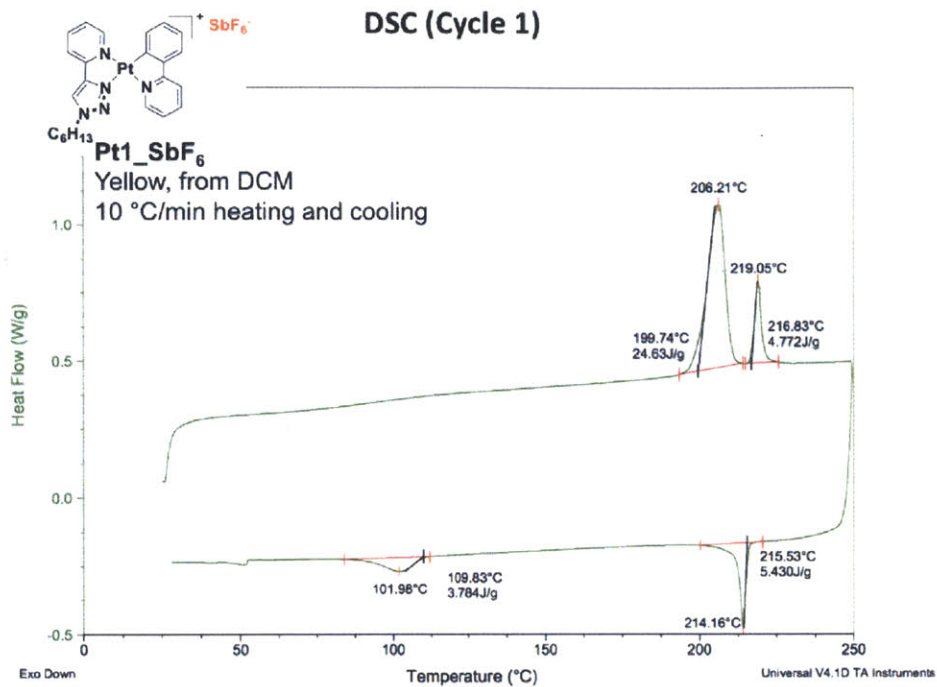
Concentration dependence of the solid-state emission of $[\text{Pt}(\text{ppy})(\text{trpy}-\text{C}_6\text{H}_{13})]\text{SbF}_6$ (**Pt1_SbF₆**) when doped into PMMA thin films

Experimental Setup

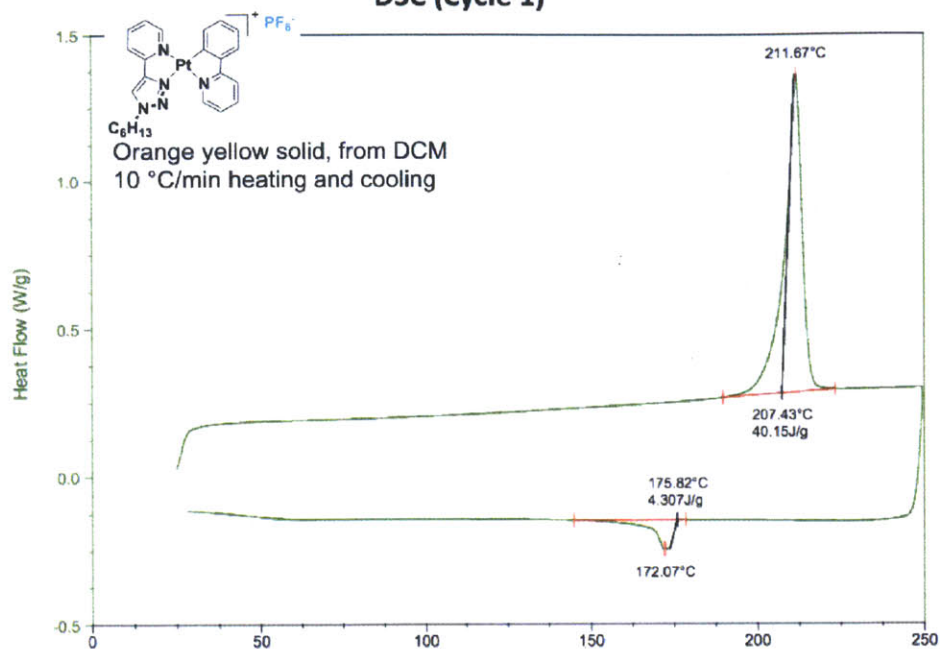


Courtesy from Wendi Chang and Gleb Akselrod in the Bulovic group@MIT

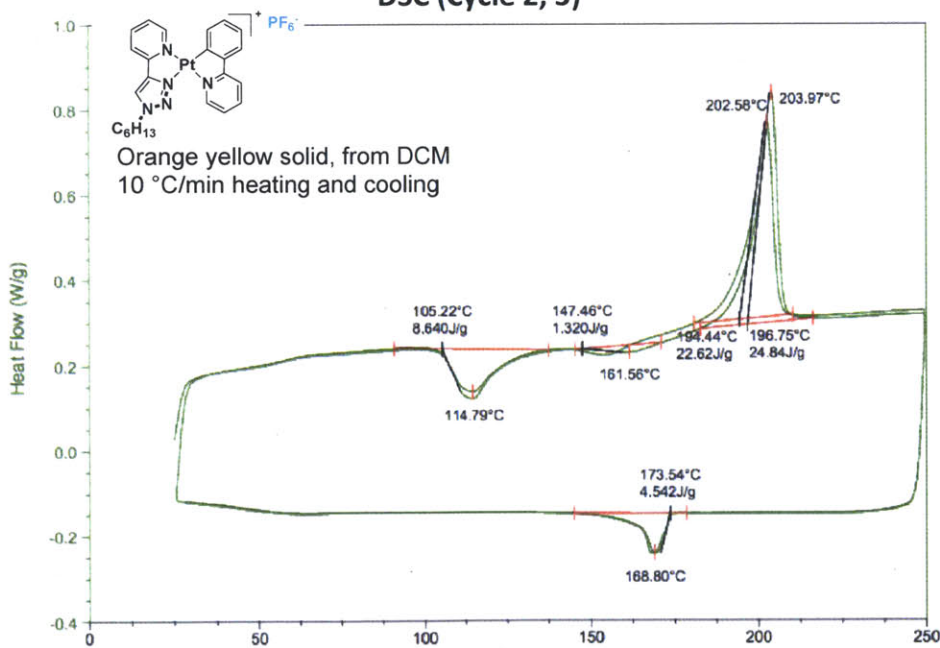
Experimental setup for the mechanochromic effect study

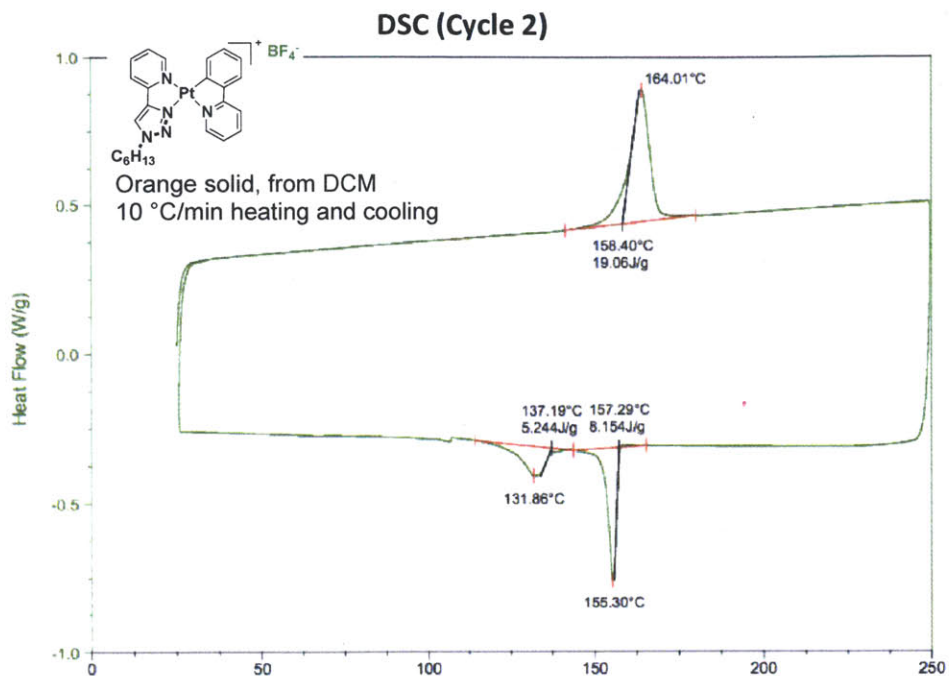


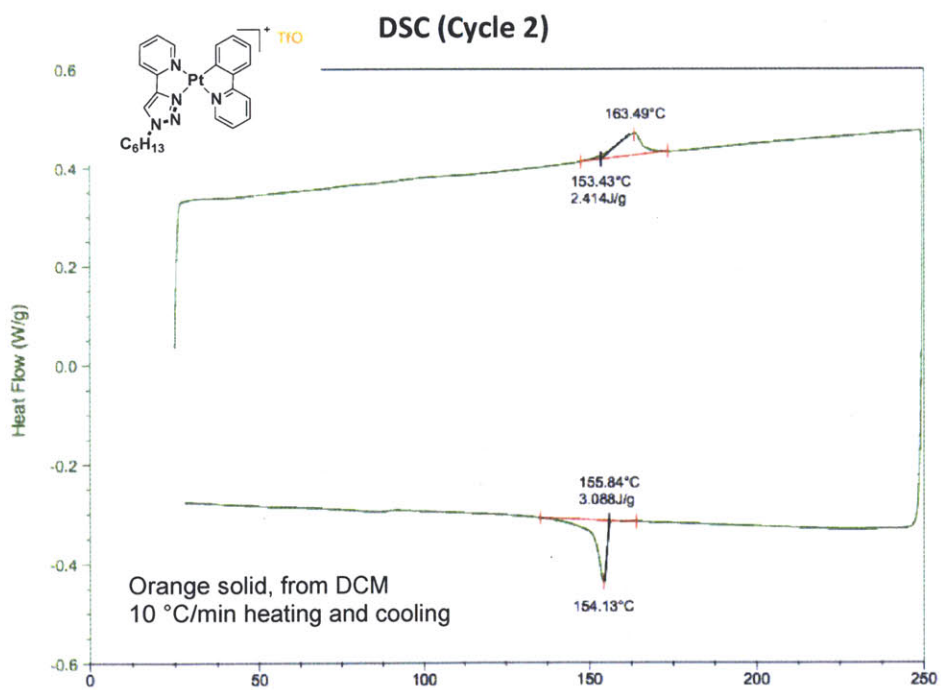
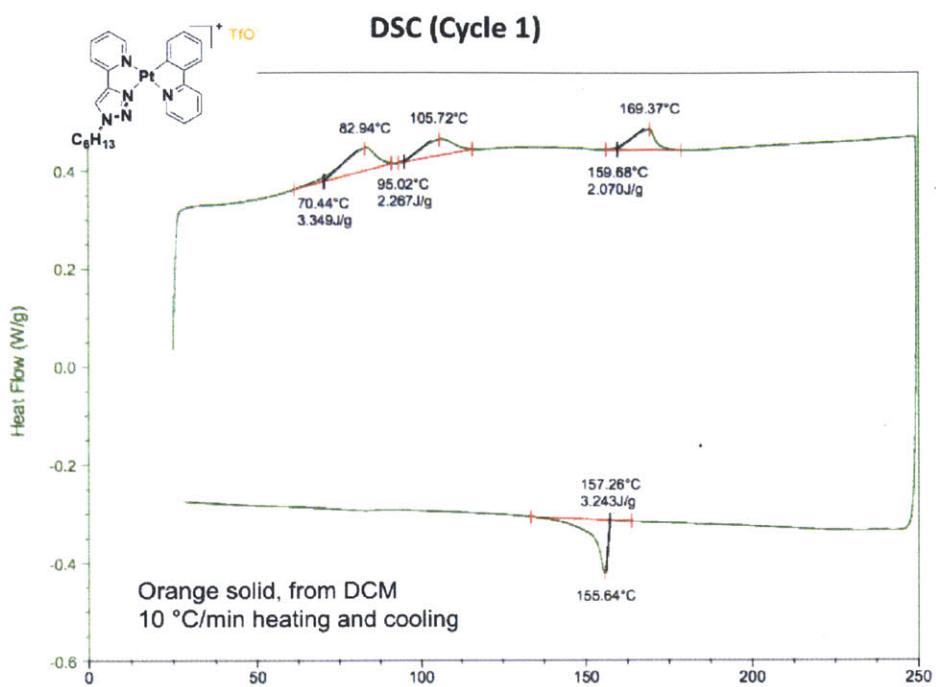
DSC (Cycle 1)

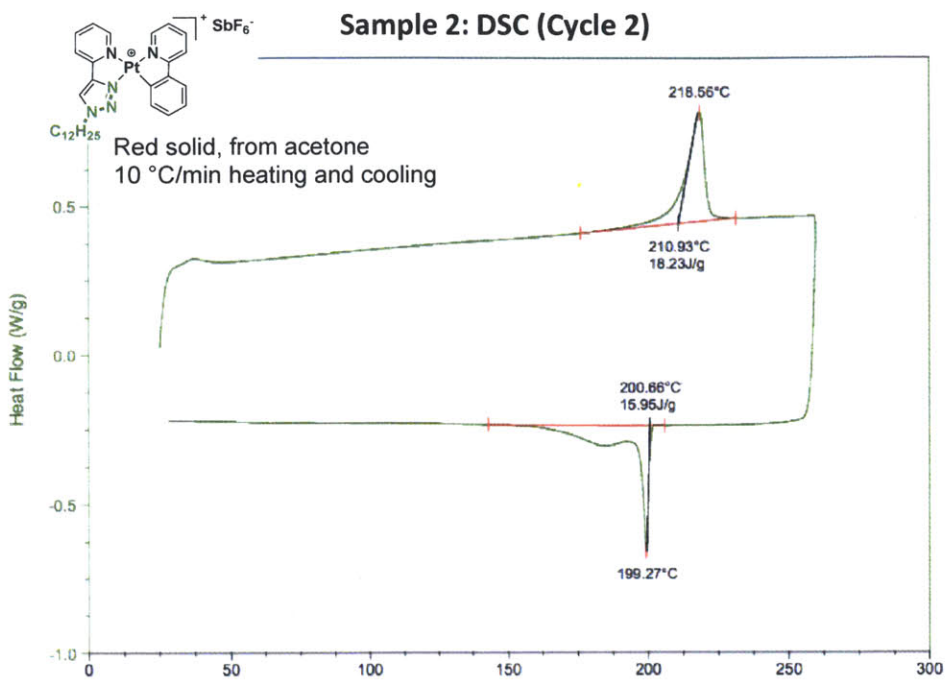


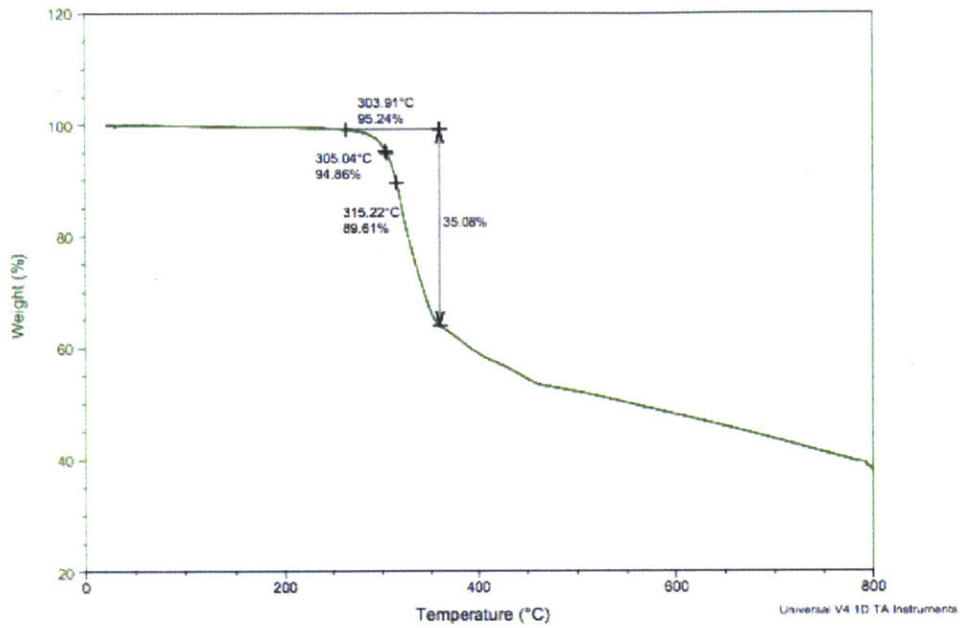
DSC (Cycle 2, 3)



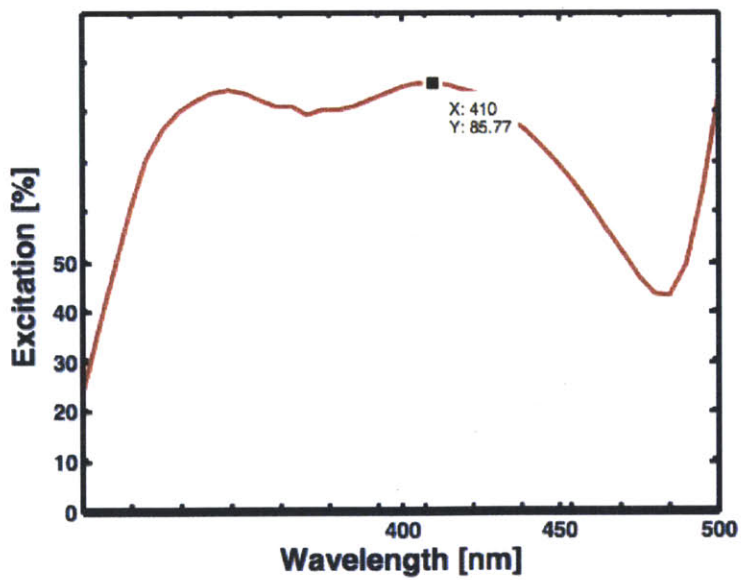




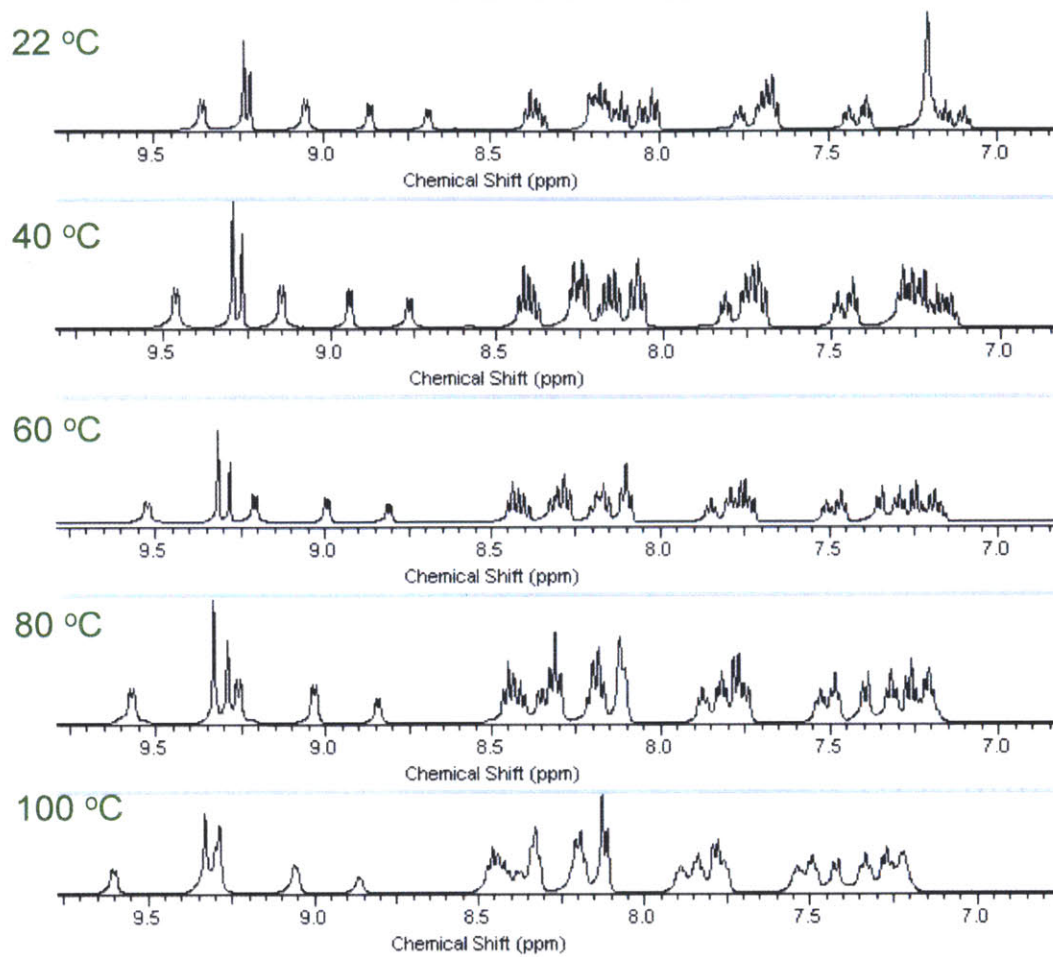




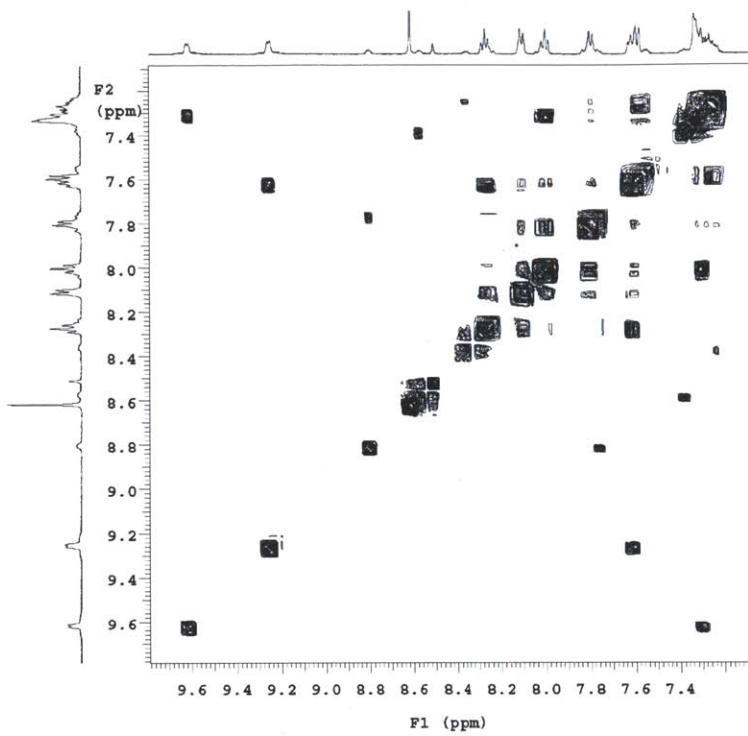
TGA data of Pt1_SbF_6



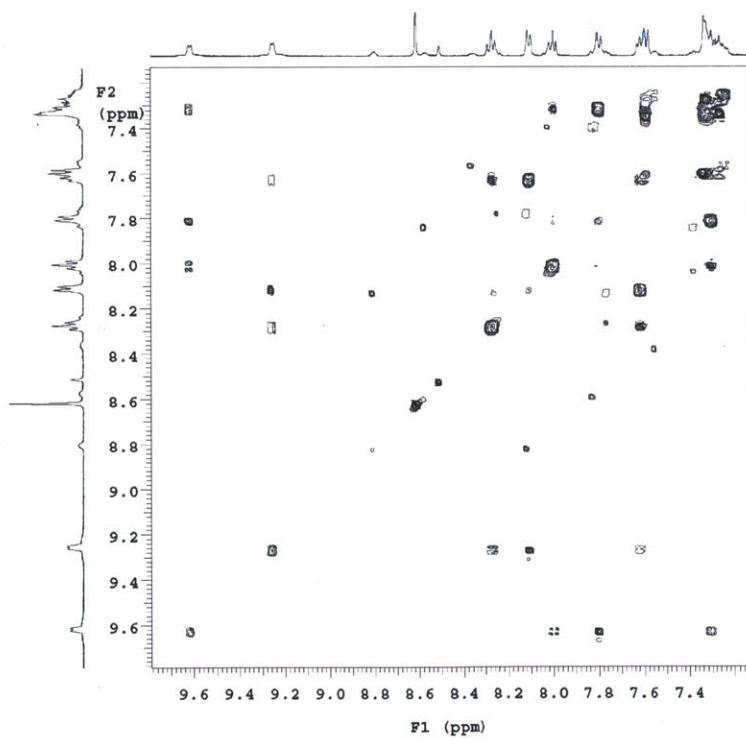
Calculations of the quantum efficiency of Pt1_SbF_6 obtained with Integrating Sphere



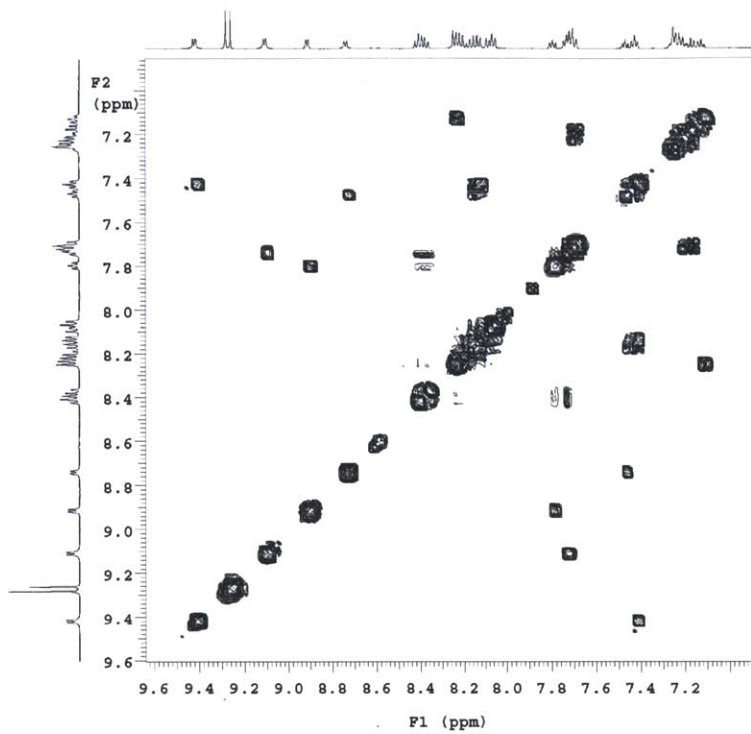
VT NMR spectra of **Pt1_SbF₆** measured in DMSO-*d*₆



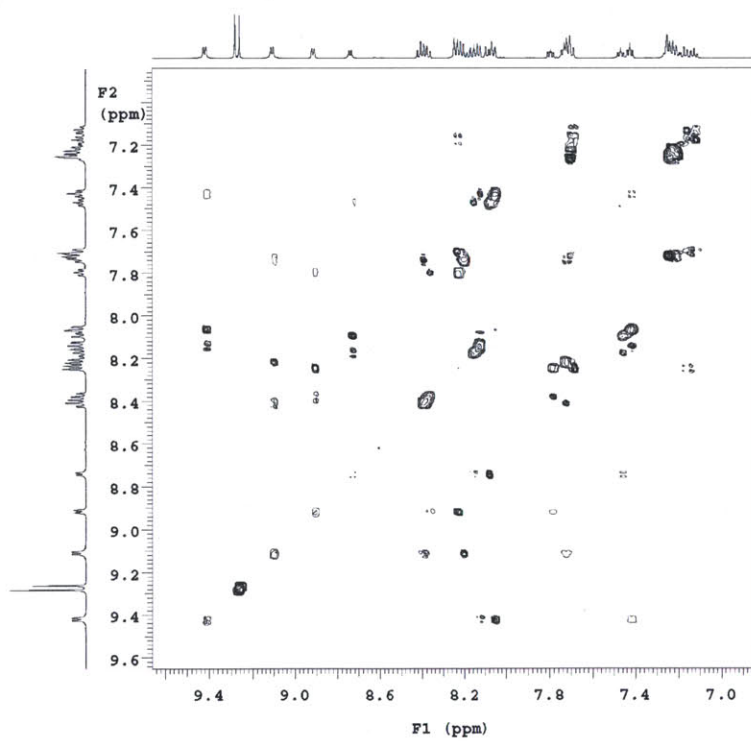
gCOSY of Pt1_SbF₆ in CD₂Cl₂



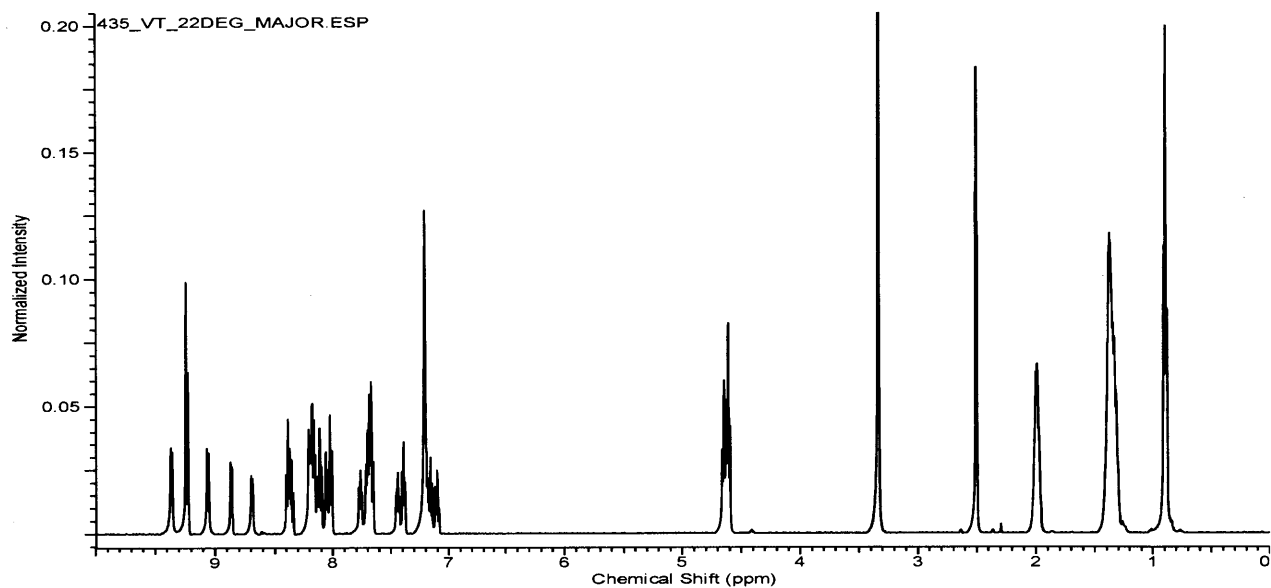
TOCSY of Pt1_SbF₆ in CD₂Cl₂



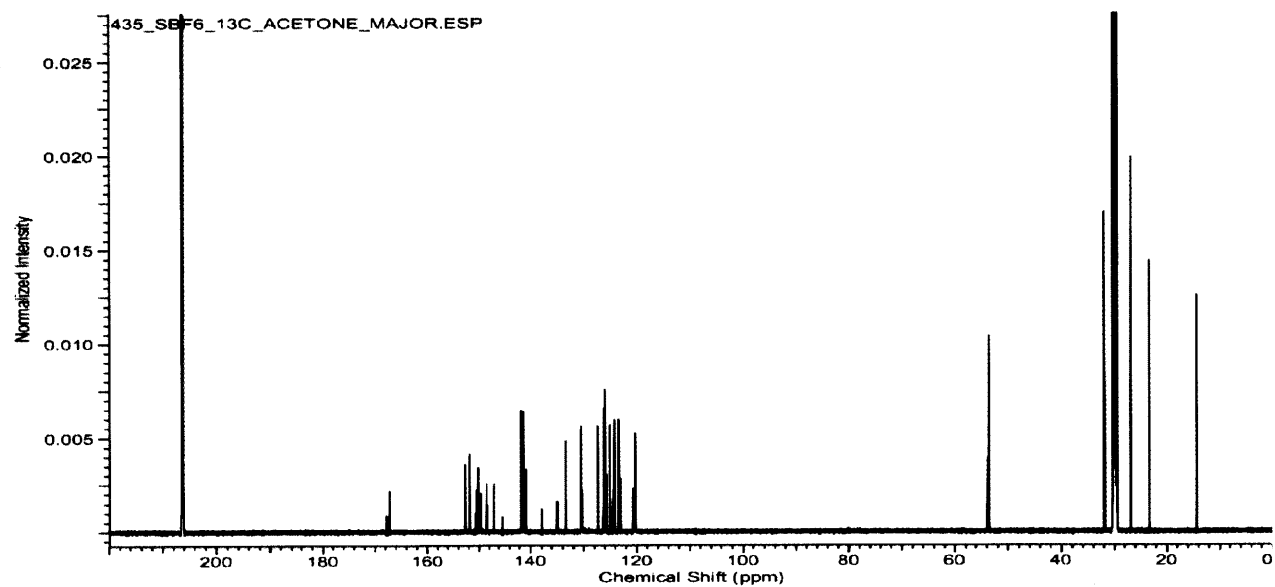
gCOSY of Pt1_SbF_6 in $\text{DMSO-}d_6$



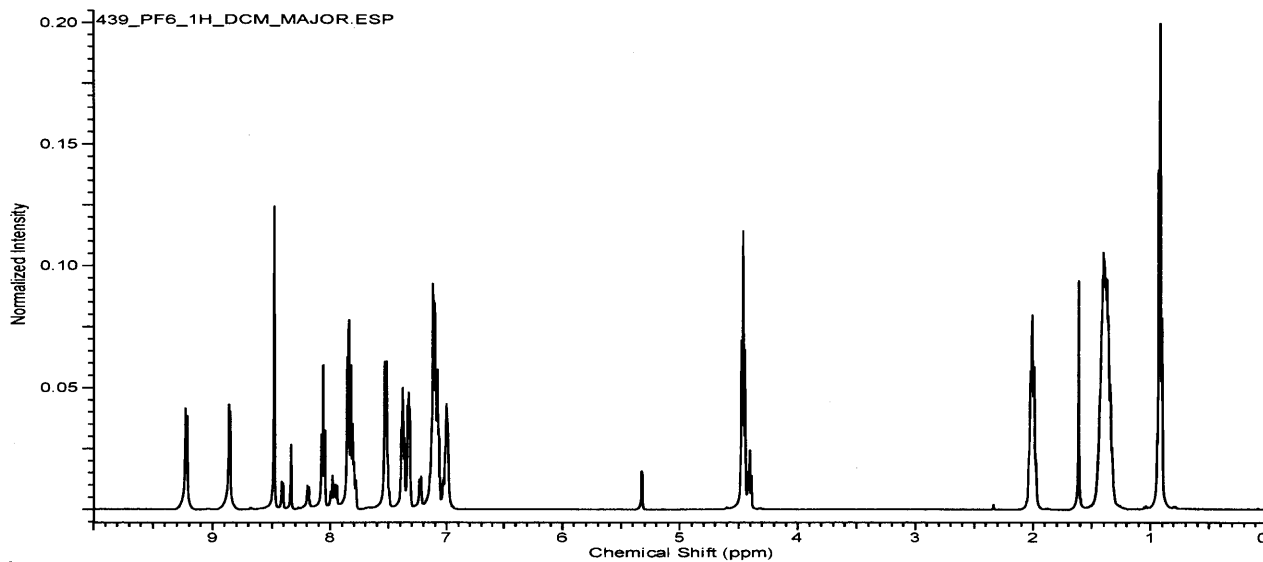
TOCSY of Pt1_SbF_6 in $\text{DMSO-}d_6$



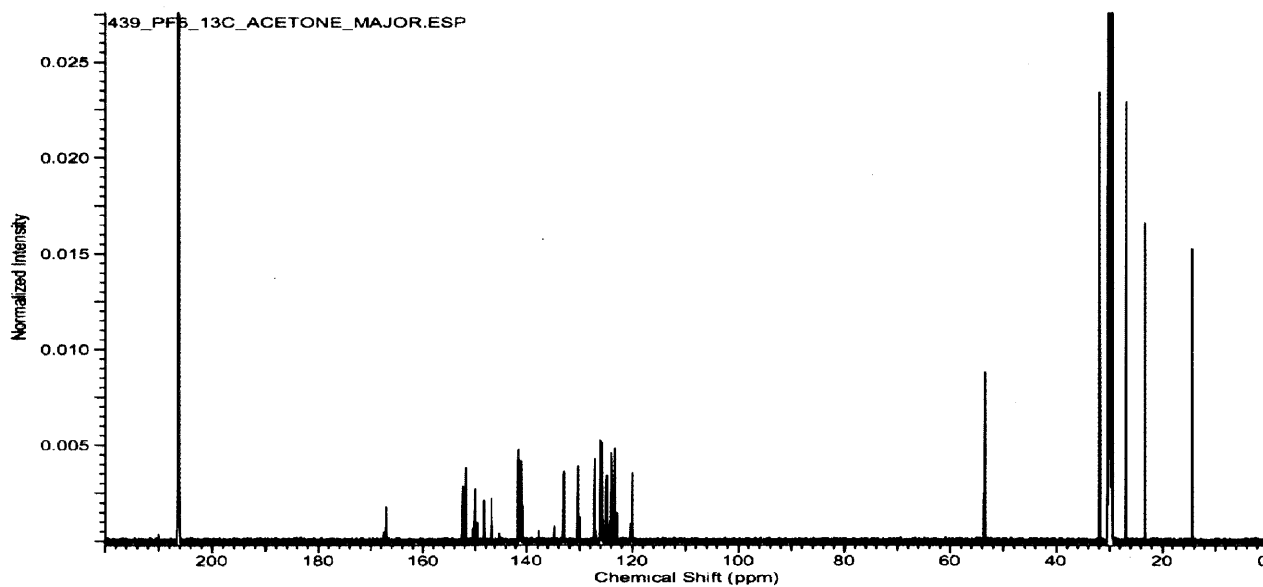
^1H NMR of **Pt1_SbF₆** in $\text{DMSO-}d_6$



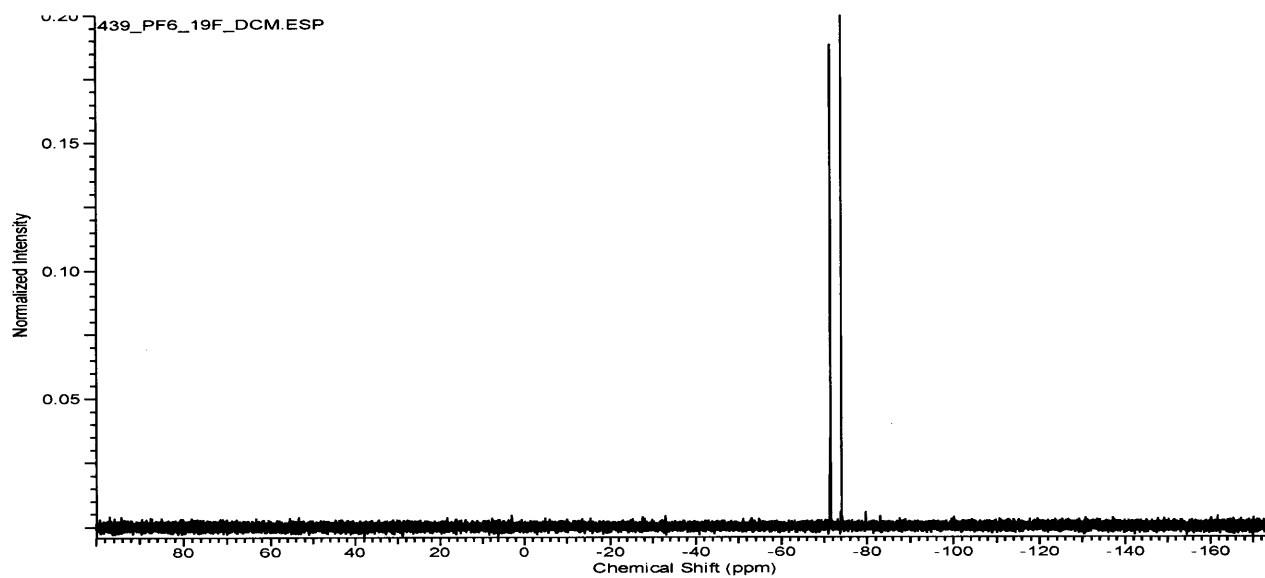
^{13}C NMR of **Pt1_SbF₆** in $\text{acetone-}d_6$



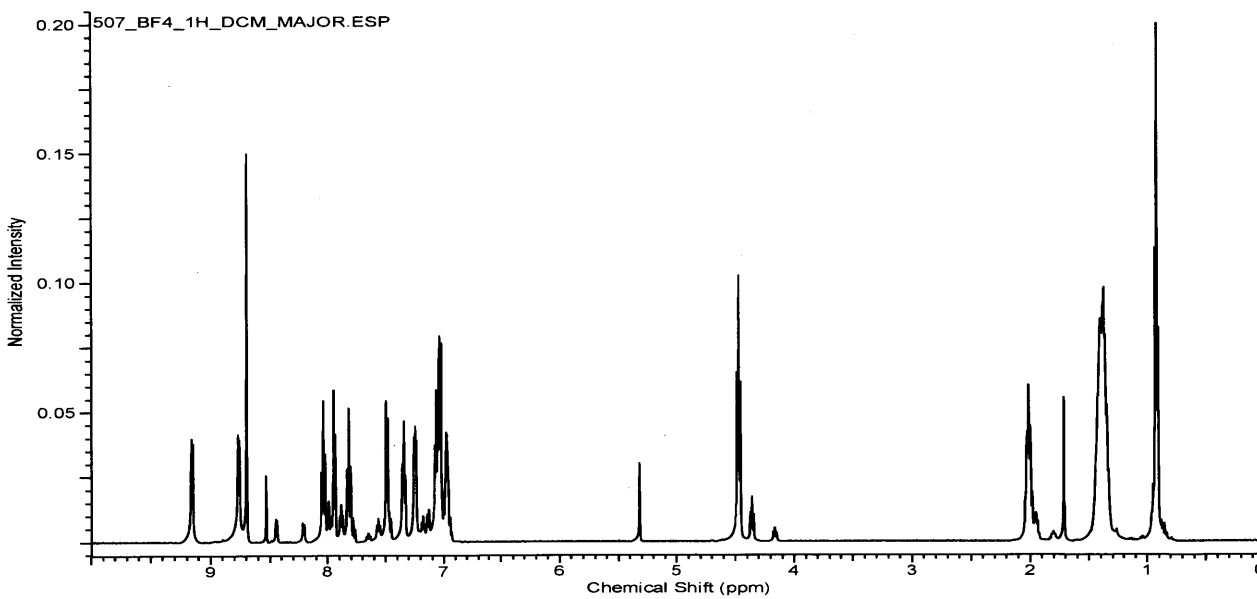
^1H NMR of Pt1_SbF_6 in CD_2Cl_2



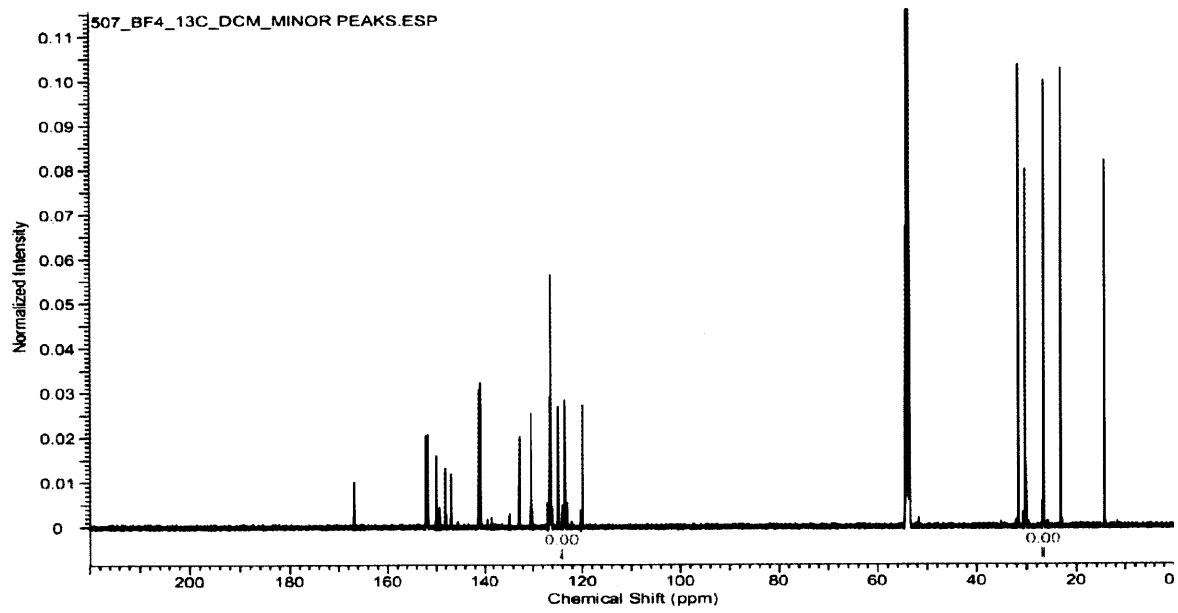
^{13}C NMR of Pt1_PF_6 in $\text{acetone-}d_6$



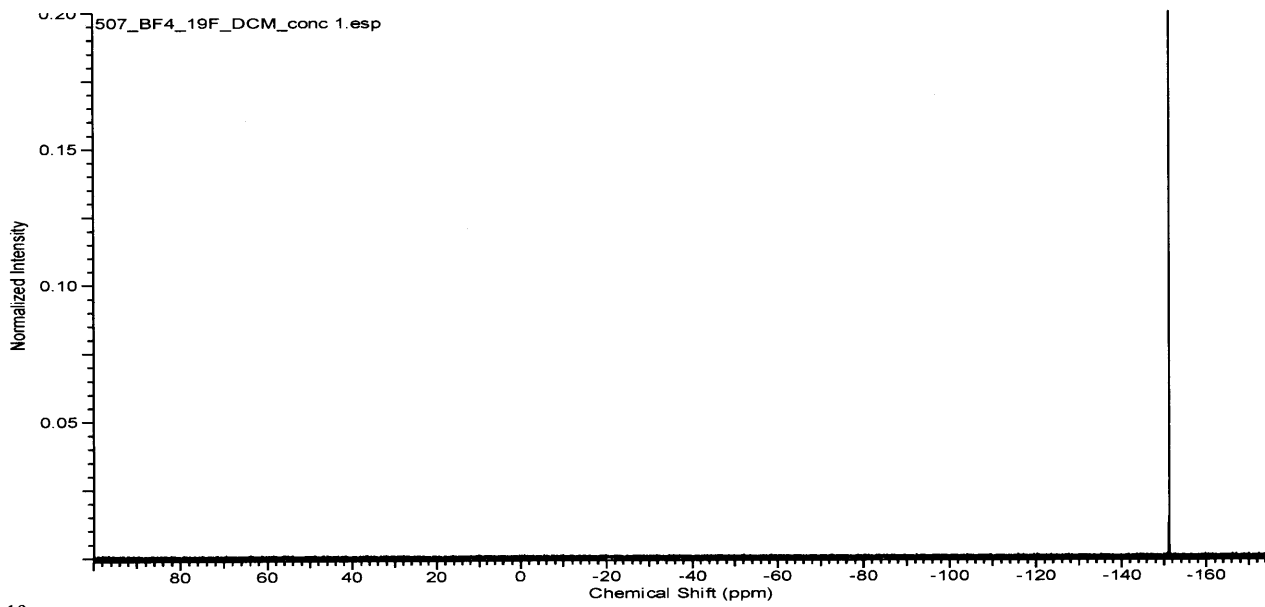
^{19}F NMR of **Pt1**_SbF₆ in CD₂Cl₂



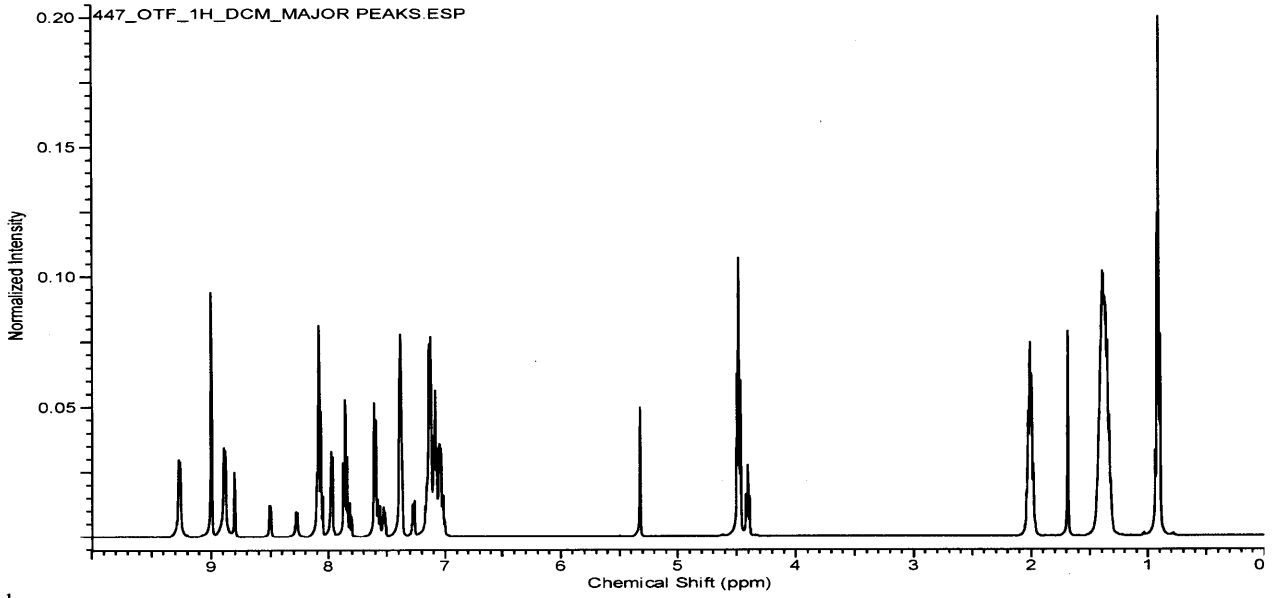
^1H NMR of **Pt1**_BF₄ in CD₂Cl₂



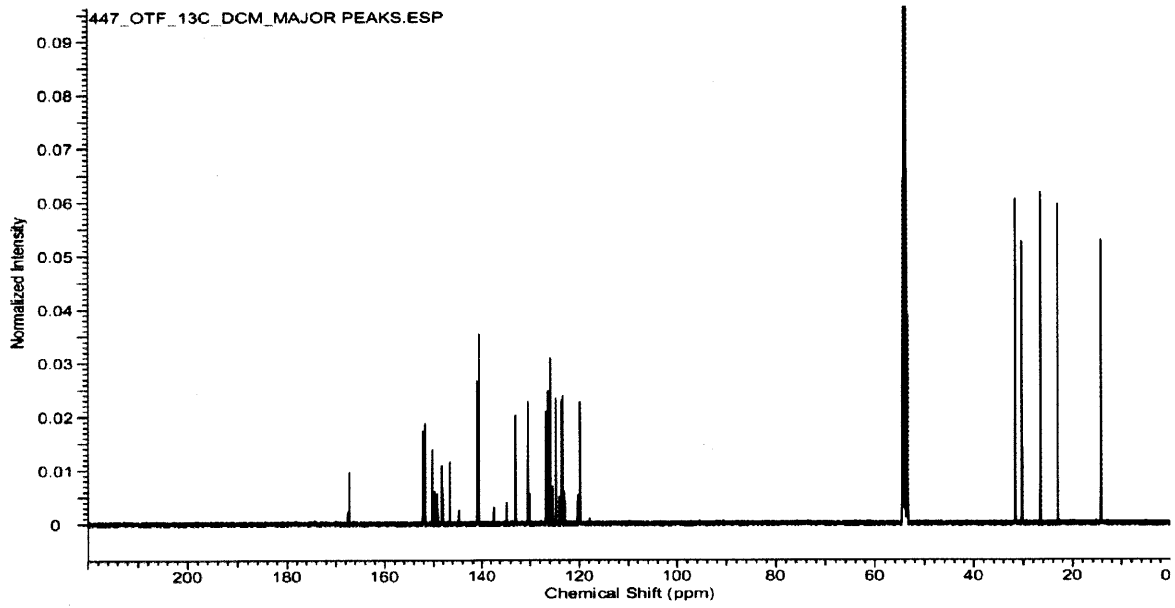
^{13}C NMR of Pt1_BF_4 in CD_2Cl_2



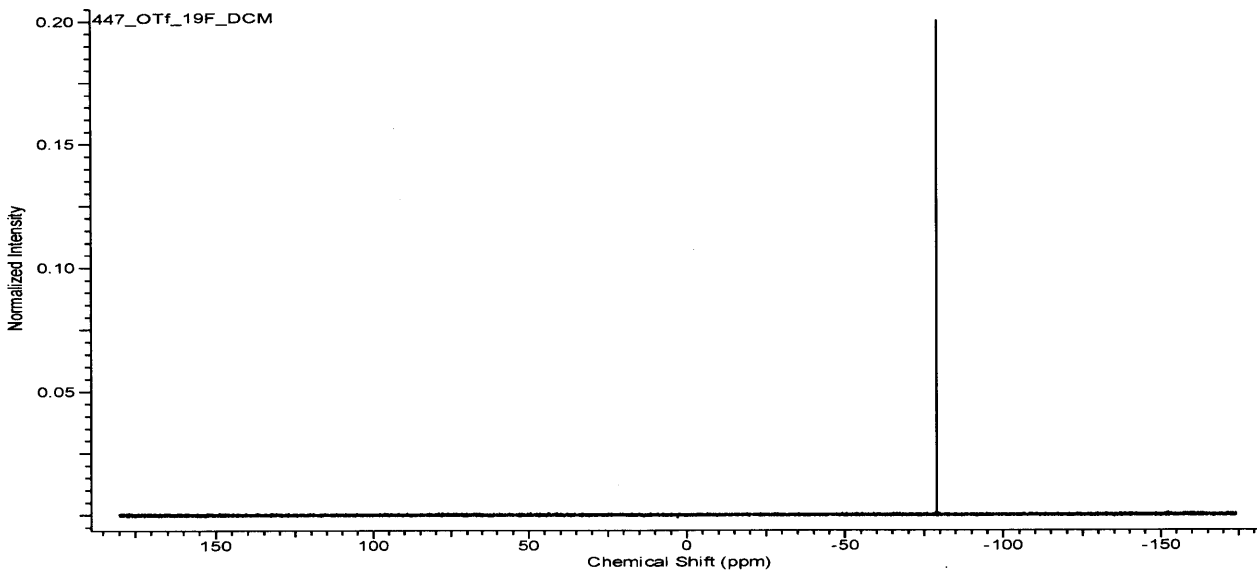
^{19}F NMR of Pt1_BF_4 in CD_2Cl_2



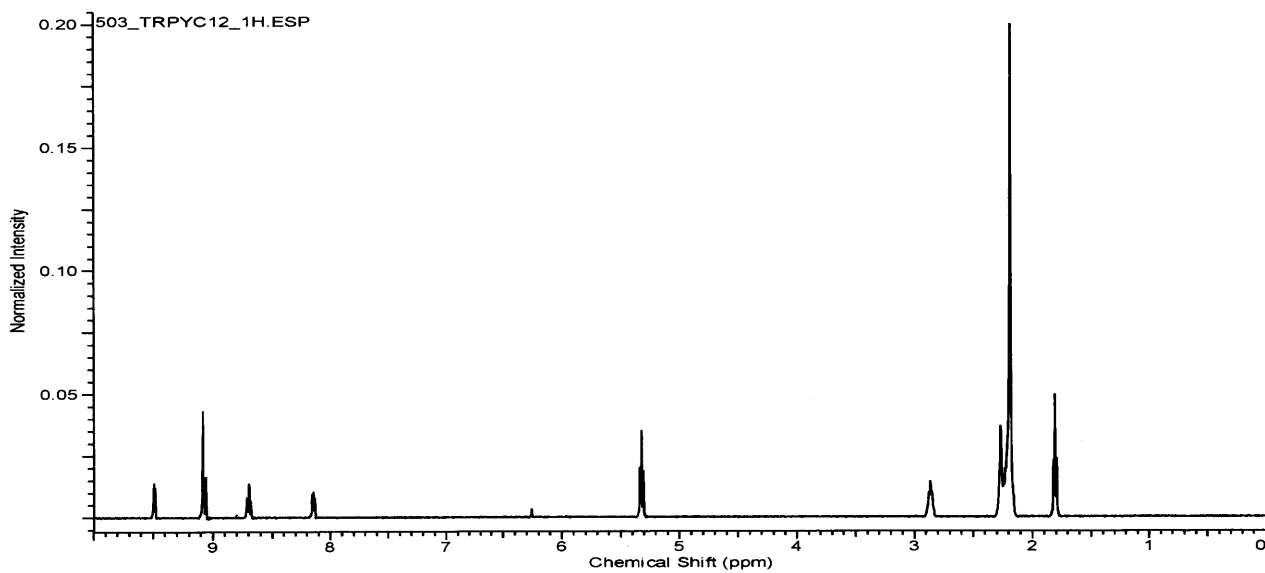
^1H NMR of Pt1_OTf in CD_2Cl_2



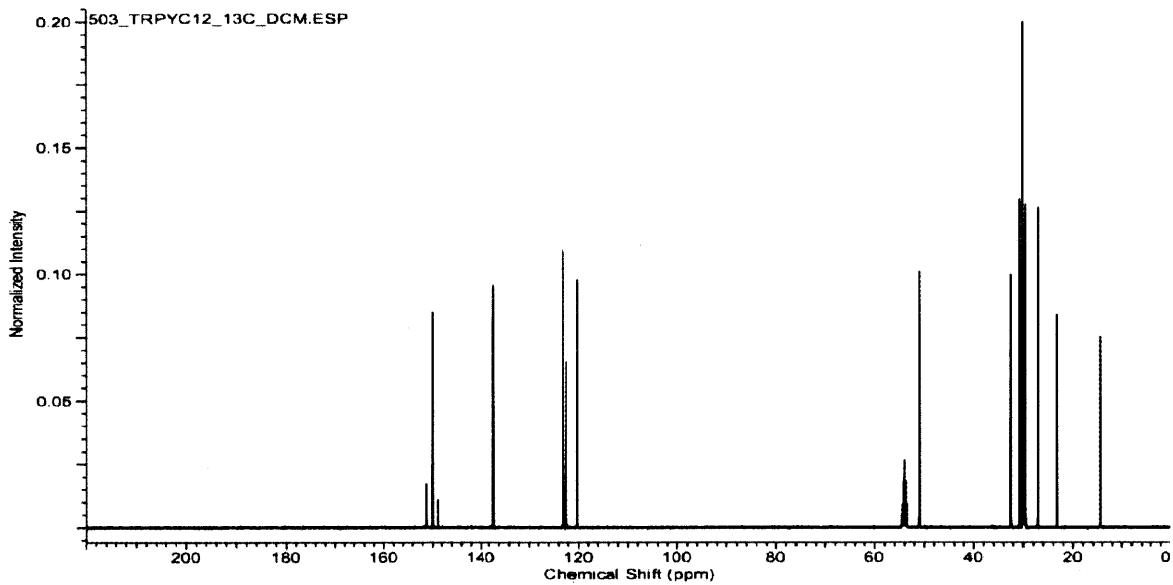
^{13}C NMR of Pt1_OTf in CD_2Cl_2



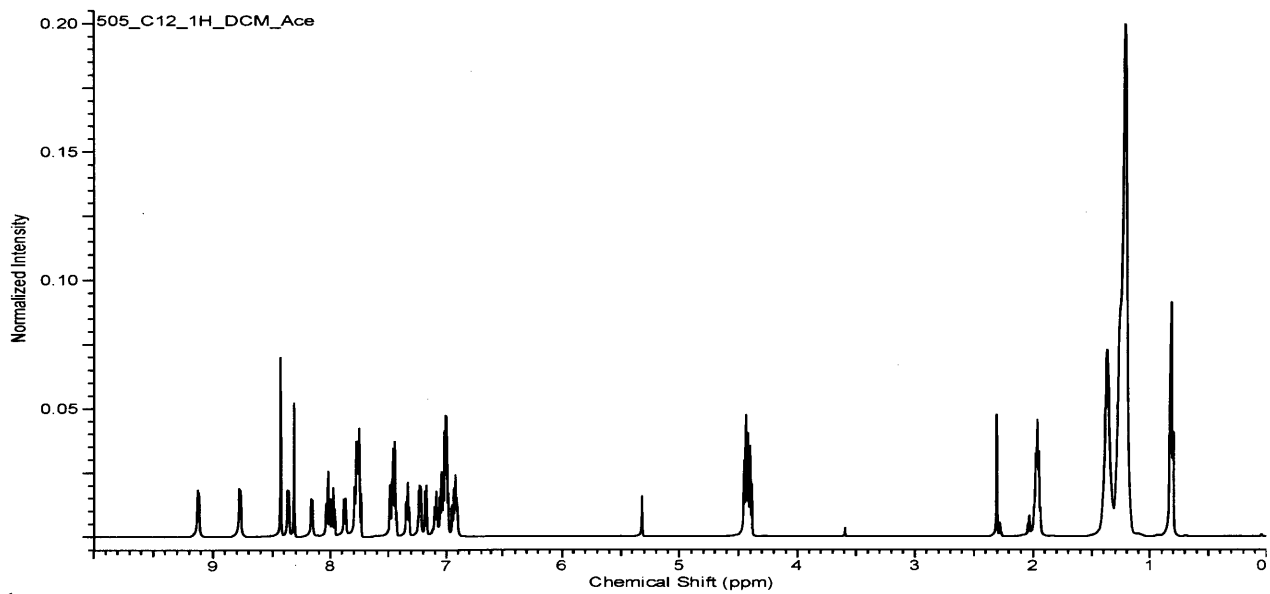
^{19}F NMR of **Pt1_OTf** in CD_2Cl_2



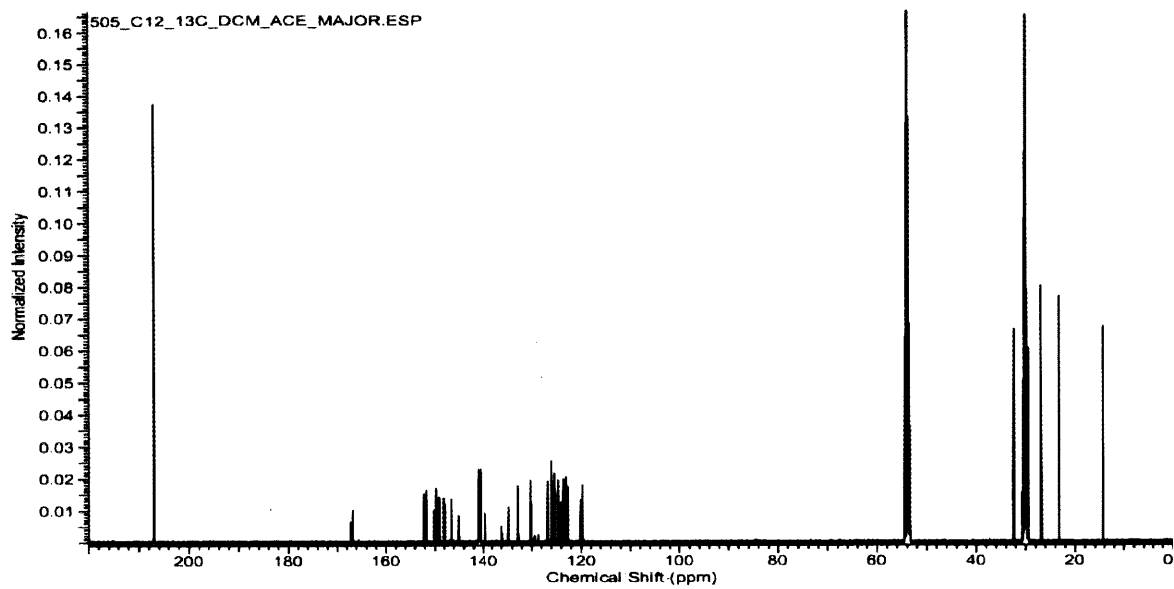
^1H NMR of **L2** in CD_2Cl_2



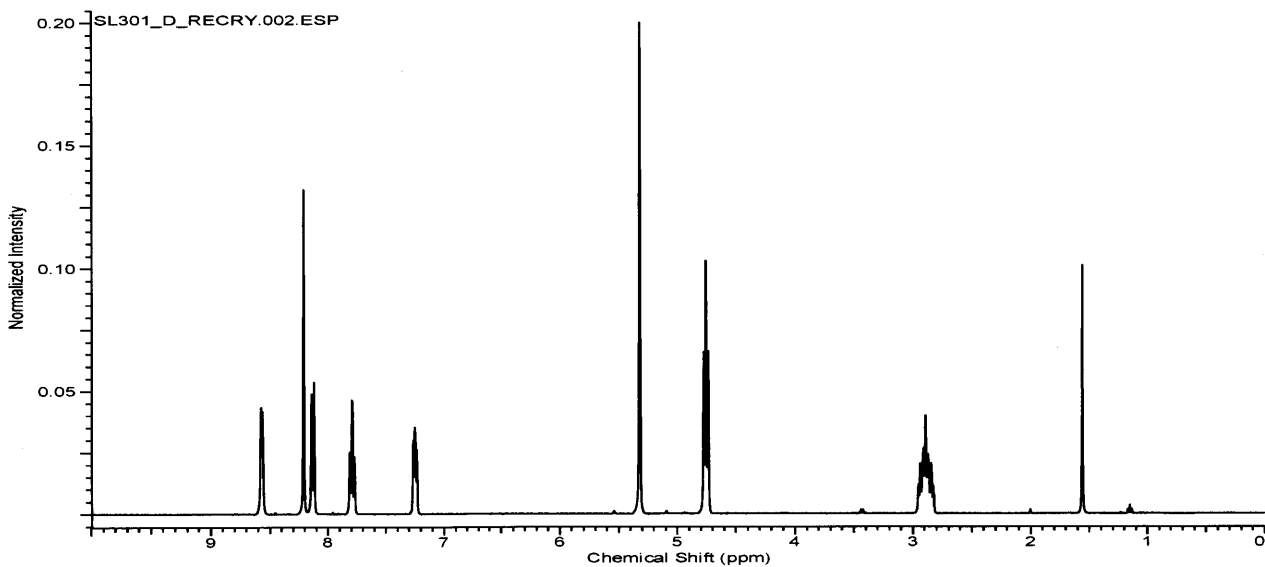
^{13}C NMR of **L2** in CD_2Cl_2



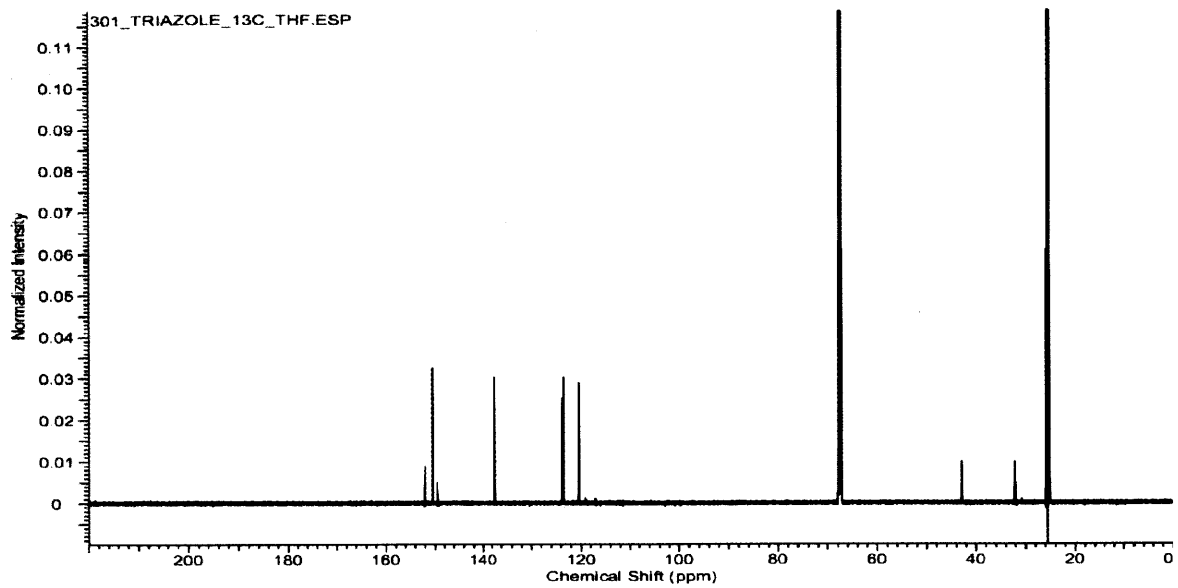
^1H NMR of **Pt2_SbF₆** in CD_2Cl_2



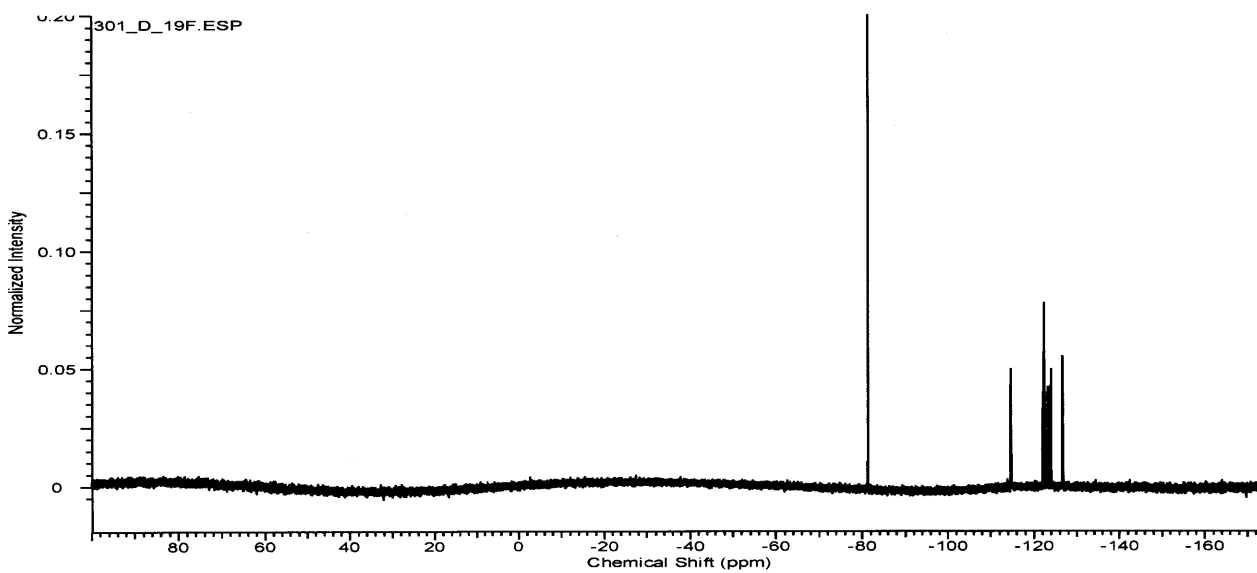
^{13}C NMR of Pt_2SbF_6 in CD_2Cl_2



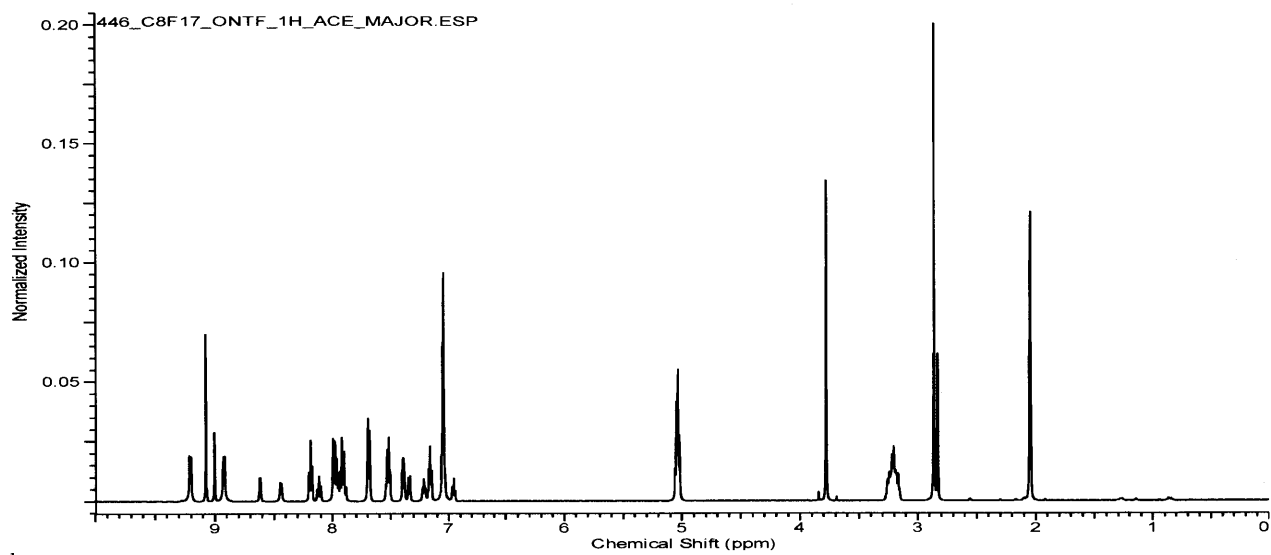
^1H NMR of L_3 in $\text{THF-}d_8$



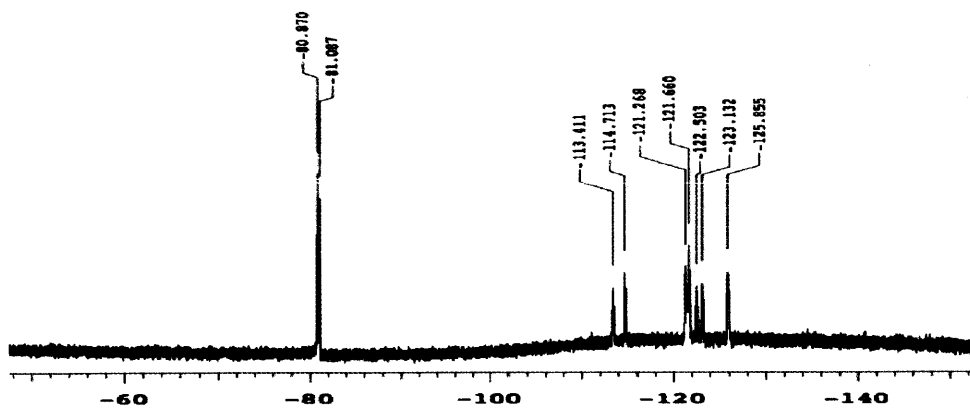
^{13}C NMR of **L3** in THF- d_8



^{19}F NMR of **L3** in THF- d_8



^1H NMR of **Pt3_ONTF** in Acetone- d_6



^{19}F NMR of **Pt3_ONTF** in Acetone- d_6

Shuang Liu

77 Massachusetts Avenue 18-034, Cambridge, MA 02139

shliu@mit.edu

EDUCATION

Massachusetts Institute of Technology (MIT), Cambridge, MA

2007–2012

- Ph.D. Candidate in Chemistry

Advisor: Professor Timothy M. Swager

Thesis: Design and Synthesis of Cyclometalated Transition Metal Complexes as Functional Phosphorescent Materials

Fudan University, Shanghai, China

- M.S. in Chemistry, *Graduated with Honors*

2004–2007

Advisor: Professor Guo-Xin Jin

Thesis: Synthesis and characterization of multinuclear complexes with dichalcogenolate carboranyl ligands

- B.S. in Chemistry, *Graduated with Honors*

2000–2004

Advisor: Professor Guo-Xin Jin

Thesis: Late-transition metals carbene complexes as efficient ethylene polymerization catalysts

RESEARCH EXPERIENCE

Massachusetts Institute of Technology, Cambridge, MA

Graduate Research Assistant

2007–present

- Established a novel synthetic method for cyclometalated platinum and iridium compounds, the most promising candidates in phosphorescence-based organic light emitting diodes (OLEDs)
- Designed platinum complexes and conjugated polymers that change color and luminescence in response to external mechanical forces and chemical environments
- Built the first thermotropic Col(h) liquid crystals with only one side-chain based on cyclometalated Pt(II) complexes with N, N-chelating “click” ligands

Fudan University, Shanghai, China

Graduate and Undergraduate Research Assistant

2002–2007

- Examined the reactivity of half-sandwiched dichalcogenolate carborane metal complexes systematically

- Evaluated late-transition metal carbene and carborane complexes with hemilabile functional groups as efficient catalysts for olefin polymerization
- Awarded funds from *Hui-Chun Chin and Tsung-Dao Lee Chinese Undergraduate Research Endowment*

SELECTED PUBLICATIONS

- **Shuang Liu**, Peter Müller, Michael K. Takase, Timothy M. Swager*. “Click” Synthesis of Heteroleptic Tris-Cyclometalated Iridium(III) Complexes: Cu(I) Triazolide Intermediates as Transmetalating Reagents”. *Inorganic Chemistry*, 2011, 7598
- **Shuang Liu**, Guo-liang Wang, Guo-Xin Jin*. “Multinuclear self-assembly via half-sandwich complexes Cp*M[S₂C₂(B₁₀H₁₀)] and pyridine-based ligands”. *Dalton Transactions*, 2008, 425
- **Shuang Liu**, Ying-Feng Han, Guo-Xin Jin*. “Formation of direct metal-metal bonds from 16-electron “pseudo-aromatic” half-sandwich complexes Cp*M[E₂C₂(B₁₀H₁₀)]”. *Chemistry Society Review*, 2007, 36, 1543 (Cover Art)
- **Shuang Liu**, Jian-qiang Wang, Guo-Xin Jin*. “Construction of trinuclear iridium clusters through ancillary ortho-carborane-1,2-diselenolato ligands, with simultaneous iridium-induced B-H activation”. *Dalton Transactions*, 2007, 3792
- **Shuang Liu**, Guo-Xin Jin*. “A facile and general approach to the Rh-M (M = Co, Rh) single bond supported by ortho-carborane-1,2-dichalcogenolato ligands”. *Dalton Transactions*, 2007, 949 (Cover Art)
- **Shuang Liu**, Jiasheng Zhang, Xin Wang, Guo-Xin Jin*. “Synthesis and characterization of binuclear half-sandwich metal (Co, Ir and Ru) complexes containing ancillary ortho-carborane-1,2-dithiolato ligands”. *Dalton Transactions*, 2006, 5225
- **Shuang Liu**, Xin Wang, Guo-Xin Jin*. “Synthesis of heteronuclear (MoRu₂) clusters from 16-electron half-sandwich complexes (*p*-cymene)Ru[E₂C₂(B₁₀H₁₀)] (E = S, Se)”. *Journal of Organometallic Chemistry*, 2006, 691(1-2), 261
- Xin Wang, Guo-Liang Wang, **Shuang Liu**, Shuyi Cai, Guo-Xin Jin*. “Half-sandwich binuclear carbaborane compounds: Closo-carbaboranes as good σ -donor ligands”. *Journal of Organometallic Chemistry*, 2008, 693, 3057
- Xin Wang, **Shuang Liu**, Lin-Hong Weng, and Guo-Xin Jin*. “A trinuclear silver(I) functionalized N-heterocyclic carbene complex and its use in transmetalation: structure and catalytic activity for olefin polymerizations”. *Organometallics*, 2006, 25, 3565
- Xin Wang, **Shuang Liu**, Lin-Hong Weng, and Guo-Xin Jin*. “Preparation and structure of mono- and binuclear half-sandwich iridium, ruthenium, and rhodium carbene complexes containing 1,2-dichalcogenolato 1,2-dicarba-closo-dodecaboranes”. *Chemistry--A European Journal*, 2006, 13(1), 188
- Xin Wang, **Shuang Liu**, Guo-Xin Jin*. “Preparation, structure and ethylene polymerization behavior of mixed-halide nickel(II) complexes and cobalt(II) complex containing imidazolium”. *Journal of*

Organometallic Chemistry, 2005, 690(12), 2934

- Xin Wang, **Shuang Liu**, Guo-Xin Jin*. "Preparation, Structure, and Olefin Polymerization Behavior of Functionalized Nickel(II) N-Heterocyclic Carbene Complexes". *Organometallics*, 2004, 23, 6002

CONFERENCE PRESENTATION

- **Shuang Liu**, Timothy M. Swager*. 243th American Chemical Society (ACS) National Meeting, Boston, CA, United States, March 25-29, 2012
- **Shuang Liu**, Timothy M. Swager*. 240th American Chemical Society (ACS) National Meeting, San Diego, MA, United States, August 22-26, 2010

AWARDS

- **2008-2009 Graduate Student Teaching Assistant Award** from the Chemistry Department at MIT
- **Distinguished Master's Thesis Award** (2008) and **Distinguished Graduate of Shanghai** (2007 and 2004) for outstanding academic achievements
- **Unilever Scholarship** (2002) and **ExxonMobil Scholarship** (2001) for outstanding performance

Acknowledgement

There are so many people who have helped me throughout my time at MIT that it is almost impossible to acknowledge everyone in such a short chapter. I cannot help thinking of the time when I was admitted to MIT. I was happily sending out emails to withdraw my applications to other universities. Moments later, I received a short note from one of the recruiting professors, saying, "It could be tough there so make sure you are well prepared. I got my Ph.D. there". Although it is something to joke about at the very end of my PhD education, that email was absolutely nerve-racking at that time.. It made me constantly wonder what I should expect next. Looking back, the five years at MIT actually turns out to be so memorable because of the people I've met and worked with.

First and foremost, I would like to thank my advisor, Prof. Timothy Swager, for his guidance, support and continuous encouragement. Tim has been an incredible advisor in every aspect. He never lacks imagination and creativity proposing new projects; his sharp intuition guided me through some difficult times; his deep understanding in a broad spectrum of research fields greatly broadened my vision. Although he is an adamant believer in training independent research ability as an indispensable part of graduate education, I never felt that I was left alone to face all the challenges. Whenever I introduce myself as Tim's student at conferences or even during interviews, people would say that I am lucky to work for him. They couldn't be more right about it.

I would also like to thank my thesis committee, Prof. Richard Schrock and Prof. Stephen Buchwald. I really appreciate them taking the time to discuss my research progress with me and offer insightful comments.

As the only inorganic chemist working on organometallic compounds in the Swager lab, I would have had a very difficult start without the generous help from the senior members in the group. Dr. Koushik Venkatesan, from whom I took over the Pt(II) theme, left the group for his independent career before I officially started. But he is always one email away. I always feel embarrassed when I read the silly questions I sent him in the early days, and extremely grateful for his timely responses. Dr. Fei Wang has been a role model and a great friend to me. Tim was not alone when he said that we looked like twins, as we were mistaken to each other quite a few times. Dr. Julian Chan was always a great resource for organic chemistry-related questions. Dr. Trisha Andrew taught me everything I know about photophysical measurements. Life in the lab is so much easier when she is around.

The Swager group has always been an amazing family to me. It is a lot of fun working with people from all over the world and with different backgrounds. I would like to thank, especially, Kathy Sweeny and Caitlin McDowell for their administrative help. I am very lucky to be among the biggest class, with Rebecca Parkhurst, Olesya Haze, Stefanie Sydlik, Jose Lobez, Jan Schnorr, and Jason Cox. They have shared with me every important moments of graduate school, from orals to thesis defenses. I wish them

all the best for their future endeavors. Dr. Eric Dane, Dr. Jeewoo Lim, Dr. Brett Van, Dr. Mindy Levine and Dr. Matt Kiesewetter have been inspiring through many in-depth discussions. Special thanks go to my wonderful office mates, Rebecca Parkhurst, Grace Han, Dr. Katherine Mirica and Dr. Baltasar Bonillo. Thanks Becca for sharing my concerns and helping me adapt to the American cultures. Grace for being such a sweet friend and reinforcing our Swager inorganic community; Kat for offering new perspectives on my research and improving my writing skills; Balta for his humorous complaints about everything and being a good company.

I was very fortunate to work with people with different expertise outside the Swager group as well. Thanks Dr. Peter Müller and Dr. Michael Takase for nailing down the problematic crystal structures; Jeff Simpson, Li Li, and Anne Gorham for the valuable trainings and advices; Gleb Akselrod and Wendi Chang from the Bulovic group for their help with the mechanochromism measurements; Phil Reusswig from the Baldo group for working on the integrating sphere setup with me; Dr. Lee-Ping Wang for breaking down the black box of DFT calculations; Dr. Smaranda Marinescu and Dr. Natalia Shustova for delightful conversations.

My final and deepest gratitude goes to my beloved family. It wasn't easy for my parents to let their only daughter to be so far away from them. But all that they've given me was their unconditional love and support through all these years. As for my dear husband, who is also my longtime classmate and best friend, thank you for cheering me up during the dark times and sharing the every little exciting moments of my life. I would have taken a completely different career path without you. I am who I am because of you, and I will never regret it.